# Fluorescence and transient kinetic analysis of the *Dictyostelium* myosin-II motor domain using Green Fluorescent Protein (GFP) and its variants as probes.

Stuart Wakelin, University of Leicester

Supervisor: Prof. C. R. Bagshaw





ProQuest LLC
789 East Eisenhower Parkway
P.O. Box 1346
Ann Arbor, MI 48106-1346

# Abstract

The determination of the structure of the myosin motor domain has made it possible to introduce fluorescent probes at defined sites, thereby allowing the resolution of the mechanochemical steps in greater detail. Here, modern genetic cloning techniques were utilised to create and express within *Dictyostelium discoideum* novel myosin-II motor fusion proteins containing various fluorescent probes, in an attempt to investigate conformational changes within the motor domain during the actin-bound stages of the crossbridge cycle. Stopped-flow analysis showed that the myosin ATPase of the single tryptophan myosin-II motor W501 was unaffected by N- and C-terminal YFP and CFP probes, whereas ATP-induced actomyosin dissociation was disrupted (potentially by the probes' propensity to dimerise in close proximity), thus rendering the system unsuitable for investigation of the actin-bound stages of the actomyosin ATPase.

By combining total internal reflection microscopy with flash photolysis of an inert caged-ATP precursor, it was shown that kinetic information for the ATP-induced dissociation of fluorescently-labelled myosin motor domains may be achieved using only nanogram quantities, while simultaneously avoiding bundling artefacts common to solution kinetics. A slight adaptation of this process could yield a highly sensitive assay for the processivity of non-classical myosin types, yielding information on their rotational and lateral movement concurrently.

Lever arm movement was assessed via the analysis of fluorescence resonance energy transfer (FRET) changes between the YFP (yellow fluorescent protein) and CFP (cyan fluorescent protein) probes. A FRET efficiency increase was observed upon nucleotide occupancy of the active site, in direct contrast to previous FRET studies. Anisotropy studies showed no change upon nucleotide binding, suggesting the FRET increase was due to a distance change, rather than a variation of relative dipole orientations. However, due to the high anisotropy (*i.e.* slow rotation in solution) of the protein, it was also shown that results from this type of FRET system are qualitative rather than quantitative.

# Acknowledgements

I would particularly like to thank the following, without whom these studies could not have been accomplished. Firstly my supervisor, Prof. Clive Bagshaw, for his teaching, advice, and guidance over the past few years in all aspects of research; from laboratory techniques and theory, to presentations and writing. Also to Dr. Andras Malnasi-Csizmadia, Dr. Mihaly Kovacs, Dr. Paul Conibear, Dr. Wei Zeng, Dr. David Floyd and Robert Woolley for their teaching, guidance, and assistance; it has been greatly appreciated.

My thanks also goes out to Dr. Peter Knight and Kavitha Thirumurugan for their electron microscopy imaging, and all the staff and colleagues in the Biochemistry department for their support, help and friendship.

My gratitude also goes out to those outside the field without whom this thesis would never have taken form; to Graham Murray, Steve Blackmore, Dr. Mick Phillips and my family whose support, and especially belief in me, greatly helped me get the job done, to Andrew Aldred for his constant selfless cleaning vigilance during my writing period, and last but not least, to Geoff. Bless Geoff.

# Fig. contents

# Contents

# 1 - Introduction

## *1.1 The study of muscle contraction*

The generation of physical movement from stored chemical energy is one of the most important fundamental processes within all life, and as such the mechanism by which this movement is achieved has been of great fascination to scientists since the time of the first Greek biologists. This thesis deals specifically with the properties of the motor domain of *Dictyostelium discoideum* myosin-II. This non-muscle myosin has close parallels with skeletal muscle myosin-II, and thus it is pertinent to first discuss the background information derived from research into the mechanism of muscle contraction. This system has been targeted for a vast number of studies, largely due to *(a)* the ease with which this tissue can be obtained and purified, *(b)* the two fundamental proteins involved (actin and myosin) comprising up to 80% of the structural proteins, *(c)* these proteins being arranged in a regular way yielding clues as to their interactions, and *(d)* muscle contraction being a macroscopic, unidirectional event allowing easy quantification of length and tension changes. Some of the earliest known experiments were concerned with muscle (Vesalius, 1543), however it is only over the last fifty years that extensive studies on the mechanism of muscle contraction have yielded an understanding of the overall process at the molecular level, though many questions still remain and many details elude us. This thesis is concerned with several approaches designed to elucidate some of the mechanistic details of actomyosin interactions which have not yet been fully established.

## *1.2 The anatomy of vertebrate skeletal muscle*

Skeletal muscle consists of bundles of specialised cells termed muscle fibres, which are enveloped and anchored to fibrous connective tissue. These cells are multi-

nucleated, with the nuclei existing near the cell periphery adjacent to the plasma membrane (the sarcolemma). Each muscle fibre is filled (~80% of the fibrous volume) with a thousand or so cylindrical structures known as myofibrils, which run the length of the muscle fibre, surrounded along their entirety by mitochondria (**Fig. 1.21, top left**).

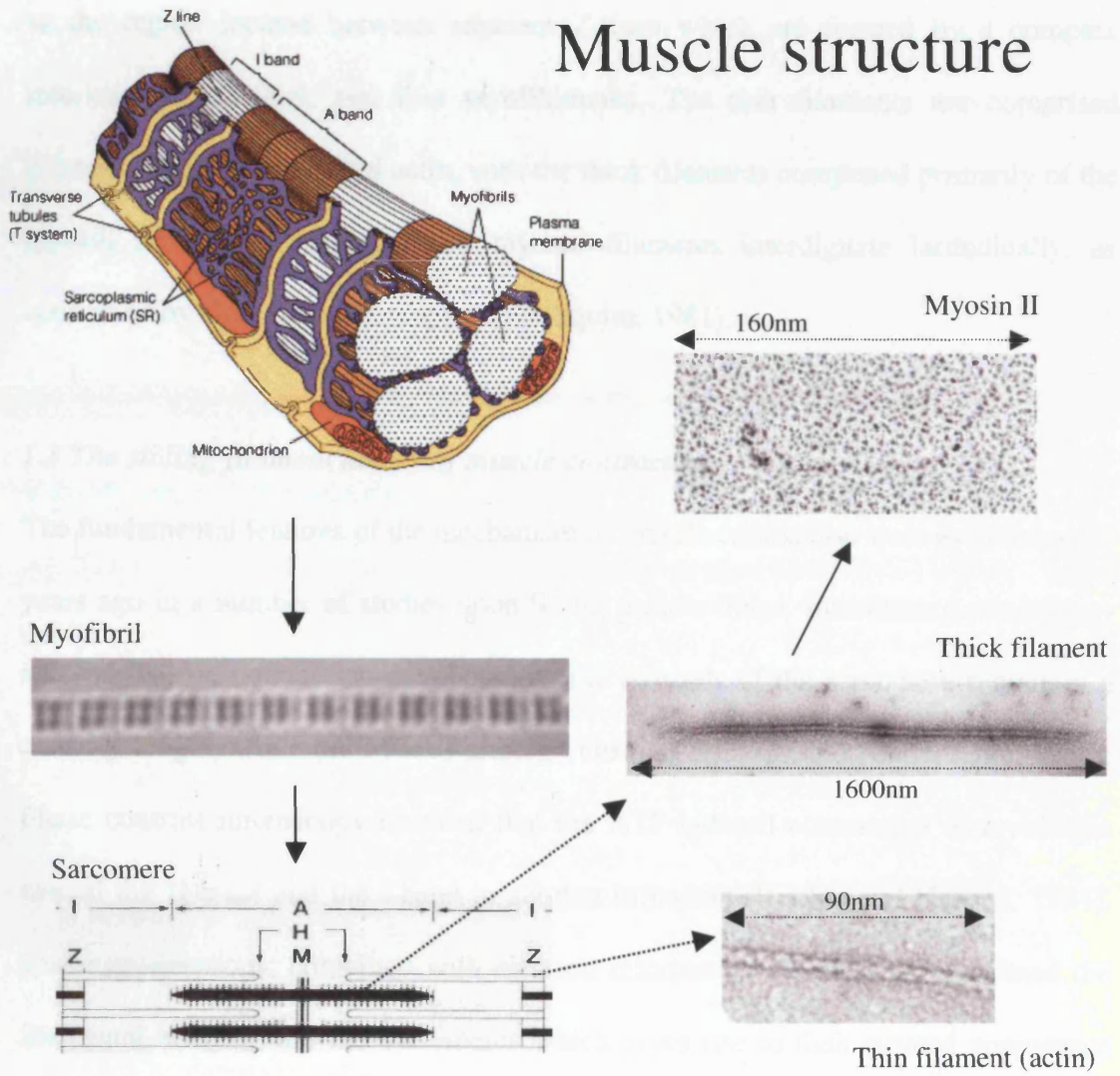


**Fig. 1.21** The anatomy of vertebrate skeletal muscle, showing a diagrammatical representation of the cross section of a muscle fibre (Becker, 2001), a myofibril viewed under phase-contrast microscopy, a diagrammatic representation of the sarcomere (Becker, 2001), and EM images of a thick filament, thin filament (Knight and Trinick, 1984) and isolated myosin molecule (Offer and Elliott, 1978).

The cytoplasm (excluding the myofibrils), is termed the sarcoplasm, the modified smooth endoplasmic reticulum (SER) is termed the sarcoplasmic reticulum (SR), with periodic invaginations of the sarcolemma forming transverse (T) tubules which separate the SR. Phase contrast microscopy revealed the myofibrils to be striated along their length, this repeating functional unit is termed a sarcomere and is defined as the region located between adjacent Z-lines which are formed by a complex interweaving of thick and thin myofilaments. The thin filaments are comprised primarily of a protein called actin, with the thick filaments comprised primarily of the myosin protein. These actin and myosin filaments interdigitate latitudinally, as confirmed by electron microscopy (EM) (Squire, 1981).

### *1.3 The sliding filament theory of muscle contraction*

The fundamental features of the mechanism of muscle contraction were established 50 years ago in a number of studies upon living muscle fibres. Interference microscopy showed that on contraction or relaxation, the A-bands of the sarcomere remain at a constant length, while the I-bands undergo changes (Huxley and Niedergerke, 1954). Phase contrast microscopy revealed that the ATP-induced contraction of myofibrils caused the H-band and the I-band to shorten in unison (Huxley and Hanson, 1954). These observations, combined with electron microscopy studies that elucidated the filamental array within the sarcomeres which gives rise to their striated appearance (Huxley, 1957), led to what is now established as the 'sliding filament theory' of muscle contraction. This involves the relative sliding of the interdigitating filaments, closing the H-band of the sarcomere, thus pulling the I-bands together and contracting the myofibril, muscle fibre, and muscle. Subsequently, electron micrographs of muscle in the *rigor* state showed small projections emanating from the myosin thick

filaments connecting to the thin actin filaments; termed crossbridges. Later it was proposed that the relative sliding was effected by the cyclic attachment and detachment of these crossbridges from the thin filament in a 'rowing' motion (the crossbridge cycle), driven by a chemical process which was identified as the hydrolysis of ATP ($ATP \rightarrow ADP + P_i$). It is now firmly accepted that interactions between the thin filament protein (actin), and the thick filament protein (myosin), form the fundaments of muscle contraction. Thus, the structure, function, interactions and conformational changes of these two proteins are of paramount importance to the investigations within this thesis.

### *1.4 The structure of contractile proteins*

#### *1.41 Myosin and its proteolytic subfragments*

Myosin (MW 520kDa) consists of six separate polypeptide chains, which under denaturing conditions dissociate into two heavy chains (MW 220kDa) and four light chains (MW 20kDa, Weeds and Lowey, 1971). The light chains are categorised into two types, the essential light chains (A-light chains) and the regulatory light chains (P-light chains), with a single myosin molecule containing two of each type. Furthermore, there exists in most fast vertebrate skeletal myosin two separate isoforms of the heavy chain (Starr and Offer, 1973) and two isoforms of the essential light chains (Periasamy *et al.*, 1984). These isoforms are assembled in what appears to be a random order when the myosin molecule in synthesised, thus any given molecule of vertebrate skeletal myosin *in vivo* may contain heavy chains or essential light chains that are structurally different to one another.

Electron microscopy visualisation of single myosin molecules (**Fig. 1.411,** Offer and Elliott, 1978) show them to be very asymmetric molecules, something first

suggested by early hydrodynamic studies. The N-terminal region of the heavy chains fold into two globular domains, termed the myosin 'heads'. It is these two globular domains which gave rise to the classification of skeletal myosin as myosin-II. Toward their C-terminal end, the heavy chains are wound together in a coiled-coil of α-helices to form the myosin 'tail', with one essential light chain and one regulatory light chain associated with each myosin head.

Many years after the isolation of myosin-II, a second type of myosin was isolated from non-muscle cells which contained only one heavy chain (one myosin head), and was thus classified as myosin-I (Pollard *et al.*, 1991). Since that time, many different types of myosin have been isolated and classified into what is now known collectively as the myosin 'superfamily', containing at present 18 distinct myosin classifications.

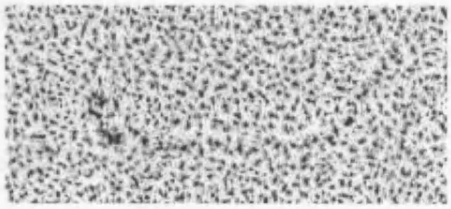

**Fig. 1.411** The structure of a single molecule of vertebrate skeletal myosin-II, viewed under electron microscopy (courtesy of Offer and Elliott, 1978). The two heavy chains each fold into a globular 'head' domain at their N-terminal end, intertwining in a coiled-coil of α-helices along their remaining length to form the 'tail' region.

Myosin is an ATPase and actin-binding protein (Engelhardt, 1939, Wollemann *et al.*, 1950), and it is widely recognised that these properties have a major role within the crossbridge cycle. The myosin head domain is also termed the motor domain, as ATP-hydrolysis and actin-binding are associated with this region (Lowey and Luck, 1969, Margossian and Lowey, 1973a), and thus generation of movement via the crossbridge cycle. Under physiological conditions, the tail regions of myosin self-aggregate to form filamentous structures very similar to those of the thick filaments *in vivo* (Huxley, 1963), and is thought to be due to the large number of exposed hydrophobic

residues present along the α-helical coiled-coil domain (McLachlan, 1984). Thus it appears that the tail region has a largely structural role, with the chemical generation of movement via actin interaction being the sole responsibility of the head domain(s).

Due to myosin's size and tendency to self-aggregate, thus rendering it largely insoluble, the structure-function relationships of myosin have been elucidated by examining its proteolytic fragments. The heavy chain is particularly susceptible to proteolytic cleavage at two sites (Weeds and Taylor, 1975), *(a)* just after the globular head domain (papain and chymotrypsin digestion), and *(b)* approximately two-thirds of the way along the coil itself from the head domain (trypsin and chymotrypsin digestion, **Fig. 1.412**). The properties of the resultant proteolytic fragments are summarised in **Fig. 1.413**, with the intrinsic functional activity (actin binding, ATP hydrolysis) of native myosin being retained by subfragment 1 (S1, Margossian and Lowey, 1973a, Margossian and Lowey, 1973b) and heavy meromyosin (HMM), justifying their use for characterisation studies. Furthermore, the viability of myosin-I as a functional motor protein suggests that the double-headed structure of myosin is not fundamental to mechanochemical coupling, making the soluble S1 a suitable myosin analogue for study. It is these S1-type proteins which are primarily involved in the research discussed within this thesis.

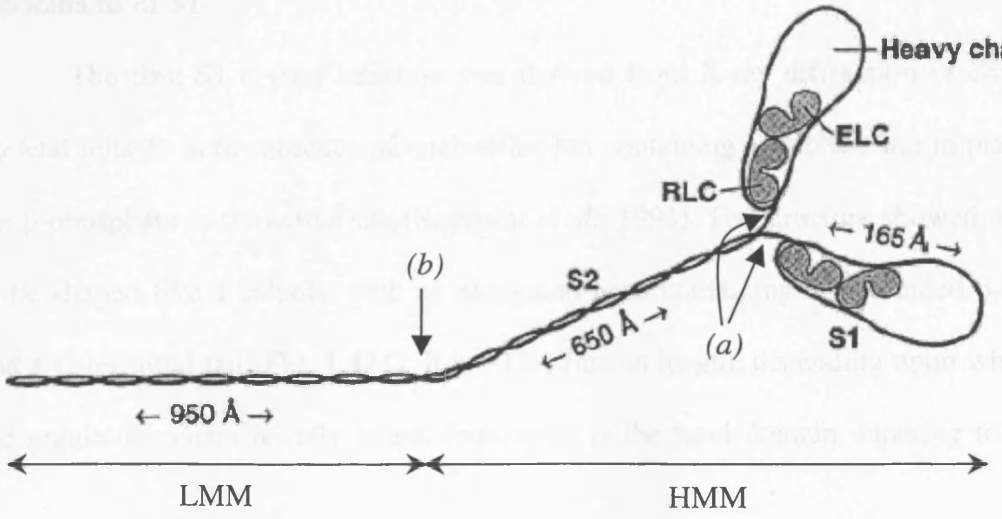

**Fig. 1.412** A diagrammatic representation of the myosin molecule, showing the main proteolytic cleavage sites. Digestion with papain and chymotrypsin (*a,* S1 fragment) yields the motor domain, complete with regulatory light chain (RLC) and essential light chain (ELC). Digestion with trypsin and chymotrypsin (*b*) yields the light meromyosin (LMM) tail fragment, and the double-headed heavy meromyosin (HMM) fragment. Adapted from Rayment and Holden (1994).

| *Protein* | *Symbol* | *MW (kDa)* | *Length (nm)* | *Self-aggregation* | *Actin/ATP binding sites* |
|---|---|---|---|---|---|
| *Myosin* | M | 520 | 160 | + | 2 |
| *Light meromyosin* | LMM | 160 | 90 | + | 0 |
| *Heavy meromyosin* | HMM | 340 | 65 | - | 2 |
| *Subfragment 1* | S1 | 120 | 15 | - | 1 |

**Fig. 1.413** A summary of the properties of myosin and a few of its proteolytic fragments (HMM, LMM and S1). Taken from Bagshaw (1993).

### *1.42 The S1 proteolytic fragment*

The S1 proteolytic fragment comprises the first 843 residues of the heavy chain domain, coupled with one regulatory and one essential light chain domain (**Fig. 1.421**). Further limited proteolysis of the S1 domain (for vertebrate skeletal muscle) yields three proposed subdomains, named after their molecular mass (in Da); the 25K (N terminal), 50K (middle), and 20K (C terminal) fragments (Mornet *et al.*, 1979). However, the proteolysis sites are now believed to mark the position of two flexible loops within the motor domain (loop1 and loop 2), rather than dividing specific subdomains of S1.

The first S1 crystal structure was derived from X-ray diffraction of chicken skeletal muscle in the absence of nucleotide, but containing a sulphate ion in place of the β-phosphate in the active site (Rayment *et al.*, 1993). The structure showed the S1 to be shaped like a tadpole, with an elongated head containing a 7-stranded β-sheet and a C-terminal tail (**Fig. 1.421**). It is ~12-17nm in length, depending upon whether the regulatory chain is fully intact, 7nm wide at the head domain, tapering to 3nm

towards the tail region. The nucleotide and actin binding sites, having been identified via *(a)* nucleotide-affinity labelling (Mahmood *et al.*, 1987, Okamoto and Yount, 1985, Szilagyi *et al.*, 1979), and *(b)* a combination of limited proteolysis and cross-linking (Mornet *et al.*, 1981a, Mornet *et al.*, 1981b), are located on opposite sides of the myosin head. They lie 4nm apart, separated by a large cleft (the 50kDa cleft) caused by several α-helices surrounding the β-sheet.

The three proteolytic fragments (25K, 50K, 20K) all contribute to the 7-stranded β-sheet, thus negating the idea that they are discrete subdomains of S1 (Vibert and Cohen, 1988).

The actin-binding sites lie on either side of the 50kDa cleft, and given that the apex of the cleft lies close to where the terminal $P_i$ of bound ATP would lie (Rayment *et al*, 1993), it has been suggested that release of this $P_i$ after hydrolysis could cause a closing of the cleft, thereby altering myosin's affinity for actin-binding, and facilitating actomyosin dissociation. The small compact region termed the converter domain (Houdusse and Cohen, 1996, Xie *et al.*, 1994), however, functions as a socket for the C-terminal α-helical tail, which is usually referred to as the regulatory domain or 'neck', to which are bound the regulatory and essential light chains. It is currently the view that the neck region acts as a lever arm to amplify rotational movements experienced by the converter domain upon ATP-binding and hydrolysis.

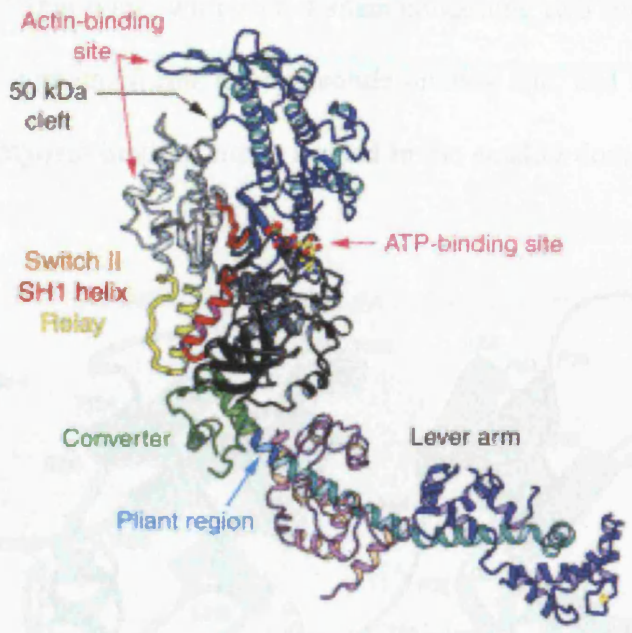


**Fig. 1.421** The crystal structure of the myosin proteolytic fragment S1, showing the main identified regions of the motor domain, together with the beginning of the C-terminal tail region and its associated light chains (1 regulatory, 1 essential). Image taken from Houdusse and Sweeney (2001).

Regarding the double-headed structure of native myosin II, observations that S1 can support relative sliding movement and generate force on an actin filament (Harada *et al.*, 1987, Kishino and Yanagida, 1988, Kron and Spudich, 1986) has led to the hypothesis that the duplex structure exists purely for the need to form a coiled-coil, either for *(a)* self-aggregation and thick filament assembly, or *(b)* the integrity of these structures (Bagshaw, 1987).

### *1.43 Actin*

Monomeric actin (G-actin) is a highly conserved protein consisting of a single polypeptide chain (MW 42kDa), with two similar domains, one slightly larger than the other, each containing a 5 strand β-sheet with surrounding α-helical regions (**Fig. 1.431**). The structure was originally solved using protein crystallography as a DNase I complex, to a resolution of 2.8Å (Kabsch *et al.*, 1990). It is asymmetrical, being

5.5nm long and 3.5nm wide, with each domain containing two subdomains. The cleft between the two domains forms the nucleotide binding site, and there is evidence to suggest that the myosin binding site is located in the smaller domain (Bertrand *et al.*, 1988).

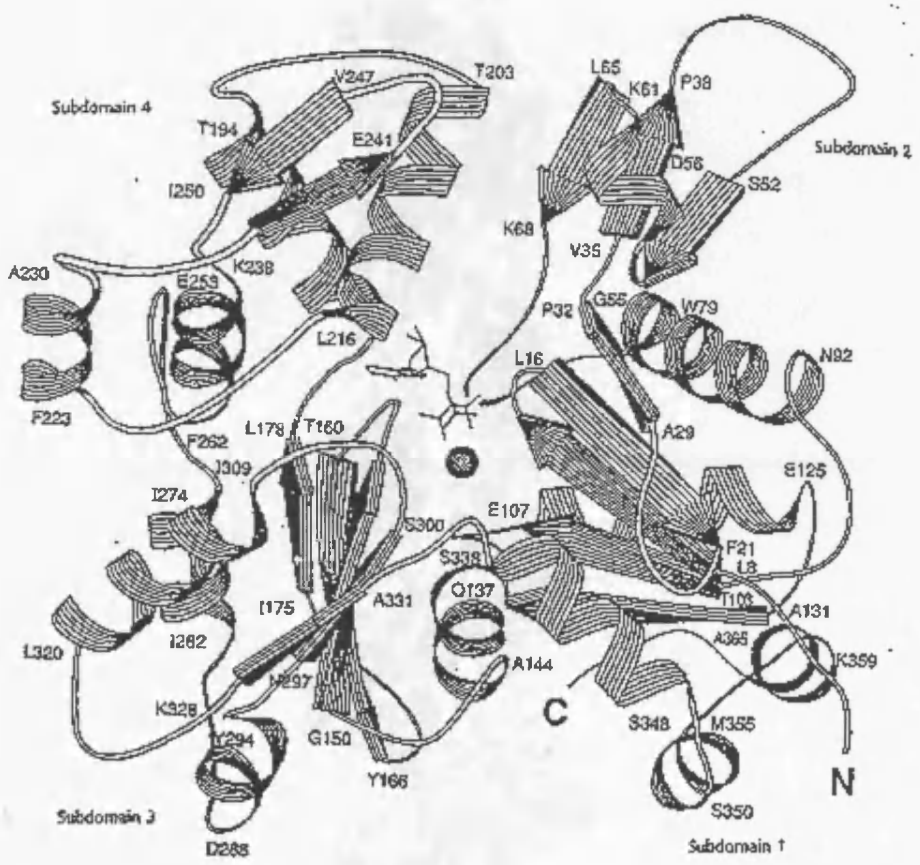


**Fig. 1.431** The crystal structure of globular actin, initially solved as a complex with DNaseI (G-actin, Kabsch *et al.*, 1990). The large domain is represented on the right and the small domain on the left, with the residue numbers corresponding to the beginning and end of each α-helix and β-sheet. In this orientation the ATP-binding cleft between the two domains is clearly visible.

Under physiological salt conditions (~0.12M), globular actin polymerises to form filaments of 2-5μm in length (F-actin). These are helical polymers which have 13 actin monomers arranged on long-pitch, left-handed helix repeating every 36nm. The thin filament helix is, in fact, comprised of two-right-hand helices intertwined (**Fig 1.432**), something which is evident from electron microscopy of isolated F-actin filaments (**Fig 1.21,** reviewed by Egelman, 1985), and X-ray diffraction patterns from

intact muscle and actin bundles (Holmes *et al.*, 1990). These studies also show that it is the small domain of actin monomers which form the filament surface, thus being free to interact with myosin.

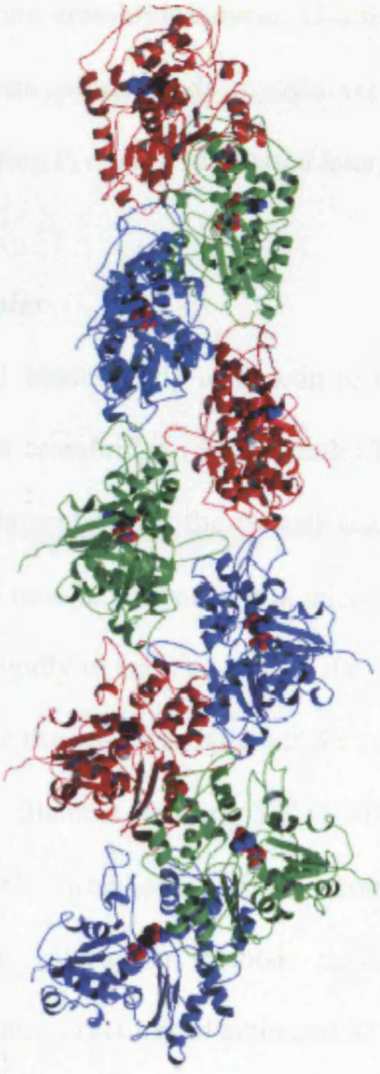

**Fig. 1.432** The structure of filamentous actin (F-actin, Holmes *et al.*, 1990, Lorenz *et al.*, 1993). In physiological salt conditions (~0.12M) actin monomers (G-actin) polymerise to form a helical structure with 13 actin monomers arranged on a long-pitch, left-handed helix repeating every 36nm. The overall F-actin structure is comprised of two of these actin helices intertwined in a double, right-hand helix with a pitch of ~350Å. Image taken from Geeves and Holmes (1999).

G-actin binds ATP (plus $Mg^{2+}$ or $Ca^{2+}$) irreversibly, however upon polymerisation this becomes hydrolysed and subsequently trapped as ADP (Carlier, 1991). An F-actin filament contains a polarity due to the asymmetry of the G-actin molecules

within it, and at physiological ionic strength the filament exists in dynamic equilibrium; with monomers being lost from the –ve (pointed) end and replaced at the +ve (barbed) end. Thus, a low ATPase activity can be detected, however this does not appear to be involved in the crossbridge cycle. G-actin binds myosin very weakly (Arata, 1990) unlike F-actin which binds myosin very strongly and activates the myosin ATPase by facilitating $P_i$ release (discussed later).

### *1.44 The actomyosin complex*

In the absence of ATP, S1 binds tightly to F-actin to form a high affinity complex known as actomyosin. One crossbridge (S1 molecule) binds to each actin monomer within these 'decorated filaments', and the overall state is taken to be an accurate model for the *rigor* state of muscle. Early electron microscopy studies showed that the head domain of S1 binds rigidly to actin at ~45° to the filament axis. Further studies, however, showed that while the head was bound at 45°, the tail region of S1 projected tangentially away from the filament at nearly 90° (Milligan *et al.*, 1990). Due to the bulky actomyosin complex's virtual insolubility, efforts to solve the structure via crystollagraphic and X-ray diffraction methods have so far proved ineffective. However, by fitting the atomic structures of actin and S1 into 3D electron microscope reconstructions of 'decorated actin' (Milligan *et al.*, 1990, Rayment *et al.*, 1993, Schroder *et al.*, 1993), a proposed structure of the actomyosin complex in the *rigor* state (in the absence of nucleotide) has provided some insight into the sub-molecular basis of the actin-S1 interaction (**Fig. 1.441**). S1 appears to bind via hydrophobic residue interactions and ionic bonds between the actin-binding site below the 50kDa cleft, and the lower subdomains and amino terminus of one actin monomer, with some additional interaction with the subdomain of the adjacent actin molecule. A final

interaction may occur via the actin-binding domain above the 50kDa cleft of S1, however this could only be achieved if a major conformational change involving closure of the 50kDa cleft were to take place. It has been proposed that this could be triggered by $P_i$ release, as previously mentioned (see ***S1 structure,* 1.42**). Furthermore, as also suggested in that section, the extended C-terminal α-helix of S1 is shown to lie distal to the actin's helical axis, and is thus in an ideal situation and orientation to function as a lever arm.

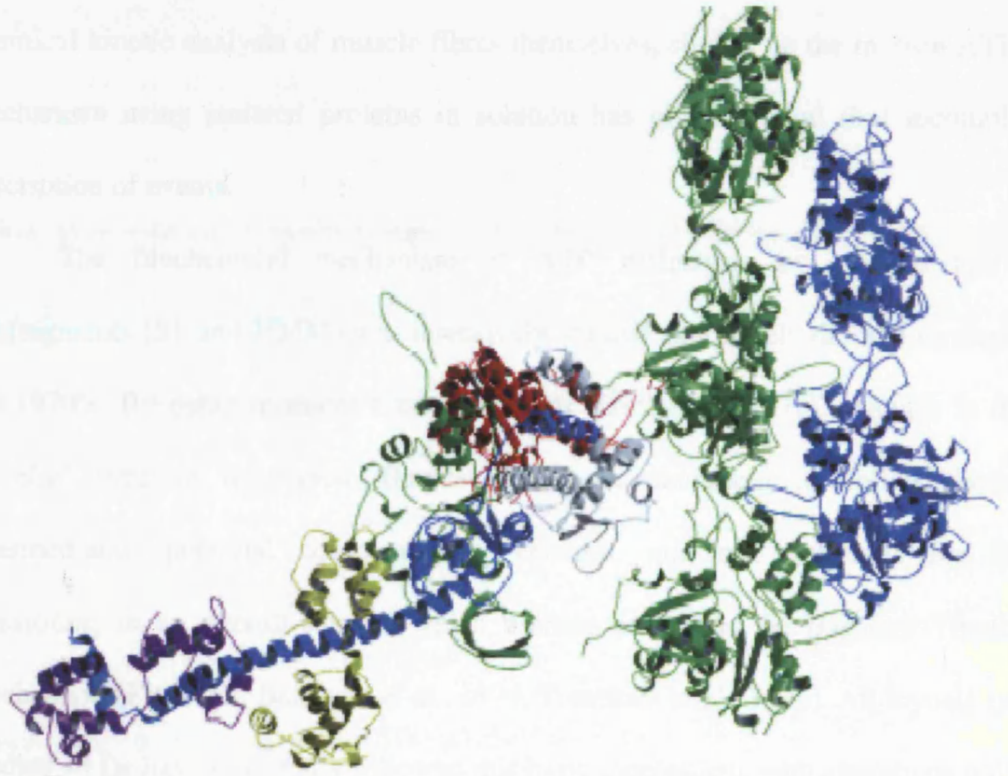

**Fig. 1.441** The proposed structure of the S1-actomyosin complex in the absence of nucleotide, constructed by fitting the atomic structures of actin and S1 into 3D electron microscope reconstructions of 'decorated actin' (Milligan *et al.*, 1990, Rayment *et al.*, 1993, Schroder *et al.*, 1993). The myosin crossbridge (*left*) is shown here making contact with two adjacent actin monomers (*right*). Image taken from Geeves and Holmes (1999).

Despite this, and other, projected structures for the various conformations of the myosin-II actomyosin complex, little has as yet been determined by direct observation of the interactions between specific regions of the molecules themselves. Thus, the

conformational changes that certain areas of myosin-II undergo while in the actomyosin complex, throughout different stages of the crossbridge cycle, are of particular interest for this thesis (discussed later).

### *1.5 The myosin ATPase*

In solving muscle contraction on a molecular basis, both chemical and mechanical events throughout the crossbridge cycle need to be related (mechanocoupling), both in extent (thermodynamics) and timecourse (kinetics). Due to the difficult nature of chemical kinetic analysis of muscle fibres themselves, studies on the myosin ATPase mechanism using isolated proteins in solution has given a good (but incomplete) description of events.

The biochemical mechanism of ATP hydrolysis by myosin and its subfragments (S1 and HMM) was intensively studied and largely defined throughout the 1970's. By using transient kinetic methods (Gutfreund, 1972), changes in these proteins' inherent tryptophan fluorescence were monitored to define chemical intermediates, potential conformational changes, and rate constants for these transitions, in an overall scheme which became known as the Bagshaw-Trentham mechanism (**Fig. 1.51,** Bagshaw *et al.*, 1974, Trentham *et al.*, 1976). All myosin types studied so far have essentially followed this basic mechanism, with alterations only in the overall ATPase rate and the individual rate constants themselves (Jontes and Milligan, 1997, Marston and Taylor, 1980, Ostap and Pollard, 1996, Ritchie *et al.*, 1993). All rate constants quoted, unless otherwise stated, refer to rabbit fast skeletal S1.

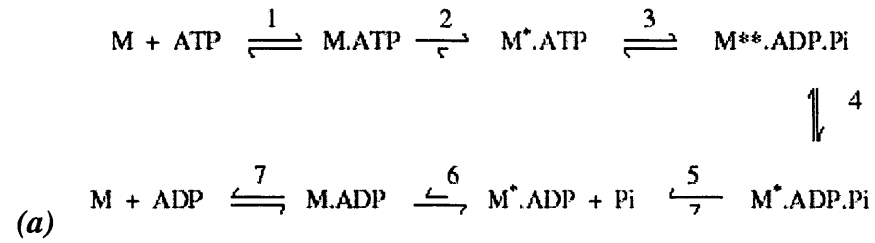


*(a)*

**Fig. 1.51** The outline of the Bagshaw-Trentham mechanism for ATP hydrolysis by fast skeletal myosin. The myosin head domain is denoted by M. Asterisks are used to denote separate levels of intrinsic tryptophan fluorescence.

ATP binds to myosin in a two-step process consisting of the initial diffusion-limited complex formation (step 1, 2nd order rate constant $2x10^6M^{-1}s^{-1}$), followed by a virtually irreversible isomerisation step which yields an ~10% increase in intrinsic protein fluorescence (step 2). The reversible hydrolysis of ATP then occurs ($k_3$>100$s^{-1}$, $k_{eqm}$=~10, Bagshaw and Trentham, 1973), resulting in a further 10% increase in tryptophan fluorescence. The products then remain tightly bound while a slow ($0.05s^{-1}$) isomerisation occurs (step 4), accompanied by a decrease in tryptophan fluorescence, before Pi is rapidly released (step 5). Following product release, ADP dissociates in a two-step reaction that is essentially the reversal of the ATP binding steps, resulting in the intrinsic tryptophan fluorescence falling to the original level.

The solving of the crystal structures for S1 in several nucleotide (or analogue) bound states has led to the coupling of the two main structures observed, termed OPEN and CLOSED states due to the conformation of the nucleotide binding pocket (**Fig. 1.52**), with specific stages of the Bagshaw-Trentham mechanism. The OPEN conformation is generally assigned to the M*ATP and M*ADP stages, as it is observed in crystals containing non-hydrolysable ATP analogues and ADP bound to the nucleotide binding site of S1. The CLOSED conformational state corresponds to M**ADP.Pi, or the 'transition state' of the hydrolysis reaction, as this structure is observed for the stable M.ADP.Vi complex. Vanadate (Vi) itself behaves as a

phosphate analogue in many biological systems. Furthermore, as tryptophans at the 440 (*Dictyostelium* 432) and 595 (*Dictyostelium* 584) do not show any evidence for environmental change between OPEN and CLOSED conformations, the change in fluorescence is primarily associated with the tryptophan at the 510 (*Dictyostelium* 501) position. This has recently been confirmed in *Dictyostelium* by construction of a mutant S1-type protein with only a single tryptophan (discussed later, Malnasi-Csizmadia *et al.*, 2001a, Malnasi-Csizmadia *et al.*, 2001b, Malnasi-Csizmadia *et al.*, 2000).

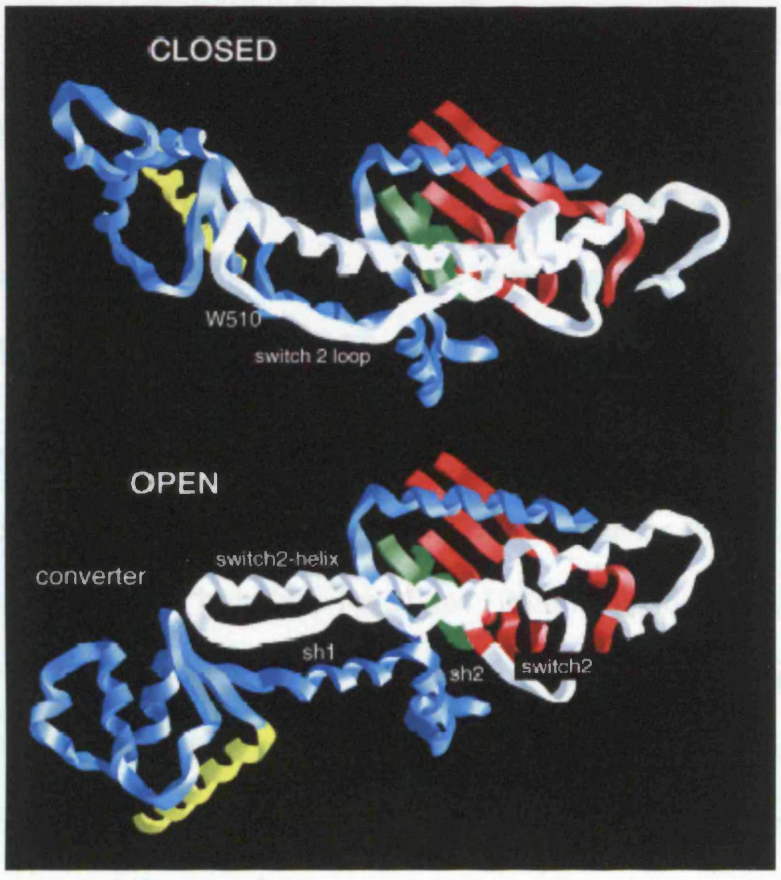


**Fig. 1.52** The OPEN and CLOSED conformations of chicken skeletal S1, showing the large orientation change of the converter domain (*left*) resulting from the inward movement of the switch-2 element (*right*), causing the bending/twisting of the switch-2 helix. Taken from Geeves and Holmes (1999).

W510 (W501) sits close to what is known as the switch-2 helix and the converter domain, and goes from a solvent-exposed to solvent-free environment as the converter

domain, lever arm, and switch-2 helix undergo considerable movement between OPEN and CLOSED conformations.

Furthermore, since the OPEN conformation appears to negate hydrolysis of ATP, then we can assume that step 3 can be further resolved into an isomerisation step, followed by hydrolysis (**Fig. 1.53**). These two stages have subsequently been resolved for the *Dictyostelium* myosin II mutant W501 (**see 1.9**) by fast-resolution pressure-jump techniques (Malnasi-Csizmadia *et al.*, 2001b).


**Fig. 1.53** Further resolution of the hydrolysis step into an initial isomerisation (3a) followed by hydrolysis itself (3b). Taken from (Geeves and Holmes, 1999)

As mentioned previously, because the crossbridge cycle involves a cyclic interaction of actin with myosin, the myosin ATPase alone gives us an incomplete picture. Thus, an understanding of the actomyosin ATPase is required.

### *1.6 The Lymn-Taylor scheme*

Early steady-state studies of the actomyosin ATPase mechanism showed that *(a)* actin increased the rate of ATP hydrolysis for S1 and HMM by up to 200-fold, depending on protein concentration and ionic strength of the environment (Eisenberg and Moos, 1968, Eisenberg *et al.*, 1968), and *(b)* ATP induced dissociation of the actomyosin complex (Eisenberg and Moos, 1968, Lymn and Taylor, 1971). The transient kinetic studies of Lymn and Taylor (1971), also yielded several important observations; *(a)* that ATP-induced dissociation of actomyosin occurs faster than the hydrolysis step, *(b)* that the rate of the hydrolysis step remains unchanged in the presence of F-actin, and *(c)* that the rate of the $P_i$ release is accelerated by the presence of actin. Collating these findings with those of the earlier studies, a model for the mechanocoupling of

ATP hydrolysis and actin-associated and actin-dissociated intermediates was proposed (**Fig 1.61**). This Lymn-Taylor cycle involves the initial formation of the *rigor* actomyosin complex (1), followed by ATP-induced dissociation of the myosin head (2), hydrolysis of ATP with an associated conformational change of the myosin head relative to the lever arm (3), re-association of myosin to the actin filament (4) and a reverse conformational change to allow actin-activated $P_i$ release, thus returning to the original actomyosin state (5). This final conformational change, a 'rowing' movement pulling the thick myosin filament along the actin filament thus causing contraction of the sarcomere via interdigitating filament sliding, is often referred to as the 'power stroke'.

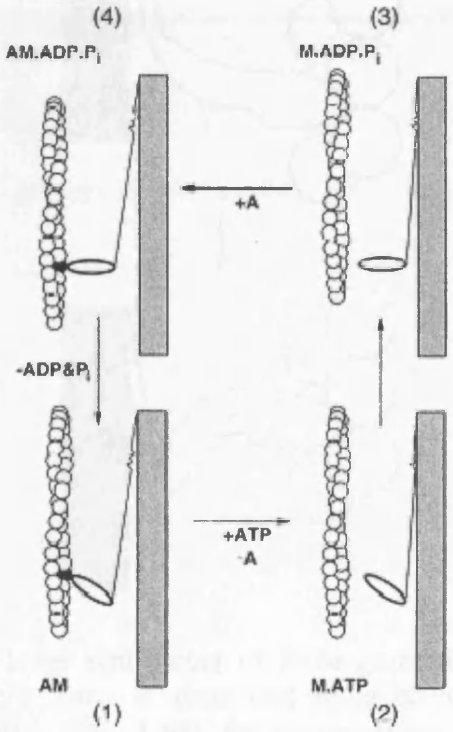


**Fig. 1.61** The Lymn-Taylor scheme relating chemical and conformational changes during the crossbridge cycle. This model involves the initial formation of the *rigor* actomyosin complex (1) followed by ATP induced dissociation (2), then ATP hydrolysis accompanied by a conformational change (3), and finally re-association to actin (4) to allow actin-activated product release and a return to the *rigor* state. Taken from Geeves and Holmes (1999).

This scheme, although still widely regarded as an accurate illustration of the concepts in the mechanochemical coupling of muscle contraction, has been shown to have some limitations throughout the years. For example, the swinging crossbridge theory, whereby the myosin head 'rolls' on the surface of the filament during the power-stroke (Huxley and Simmons, 1971, Irving, 1987), has since been replaced by the 'swinging lever-arm' theory due to a number of structural and spectroscopic observations (see Cooke, 1986). Here the power-stroke is generated by the distal part of the myosin crossbridge moving as a lever arm (**Fig. 1.62**).

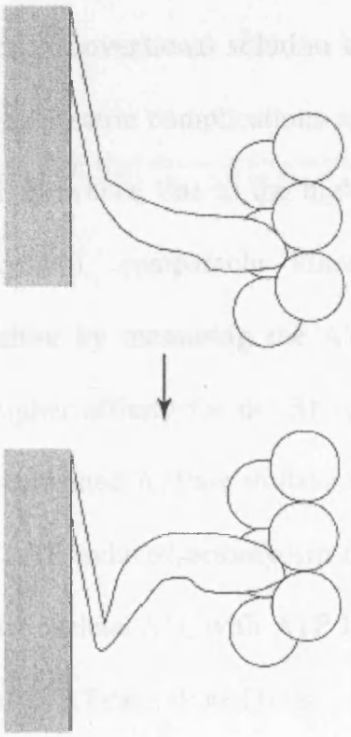

**Fig. 1.62** The swinging lever arm theory of force-generation. Unlike the swinging crossbridge theory, where force is generated by a change in the angle of the crossbridge relative to actin (**Fig. 1.61**), the power-stroke here is generated by the distal part of the crossbridge moving as a lever arm. Taken from Geeves and Holmes (1999).

Furthermore, the assumption that the M.ATP complex has a lower affinity for actin than M.ADP.Pi, thus driving a cyclic attachment-detachment cycle during each ATP-hydrolysis reaction, was later disproved by studies into the actin-activated S1 ATPase

(discussed in the following section). These showed the M.ATP and M.ADP.Pi complexes to have relatively equal, weak affinities for actin, termed the 'weak-binding states'. Therefore, this suggests that the hydrolysis step does not drive the re-association of myosin to actin. However, the alternation of the myosin intermediates between weak and strong (M.ADP & M) binding states still allows the basic concepts to be retained.

### *1.7 The actomyosin ATPase*

Standard kinetic analysis of the myosin ATPase showed it to be activated by F-actin, but not by monomeric G-actin. Conventional solution kinetics are applicable to S1 interaction with F-actin, however steric complications arise with HMM and myosin due to tethering of the heads. However, due to the high concentration of protein in muscle (~100mg/ml actomyosin), comparable kinetic analysis can only be realistically achieved in solution by measuring the ATPase at low ionic strength (10mM) where actin has a higher affinity for the S1 intermediates. These types of studies have shown the actin-activated ATPase to have a $V_{max}$ of $20s^{-1}$, compared to the $0.05s^{-1}$ of myosin alone. ATP-induced actomyosin dissociation appears to occur very quickly ($>1000s^{-1}$ for fast skeletal S1), with ATP hydrolysis occurring at a rate comparable to that of the myosin ATPase alone ($100s^{-1}$). Subsequent re-association of the actin (rapidly reversible, thus difficult to resolve) presumably causes a conformational change facilitating $P_i$ release to achieve overall activation. As with the myosin ATPase, the subsequent $P_i$ and ADP steps have been resolved and suggest that $P_i$ release occurs first (**Fig. 1.71**).

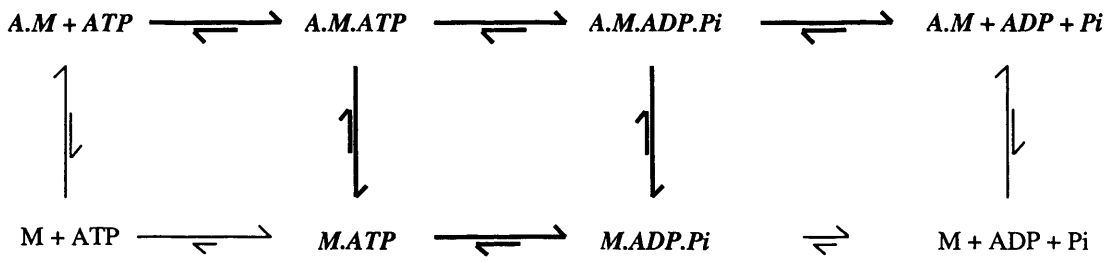


**Fig. 1.71** The proposed actomyosin ATPase mechanism. Shown is a summary of all the proposed states of actomyosin interaction, with the widely accepted kinetic pathways for actin-myosin interaction during the crossbridge cycle, including dissociative (Lymn-Taylor) and non-dissociative hydrolysis of ATP, shown in bold.

This dissociative pathway proposed by (Lymn and Taylor, 1971) provided a reasonable model of contraction, but, as previously mentioned, failed to consider the reversibility of steps in the pathway, assumed that M.ATP had a lower actin affinity than M.ADP.$P_i$, and did not clearly define events at high [actin]. Subsequently these complexes were shown to have a similar, weak affinity for actin. Furthermore, steady-state studies showed that one actin monomer could dissociate from one S1 and bind to another within the ATP turnover time, thus it was not possible to assign the $V_{max}$ ($20s^{-1}$) to the $P_i$ release step, as with the myosin ATPase. These ambiguities have proved hard to resolve due to *(a)* the ionic dependence of actin affinities, and *(b)* that at high [actin] solutions become viscous thus decreasing the accuracy of measurements.

Overall, a single rate-limiting step has not been identified for the actomyosin ATPase although the predominant states have been identified (**Fig. 1.71**). However the dominant pathway which occurs during the actomyosin ATPase is still widely debated.

Nevertheless, by utilising modern genetic cloning methods to express myosin mutants within eukaryotic organisms such as *Dictyostelium discoideum*, myosin motors may now be re-engineered to specifically investigate certain protein regions, and follow biochemical changes of these regions in real-time. Thus by separately

probing for conformational changes within the actin-binding sites, ATP-binding site, lever-arm domain, converter domain, etc., the interactions of myosin and actin could be monitored in real-time throughout the actin-bound stages of the crossbridge cycle, potentially resolving the actomyosin ATPase.

### *1.8 Dictyostelium discoideum & genetic manipulation*

Huge developments in genetic manipulation, such as point mutations, truncations, specific deletion of supposed vital functional units, and the creation of fluorescent chimeras and protein tags, have proved useful in the analysis of protein function. However, they have also shown to be a powerful adjunct to structural studies, due to the ease with which specific and well-defined units and subdomains can be produced. Unfortunately in the case of myosin, prokaryotic expression cannot be successfully achieved, and thus eukaryotic hosts such as *Dictyostelium discoideum* and SF9 insect cells (*Spodoptera frugperda*) have become the main expression hosts for genetically modified myosin constructs. For SF9 cells, particular success has been obtained using baculovirus to express chicken smooth-muscle constructs, however it is the plasmid induced over-expression of myosin II constructs in *Dictyostelium discoideum* which is of great relevance to the work contained within this thesis, and thus it is this system which will be discussed in detail.

*Dictyostelium discoideum* is a cellular slime mold, which feeds on soil bacteria and exists as a singular cellular entity until the onset of starvation. Following this, cAMP induced chemotaxis aggregate the amoebae, eventually forming an organism which undergoes cell-differentiation and morphogenesis. The resultant fruiting body consists of a ball of spores suspended on a stalk (**Fig. 1.81**), and thus the first known

observer of *Dictyostelium* (Brefeld, 1869) named them so because of these structural elements (*Dicty* means net, *stelium* means tower).

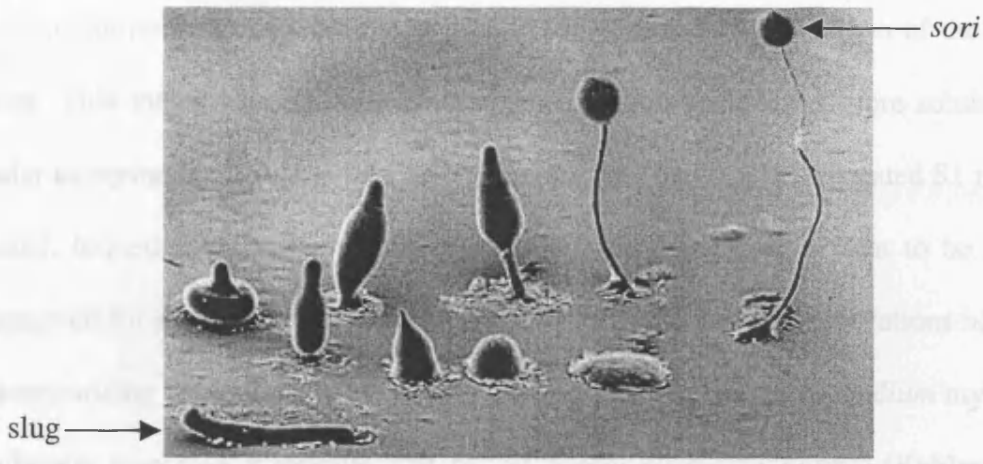


**Fig. 1.81** A gallery of REM images showing *Dictyostelium discoideum* through slug (aggregation of amoebae) and *sori* (fruiting body, spore) formation. Image taken from the Dept. of Genetics homepage, Kassel University, Germany (www.uni-kassel.de/fb19/genetics/Welcome.html) and originally compiled by L. Blanton & M. Grimson of Texas Tech. University.

*Dictyostelium* itself contains a variety of extra-chromosomal plasmids, divided into four separate families, Dpd1 and Dpd2 (Gonzales *et al.*, 1999) and Dpp1 and Dpp3 (Kiyosawa *et al.*, 1993). The Dpd2 family contains *rep* genes that code for proteins required for autonomous plasmid replication (Slade *et al.*, 1990), and plasmid maintenance (Shammat and Welker, 1999), and thus Dpd2 genes were subsequently utilised as origins of replication to create cloning vectors for the expression of novel protein (*e.g* myosin II) constructs in *Dictyostelium* (Manstein *et al.*, 1995). DNA can be introduced into *Dictyostelium* amoebae either as a calcium phosphate precipitate or by electroporation (Firtel *et al.*, 1985, Nellen *et al.*, 1984), with selection of successfully transformed amoeba usually occurring by incorporating G418 (geniticin) resistance into the transformation vectors. Regarding the work undertaken for this thesis, the most useful element of *Dictyostelium* is that it has one conventional myosin (myosin II), and thus offers the biochemical facility to isolate mutants of myosin II whose mechanisms and motor functions can then be examined in subsequent *in vitro*

studies. These myosin-II mutants usually involve a minimal model of the myosin motor; truncation of the polypeptide chain removes the neck and light chain regions of S1, leaving an intact converter domain and globular N-terminal region of the heavy chain. This yields a more symmetrical protein which has proved more soluble and easier to crystallise (Fisher *et al.*, 1995, Gulick *et al.*, 1997). This truncated S1 myosin model, termed the myosin motor, or myosin 'core', has been shown to be highly conserved for all myosin types (Cope *et al.*, 1996), with the major variations between classes arising from the neck regions. It has been shown that *Dictyostelium* myosin II molecules truncated at residues 759, or 761 appear kinetically normal (Kuhlman and Bagshaw, 1998), and as such provide an excellent basis for the production of genetic mutants to investigate the structure-function relationship of myosin. In particular, the 761 residue, *Dictyostelium* myosin II single tryptophan mutant W501 (Malnasi-Csizmadia *et al.*, 2001a, Malnasi-Csizmadia *et al.*, 2001b, Malnasi-Csizmadia *et al.*, 2000) has provided the core for all of the fusion proteins designed, discussed and investigated within this thesis.

### *1.9 W501*

Tryptophan residues in proteins usually comprise the dominant source of UV absorption and fluorescence emission, and as such are particularly useful as biochemically sensitive probes. In particular tryptophan fluorescence has long been used as an empirical probe of myosin conformation during ATPase activity, as mentioned previously (Bagshaw *et al.*, 1974, Bagshaw and Trentham, 1973, Werber *et al.*, 1972). The use of modern molecular genetic cloning methods to mutate tryptophan residues to phenylalanine, thus leaving a single conformationally sensitive tryptophan residue within a protein, is an attractive approach because *(a)* the signal

arises from a single location, *(b)* any heterogeneity in the signal can be less ambiguously analysed, and *(c)* due to a lower background from other tryptophan residues, the overall signal changes may be larger and more clearly defined. Thus, Bagshaw and colleagues (Malnasi-Csizmadia *et al.*, 2001a, Malnasi-Csizmadia *et al.*, 2001b, Malnasi-Csizmadia *et al.*, 2000) created the truncated S1 (761 residue) *Dictyostelium* myosin II mutant containing a single tryptophan at the 501 position (**Fig. 1.92**), with all other tryptophans mutated to phenylalanine. The 501 position is equivalent to the 510 position of chicken skeletal myosin, situated close to the switch-2 helix and the converter region as mentioned previously, thus undergoes a considerable environmental change during the OPEN-CLOSED transition. It was subsequently shown that the tryptophan fluorescence of W501 was indeed sensitive to this conformational change upon ATP-binding and hydrolysis, while retaining its native functionality (**Fig. 1.91,** Malnasi-Csizmadia *et al.*, 2000).

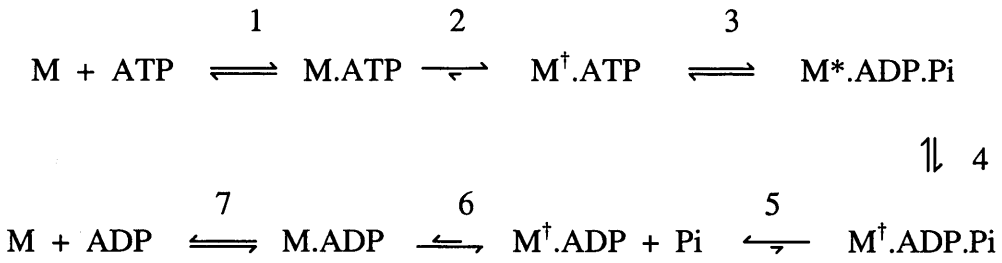


**Fig. 1.91** The ATPase mechanism of the *Dictyostelium* myosin II motor domain mutant W501. This overall mechanism is the same as fast skeletal S1, however the intrinsic tryptophan changes observed differ slightly; a small quench is denoted by a dagger ($M^{\dagger}$.ATP), with an enhancement denoted by an asterisk (M*.ADP.Pi). As before, M represents the myosin head domain.

Therefore, W501 provided an excellent starting point for the genetic engineering of myosin II motor-FP fusion proteins, with a view to monitoring FRET changes (Suzuki *et al.*, 1998) during the actin-bound stages of the crossbridge cycle, as it gave an inherent assay into the myosin motors' functionality.

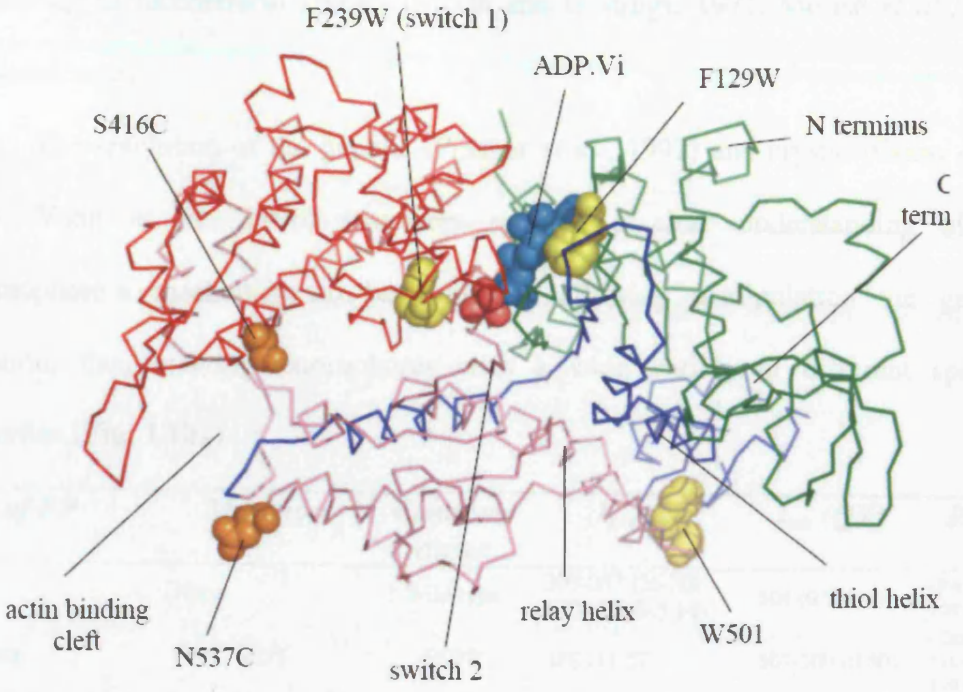


**Fig. 1.92** The structure of the 761 residue *Dictyostelium* myosin II motor in the CLOSED conformation. Also shown are the sites of some of the fluorescent probes used to elucidate aspects of the myosin ATPase. The positions of W501 and the N- and C-termini are of particular relevance to this thesis. Taken from Zeng *et al.* (2004).

### *1.10 Green Fluorescent Protein (GFP) and its derivatives*

Since 1996, the green fluorescent protein (GFP, *gfp10*) has become one of the most widely studied and exploited proteins in biochemistry and cell biology. Discovered by (Shimomura *et al.*, 1962), as a companion protein to aequorin from the *Aequorea victoria* jellyfish, its ability to generate an efficient, highly visible, stable fluorescent signal has made it particularly useful as a marker of gene expression and protein targeting for cells and micro-organisms *in vivo*. The spectral properties of GFP were also first characterised by Johnson *et al.* (1962), showing an emission peak of 504nm and excitation peak of 470-475nm, which also corresponds to the emission peak (~470nm) of aequorin. It was subsequently shown that GFP was excited by radiationless energy transfer from excited aequorin (fluorescence resonance energy transfer, or FRET) something which created great opportunities for the sensitive

monitoring of biochemical signals (Morin and Hastings, 1971, Morise *et al.*, 1974 discussed later).

The resolution of the genetic (Prasher *et al.*, 1992) and crystal (Ormo *et al.*, 1996, Yang *et al.*, 1996) structures enabled a clear understanding of the chromophore's mechanism to be achieved, allowing manipulation via genetic mutation, thus creating fluorophores with a wide variety of different spectral properties (**Fig. 1.101**).

| *Class of FP* | *Mutation* | *Common name* | $\lambda_{exc}$ ($\varepsilon$) | $\lambda_{em}$ (*QY*) | *References* |
|---|---|---|---|---|---|
| *1* wild-type | None | Wild-type | 395-397 (25-30)<br>470-475 (9.5-14) | 504 (0.79) | (Patterson *et al.*, 1997, Ward, 1997) |
| *2* phenolate anion | F64L, S65T | EGFP | 488 (55-57) | 507-509 (0.60) | (Cubitt *et al.*, 1999, Patterson *et al.*, 1997, Ward, 1997) |
| *3* neutral phenol | S202F, T203I | H9 | 399 (20) | 511 (0.60) | (Cubitt *et al.*, 1999) |
| *4* YFPs (*2* with stacked $\pi$-electron system) | S65G, V68L, S72A, T203Y | 10C | 514 (83.4) | 527 (0.61) | (Cubitt *et al.*, 1999) |
| *5* CFPs (indole in chromophore) | F64L, S65T, Y66W, N146I, M153T, V163A | ECFP | 434 (32.5)<br>452 | 476 (0.4)<br>505 | (Cubitt *et al.*, 1999) |
| *6* BFPs (imidazole in chromophore) | Y66H | BFP | 384 (21) | 448 (0.24) | (Cubitt *et al.*, 1999) |

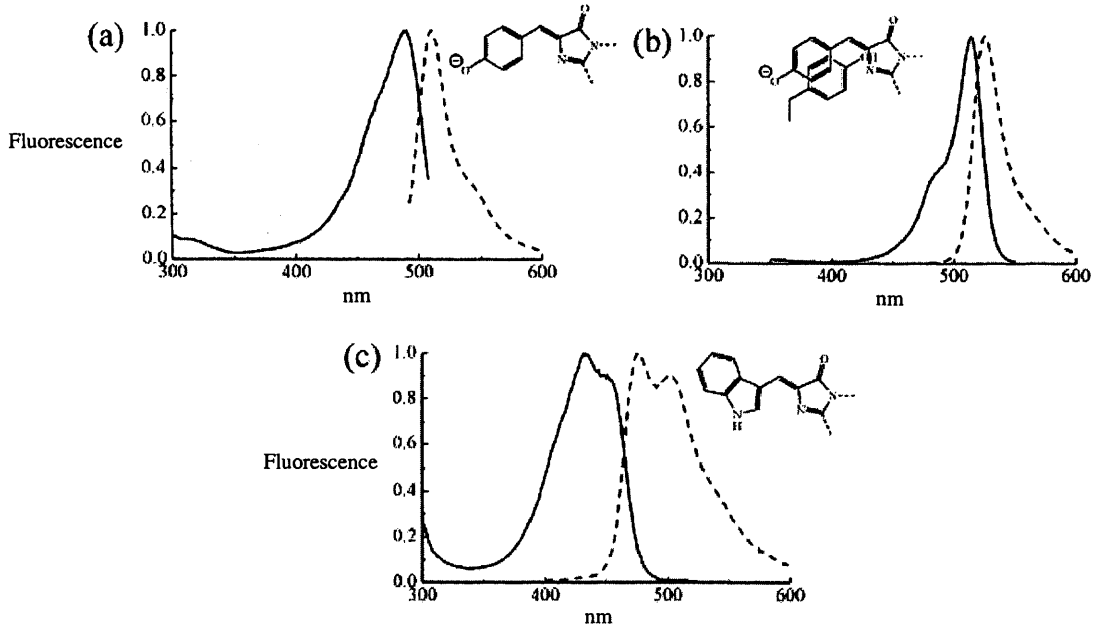


**Fig. 1.101** The spectral properties of the main classes of fluorescent proteins (FPs, *top*). Also shown (*bottom*) are the reported excitation and emission spectra for *(a)* EGFP, *(b)* YFP and *(c)* CFP, which are of particular relevance to this thesis, together with the proposed structures of their chromophores. Derived from Tsien (1998).

The EGFP mutation (S65T to improve chromophore ionisation, F64L to improve folding at 37°C, Clontech laboratories, (Yang *et al.*, 1996) exhibits a slight red shift in the excitation and emission peaks ($\lambda_{ex}$=488nm, $\lambda_{em}$=507-509nm) with a 2-fold increase in the extinction coefficient, and as such is now widely used in preference to wildtype GFP, to the extent that GFP now generally refers to this mutant and not the wildtype protein. Other GFP mutants that are of particular importance to this thesis are the ECFP ($\lambda_{ex}$=434, 452nm, $\lambda_{em}$=476, 505nm) and 10C YFP ($\lambda_{ex}$=514nm $\lambda_{em}$=527nm) fluorophores.

GFP itself exists as a stable, 11-stranded β-barrel structure, with an α-helix threaded through the central axis of the cylinder (**Fig. 1.102**). The chromophore itself is fixed to the end of this helix, placing it almost precisely in the centre of the β-barrel, thereby effectively shielding it from environmental changes. The chromophore itself is a *p*-hydroxybenzylideneimidazolinone (**Fig. 1.102,** Cody *et al.*, 1993, Prasher *et al.*, 1992), formed from the 65-67$^{th}$ residues (Ser-Tyr-Gly in native GFP) of the sequence, with Gly being conserved in all known mutations of GFP which preserve fluorescence. This is presumably as it performs a vital nucleophilic cyclisation to form the chromophore following the correct folding of the β-barrel. Following this, molecular oxygen is thought to dehydrogenate the α-β bond of residue 66 to conjugate the aromatic group with the imidazolinone, as oxygen is required for GFP to exhibit fluorescence (Heim *et al.*, 1994, Inouye and Tsuji, 1994). Thus, one problem with GFP may be that as a result of oxidative dehydrogenation, $H_2O_2$ would be released which could potentially be damaging to cells or organisms over-expressing the protein.

GFP and its derivatives are particularly insensitive to photobleaching, presumably because the chromophore is fairly protected within the β-barrel from

chemical reactants such as $O_2$. The BFP class of GFP derivatives are most susceptible to photobleaching, however with high laser power any class can be photobleached should the need arise.

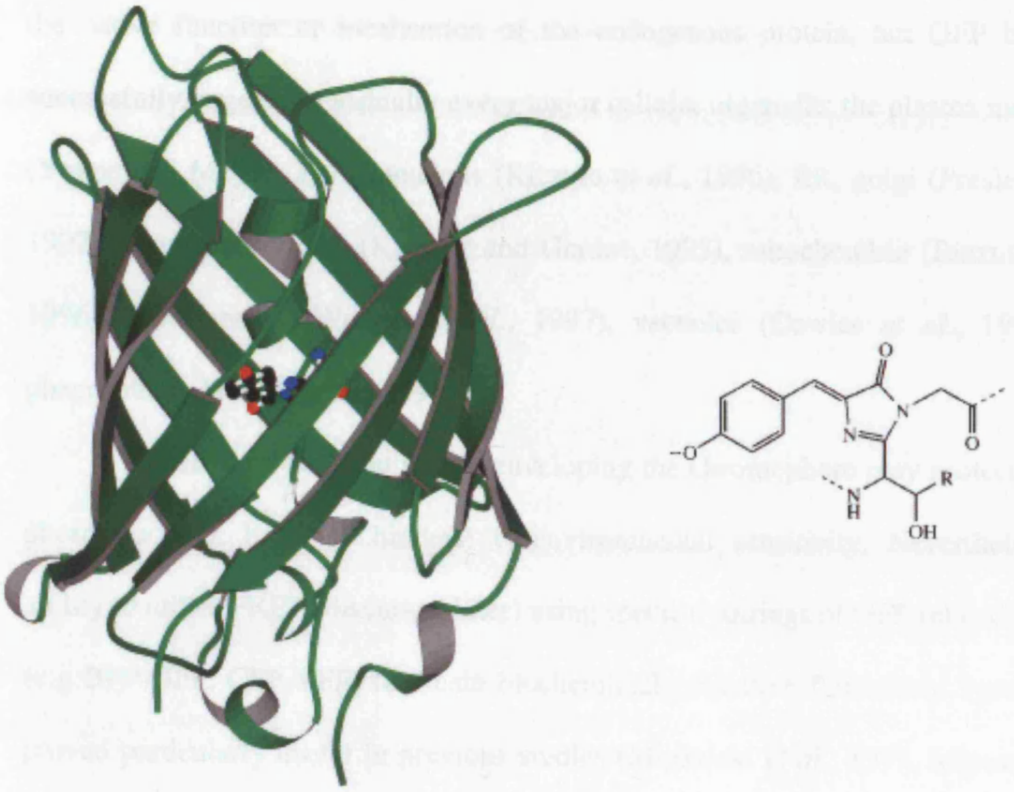


**Fig. 1.102** The structure of GFP and its deprotonated chromophore (the fluorescent state). GFP consists of an 11-stranded β-barrel structure, with an α-helix threaded through the central axis of the cylinder to which the chromophore (shown in space-fill form) is fixed. This effectively places it in the centre of the β-barrel, thus shielding it from environmental changes. The structural image comes courtesy of the Laboratoire de PhotoPhysique moléculaire website (www.ppm.u-psud.fr/persos/severine/), and the chromophore structure was taken from Tsien (1998).

The first proposed application for GFP was as a fluorescent marker to detect gene expression *in vivo* (Chalfie *et al.*, 1994). It has had varying success as a gene-tag (Cheng *et al.*, 1996, Muldoon *et al.*, 1997), presumably due to *(a)* its need for strong promoters to drive expression sufficiently for detection, and *(b)* its lack of amplification, as it does not catalytically process substrates, with one GFP molecule producing one fluorophore. The most successful application of GFP has been as a genetic fusion protein to monitor the localisation and fate of proteins *in vivo*. The GFP

gene is fused in-frame at the N- or C-terminus of the gene encoding the endogenous protein, and the resulting fusion protein (chimera) expressed in the cell or microorganism being studied. Not all fusions are successful with regard to retaining the native function or localisation of the endogenous protein, but GFP has been successfully targeted to virtually every major cellular organelle; the plasma membrane (Yokoe and Meyer, 1996), nucleus (Rizzuto *et al.*, 1996), ER, golgi (Presley *et al.*, 1997), secretory vesicles (Kaether and Gerdes, 1995), mitochondria (Rizzuto *et al.*, 1996), peroxisomes (Wiemer *et al.*, 1997), vacuoles (Cowles *et al.*, 1997) and phagosomes (Maniak *et al.*, 1995).

The stable β-barrel structure enveloping the chromophore may protect it from photobleaching, but also hinders its environmental sensitivity. Nevertheless, the ability to utilise FRET (discussed later) using specific pairings of GFP related proteins (e.g BFP-GFP, CFP-YFP) to create biochemically sensitive fluorescent systems has proved particularly useful in previous studies (Miyawaki *et al.*, 1997, Miyawaki and Tsien, 2000, Romoser *et al.*, 1997, Suzuki *et al.*, 1998), and is of particular importance to this thesis. Using this technique, any biochemical signal that changes the distance between the fluorophores, or the relative orientations of their transition dipoles, will change the efficiency of the FRET. Thus, these changes can be monitored and interpreted in terms of mechanistic and structural changes.

### *1.11 Anisotropy*

The anisotropy ($a$) of a light source is defined as the ratio of the polarised component ($p$) relative to the total intensity of all components ($T$). Furthermore, for partially polarized light travelling along the x-axis, the polarised component of that light ($p$) is defined as $p = I_z - I_y$, where $I_z$ is the intensity in the z-plane and $I_y$ is the intensity in

the y-plane, if the detector is also oriented along the x-axis. Thus, the anisotropy would be defined as

$$a = \frac{p}{T} = \frac{Iz - Iy}{Ix + Iy + Iz}$$

When the excitation is polarised around the z-axis (vertical excitation), it is symmetric with respect to x and y, thus the resultant dipolar radiation from a fluorophore excited in this way would also be symmetric with respect to x and y. Thus, as $I_x = I_y$, the equation becomes

$$a = \frac{Iz - Iy}{Iz + 2Iy}$$

Thus, if the intensity of the emission (from vertically polarised excitation) is measured through a polarizer parallel to the excitation (intensity = $I_{\parallel} = I_z$) and then through a polarizer perpendicular (intensity = $I_{\perp} = I_y$) to the excitation the anisotropy may be calculated for light travelling along the x-axis.

In practical terms, the anisotropy is typically used as a measure of the speed of rotation in solution of a fluorophore relative to its fluorescent lifetime, although more accurately it is a measure of the orientation of a fluorophore's emission dipole relative to its excitation dipole. In solution, anisotropy has a theoretical maximum of 0.4 for totally immobile fluorophores, a value of 0 for infinitely fast rotations (fully depolarised emission), and a theoretical minimum of -0.2 for immobile fluorophores where the emission and absorption dipoles are 90° relative to each other. Furthermore, the anisotropy can be expressed as a product of the angle of the emission dipole relative to the z-axis ($\theta$).

$$a = \frac{\left(3\cos^2\theta\right) - 1}{2}$$

This equation, applicable to aligned fluorophores within a crystal, has a theoretical range from 1 to -0.5 ($\cos^2$=1 and 0 respectively). However, integrating for randomly distributed molecules in solution introduces a factor of 2/5, which changes the theoretical limits to 0.4 and -0.2 as mentioned previously;

$$a = \frac{2}{5}\left(\frac{\left(3\cos^2\theta\right)-1}{2}\right) = \frac{\left(3\cos^2\theta\right)-1}{5}$$

$$\text{Therefore; } \cos^{-1}\sqrt{\left(\frac{5a+1}{3}\right)} = \theta$$

It is this value ($\theta$) which may be used to calculate a range for the orientation factor ($\kappa^2$) of the Förster equation (used to quantify FRET changes), as discussed in the following chapter.

### *1.12 Fluorescence Resonance Energy Transfer*

Fluorescence resonance energy transfer (FRET) is the transfer of energy from the excited state of a donor to an acceptor fluorophore, without the appearance of a photon, and is primarily due to dipole-dipole interactions between the two fluorophores themselves. The rate of this energy transfer depends upon *(a)* the extent of the overlap between the donor emission spectrum and the acceptor excitation spectrum, *(b)* the relative orientation of the donor and acceptor dipoles, and *(c)* the distance between the two fluorophores. Measurements of this distance can thus be achieved via the analysis of FRET changes, provided that the donor-acceptor pair are separated by a single distance that does not vary during the excited-lifetime of the donor fluorophore.

The rate of energy transfer from a specific donor to a specific acceptor ($k_T$), as derived from Förster's theory (Forster, 1948) is given by

$$k_T = \frac{1}{\tau_d}\left(\frac{R_o}{r}\right)^6$$

Where $\tau_d$ is the fluorescent lifetime of the donor in the absence of the acceptor, $r$ is the distance between donor and acceptor, and $R_o$ is a specific donor-acceptor separation known as the Förster distance. This is defined as the distance at which the transfer rate ($k_T$) is equal to the decay rate of the donor in the absence of the acceptor, *i.e.* the distance at which exactly 50% of the donor molecules' excited states decay by energy transfer to the acceptor. This is given by

$$R_0^6 = 8.8\times10^{-25}\left(\kappa^2 n^{-4}\phi_d J\right)$$

where $J$ is the overlap integral, which expresses the degree of spectral overlap between the donor emission and acceptor absorption, $\phi_d$ is the quantum yield of the donor in the absence of the acceptor, $n$ is the refractive index of the medium, and $\kappa^2$ is a factor describing the relative orientation of the transition dipoles of the donor and acceptor. This orientation factor has theoretical maximum and minimum values of 4 and 0 respectively, and can be defined by

$$\kappa^2 = \left(\cos\theta_T - 3\cos\theta_D\cos\theta_A\right)^2$$

where $\theta_T$ is the angle between the emission transition dipole of the donor and the absorption transition of the acceptor, and $\theta_D$ and $\theta_A$ are the angles between these dipoles and the vector joining the donor and acceptor (**Fig. 1.121**) A $\kappa^2$ value of 0.67 can be deduced for pairs of rapidly rotating fluorophores, however for fluorophores which may be tethered to bulky molecules rendering them relatively immobile on the timescale of their fluorescent lifetimes, this value may prove inaccurate. Nevertheless, by noting that $\theta_T$ is equal to $\theta$ (the angle of the emission dipole relative to the $z$-axis)

in the equation defining anisotropy (**see 1.11**), it follows that anisotropy values could be used to give a range of possible $\kappa^2$ values.

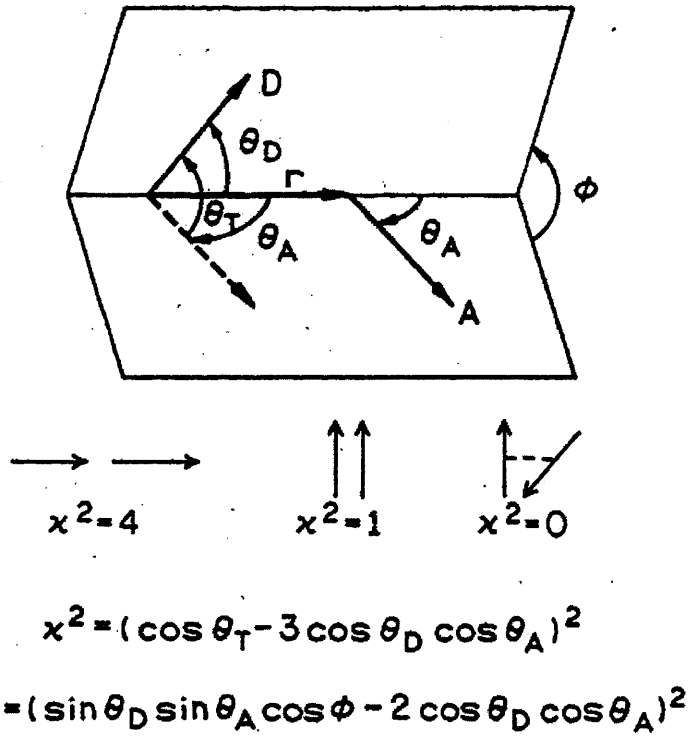


**Fig. 1.121** The definition of $\kappa^2$ ($x^2$), with respect to the angles relating the donor and acceptor dipoles. $\theta_T$ represents the angle between the emission dipole of the donor and the absorption dipole of the acceptor ($\theta$ obtained from anisotropy). $\theta_D$ and $\theta_A$ represent the angles between these dipoles and the vector joining them (r). Note: for a fixed $\theta_T$, either $\theta_D$ or $\theta_A$ must be equal or greater than $\theta_T$. This is of importance when calculating a possible range of $\kappa^2$ from a known $\theta_T$. Diagram taken from Lacowicz (1999).

The efficiency of energy transfer between donor and acceptor ($E$) can be directly related to the separating distance using

$$E = \frac{R_0^6}{R_0^6 + r^6}$$

thus, it can be seen that FRET is inversely dependent upon the separating distance to the sixth power. This highly sensitive dependence has resulted in a wide variety of applications within biochemical and biological research, as any phenomenon which

alters the donor-acceptor distance will consequently affect the FRET efficiency and can thus be quantified. The elegant approach adopted by (Suzuki *et al.*, 1998) involved the genetic fusion of a BFP and GFP fluorophore to the N- and C-termini of the *Dictyostelium* myosin II motor domain (S1dC, **Fig. 1.122**), effectively replacing the lever arm with a viable FRET pairing.

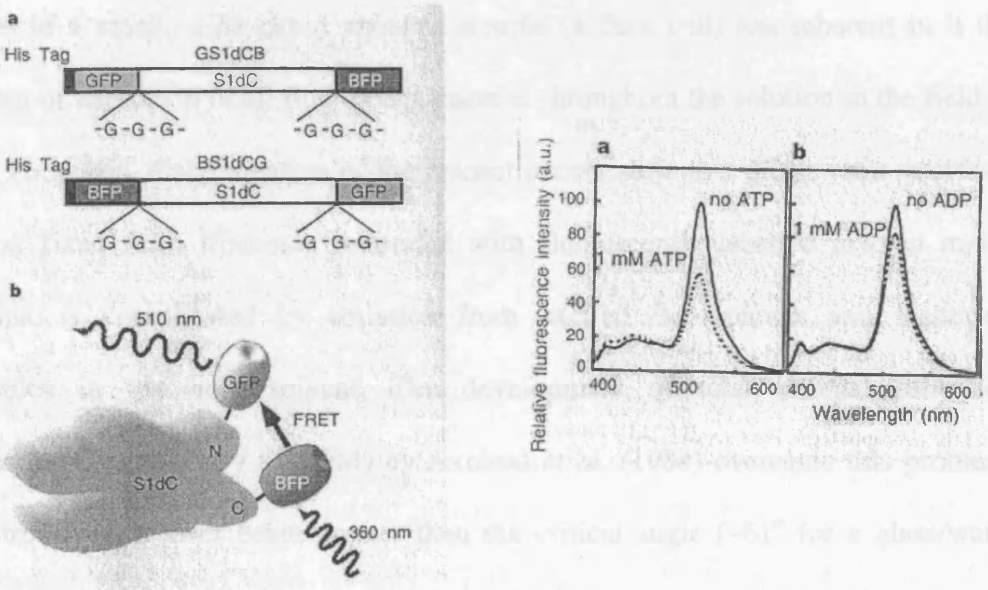


**Fig. 1.122** The structure of the *Dictyostelium discoideum* myosin II motor domain (S1dC) fusion proteins containing C-terminal and N-terminal BFP or GFP fluorophores, linked via a flexible triple-Gly region, to form a FRET pairing (left, taken from Suzuki *et al.* (1998). Also shown (right) are the changes observed for these chimeras upon ATP (40% decrease in GFP emission via FRET) and ADP (15% quench in GFP emission) binding, corresponding to an increase in the donor-acceptor distance of 1.5 and 0.2nm respectively.

Thus, conformational changes occurring within the motor domain were monitored and quantified by analysis of the FRET changes in several ligand bound states. It must be noted, however, that the value of $\kappa^2$ was assumed in this case to be 0.67 for pairs of rapidly rotating fluorophores. The large molecular volume of GFP and BFP themselves, aside from their tethering to the *Dictyostelium* myosin II motor domain, suggests that they would be slowly rotating in solution relative to their fluorescent lifetimes (~3ns) and therefore this value would be unsuitable.

### *1.13 Total internal reflection fluorescence microscopy (TIRFM)*

The development of microscope-based equivalents to solution-based assays is of considerable significance, as it enables the scaling down of measurements and thus the analysis of systems only available in very small quantities. However, in standard fluorescence microscopy using epi-illumination, the visualisation of fluorescent entities in a small, slide based aqueous sample (a flow cell) has inherent in it the problem of excitation of all fluorescent material throughout the solution in the field of view. Therefore, discrimination of fluorescent events close to a glass-water interface, such as fixed actin filaments decorated with fluorescently labelled myosin motor domains, is complicated by emission from excited fluorophores and scattering molecules in the bulk solvent. The development of total internal reflection fluorescence microscopy (TIRFM) by Axelrod *et al.* (1984) overcame this problem. By introducing a laser beam greater than the critical angle (~61° for a glass/water interface, ~65° for silica/water; derived from Snells's law) by use of a cubic prism, the excitation light passes through the upper face of the slide/coverslip, and is internally reflected from the lower face away from the field of view (**Fig. 1.132**). This generates an ellipse of excitation ~150μm in length, which penetrates ~150nm into the solution, and is termed the evanescent field (**Fig. 1.131**). This effectively excites fluorescent material fixed, or close to, the upper slide/coverslip of a flow cell, drastically reducing background noise from the excitation of fluorophores or scattering molecules in solution. An alternative method is to introduce the beam via the periphery of the back-focal plane of a high numerical aperture (NA>1.33) objective lens from a microscope (**Fig. 1.132**). This has the same effect, only upon the lower slide/coverslip in contact with the objective lens.

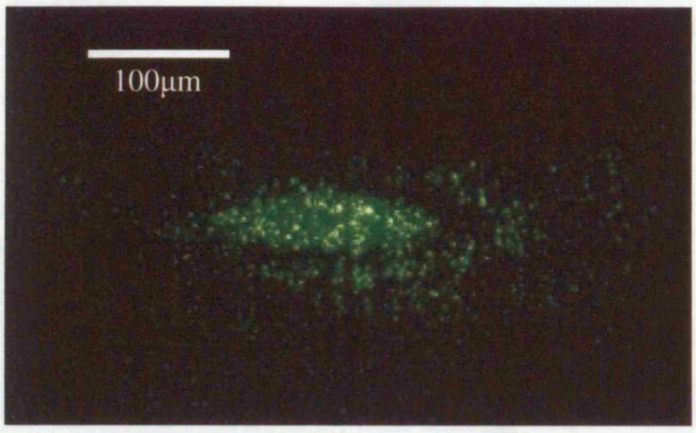


**Fig. 1.131** The elliptical field of excitation (the 'footprint') produced by total internal reflection fluorescence microscopy (TIRFM). Outside of this field diffraction rings give varying degrees of excitation, thus fluorescence intensities outside the footprint cannot be accurately analysed. The evanescent field only penetrates 150nm or less into the flow cell, effectively decreasing background noise caused by fluorescent and scattering particles in solution.

This method has proved particularly useful in the study of events at or near the cell surface (Axelrod, 1999, Gingell *et al.*, 1985), for following the binding of proteins to lipid bilayers (Thompson *et al.*, 1993), and in recent years for the visualisation of single immobilised fluorophores (Conibear and Bagshaw, 2000, Conibear *et al.*, 1998, Funatsu *et al.*, 1995). However, the combination of TIRFM with flash photolysis from a separate UV source (*e.g.* a Xe flash lamp, **Fig. 1.132**) to initiate reactions via the release of active substrates from inert caged-precursors in solution (McCray and Trentham, 1989) provides opportunities to study the interaction of myosin and F-actin at the molecular level, rather than using standard transient kinetic methods. Furthermore, flash photolysis provides better time-resolution and reduces the potential for movement artefacts compared to flow-cell solution exchange methods (Oiwa *et al.*, 2000, Sowerby *et al.*, 1993). Previous studies have also shown that information on the ATP-induced dissociation kinetics of fluorescently labelled truncated S1 myosin may be obtained by combining fluorescence microscopy with flash photolysis of inert caged-ATP (Weiss *et al.*, 2000). These assays require <μg of protein, and are thus considerably more sensitive relative to stopped-flow and quenched-flow methods,

which typically require milligram amounts of protein. By utilising TIRFM in a similar way, the sensitivity of these assays could be developed to require «µg of protein.

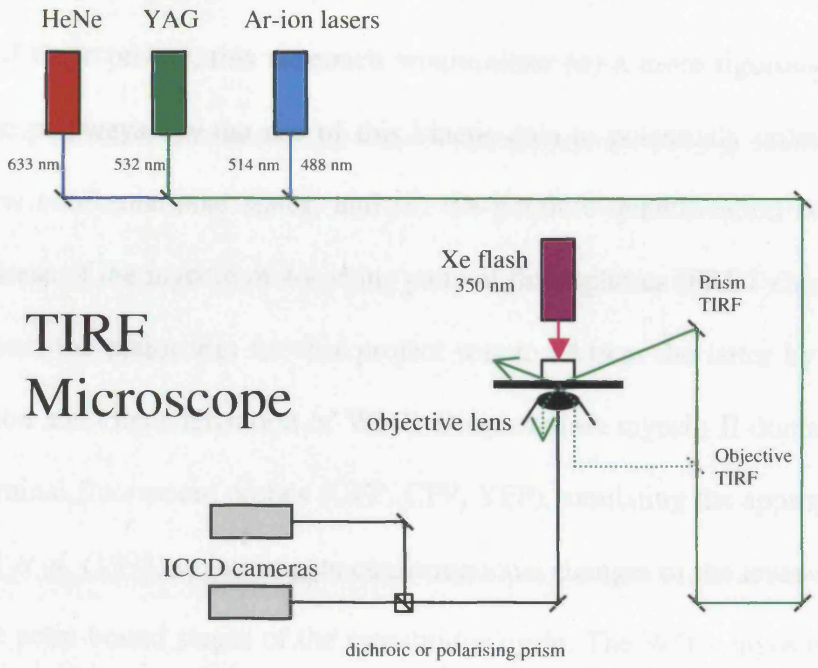


**Fig. 1.132** A basic schematic representation of the TIRFM setup used for caged-ATP flash photolysis studies of ATP-induced actomyosin dissociation kinetics. YAG represents a yitrium aluminium garnet laser source.

### *1.14 Project goals and aims*

The myosin ATPase has been widely studied and well characterised, both in kinetic and structural terms (as previously described), over the years. The actomyosin ATPase however has proved difficult to resolve kinetically, and to date no accurate structural observations have been obtained for the various conformations of the actomyosin complex, something which is largely due to its resistance to crystallisation. Thus, the global question still remains; 'What is the nature of the conformational changes which occur within the cross-bridge during the actin-bound stages of the crossbridge cycle?'

In an attempt to address this question, it seemed pertinent to introduce fluorescent probes into specific areas of the myosin crossbridge using modern genetic cloning techniques. Using the crystal structures of myosin to rationally assign the position of these probes, this approach would allow *(a)* a more rigorous analysis of the kinetic pathways, *(b)* the use of this kinetic data to potentially order events and define new conformational states, and *(c)* the possible quantification of movement between areas of the myosin motor using pairs of fluorophores (FRET changes).

Thus, the major aim for this project was to address the latter by the genetic construction and characterisation of W501 *Dictyostelium* myosin II domains with N- and C-terminal fluorescent probes (GFP, CFP, YFP), emulating the approach adopted by Suzuki *et al.* (1998) to investigate conformational changes of the lever-arm domain during the actin-bound stages of the crossbridge cycle. The W501 myosin motor was chosen for its inherent tryptophan probe for the myosin ATPase, allowing simple characterisation in this way via standard transient kinetic techniques. A FRET pairing of YFP and CFP (unlike BFP/GFP, Suzuki *et al.*, 1998) was chosen as *(a)* they exhibit a better spectral overlap, therefore should give larger FRET signals, and *(b)* BFP and other class 6 FP fluorophores are susceptible to photobleaching, thus CFP as a donor may give more stable fluorescent signals. Furthermore, the single W501-FP fusion protein intermediates could provide an excellent opportunity for the development of sensitive, microscope-based kinetic assays. In summary, the more specific initial goals of the project were;

(i) The cloning of fluorescently labelled myosin motors, containing FP fluorophores fused to the C-terminal (W501.gGFP), N-terminal

(rYFP.W501), or both (gYFP.W501.gCFP; rYFP.W501.gCFP) of W501.

(ii) The characterisation of the functionality of the myosin motor of the fusion proteins using standard transient kinetic methods.

(iii) The development of sensitive, microscope-based assays, using single FP-W501 fusion proteins. In particular the TIRFM caged-ATP flash photolysis assays into actomyosin dissociation kinetics (continuation of the studies of Weiss *et al.* (2000).

(iv) FRET studies in the absence (Suzuki *et al.*, 1998) and then presence of actin, to determine conformational changes associated with the lever arm domain during the actin-bound stages of the crossbridge cycle.

# 2 - Materials and Methods

## *2.1 DNA cloning techniques*

### *2.11 The design of novel oligonuclueotides*

Oligonucleotides (upstream 5'-3', downstream 5'-3' reverse complementary) for use as primers in the PCR synthesis and amplification of novel DNA fragments were designed with optimal properties of *(a)* a length of 18-35bp, *(b)* a melting temperature ($T_m$) of 48-55°C given by equation ***(i)***, and *(c)* a G-C rich 3' terminal region. The oligonucleotides, once obtained, were diluted to a final concentration of 40mM in de-ionised water, and stored at -20°C.

***(i)*** $$T_m = 64.9 + 41\left(\frac{G+C}{n}\right) - \frac{600}{n}$$

**Fig. 2.111** The equation for calculating the melting temperature ($T_m$) of oligonucleotides, where *G* and *C* represent the number of guanine and cytosine bases present in the oligonucleotide sequence, *n* is the length of the oligonucleotide in base-pairs, and $T_m$ is given in Celsius.

### *2.12 Polymerase chain reaction (PCR) amplification of DNA fragments*

In a sterile, nuclease free microcentrifuge tube, the following components were assembled (on ice);

| | | ***Final concentration*** |
|---|---|---|
| *Pfu* DNA Polymerase 10x buffer | 5µl | 1x |
| dNTP mix (10mM of each) | 1µl | 200µM of each |
| Upstream primer | 5-50pmol | 0.1-1.0µM |
| Downstream primer | 5-50pmol | 0.1-1.0µM |
| DNA Template | - | <0.5µg/µl |
| *Pfu* DNA Polymerase (2-3u/µl) | - | 1.25u/50µl |
| Nuclease free water to a final vol. of | 50µl | |

**Fig. 2.121** The components of a typical PCR reaction mixture. *Pfu* DNA Polymerase 10x buffer consisted of Tris-HCl (200mM, pH 8.8 at 25°C), KCl (100mM), $(NH_4)_2SO_4$ (100mM), $MgSO_4$ (20mM), nuclease-free BSA (1mg/ml), Triton® X-100 (1%). The dNTP mix contained 10mM final concentrations of dATP, dCTP, dGTP and dTTP in de-ionised water.

The *Pfu* DNA polymerase was added last to ensure that the proofreading (3'-5' exonuclease) activity did not degrade the primers, leading to non-specific amplification and reduced product yield. The reaction mixture was then immediately placed into a Helena Biosciences Proteus II thermal cycler (with heated lid) preheated to 95°C. The sample was then heated at 95°C for 1-2mins to ensure the target DNA was completely denatured. Denaturing for longer than 2mins risked damage to the DNA and reduction of the overall yield. PCR amplification of the desired DNA fragments was then performed by a thermal cycling profile such as that illustrated in Fig. **2.122**. The temperature of the annealing step was usually ~5-10°C below that of the melting temperature ($T_m$) of the primers, with the length of the extension step being ~2mins/1kb of DNA to be amplified.

| *Step* | *Temperature* | *Time* | *No. of cycles* |
|---|---|---|---|
| Initial denaturation | 95°C | 1-2mins | 1 |
| Denaturation | 95 °C | 0.5-1min | |
| Annealing | 42-65 °C | 30s | 25-35 |
| Extension | 72-74 °C | 2-4mins | |
| Final extension | 72-74 °C | 5mins | 1 |
| Soak | 4 °C | indefinite | 1 |

**Fig. 2.122** Typical thermal cycling conditions for *Pfu* DNA Polymerase-mediated PCR amplification of novel DNA fragments.

The amplified DNA fragment was then analysed and isolated by agarose gel (1%) electrophoresis of the whole PCR sample.

### *2.13 Preparing and running agarose DNA gels*

Agarose powder was mixed with Tris-acetate-EDTA buffer (TAE, 40mM Tris-HCl, 11ml/l glacial acetic acid, 1mM EDTA) to a concentration of 1.0% w/v, heated in a microwave oven until completely melted, and allowed to cool at room temperature. From this stock, the desired quantity was weighed out (30g or 80g), heated again in a

microwave oven until completely melted, and allowed to cool for 5 minutes at room temperature. Ethidium bromide (to a final concentration of 0.5-1μg/ml) was then added to the 1% agarose to facilitate visualisation of DNA after electrophoresis, and mixed by gentle swirling. The solution was then cooled to approximately 60°C, poured into a casting tray containing a sample comb and allowed to solidify at room temperature.

After the gel had solidified, the comb was removed, taking care not to rip the bottom of the wells. The gel and casting tray were then placed into the electrophoresis chamber (sample wells towards the cathode, the bottom of the gel towards the anode) and covered with ~1cm of TAE buffer. Samples containing DNA mixed with loading buffer (to a final concentration of; 2.5-3% w/v ficoll, 0.04% w/v xylene cyanol, 0.04% w/v bromophenol blue) were loaded into the sample wells, alongside a single well loaded with 5-10μl of molecular weight DNA marker (New England Biolabs 1kb DNA ladder). The gel was then run at 120V, 100mA (5V / cm between electrodes) for 45-60mins. The approximate distance that the DNA had migrated was judged by visually monitoring the migration of the tracking dyes in the loading buffer; Bromophenol blue and xylene cyanol dyes migrate through agarose at approximately the same rate as double-stranded DNA fragments of 300 and 4000bp respectively.

The DNA fragments were then visualised under UV illumination, and recorded via printout or computer frame capture. If the DNA fragments were to be excised and retained for further cloning procedures, exposure to UV was minimised as much as possible to reduce damage to the DNA.

### *2.14 DNA purification from agarose gels*

DNA purification from 1% agarose gel slices was carried out using the GENECLEAN® range of spin kits. Gently resuspended GENECLEAN® SPIN GLASSMILK® (400µl) was transferred to a GENECLEAN® SPIN filter, to which was added the agarose gel slice (300mg maximum/filter). The resultant mixture was then heated to 55°C for 5mins to dissolve the agarose, while flicking and inverting the tube every minute to prevent settling of the matrix (for >5µg DNA, the sample was divided into multiple preps). The DNA was then bound to the filter and the supernatant eluted into the catch tube (then discarded) by centrifugation for 30s at ~14000g (12.5krpm, FA45-30-11 rotor). GENECLEAN® SPIN NEW Wash (500µl) was then transferred to the filter, the wash solution eluted and discarded by centrifugation for 30s at ~14000g (12.5krpm, FA45-30-11 rotor), this wash step repeated, and the DNA pellet dried by centrifugation of the empty catch tube for 2mins at ~14000g (12.5krpm, FA45-30-11 rotor). After transferring the spin filter to a fresh catch tube, GENECLEAN® SPIN Elution Solution (10-25µl) was added, and the GLASSMILK® resuspended by gentle pipetting (a large bore pipette would have been used for DNA>10kbp to prevent shearing). Elution of the DNA was achieved by centrifugation for 30s at ~14000g (12.5krpm, FA45-30-11 rotor), a 2$^{nd}$ elution was occasionally carried out to increase yield by 10-15%, and the DNA stored at -20°C until use.

### *2.15 Quantification of DNA concentration*

An approximate estimate of the mass of DNA present in a sample was achieved by running a known quantity (1-10µl) against a 1kb DNA ladder (0.5µg-2µg [1-4µl]

loading, New England Biolabs) on an ethidium bromide agarose gel (1%). Thus, quantification was achieved via a visual comparison of the fluorescent intensity of the DNA band with the ladder band of closest size;

| *Ladder fragment size (kbp)* | *DNA mass (ng)* |
|---|---|
| 10.0 | 42 |
| 8.0 | 42 |
| 6.0 | 50 |
| 5.0 | 42 |
| 4.0 | 33 |
| 3.0 | 125 |
| 2.0 | 48 |
| 1.5 | 36 |
| 1.0 | 42 |
| 0.50 | 42 |

**Fig. 2.151** The DNA mass present in each band of a 1kb DNA ladder (NEB). Thus, when run on an ethidium bromide agarose gel (1%) alongside DNA of unkown concentration, an approximate quantification of the sample DNA can be made.

The concentration of the DNA sample can then be calculated using the following equation, where *N* represents the length of the oligonucleotide in base pairs;

$$\text{pmol of oligo} = \frac{\mu g(oligo) \times 3{,}030}{N}$$

### *2.16 Restriction digestion of circular or linear DNA*

Restriction enzyme digests were usually performed on 0.2-1.5μg of substrate DNA, using a 2- to 10-fold excess of enzyme over DNA. The following typical reaction mixture (**Fig. 2.161**, total vol. 20μl) was assembled in a sterile microcentrifuge tube. The components were assembled in the order represented, with gentle mixing by pipetting before the final addition of the restriction digest enzyme.

| *Component* | *Volume (μl)* |
|---|---|
| De-ionised water | 16.3 |
| Restriction-enzyme buffer (10x) | 2 |
| Acetylated BSA (10μg/μl) | 0.2 |
| Sample DNA (~1μg/μl) | 1 |
| Restriction digest enzyme (10U/μl) | 0.5 |

**Fig. 2.161** The reaction mixture for a typical restriction digestion.

Following gentle mixing once more, the microcentrifuge tube was closed, the mixture centrifuged for ~10s, and the reaction incubated at the optimum temperature for the optimum time. Overnight digest reactions were avoided wherever possible as these may result in degradation of the DNA. The reaction was then stopped by agarose gel (1%) analysis of the whole sample.

### *2.17 Ethanol precipitation of DNA*

To the mini / midiprep DNA stock contained in a sterile eppendorf tube, NaAc (to a final concentration of 0.3M) and EtOH (100%, 2.5x the volume of DNA stock after NaAc addition) were added. This solution was then stored at -20°C for 30mins, centrifuged for 20mins at ~14000g (12.5krpm, FA45-30-11 rotor), the supernatant *carefully* decanted and discarded and the pellet dried in filtered air for 20mins.

### *2.18 Treatment of vector DNA with calf intestinal alkaline phosphatase (CIAP)*

Prior to the ligation of linearised cloning vector and DNA insert, the cloning vector was treated with calf alkaline intestinal phosphatase. This prevents any spontaneous recircularisation and religation of the cloning vector by removing phosphate groups from both 5'-termini.

The linearised cloning vector DNA was purified by ethanol precipitation and resuspended in Tris-HCl (40µl, pH 8.0). To this, CIAP reaction buffer (10x, Promega, 5µl, (1x) 50mM Tris-HCl (pH9.3 at 25°C) 1mM $MgCl_2$, 0.1mM $ZnCl_2$, 1mM spermidine) was added, followed by ~0.01U of CIAP (Promega) for every pmol of DNA ends (1µg of 1kbp DNA = 1.52pmol DNA = 3.03pmol of ends). The reaction mixture was then made up to a final volume of 50µl using nuclease-free water and incubated at 37°C for 30mins. A further 0.01U of CIAP was then added, and the

mixture incubated at 37°C for a further 30mins before the addition of CIAP stop buffer (300µl, Promega, 10mM Tris-HCl pH 7.5, 1mM EDTA pH 7.5, 200mM NaCl, 0.5% SDS). The DNA was then analysed and isolated by ethidium bromide agarose gel (1%) electrophoresis.

Alternatively, CIAP reaction buffer (10x, 5µl), CIAP 0.01u/pmol ends, and de-ionised water (to a final vol of 50µl) could be added directly to a restriction digest reaction, and the protocol followed as previously described. Both these methods were suitable for up to 5pmol of linearised vector DNA, equivalent to 10pmol of 5'-ends.

Furthermore, when 5'-recessed or blunt end DNA fragments were used as a substrate, incubation for 15mins at 37°C, then for 15mins at 56°C was employed for each 30min incubation period, to ensure accessibility of the recessed end.

### *2.19 Ligation of vector and insert DNA*

Typically, a 1:3 or 1:6 molar ratio of vector:insert was used for the ligation of DNA fragments into pDXA-3H based cloning vectors. The exact amounts of DNA required for any given ligation varied with the size of the insert, and were calculated by using the following equation relating molar ratio to mass ratio;

$$\frac{\text{ng of vector} * \text{kb size of insert}}{\text{kb size of vector}} * \text{molar ratio of } \frac{\text{insert}}{\text{vector}} = \text{ng of insert}$$

Ligation reactions were assembled in sterile microcentrifuge tubes, into which 1µl of ligase buffer (10x, Promega, 300mM Tris-HCl pH 7.8, 100mM $MgCl_2$, 100mM DTT, 10mM ATP), 1u of T4 DNA ligase (Promega, Weiss units), vector and insert DNA (typically 100-200ng of vector DNA), and nuclease free water were mixed to a final

volume of 10µl. The reaction mixture was then incubated at room temperature for 3hrs for sticky-end ligations, or overnight for blunt-end ligations.

### *2.110 Transformation of plasmid DNA into competent bacterial cells*

For the amplification of plasmid DNA, either HB101 (Promega) or JM109 (Promega) competent cells were used, both having a minimum transformation efficiency of $1x10^7$ colony forming units / µg of control DNA, when plated on Luria-Bertani plates containing 100µg/ml ampicillin (LB-Amp plates, 1g/ml proteose peptone, 0.5g/ml yeast, 0.17M NaCl, 1.2% bacteriological agar w/v, 100µg/ml ampicillin, pH 7.0).

Sterile microcentrifuge tubes were chilled on ice for 10mins, while the frozen competent cells were removed from -80°C storage and thawed on ice. The competent cells were then quickly mixed by flicking, and 50µl transferred to each of the sterile microcentrifuge tubes. To these aliquots 1-50ng of supercoiled plasmid DNA, or 100-200ng of ligated vector DNA were quickly added, mixed by quickly flicking the microcentrifuge tubes several times, and immediately returned to ice for 30mins. The competent cells were then subjected to a heat-shock by immersing the microcentrifuge tubes in a water bath at exactly 42°C for 90 seconds, before immediately returning to ice for 5mins. Using standard laboratory aseptic technique, 500µl of LB media (1g/ml proteose peptone, 0.5g/ml yeast, 0.17M NaCl,, 100µg/ml ampicillin, pH 7.0) was then added to each transformation reaction and the cells incubated at 37°C for 1hr. Again using aseptic technique, 100µl-500µl of transformed cells were spread onto LB plates containing 100µg/ml ampicillin and incubated at 37°C for 12-24hrs.

*2.111 Small scale purification of plasmid DNA from competent bacterial cells*

The purification of plasmid DNA from a small scale (5-10ml culture) amplification was carried out using the Promega Wizard® *Plus* SV Miniprep DNA Purification System, with all centrifuge steps being carried out at room temperature using an eppendorf 5417R centrifuge fitted with an FA45-30-11 rotor.

A single, well-isolated colony from a transformed LB-Amp plate was picked using a sterile 200µl Gilson tip, and transferred to 5ml of LB culture medium using standard laboratory aseptic technique. This culture was then incubated overnight (12-16 hours) at 37°C in a shaking incubator set to 200rpm. The cells were harvested by centrifugation for 5mins at ~10000g (10.6krpm, FA45-30-11 rotor), the supernatant removed and the inverted tube blotted on a paper towel to remove excess media. The cell pellet was fully resuspended in 250µl of cell resuspension solution (50mM Tris-HCl (pH 7.5), 10mM EDTA, 100µg/ml Rnase A) and transferred to a 1.5ml microcentrifuge tube before the addition of 250µl of cell lysis solution (0.2M NaOH, 1% SDS). This solution was then mixed by multiple tube inversions and allowed to stand at room temperature until a partial clearing of the lysate was observed (1-5mins). Mixing by vortex or pipette methods was not carried out as this could cause shearing of the chromosomal DNA. To inactivate endonucleases released during cell lysis, 10µl of alkaline protease solution was then added and the solution mixed by multiple inversions. After the addition of 350µl of neutralization solution (4.09M, guanidine hydrochloride, 0.759M potassium acetate, 2.12M glacial acetic acid) and immediate mixing by inversion, the bacterial lysate was centrifuged for 10mins at ~14000g (12.5krpm, FA45-30-11 rotor) to sediment the precipitate. The cleared lysate was transferred to a spin column, itself inserted into a 2ml collection tube, taking care not to disturb any of the white precipitate when removing the supernatant. The spin

column was then centrifuged for 1min at ~14000g (12.5krpm, FA45-30-11 rotor) and the flowthrough in the collection tube discarded. After the addition of 750µl of column wash solution (162.8mM potassium acetate, 22.6mM Tris-HCl(pH 7.5), 0.109mM EDTA(pH 8.0)), the spin column and collection tube were again centrifuged for 1min at ~14000g (12.5krpm, FA45-30-11 rotor) and the flowthrough discarded. This wash step was then repeated with a further 250µl of column wash solution, before a final centrifugation for 2min at ~14000g (12.5krpm, FA45-30-11 rotor) to ensure that all of the column wash solution had been removed. The spin column was then placed into a sterile 1.5ml microcentrifuge tube and the plasmid DNA eluted by the addition of 50-100µl of nuclease free water, followed by centrifugation for 1min at ~14000g (12.5krpm, FA45-30-11 rotor). The plasmid DNA was then stored at -20°C for up to 6 months.

### *2.112 Large scale purification of plasmid DNA from competent bacterial cells*

The purification of plasmid DNA from a large scale (25-50ml culture) amplification was carried out using the QIAGEN® Midi Plasmid Purification Kit, with all centrifuge steps being carried out at 4°C using a Sorvall RC-5B refrigerated superspeed centrifuge fitted with an Sorvall SS-34 rotor.

A single, well-isolated colony from a transformed LB-Amp plate was picked using a sterile 200µl Gilson tip, and transferred to 25-50ml of LB culture medium using standard laboratory aseptic technique. This culture was then incubated overnight (12-16 hours) at 37°C in a shaking incubator set to 200rpm. The cells were harvested by centrifugation for 15mins at 6000g (8000rpm), the supernatant removed and the inverted tube blotted on a paper towel to remove excess media. The cell pellet was *fully* resuspended in 4ml of resuspension buffer (50mM Tris-Cl pH 8.0, 10mM

EDTA, 100μg/ml RNase A) before the addition of 4ml of lysis buffer (200mM NaOH, 1% SDS w/v). This solution was then mixed by multiple tube inversions and allowed to stand at room temperature until a partial clearing of the lysate was observed (5mins). Mixing by vortex or pipette methods was not carried out as this could cause shearing of the chromosomal DNA. After the addition of 4ml of neutralization buffer (3M KAc, pH 5.5) and immediate mixing by inversion, the bacterial lysate was incubated on ice for 15mins before sedimenting the precipitate by centrifugation for 30mins at 20000g (15krpm). The cleared lysate was then *carefully* removed, transferred to a fresh centrifuge tube and centrifuged for 15mins at 20000g (15krpm) to ensure that no particulate matter remained in the supernatant. A QIAGEN-tip 100 was equilibrated by applying 4ml of equilibration buffer (750mM NaCl, 50mM MOPS pH 7.0, 15% isopropanol v/v, 0.15% Triton X-100 v/v) and allowed to empty by gravity flow, before the cleared lysate was applied to the QIAGEN-tip. Once this had entered the resin by gravity flow, 2x10ml of wash buffer (1M NaCl, 50mM MOPS pH 7.0, 15% isopropanol v/v) was applied to the QIAGEN-tip and allowed to drain completely under gravity. The DNA was then eluted by applying 5ml of elution buffer (1.25M NaCl, 50mM Tris-Cl pH 8.5, 15% isopropanol v/v) to the QIAGEN-tip. The DNA was subsequently precipitated by adding 3.5ml of room temperature isopropanol to the eluant, mixed by inversion and sedimented by immediate centrifugation for 30mins at 15000g (13krpm). The supernatant was carefully removed and the DNA pellet washed with 2ml of room temperature 70% EtOH, before further centrifugation for 10mins at 15000g (13krpm). The supernatant was again discarded, the DNA pellet air-dried for 10mins and then redissolved in 500μl of nuclease free water or TE buffer (10mM Tris-Cl pH 8.0, 1mM EDTA). The DNA was subsequently stored at -20°C for up to 6 months.

### *2.113 DNA sequencing*

DNA sequencing and primer synthesis was carried out by the Protein and Nucleic Acid Chemistry Laboratory (PNACL). Primers were *(a)* designed with optimal properties as described previously (**see 2.11**, 18-35bp, $T_m$=48-55°C, G-C rich 3' end) without runs of identical bases or complimentarity, *(b)* designed to initiate sequencing ~100bp prior to the region of interest, and *(c)* supplied in a 10µl sample of 0.8-1.0pmol/µl diluted in nuclease free water. The sample of substrate DNA was also supplied in this manner.

## *2.2 Protein culture and purification*

### *2.21 Culturing Dictyostelium discoideum*

The *Dictyostelium discoideum* used to express the myosin II mutants was an AX3-$Orf^+$ strain containing integrated copies of the Dpd2 *ORF* gene, whose product is essential for autonomous replication of transformed plasmid vectors. The $Orf^+$ strain also contained an inherent resistance to penicillin and streptomycin.

Liquid cultures were maintained in conical flasks of 100-1000mls, which were sealed with a sterilised sponge bung and foil covering to minimise exposure to outside contaminants while still allowing oxygenation of the cells. Sterilisation was achieved via autoclaving of all the relevant apparatus and growth media (121°C, Falcon 30 autoclave). The cultures were grown in darkness, at 22°C, in a Brunswick C25KC incubator shaker set at 120rpm. During the following procedures all manipulation of *Dictyostelium discoideum* was carried out under sterile conditions, with the outside of all equipment being sterilised before use by thoroughly wiping with 70% ethanol, then placed in a sterile hood (Airone LF-640) where *Dictyostelium* could be safely

exposed to the air without great risk of contamination. The cells were cultured in HL5 liquid growth media (14.3g/l protease peptone, 7.16g/l yeast extract, 4mM, $KH_2PO_4$, 4mM $Na_2HPO_4.2H_2O$, with the addition of 6µl/ml Pen/Strep(10000u/ml), 100µg/ml G418, and 154mg/ml glucose prior to use), and maintained at a density of $5x10^5$-$1x10^7$ cells/ml wherever possible.

### *2.22 Production and storage of* Dictyostelium discoideum *spores*

Wildtype *Dictyostelium discoideum* ($Orf^+$ strain) was grown to a density of $5x10^6$-$1x10^7$ cells/ml, 50ml of cells were then transferred to a sterile centrifuge tube and pelleted by centrifugation for 10mins at 300g (1500rpm, Harrier 43124-141 rotor), and the supernatant discarded. The cells were then resuspended in MES buffer (50ml, 20mM MES (pH6.8), 0.2mM $CaCl_2$, 2.0mM $MgCl_2$), pelleted by centrifugation as before, and resuspended in fresh MES buffer to a final concentration of $2x10^7$ cells/ml. A sample (9ml) of this suspension was then transferred to a MES agar plate (20mM MES (pH6.8), 0.2mM $CaCl_2$, 2.0mM $MgCl_2$, 2% w/v bacteriological agar), left to stand at room temperature for 20mins (with plate lid on), the excess fluid carefully removed by pipetting and the plate incubated in the sterile hood (without lid) for 20mins or until dry. The lid was then replaced and the plate incubated in darkness at 20°C for 24 to 48hrs, to allow the spore cases (*sori*) to develop. The spherical *sori* were then harvested from their stalks by tapping the inverted plate sharply onto a solid surface. Following resuspension of the *sori* in 1-3ml of glycerol (10%), the mixture was separated into aliquots (200µl), flash-frozen in dry-ice cooled ethanol, and stored at -80°C until use.

To convert the spores to a viable cell-culture, the aliquots were thawed at room temperature, transferred to a plate containing HL5 growth media (~15ml) and

stored static, in darkness, at 22°C until confluent (5-7days). The 15ml of cells were then transferred to 100ml of HL5 growth media in a conical flask, and stored shaken at 22°C until ready for electroporation (density of $5x10^6$ cells/ml).

### *2.23 Electroporation of novel plasmid constructs into Dictyostelium discoideum*

During this procedure, in order to ensure an efficient transformation the buffers, cuvettes and centrifuge tubes were kept on ice at all possible times, with the centrifuges and centrifuge rotors pre-cooled to 4°C prior to use.

Wildtype *Dictyostelium discoideum* ($Orf^+$ strain) was grown to a density of $5x10^6$ cells/ml (log phase) in 100ml of HL5 growth media. The cells were then transferred to 50ml sterile tubes and pelleted by centrifugation for 10mins at 300g (1500rpm, Harrier 43124-141 rotor). The supernatant was then discarded and the cell pellet resuspended in ice-cold electroporation buffer (50mM sucrose, 10mM $NaH_2PO_4$, 2mM $Na_2HPO_4.2H_2O$, pH 6.1). This centrifugation/resuspension step was then repeated to ensure the complete removal of HL5 growth media, followed by a final centrifugation and resuspension in 1-2ml of ice-cold electroporation buffer. The cell density of a small sample of this (10x diluted) was then analysed, and the density of the remainder of the cells adjusted to $5x10^7$ cells/ml in ice-cold electroporation buffer. The cell suspension (400µl) was then transferred to a cold electroporation cuvette (0.2cm), before the addition of plasmid DNA (~20µl) and gentle mixing by pipetting. After being left to stand on ice for 10mins, the settled cells were gently resuspended by pipetting before electroporation (1.2kV, 3µF, 400Ω, T.C.≈0.35 for $Orf^+$). The suspension was then left on ice for 10mins, before the addition and gentle mixing of curing buffer (8µl, 100mM $CaCl_2$, 100mM $MgCl_2$). Samples of the cured cells (20µl, 50µl, and 100µl) were then transferred to separate petri dishes, and left to

stand at room temperature for 15mins to allow the cells to settle. HL5 growth media (15mls, *no* G418) was then carefully added to the dishes so as to slightly, but not completely, disturb the cells, and the culture incubated in darkness, unshaken, at 22°C for 18-24hrs. The HL5 media was then carefully removed (cells should be fixed to the surface of the petri dish) and replaced with fresh HL5 containing geniticin (100µg/ml G418) to select for electroporated cells. From this point on, all HL5 growth media contained penicillin, streptomycin and geniticin. When distinct, separate colonies had formed (~5days) the media was carefully removed, the colonies scraped with a pipette tip and transferred to separate microtitre wells containing 200µl of fresh HL5. When a large clump of cells was clearly visible at the base of the wells (3-5days) they were transferred to individual petri dishes, 15mls HL5 added, and incubated in darkness, unshaken, at 22°C until confluent (5-8days). The entire mass of cells from one Petri dish was then transferred to 100mls of HL5 in a conical flask, incubated in darkness, shaken, at 22°C until the cell density was $5x10^6$-$1x10^7$ cells/ml. An expression assay was then carried out on a small sample of the cells (**see 2.43**), and the culture (if suitable) grown to the required volume (2.5-5l, maintaining $5x10^5$-$1x10^7$ cells/ml) for protein purification (7-10days).

### *2.24 Purification of His-tagged myosin fusion proteins from Dictyostelium discoideum*

An electroporated $Orf^+$ cell-line was grown to a concentration of $5x10^6$-$1x10^7$ cells/ml in 2.5-5l of HL5 growth media, the volume being dependent on the estimated expression level of the cell-line. The cells were then pelleted by centrifugation for 10mins at 2000g (3500rpm, Beckman Avanti J-20 XP, JA-1 rotor, using 4-6 500ml or 1l centrifuge tubes) and the supernatant discarded. To remove any residual HL5 media, the cell pellets were then resuspended in a small volume of ice-cold PBS and

transferred to a single pre-weighed centrifuge tube, which was then filled with ice-cold PBS. The cells were again pelleted by centrifugation for 10mins at 2000g (3500rpm, JA-10 rotor), and the wet weight of the cell pellet determined (usually 25-35g). 2 mls of lysis buffer (50mM TrisHCl pH 8.0, 2mM EDTA, 0.2mM EGTA, with *freshly* added 3mM DTT, 5mM benzamidine, and 2000x protease inhibitor mix [15mg pepstatin, 2 or 3.3mg leupeptin, 66mg TPCK, 25mg TLCK, and 66mg PMSF in 1ml DMSO]. The lysis buffer was always vigorously stirred during the addition of the 2000x protease inhibitor mix, to avoid it precipitating and adhering to the walls of the container) per g of cells was placed into a large homogeniser containing 1% w/v Triton X-100, and the Triton *fully* resuspended by homogenisation to prevent localised concentrations from damaging the protein. Then, 100 units of calf intestinal phosphatase were added and mixed by further homogenisation. The cells were then transferred to the homogeniser and resuspended by *gentle* homogenisation, avoiding bubbles as much as possible. The suspension was then added immediately to 4ml lysis buffer (*without* Triton X-100 or calf intestinal phosphatase) per g of cells, mixed by gentle swirling, and sonicated (Soniprep 150, 2x1min, 0.75" tip, 8-10 power setting, 50% duty cycle. The suspension was kept ice-cold during sonication by placing in a bath of iced water) to fully lyse the cells. A small sample of the suspension was then placed on a haemocytometer and viewed under a standard light microscope (25x magnification). If intact cells were observed, then the sonication step was repeated until all cells had been lysed. The lysate was then incubated on ice for 1hr to allow cellular ATP to be completely hydrolysed, extra lysis buffer used to ensure that all the tubes were fully filled, and then centrifuged for 1hr at 250000g (45krpm, 4°C, Beckmann L7-65 ultracentrifuge, 50.2Ti rotor). The supernatant was discarded, the pellets carefully removed from the centrifuge tubes and then resuspended by gentle

homogenisation in 50-70ml of extraction buffer (50mM HEPES pH 7.3, 30mM KAc, 10mM MgAc, with *freshly* added 7mM βME, 5mM benzamidine, 40μg/ml PMSF). This solution was then centrifuged for 1hr at 250000g (45krpm, 50.2Ti rotor, fully filled tubes), and the supernatant discarded. The pellets were then carefully removed from the centrifuge tubes, and resuspended by gentle homogenisation in 40-60ml of extraction buffer (containing an additional 20mM ATP, 10mM $MgCl_2$, re-pH to 7.3) to extract the myosin fusion proteins from cellular F-actin. This solution was then centrifuged for 1hr at 250000g (45krpm, 50.2Ti rotor, fully filled tubes), the supernatant carefully removed and stored overnight at 4°C.

A $Ni^{2+}$-NTA purification column (15-20ml, Novagen $Ni^{2+}$-NTA His-bind resin) was then cleaned and equilibriated by washing with 1-2 column volumes of 100% imidazole (0.5M imidazole, 50mM HEPES pH 7.3, 30mM KAc, 0.01% w/v $NaN_3$, with *freshly* added 3mM benzamidine, 3mM βME), followed by 2-3 column volumes of low salt buffer (50mM HEPES pH 7.3, 30mM KAc, 0.01% w/v $NaN_3$, with *freshly* added 3mM benzamidine, 3mM βME), both of which were applied to the column at a flow rate of ~1ml/min using a peristaltic pump (LKB 2120 varioperpex II). The supernatant containing the myosin fusion protein was then added to the column at the same flow rate and immediately washed with 1-2 column volumes of low salt buffer, 1-2 column volumes of high salt buffer (50mM HEPES pH 7.3, 300mM KAc, 0.01% w/v $NaN_3$, with *freshly* added 3mM benzamidine, 3mM βME) and 1-2 volumes of low salt buffer to remove non-bound and non-specifically bound proteins. Then a 10-17% imidazole (50-85mM imidazole in low salt buffer) solution was applied to the column to remove any proteins bound by a *His*-tag of 4-5 or less histidines. This high stringency wash was continued until the eluted protein reached a steady baseline, determined by placing a single drop of eluate into 500μl of Bradford

reagent at 5-10min intervals. Once this was achieved, the myosin fusion protein was eluted by applying a 90% imidazole (0.45M imidazole in low salt buffer) solution to the column at a flow rate of 0.5ml/min or less. The eluate was collected in 1.5ml fractions, each fraction being analysed using Bradford reagent as before, until the entire elution peak had been observed. The most concentrated fractions were then pooled and dialysed overnight at 4°C in ice-cold assay buffer (20mM HEPES, 40mM NaCl, 2mM $MgCl_2$, pH7.5, with freshly added 5mM βME, 0.01% w/v $NaN_3$), then for a further 3hrs at 4°C in fresh, ice-cold assay buffer. The dialysate was then transferred to 1.5ml eppendorf tubes and centrifuged for 15mins at ~14000g (12.5krpm in eppendorf 5417R, FA45-30-11 rotor, pre-cooled to 4°C) to pellet any remaining endogenous cellular myosin which had precipitated. The supernatant containing the soluble purified myosin fusion protein was then *carefully* transferred to a 10ml tube using a Gilson pipette and stored on ice, in darkness, at 4°C.

### *2.25 Preparation of acetone-dried rabbit powder*

The preparation and storage of acetone-dried rabbit powder was carried out for use as a source material for the purification of fresh actin. With the exception of the initial dissection, all steps in this protocol were carried out in a chilled environment (4°C) unless otherwise stated.

The rabbit back and leg white muscles were removed by dissection as quickly as possible, and then minced using a small gauge attachment. After manually removing any large strands of connective tissue, the minced muscle was weighed and placed in 3 volumes (w/v) of Guba-Straub buffer (0.3M KCl, 0.15M $KH_2PO_4$, 0.25M $K_2HPO_4$, pH 6.5). The mixture was then gently stirred for 30mins to extract the myosin. This suspension was *slowly* and carefully diluted, with constant and thorough

stirring, into approximately 15l of chilled (4°C) deionised water, and then filtered through a layer of fine gauze net curtain. The filtrate was retained for the purification of rabbit myosin, while the mince was placed in 5l of actin buffer 1 (4% $NaHCO_3$ w/v, 0.1mM $CaCl_2$) and stirred gently for 30mins. The resulting mixture was filtered through fine gauze net curtain and the remaining solid stirred in 1l of actin buffer 2 (10mM $NaHCO_3$, 10mM $Na_2CO_3$, 0.1mM $CaCl_2$) for 10mins. Ten litres of chilled deionised water was then added and the mixture quickly stirred before further filtration through fine gauze net curtain. The residue was subsequently placed in 2.5l of cold acetone and stirred for 20mins in a fume cupboard at room temperature. The mixture was again filtered through fine gauze net curtain and the solid stirred for 20mins in another 2.5l of cold acetone at room temperature. After a final filtration through fine gauze net curtain the solid material was spread between two large layers of filter paper and dried in a fume cupboard overnight. The acetone dried rabbit powder was then forced through a sieve to remove most of the connective tissue and stored at -20°C for up to 3 months.

### *2.26 Purification of rabbit skeletal filamentous actin*

Rabbit skeletal F-actin was purified essentially as described by (Pardee and Spudich, 1982). Unless otherwise stated, all solutions were kept on ice at all times.

Acetone-dried rabbit muscle powder (~5g) was suspended in 80-100ml of actin buffer 1 (0.5mM $Na_2ATP$, 0.5mM DTT, 0.2mM $CaCl_2$, 1mM Trizma base, pH 8.5), which had been chilled to 0°C by standing on ice overnight. The mixture was then incubated on ice for 30-60mins with frequent gentle stirring, before filtering through a fine nylon mesh which had been previously prewashed, boiled and chilled. The cloudy filtrate was then centrifuged for 1hr at 250000g (45krpm, 4°C, Beckmann

L7-65 ultracentrifuge, 50.2Ti rotor) ensuring that all centrifuge tubes were full by the extra addition of ice-cold actin buffer 1. The supernatant was then filtered through Whatman no.1 filter paper and the volume of the filtrate determined. To this filtrate the following compounds were then added to final concentrations of 1mM $MgCl_2$, 10mM NaPi (pH 7.0), and 50mM KCl, in that respective order, to induce actin polymerisation. The mixture was then allowed to polymerise at room temperature for 1hr, then solid KCl was added to a final concentration of 0.85M, dissolved by *gentle* stirring, and the mixture allowed to stand at 4°C overnight to dissociate tropomyosin from the filamentous actin. This mixture was then centrifuged for 3hrs at 25000g (45krpm, 4°C, 50.2Ti rotor), the supernatant discarded, and the pellet allowed to soften in ~6mls of ice-cold depolymerisation buffer (2mM Trizma base, 100μM DTT, 100μM ATP, pH 8.0) for 30mins. The pellet was then carefully resuspended using a 10ml manual glass homogeniser. The suspension was then dialysed at 4°C in 700ml of ice-cold depolymerisation buffer for 3hrs, overnight, and for a further 3hrs, changing the dialysis buffer for fresh depolymerisation buffer each time. The dialysate was then centrifuged for 1hr at 386000g (100krpm, 4°C, Beckmann TL-100 tabletop ultracentrifuge, TLA-100 rotor) and the G-actin concentration determined by measuring the absorbance at 290nm (Varian Cary 50 Probe UV visible spectrophotometer, $\varepsilon=26600M^{-1}$). At least half of the final purified G-actin was usually polymerised to F-actin by the addition of 100mM NaCl or KCl and 2mM $MgCl_2$ (final concentrations). Both G-actin and F-actin could then stored on ice for up to 2-3 weeks.

*2.27 Purification of rabbit myosin*

With the exception of the initial dissection, all steps in this protocol were carried out in a chilled environment (4°C) unless otherwise stated. The overall method was based on that previously described by (Margossian and Lowey, 1982).

The rabbit back and leg white muscles were removed by dissection as quickly as possible, and then minced using a small gauge attachment. After manually removing any large strands of connective tissue, the minced muscle was weighed and placed in 3 volumes (w/v) of Guba-Straub buffer (0.3M KCl, 0.15M $KH_2PO_4$, 0.25M $K_2HPO_4$, pH 6.5). The mixture was then gently stirred for 30mins to extract the myosin. This suspension was *slowly* and carefully diluted, with constant and thorough stirring, into approximately 15l of chilled (4°C) deionised water, and then filtered through a layer of fine gauze net curtain. The mince was retained for acetone-dried rabbit powder preparations to obtain a source of fresh actin. The filtrate was then diluted into a further 15l of chilled deionised water, and allowed to stand for a minimum of 2hrs until the myosin precipitate had formed and sedimented by gravity. Subsequently, the supernatant was removed by manual siphoning and the precipitate pelleted by centrifugation for 45mins at 5000g (5000rpm, 4°C, Beckman Avanti J-20 XP, JA-10 rotor). The pelleted myosin was then resuspended in a *final volume* of 250mls of myosin buffer 1 (0.6M KCl, 5mM imidazole pH 7.0) and left overnight to completely dissolve. The following day 285mls of chilled deionised water was *slowly* and carefully added to the myosin solution (1.14x dilution) and the actomyosin precipitate pelleted by centrifugation for 5mins at 5000g (5krpm, 4°C, JA-10 rotor) and then discarded. The supernatant was diluted by a further 7x the initial volume in chilled deionised water, left to stand for 15mins, and the precipitated myosin pelleted by centrifugation for 45mins at 5000g as before. The pellet was again resuspended in

250mls of myosin buffer 1 and the actomyosin extraction repeated, although it was not usually necessary to leave the suspension overnight at this stage. The final myosin pellet was then resuspended in *up to* 150mls of myosin buffer 2 (1.2M KCl, 10mM NaPi, 3mM $MgCl_2$, 0.2mM EGTA, 3mM $NaN_3$) and the protein concentration measured using a standard Bradford assay. Glycerol was added to the myosin solution to a final concentration of 51-55%, thoroughly mixed, and stored at -20°C.

### *2.28 Purification of rabbit heavy meromyosin (HMM)*

Rabbit skeletal HMM, although not carried out personally, was isolated from purified rabbit myosin by digestion with α-chymotrypsin as described by (Weeds and Taylor, 1975).

### *2.29 Purification of thick myosin filaments from molluscan white catch muscle*

Molluscan white catch muscle was purified essentially as described by (Sellers *et al.*, 1991) Unless otherwise stated, all steps were carried out in a chilled (4°C) environment, with all centrifuges and centrifuge tubes also pre-chilled to 4°C.

The white catch muscles were carefully removed from fresh mussels, cut into small pieces, placed in 20mls of chilled buffer A (10mM $MgCl_2$, 1mM EGTA, 20mM MOPS, 3mM $NaN_3$, 1mM DTT, 0.1M PMSF, 10mM ATP, pH 7.0) and stirred thoroughly. If the catch muscle had been previously glycerinated, care was taken to drain the catch muscles thoroughly before immersing into the buffer. The muscle was removed, placed in 20ml of fresh chilled buffer A, stirred thoroughly, and the process repeated once more to ensure that a constant supply of fresh ATP kept the actin and myosin thick filaments dissociated. The muscle was subsequently homogenised (Polytron mechanical homogeniser) in the final 20ml of buffer A, first at a slow speed

until a cloudy solution was produced, then at a slowly increasing speed until the whole sample was homogenised. This ensured that as few bubbles as possible were introduced into the homogenate. The homogenised muscle was then mixed with an equal volume of buffer B (buffer A + 0.1% w/v Triton X-100) and allowed to stand on ice for 5mins. Extraneous muscle tissue was sedimented by centrifugation for 5mins at 500g (2800rpm, SS34 rotor) and the top ⅔ of the supernatant *carefully* removed and retained. The thick filaments were then sedimented from the supernatant by centrifugation for 30mins at 5000g (7500rpm, SS34 rotor). After resuspension of the pellet in 30mls of buffer A, the solution was left for 20mins to allow large aggregates to dissociate. Any remaining aggregates were sedimented by centrifugation for 5mins at 500g (2800rpm, SS34 rotor). The supernatant was then carefully removed and the thick myosin filaments sedimented again by centrifugation of the supernatant for 30mins at 5000g. The molluscan myosin thick filaments were then resuspended in 100-500µl of assay buffer (20mM HEPES, 40mM NaCl, 2mM $MgCl_2$, pH7.5, with freshly added 5mM βME, 0.01% w/v $NaN_3$) and stored on ice for up to 2-3 weeks. For the purposes of our experiments, a final set of washes and sedimentation steps to remove all traces of ATP from the molluscan myosin thick filaments was not required due to the high dilution factors involved before use.

## *2.3 Solution-based analytical techniques*

### *2.31 Quantification of protein concentration and purity*

The concentration of the novel fusion proteins was usually calculated from the relevant intensity (background corrected) of the absorbance spectrum, using the published extinction coefficient (Tsien, 1998) of the fluorescent probe in question (**Fig. 2.311**). The purity of the isolated fusion proteins was assessed by a comparison

of this concentration value and that obtained via a standard Bradford Reagent assay (total protein).

$$c = \frac{A}{\varepsilon l}$$

**Fig. 2.311** The equation utilised for novel fusion protein concentration determination, where $A$ denotes the absorbance at a certain wavelength, $\varepsilon$ ($cm^{-1}M^{-1}$) is the extinction coefficient for a given fluorophore, $l$ is the path length (cm) of the sample (usually 1), and $c$ is the concentration (M).

### *2.32 Stopped-flow and spectral analysis*

Solution kinetics were performed using SF18MV stopped-flow apparatus (Sowerby *et al.*, 1993) equipped with a Hg-Xe arc lamp (Applied Photophysics, Leatherhead, UK). Absorbance spectra were obtained using a Varian Cary 50 Probe UV visible spectrophotometer, with emission and excitation spectra obtained using a Varian Cary Eclipse fluorescence spectrophotometer, all of which were supplied with their own software. Anisotropy values were determined using an SLM 48000S fluorescence spectrophotometer with Glan-Thompson polarisers.

### *2.33 Anisotropy measurements*

Anisotropy was measured as discussed previously (see 1.11), however an additional factor in practice is the sensitivity ratio of the monochromator and polarisers to vertically and horizontally polarised light (the G factor). This can be measured by introducing horizontally polarised excitation light to the sample, thus any emission detected would be a result of depolarisation, equal in intensity in both planes. Therefore the ratio of sensitivity can be calculated and applied to the relevant equations to obtain a corrected anisotropy value (**Fig. 2.331**).

$$a = \frac{Iz - GIy}{Iz + 2GIy}$$

**Fig. 2.331** The equation for measurement of anisotropy, taking into account the relative sensitivity of monochromator and filters to horizontally and vertically polarized light (The G factor).

## *2.4 Microscope-based analytical techniques*

### *2.41 Fluorescence microscopy setup*

TIRFM Images were obtained with a Zeiss Axiovert 135TV microscope using an optical setup based on that of Gingell *et al.* (1985) with alternative laser sources and new detectors, as described in detail previously (Conibear *et al.*, 1998). Excitation light was provided by a Lexel 85-1 argon-ion laser (Lambda Photometrics Ltd, Harpenden, UK), yielding 250mW at 488 and 514nm, which was focussed at the sample position 1.7m away with a convergence of ~1°. For TIRFM, the laser beam was directed towards a 15mm cubic (or modified; Conibear and Bagshaw, 2000) Spectrosil B prism (fixed to the top face of the coverslip with glycerol) so that it underwent total internal reflection at the sample/coverslip interface (**Fig. 2.411**). Fluorescence was observed using either a 63x Zeiss plan-apochromat 1.36 NA oil-immersion objective lens (epifluorescent microscopy), or an Zeiss 60x 1.2 NA water-immersion objective lens (TIRFM). Fluorescent emission was selected using Omega 455DF70/510AF23 (GFP excitation/emission) or Omega 500AF25/545AF35 (YFP excitation/emission) filters, and recorded using a Hamamatsu C2400-08 SIT camera or a Hamamatsu 3500 ICCD camera coupled to an Argus 10 image processor (Hamamatsu). Individual frames were grabbed directly or from video records (VHS, Panasonic FS88) by using a Scion LG3 card interfaced to a 7100 Macintosh PowerPC running NIH imaging software. For the purposes of flash photolysis experiments, an

output signal from the LG3 card was used to briefly close a protective electronic shutter (Ealing Electro-Optics; 22-8411) in front of the camera, while simultaneously triggering the Xe flash lamp (XF-10, Hi-tech Scientific, UK), whose emission was selected to produce an ~350nm flash. The shutter re-opened approximately 10-20ms after the 4ms flash.

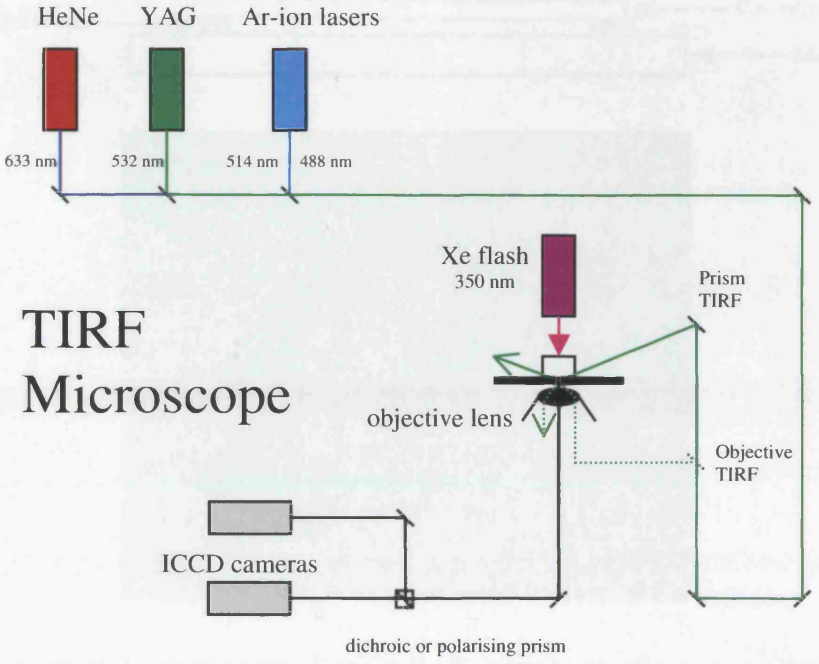


**Fig. 2.411** A basic schematic representation of the TIRFM setup used for caged-ATP flash photolysis studies of ATP-induced actomyosin dissociation kinetics. YAG represents a yitrium aluminium garnet laser source.

### *2.42 Construction of a flow cell*

A microscopy flow cell consisted of a coverslip (22x40mm) fixed to a brass slide mount with two strips of double-sided adhesive tape. Two small strips of cut glass (usually 0 or 1 coverslips) were aligned on top of the fixed coverslip, either side of the viewing hole of the brass slide mount. Just inside these spacers two lines of grease were applied using a syringe, with a second coverslip (18x18mm) placed ontop of the glass spacers and grease lines, forming a sealed cell of ~50µl (**Fig. 2.421**). The mount was then aligned at ~45° to the vertical, and solutions were applied to the top of the

flow cell, while simultaneously leeching previous solutions out from the bottom of the flow-cell using strips of Whatman filter paper. Solutions were typically incubated for 1-2mins before washing out with assay buffer and/or replacement with a subsequent solution.

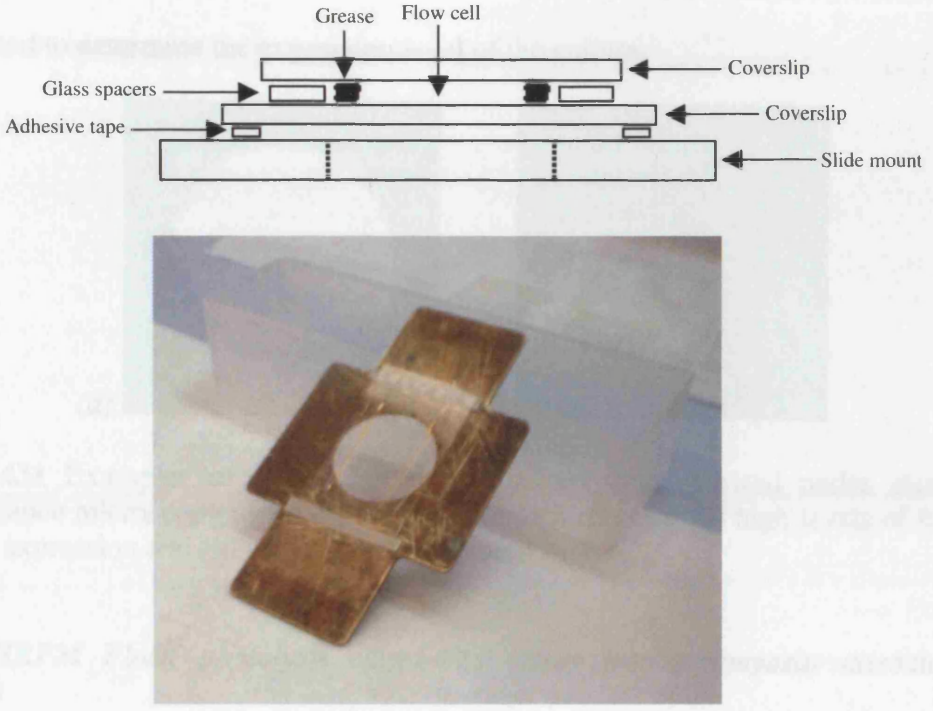


**Fig. 2.421** A typical microscopy flow-cell, diagrammatically represented from the side (*top*), and aligned at ~45° ready for perfusion of various solutions prior to visualisation under TIRFM (*bottom*).

### *2.43 Microscope-based assay for the expression of FP fusion proteins in* **Dictyostelium discoideum**

An electroporated $Orf^+$ cell-line was grown to a concentration of $5x10^6$-$1x10^7$ cells/ml in 100ml of HL5 growth media. A small sample of cells (~10ml) was pelleted by centrifugation at 300g (1000rpm, Harrier 43124-141 rotor), resuspended in 10ml of microscopy buffer (20mM HEPES, 40mM NaCl, 2mM $MgCl_2$, 0.1mM EGTA, 10mM DTT, 0.01% w/v $NaN_3$, at 20°C), allowed to stand for 10min, pelleted by centrifugation in the same manner and resuspended in ~1ml of microscopy buffer. A sample of the cells (10µl) was then placed on a glass coverslip (22x40mm) fixed to a

brass slide mount, another glass coverslip (18x18mm) placed directly onto the sample and any excess liquid carefully removed with filter paper. The cells were then visualised under epi-fluorescent illumination with appropriate dichroic filters applied to the emission, and the ratio of brightly fluorescent:non-fluorescent cells (**Fig. 2.431**) calculated to determine the expression level of the culture.

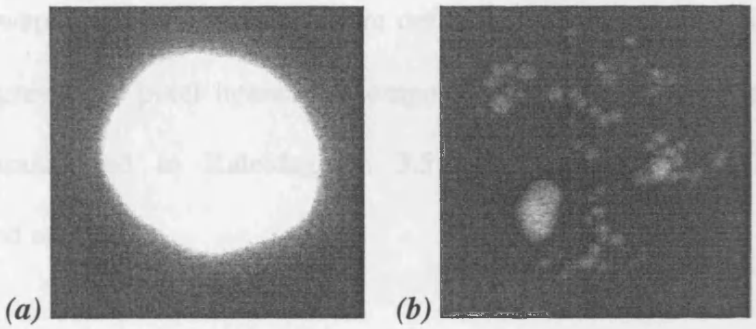


**Fig. 2.431** Examples of *Dictyostelium discoideum* cells, viewed under standard fluorescence microscopy using epi-illumination, which show *(a)* high levels of fusion protein expression and *(b)* virtually no expression.

### *2.44 TIRFM Flash photolysis caged-ATP assay into actomyosin dissociation kinetics*

To the top of a flow cell angled at ~45°, aged rabbit HMM (50µl, 0.2-1mg/ml) was perfused and allowed to stand for 2min. This was washed out with 2x50µl perfusions of microscopy buffer (20mM HEPES, 40mM NaCl, 2mM $MgCl_2$, 0.1mM EGTA, 10mM DTT, 0.01% w/v $NaN_3$, at 20°C), aided by simultaneous leeching of the previous solution from the bottom of the flow cell using a small strip of filter paper. BSA (1-2mg/ml) was then introduced to the flow cell to block any HMM-uncovered glass surface, allowed to stand for 1min and washed out with 2x50µl of microscopy buffer. F-actin (10-40nM) was then perfused into the flow-cell, allowed to stand for 2min, then directly replaced with fusion protein (10-40nM) to decorate any actin filaments bound to the HMM monolayer within the flow-cell. After a further 2min, the flow-cell was thoroughly washed with 4x50µl of microscopy buffer, before

visualisation under TIRFM. Caged-ATP was then perfused into the flow cell, taking great care not to disturb the sample itself. Following re-visualisation of the decorated filaments, ATP-induced actomyosin dissociation was initiated by UV flash photolysis (350nm) of caged-ATP, and the resultant fluorescence changes recorded via video records. Subsequent to capture of the images and processing of frame stacks into NIH imaging software, regions of interest were defined around individual filaments, and the average grey-scale pixel intensities computed as a function of time. These data were then transferred to Kaleidagraph 3.51 (Synergy Software) for plotting, processing and analysis.

# 3 - Cloning and basic characterisation of novel FP-myosin fusion proteins from *Dictyostelium discoideum*

## *3.1 Plasmid construction*

In emulating the cloning of a double-FP *Dictyostelium* myosin-II fusion protein for FRET studies, as performed by Suzuki *et al.* (1998), particular interest was placed in the intervening linkers between the myosin motor and the fluorescent probes. The nature of these regions was of considerable importance as they could affect *(a)* the flexibility of the probes, and *(b)* the orientation of the probes relative to the motor domain and each other. Both these factors could, in turn, have a significant effect on the level of FRET in the *apo* protein, and the type and magnitude of FRET changes upon ligand binding. Thus, double fusion proteins with and without the triple-gly linkers employed by Suzuki *et al.* (1998) were cloned. The 'g' terminology represented the presence of a triple-gly linker (*e.g.* W501.gGFP), with the absence of this linker denoted by 'r' (*i.e* a potentially more rigid link; rYFP.W501). Furthermore, within the nomenclature the left-hand corresponded to the N-terminal or 5' end of protein / DNA (*e.g.* rYFP.W501), with the right-hand corresponding to the C-terminal or 3' end (*e.g.* W501.gGFP).

### *3.11 Single tryptophan Dictyostelium myosin II mutant (pDXA.W501)*

The template from which the *Dictyostelium* myosin II-FP fusions were constructed was a 2283bp S1-type *Dictyostelium* myosin II DNA fragment, with all tryptophan residues replaced by phenylalanine save for the 501 position (*w501*). The 501 tryptophan residue has been shown to be sensitive to the binding and hydrolysis of ATP (Malnasi-Csizmadia *et al.*, 2001a, Malnasi-Csizmadia *et al.*, 2001b, Malnasi-

Csizmadia *et al.*, 2000), and could therefore be used as an effective tool for the analysis of the functionality of novel fusion proteins.

The *Dictyostelium* myosin II fusions were expressed by insertion of the novel DNA fragments into the multiple cloning site of the pDXA-3H *Dictyostelium discoideum* expression vector (Manstein *et al.*, 1995), which was subsequently transformed into *Dictyostelium* ($Orf^+$ strain). This vector contained a complementary *beta lactamase* gene, conferring ampicillin and penicillin resistance for bacterial selection and to prevent unwanted bacterial contamination, and a complementary aminoglycoside 3' phosphotransferase gene (*APH 3'*), conferring kanamycin, neomycin and geniticin (G418) resistance to enable easy selection of fully transformed cells following electroporation. The origin of replication was a *Dictyostelium ori* sequence from plasmid Dpd2 (Chang *et al.*, 1990, Leiting *et al.*, 1990), situated immediately prior to an actin 15 (*act15*) promoter which provided strong, constitutive expression in *Dictyostelium discoideum* of any DNA fragment

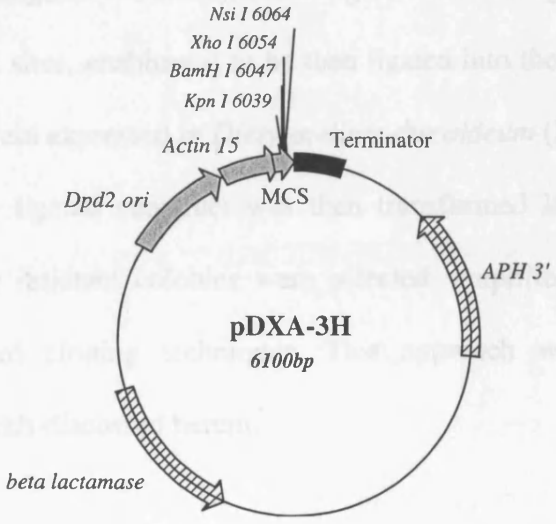


**Fig. 3.111** The pDXA-3H *Dictyostelium discoideum* expression vector (Manstein *et al.*, 1995), containing a complementary *Beta lactamase* gene for bacterial selection and prevention of bacterial contamination, a complementary *APH 3'* gene conferring geniticin (G418) resistance to transformed cells, thus allowing antibiotic selection, a *Dictyostelium* high copy *Dpd2* origin of replication, a constitutive actin promoter (*act15*) and an 8 His-tag sequence prior to the terminator to allow purification of expressed proteins on a $Ni^{2+}$-NTA filtration column (Janknecht *et al.*, 1991).

inserted into the multiple cloning site. The pDXA-3H vector also contained an 8 residue poly-His tag sequence (Janknecht *et al.*, 1991) situated immediately prior to the terminator. This His-tag was thus fused to the C-terminal end of any expressed proteins, allowing quick and easy purification using a $Ni^{2+}$-NTA filtration column.

The pDXA.W501 plasmid construct was designed for the expression of S1-type *Dictyostelium* myosin II containing only a single Trp at the 501 position (W501, Malnasi-Csizmadia *et al.*, 2001a, Malnasi-Csizmadia *et al.*, 2001b, Malnasi-Csizmadia *et al.*, 2000), and provided an excellent starting point for the construction of plasmids for the expression of the novel FP-myosin II fusion proteins. These fusion proteins were intended for use in a wide variety of studies, including kinetic studies in solution, fluorescence resonance energy transfer (FRET) studies, and the development of sensitive, microscope based kinetic assays. The *w501* DNA fragment was cloned as described previously (Yengo *et al.*, 2000), resulting in a *w501* fragment flanked by *BamHI* restriction digest sites, enabling it to be then ligated into the MCS of pDXA-3H and the resultant protein expressed in *Dictyostelium discoideum* (**Fig. 3.112**).

The successfully ligated construct was then transformed into *E. coli*, after which viable ampicillin resistant colonies were selected, amplified, and the DNA extracted using standard cloning techniques. This approach was used for all subsequent fusion plasmids discussed herein.

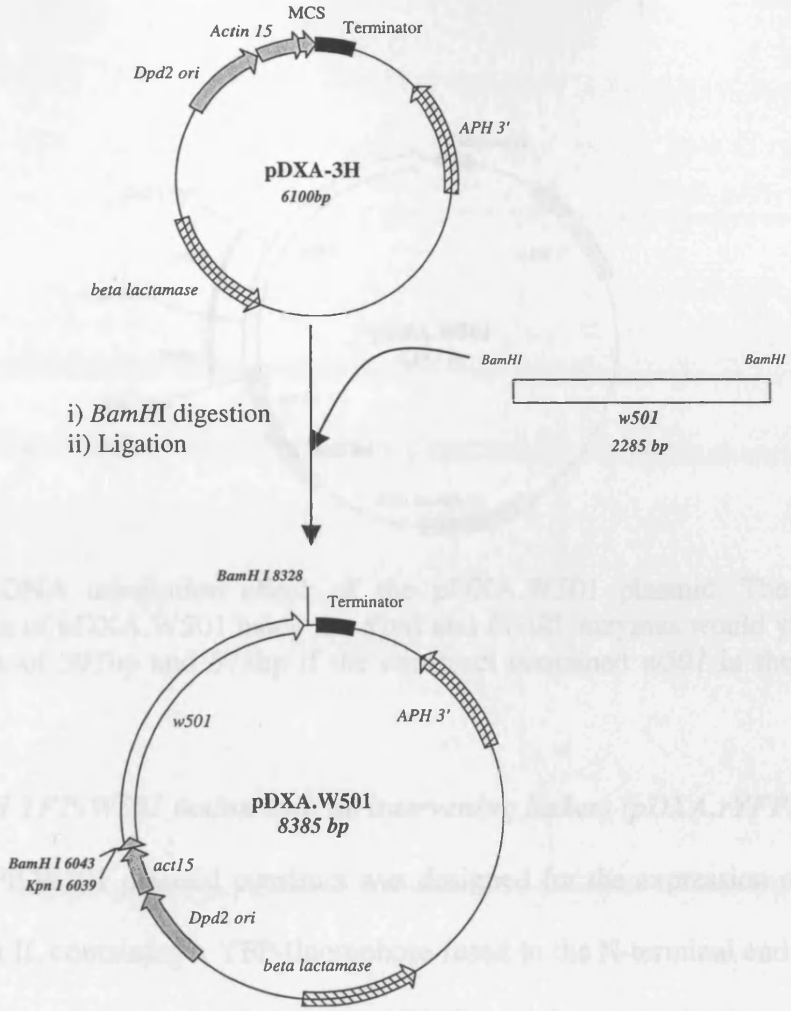


**Fig. 3.112** The construction of the pDXA.W501 plasmid. The *w501 Dictyostelium* S1-type myosin II DNA fragment, flanked by *BamH*I restriction digest sites, was ligated into the pDXA-3H *Dictyostelium* expression vector (Manstein *et al.*, 1995) following linearisation of the plasmid with *BamH*I.

Prior to a final DNA sequence analysis, the presence and orientation of the *w501* myosin II domain were determined by double restriction digest using the *Kpn*I and *EcoR*I enzymes. The *Kpn*I enzyme was unique to the pDXA-3H plasmid, just prior to the *BamH*I digestion site within the multiple cloning site (MCS). The *EcoR*I enzyme, however, was unique to the *w501* sequence, with two sites existing towards the 5'-end, 575bp apart. Thus, following the double-digest a 575bp fragment signified the presence of the *w501* sequence, while a 393bp fragment signified that it was in the correct orientation.

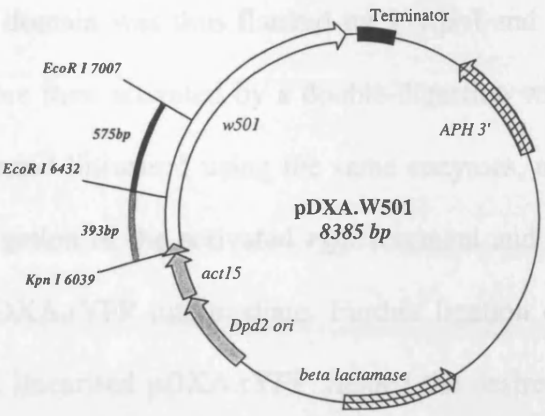


**Fig. 3.113** A DNA orientation check of the pDXA.W501 plasmid. The double restriction digest of pDXA.W501 using the *Kpn*I and *EcoR*I enzymes would yield two small fragments of 393bp and 575bp if the construct contained *w501* in the correct orientation.

### *3.12 N-terminal YFP-W501 fusion with no intervening linkers (pDXA.rYFP.W501)*

The pDXA.rYFP.W501 plasmid construct was designed for the expression of W501 S1-type myosin II, containing a YFP fluorophore fused to the N-terminal end with no intervening linker region (rYFP.W501). The YFP fluorophore contained 4 mutations from wildtype GFP (GFP-10C or YFP; S65G, V68L, S72A, T203Y, Cubitt *et al.*, 1999) which increased not just the excitation and emission wavelength ($\lambda_{exc}$=514nm $\lambda_{em}$=527nm), but also the extinction coefficient ($\varepsilon$=83.4x10$^3$M$^{-1}$cm$^{-1}$, QY=0.61) thus increasing the overall brightness relative to native GFP ($\lambda_{exc}$=470-475nm, $\lambda_{em}$=504nm, $\varepsilon$=9.5-14x10$^3$M$^{-1}$cm$^{-1}$, QY=0.79). The rYFP.W501 protein was intended for use in the development of novel sensitive microscope-based kinetic assays, solution kinetic studies and other control experiments relating to the functionality of novel myosin II fusion proteins with an N-terminal FP moiety. Also, the pDXA.rYFP.W501 plasmid was intended as a precursor to the pDXA.rYFP.W501.gCFP plasmid construct, the fusion protein from which would be utilised in FRET studies.

The *ryfp* DNA fragment was amplified by PCR using *KpnGFUP* (upstream) and *BamGFDOr* (downstream) primers (**App 7.2a, 7.2b**) and the pet-YFP plasmid as

a template. The YFP domain was thus flanked by 5' *Kpn*I and 3' *BamH*I restriction digest sites. These were then activated by a double-digestion with *Kpn*I and *BamH*I, the pDXA.W501 plasmid linearised using the same enzymes, and the excised *w501* fragment retained. Ligation of the activated *ryfp* fragment and the linearised pDXA vector yielded the pDXA.rYFP intermediate. Further ligation of the retained *w501* fragment into *BamH*I linearised pDXA.rYFP yielded the desired pDXA.rYFP.W501 plasmid (**Fig. 3.121**).

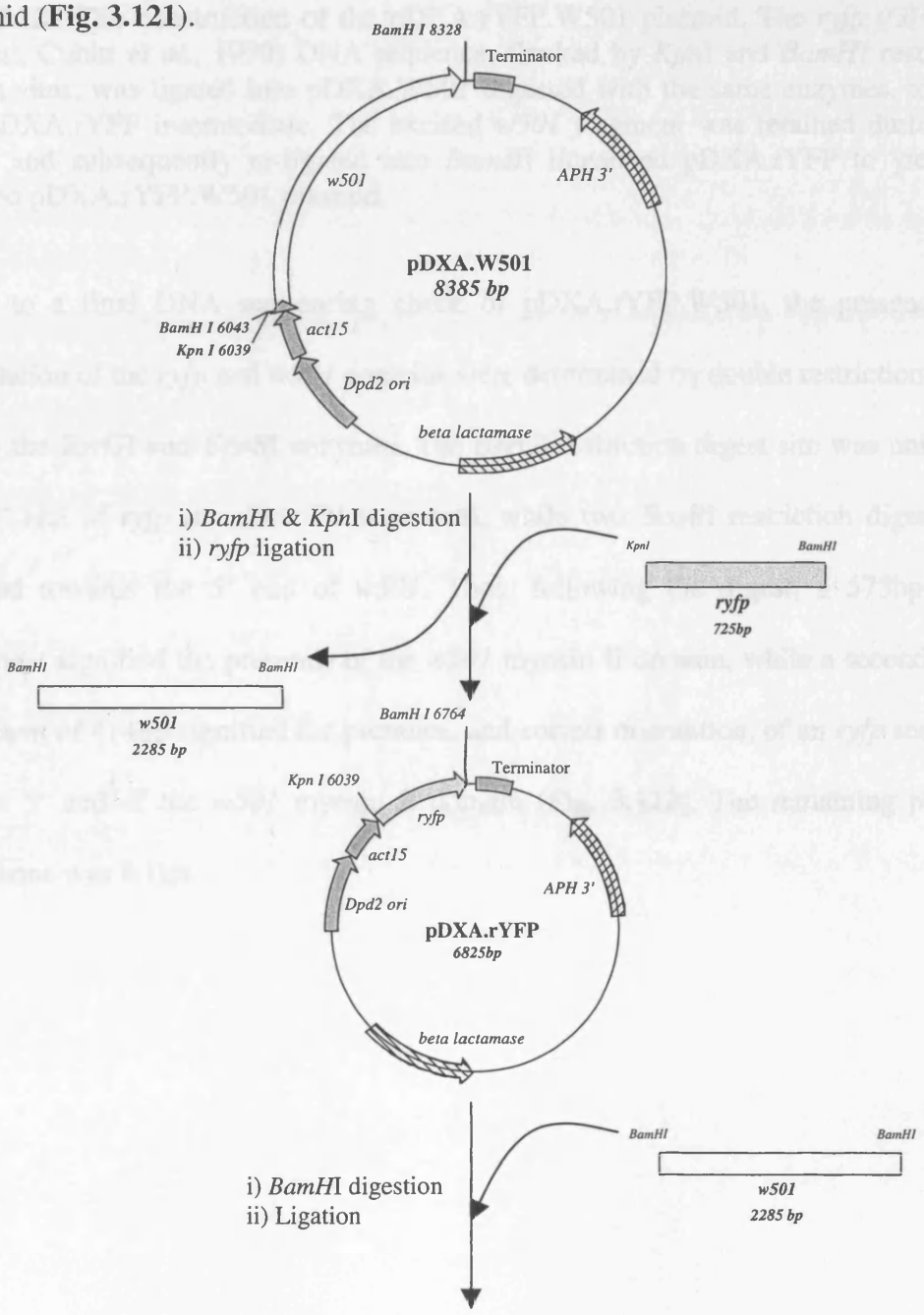

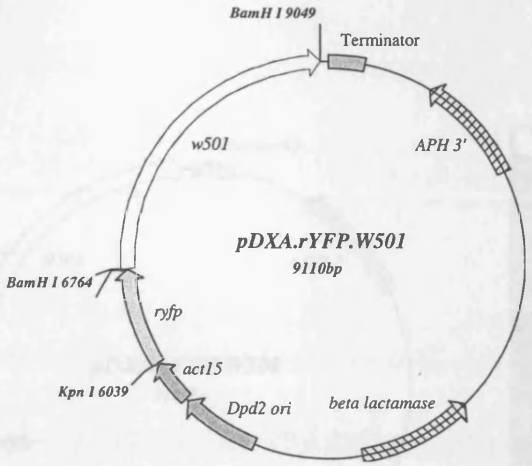


**Fig. 3.121** The construction of the pDXA.rYFP.W501 plasmid. The *ryfp* (GFP-10C mutant, Cubitt *et al.*, 1999) DNA sequence, flanked by *Kpn*I and *BamH*I restriction digest sites, was ligated into pDXA.W501 digested with the same enzymes, to yield the pDXA.rYFP intermediate. The excised *w501* fragment was retained during this stage and subsequently re-ligated into *BamH*I linearised pDXA.rYFP to yield the desired pDXA.rYFP.W501 plasmid.

Prior to a final DNA sequencing check of pDXA.rYFP.W501, the presence and orientation of the *ryfp* and *w501* domains were determined by double restriction digest using the *BsrG*I and *Eco*RI enzymes. The *BsrG*I restriction digest site was unique to the 3' end of *ryfp* (or other FP sequence), while two *Eco*RI restriction digest sites existed towards the 5' end of *w501*. Thus, following the digest, a 575bp DNA fragment signified the presence of the *w501* myosin II domain, while a second DNA fragment of 414bp signified the presence, and correct orientation, of an *ryfp* sequence at the 5' end of the *w501* myosin II domain (**Fig. 3.122**). The remaining plasmid backbone was 8.1kb.

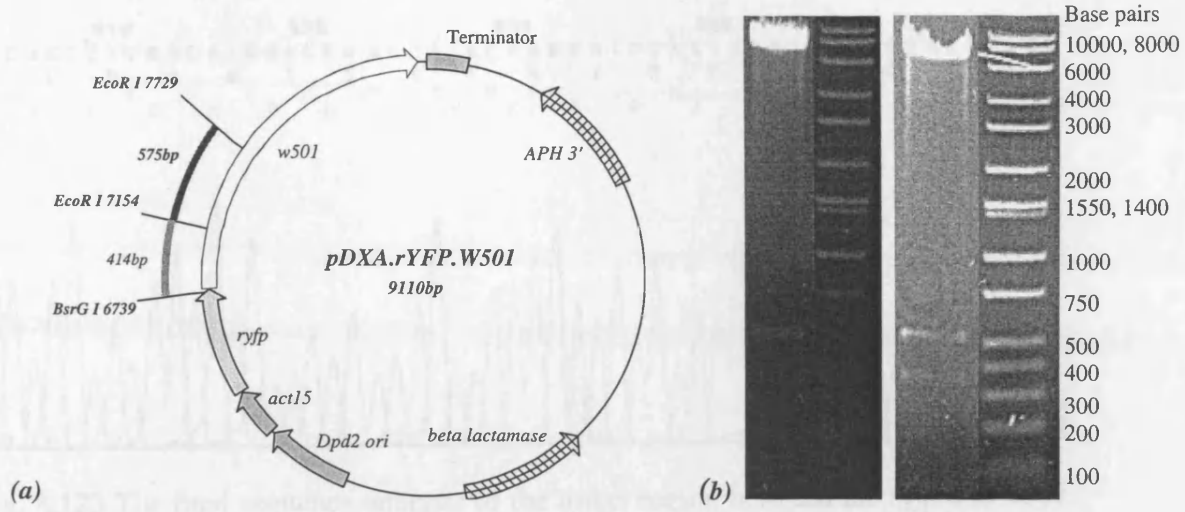


**Fig. 3.122** A DNA check prior to sequencing of the final plasmid contruct. The double restriction digest using the *BsrG*I and *Eco*RI enzymes yielded two small fragments of 414bp and 575bp if the construct contained *ryfp* at the 5' end of *w501* in the correct relative orientation ***(a)***. A standard 5% ethidium bromide agarose gel after double digestion of pDXA.rYFP.W501 gave the result shown ***(b)***.

To determine that there was no linker region between the YFP and W501 domains of pDXA.rYFP.W501, standard DNA sequencing was employed using the *seq3* (downstream, **App 7.2c**) oligonucleotide as a primer. The sequence analysis (**Fig. 3.123**, 3rd translation; shown in red) clearly showed the final residues from the C-terminal end of native GFP (minus the final TSS sequence, *MDELYK**[TSS]***, 916-933) followed immediately by the beginning N-terminal residues of the original W501 domain (minus the very first M residue, *[M]DPIHDR*..., 934+). Thus, the pDXA.rYFP.W501 plasmid construct contained a *w501* sequence with a 5' *ryfp* fused via a four residue deletion from the native sequences.

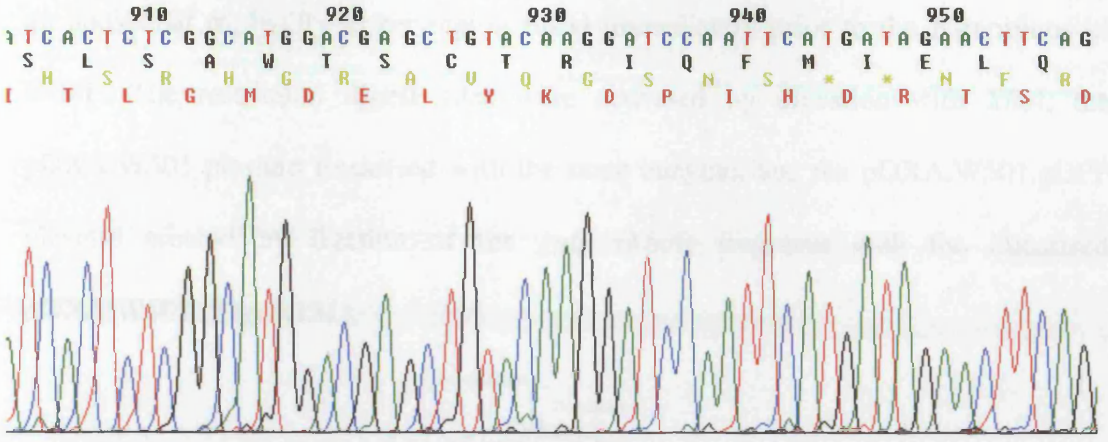


**Fig. 3.123** The final sequence analysis of the linker region between the *ryfp* and *w501* domains of pDXA.rYFP.W501 (3rd translation, shown in red). The final C-terminal residues of native GFP (minus the final TSS sequence, *MDELYK[TSS]*) were followed immediately by the beginning N-terminal residues of W501 (minus the very first M residue, *[M]DPIHDR*), thus indicating that this was the desired pDXA.rYFP.W501 plasmid construct, containing a *w501* sequence with a 5' *ryfp* fused via a four residue deletion from the native sequences.

### *3.13 C-terminal FP-W501 fusion with Gly-Gly-Gly linker (pDXA.W501.gGFP)*

The pDXA.W501.gGFP plasmid construct was designed for the expression of W501 S1-type myosin II, containing an EGFP fluorophore fused to the C-terminal end via a triple-Gly linker (W501.gGFP). The EGFP fluorophore contained 2 mutations from the wildtype GFP (EGFP; F64L, S65T, Cubitt *et al.*, 1999, Patterson *et al.*, 1997, Ward, 1997) to increase the absorbance extinction coefficient 5 fold ($\lambda_{exc}$=488nm, $\lambda_{em}$=507-509nm, $\varepsilon$=55-57x$10^3 M^{-1}cm^{-1}$) while retaining the quantum yield (QY=0.60), thus increasing the overall brightness of the fluorophore. The W501.gGFP protein was intended for use in the development of novel sensitive microscope-based kinetic assays, solution kinetic studies and other control experiments relating to the functionality of novel myosin II fusion proteins with a C-terminal FP-type moiety.

The *ggfp* DNA fragment was amplified by PCR using *XhoGFPUP* (upstream) and *XhoGFDO* (downstream) as primers (**App 7.2d, 7.2e**) and the pet-GFP plasmid as a template. The EGFP domain was thus flanked by *Xho*I restriction digest sites, with

an additional triple-Gly linker region fused immediately prior to the N-terminus of EGFP. The restriction digest sites were activated by digestion with *Xho*I, the pDXA.W501 plasmid linearised with the same enzyme, and the pDXA.W501.gGFP plasmid created by ligation of the *ggfp* (*Xho*I) fragment with the linearised pDXA.W501 (**Fig. 3.131**).

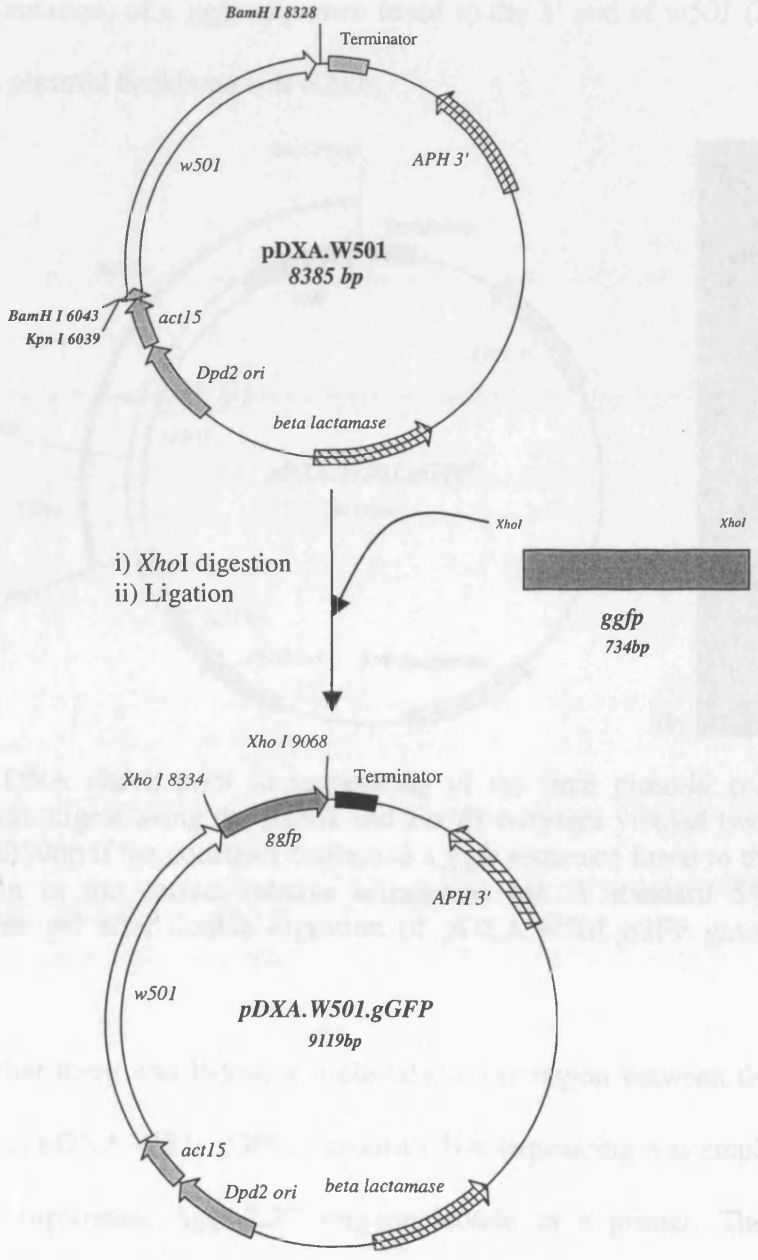


**Fig. 3.131** The construction of the pDXA.W501.gGFP plasmid. The *ggfp* (2 mutations from wildtype, Cubitt *et al.*, 1999, Patterson *et al.*, 1997, Ward, 1997) DNA sequence, flanked by *Xho*I restriction digest sites and including a 5' triple-Gly sequence, was ligated into the *Xho*I linearised pDXA.W501 plasmid construct.

Again, prior to the final sequencing check of pDXA.W501.gGFP, the presence and orientation of the *ggfp* and *w501* domains were determined by a double restriction digest using the *BsrG*I and *EcoR*I enzymes. As before (**see 3.12, Figs. 3.122(*a*)-(*b*)**), following the digest a 575bp DNA fragment signified the presence of the *w501* myosin II domain, however a second DNA fragment of 2050bp signified the presence, and correct orientation, of a *ggfp* sequence fused to the 3' end of *w501* (**Fig. 3.132**). The remaining plasmid backbone was 6.5kb.

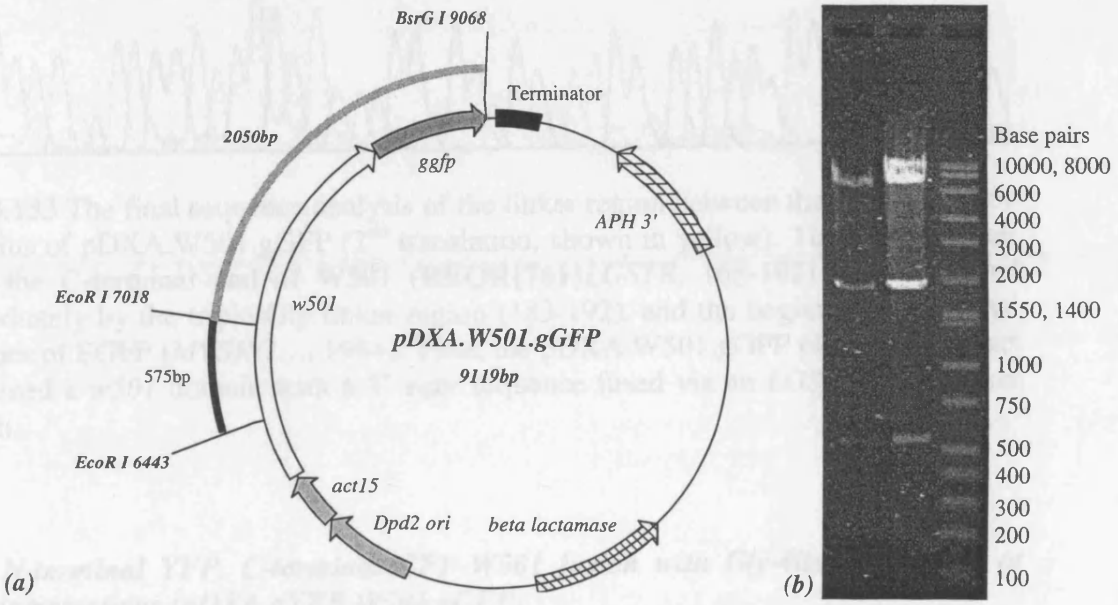


**Fig. 3.132** A DNA check prior to sequencing of the final plasmid contruct. The double restriction digest using the *BsrG*I and *EcoR*I enzymes yielded two fragments of 575bp and 2050bp if the construct contained a *ggfp* sequence fused to the 3' end of a *w501* domain in the correct relative orientation ***(a)***. A standard 5% ethidium bromide agarose gel after double digestion of pDXA.W501.gGFP gave the result shown in ***(b)***.

To determine that there was indeed a triple-Gly linker region between the *ggfp* and *w501* domains of pDXA.W501.gGFP, standard DNA sequencing was employed using the *T706WUP* (upstream, **App 7.2f**) oligonucleotide as a primer. The sequence analysis (**Fig. 3.133**, 2nd translation; shown in yellow) clearly showed the final residues from the C-terminal end of W501 (**REQR{761}***LGSTR*, 168-182, R761 is the final residue of the *Dd* myosin II motor domain) followed by the triple-Gly linker

region (183-192), and the beginning N-terminal residues of native EGFP (*MVSKG*..., 193+). Thus, the pDXA.W501.gGFP plasmid construct contained a *w501* domain with a 3' *egfp* sequence fused via an *LGSTR-GGG* linker region.

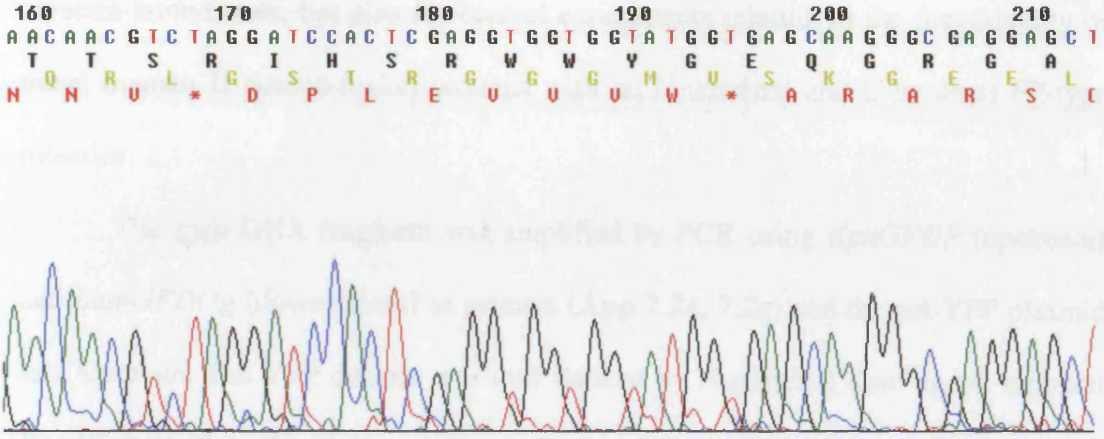


**Fig. 3.133** The final sequence analysis of the linker region between the *ggfp* and *w501* domains of pDXA.W501.gGFP (2nd translation, shown in yellow). The final residues from the C-terminal end of W501 (**REQR{761}***LGSTR*, 168-182) were followed immediately by the triple-Gly linker region (183-192), and the beginning N-terminal residues of EGFP (*MVSKG*..., 193+). Thus, the pDXA.W501.gGFP plasmid construct contained a *w501* domain with a 3' *egfp* sequence fused via an *LGSTR-GGG* linker region.

### *3.14 N-terminal YFP, C-terminal CFP-W501 fusion with Gly-Gly-Gly linkers at both intersections (pDXA.gYFP.W501.gCFP)*

The pDXA.gYFP.W501.gCFP plasmid construct was designed for the expression of W501 S1-type myosin II, containing a YFP fluorophore fused to the N-terminus via a triple-Gly linker, and a CFP fluorophore fused to the C-terminus, also via a triple-Gly linker (gYFP.W501.gCFP). The YFP fluorophore was the GFP-10C variant described previously (**see 3.12,** Cubitt *et al.*, 1999), which contained 4 mutations from wildtype GFP. The CFP fluorophore, however, contained 6 mutations from wildtype GFP (ECFP; F64L, S65T, Y66W, N146I, M153T, V163A, Cubitt *et al.*, 1999) which decreased the excitation and emission wavelength ($\lambda_{exc}$=434 and 452nm, $\lambda_{em}$=476 and 505nm, $\varepsilon$=32.5x10$^{3}$M$^{-1}$cm$^{-1}$, QY=0.4) such that fluorescence resonance energy

transfer was possible between the ECFP and YFP fluorophores as donor and acceptor respectively. The gYFP.W501.gCFP protein was intended primarily for use in FRET studies investigating the kinetics and physical movement of an S1-type myosin II in an actin-bound state, but also for control experiments relating to the functionality of novel myosin II double-fusion proteins with an N-terminal and C-terminal FP-type moieties.

The *gyfp* DNA fragment was amplified by PCR using *KpnGFUP* (upstream) and *BamGFDOg* (downstream) as primers (**App 7.2a, 7.2g**) and the pet-YFP plasmid as a template. The YFP domain was thus flanked by N-terminal *Kpn*I and C-terminal *BamH*I restriction digest sites, with an additional triple-Gly linker region fused to the C-terminal end of YFP. The digest sites were then activated by a double-digestion with *Kpn*I and *BamH*I, the pDXA.W501 plasmid linearised using the same enzymes, and the excised *w501* fragment retained. Ligation of the activated *gyfp* fragment into the linearised pDXA vector yielded the pDXA.gYFP intermediate.

The *gcfp* DNA fragment was amplified by PCR using *GFPBal* (upstream) and *NsiGF2* (downstream) as primers (**App 7.2h, App 7.2i**) and the pet-ECFP plasmid as a template. The ECFP domain was thus flanked by N-terminal *BamH*I and C-terminal *Nsi*I restriction digest sites, with an additional triple-Gly linker region fused to the N-terminal end of ECFP. The digest sites were then activated by a double-digestion with *BamH*I and *Nsi*I, the pDXA.gYFP intermediate linearised using the same enzymes, and the secondary intermediate plasmid vector pDXA.gYFP.gCFP created by ligation of the activated *gcfp* fragment into the linearised pDXA.gYFP. The retained *w501* fragment was then ligated into *BamH*I linearised pDXA.gYFP.gCFP to create the desired pDXA.gYFP.W501.gCFP plasmid (**Fig. 3.141**).

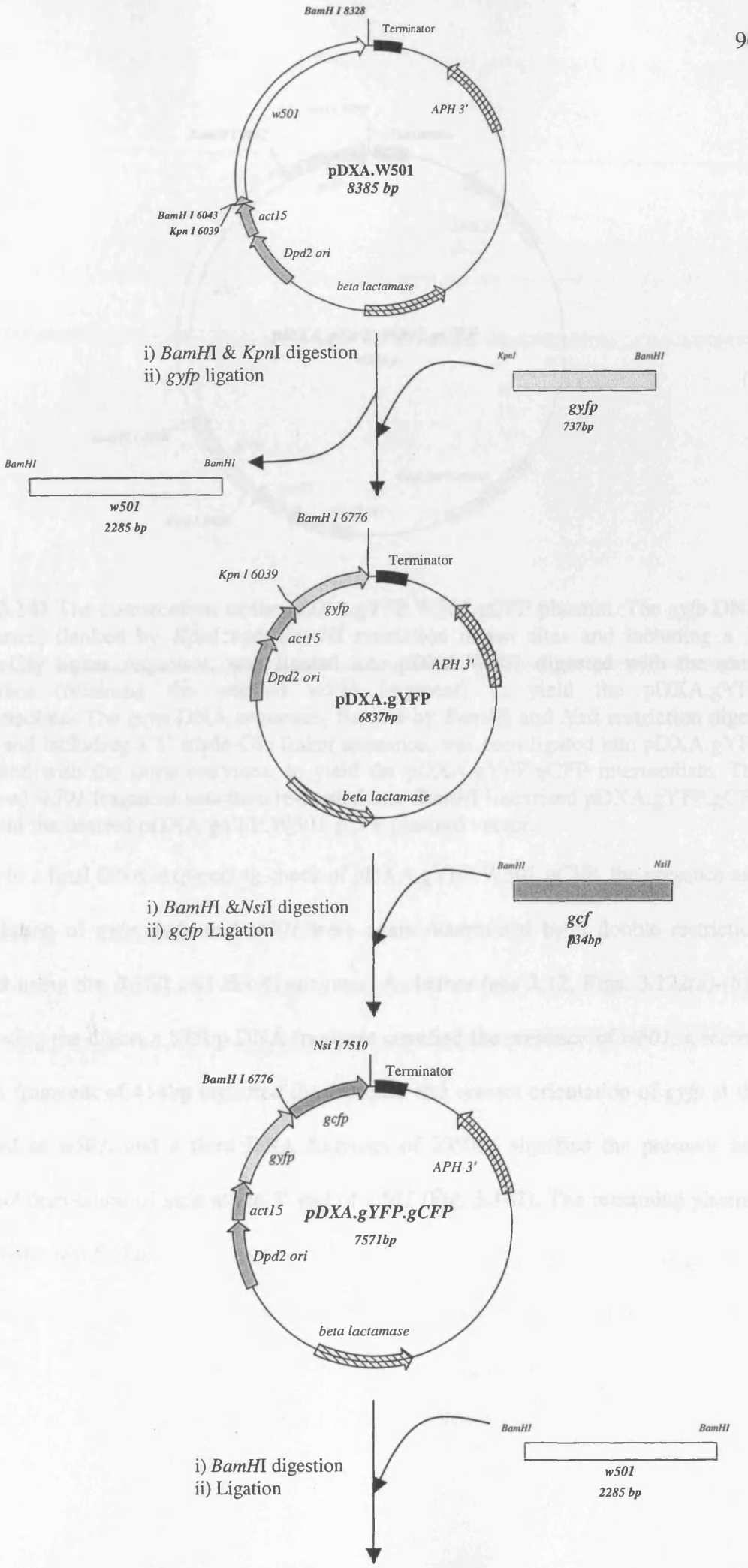
BamH I 8328
Terminator
w501
APH 3'
pDXA.W501
8385 bp
BamH I 6043
Kpn I 6039
act15
Dpd2 ori
beta lactamase
i) BamHI & KpnI digestion
ii) gyfp ligation
KpnI
BamHI
gyfp
737bp
BamHI
BamHI
w501
2285 bp
BamH I 6776
Terminator
Kpn I 6039
gyfp
act15
APH 3'
Dpd2 ori
pDXA.gYFP
6837bp
beta lactamase
i) BamHI &NsiI digestion
ii) gcfp Ligation
BamHI
NsiI
gcf
734bp
Nsi I 7510
Terminator
BamH I 6776
gcfp
gyfp
APH 3'
act15
pDXA.gYFP.gCFP
7571bp
Dpd2 ori
beta lactamase
i) BamHI digestion
ii) Ligation
BamHI
BamHI
w501
2285 bp

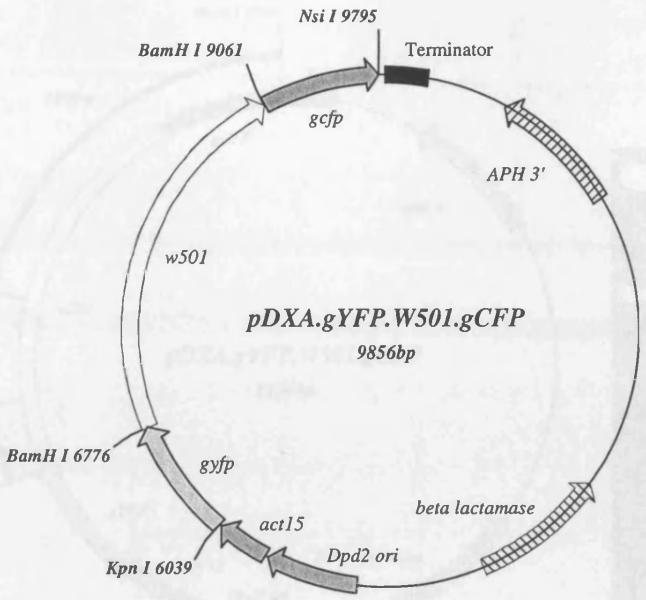


**Fig. 3.141** The construction of the pDXA.gYFP.W501.gCFP plasmid. The *gyfp* DNA sequence, flanked by *Kpn*I and *BamH*I restriction digest sites and including a 3' triple-Gly linker sequence, was ligated into pDXA.W501 digested with the same enzymes (retaining the excised *w501* fragment) to yield the pDXA.gYFP intermediate. The *gcfp* DNA sequence, flanked by *BamH*I and *Nsi*I restriction digest sites and including a 5' triple-Gly linker sequence, was then ligated into pDXA.gYFP digested with the same enzymes, to yield the pDXA.gYFP.gCFP intermediate. The retained *w501* fragment was then re-ligated into *BamH*I linearised pDXA.gYFP.gCFP to yield the desired pDXA.gYFP.W501.gCFP plasmid vector.

Prior to a final DNA sequencing check of pDXA.gYFP.W501.gCFP, the presence and orientation of *gyfp*, *gcfp* and *w501* were again determined by a double restriction digest using the *BsrG*I and *EcoR*I enzymes. As before (**see 3.12, Figs. 3.122*(a)-(b)***), following the digest a 575bp DNA fragment signified the presence of *w501*, a second DNA fragment of 414bp signified the presence and correct orientation of *gyfp* at the 5' end of *w501*, and a third DNA fragment of 2050bp signified the presence and correct orientation of *gcfp* at the 3' end of *w501* (**Fig. 3.142**). The remaining plasmid backbone was 6.8kb.

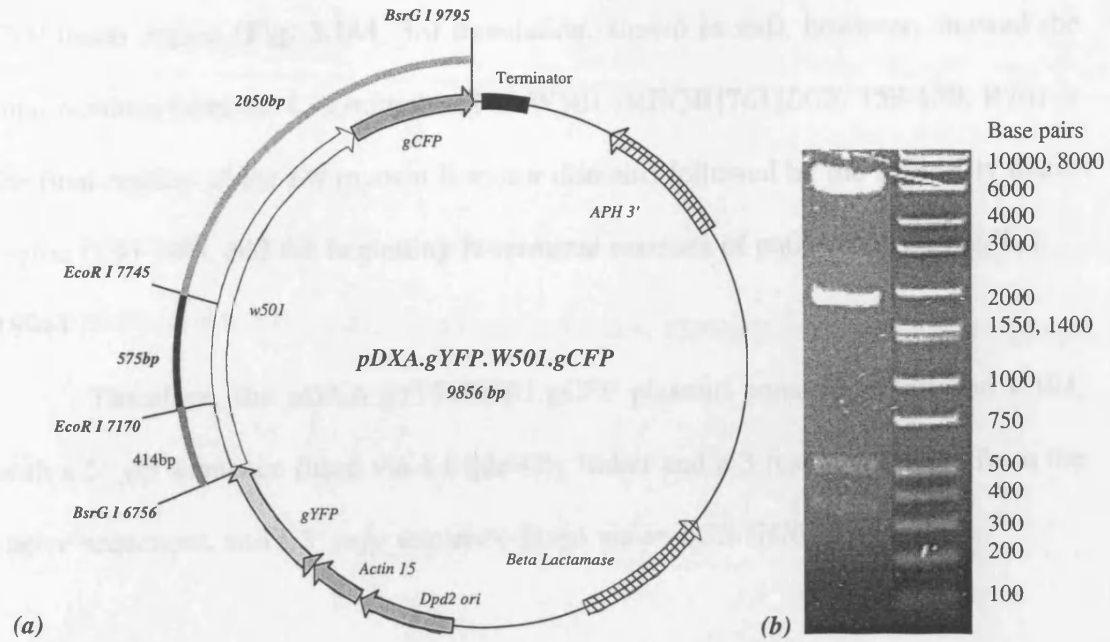


**Fig. 3.142** A DNA check prior to sequencing of the final plasmid contruct. The double restriction digest using the *BsrG*I and *Eco*RI enzymes yielded fragments of 414bp, 575bp and 2050bp if the construct contained *gyfp* and *gcfp* at the 5' and 3' ends of *w501* in the correct relative orientation ***(a)***. A standard 5% ethidium bromide agarose gel after double digestion of pDXA.gYFP.W501.gCFP gave the result shown in ***(b)***.

To determine that there were triple-Gly linker regions between the YFP / CFP domains and the W501 domain of pDXA.gYFP.W501.gCFP, standard DNA sequencing was employed using two separate reactions. The triple-Gly linker region between the N-terminal YFP and the W501 domain of pDXA.gYFP.W501.gCFP was analysed using the *seq3* (downstream, **7.2c**) oligonucleotide as a primer, whereas the triple-Gly linker between the C-terminal CFP and the W501 domain required the *T706WUP* (upstream, **7.2e**) oligonucleotide as a primer.

The sequence analysis of the YFP-W501 linker region (**Fig. 3.143**, 3rd translation, shown in red) clearly showed the final residues from the C-terminal end of native EGFP (again minus the final TSS sequence, *MDELYK[TSS]*, 849-866), followed by a triple-Gly linker (867-875) and the beginning N-terminal residues of the original W501 domain (*MDPIHDR*..., 876+). The sequence analysis of the W501-

CFP linker region (**Fig. 3.144**, 3rd translation, shown in red), however, showed the final residues from the C-terminal end of W501 (**REQR{761}***LGS*, 159-179, R761 is the final residue of the *Dd* myosin II motor domain) followed by the triple-Gly linker region (180-188), and the beginning N-terminal residues of native EGFP (*MVSKG*..., 189+).

Therefore, the pDXA.gYFP.W501.gCFP plasmid construct contained *w501*, with a 5' *yfp* sequence fused via a triple-Gly linker and a 3 residue deletion from the native sequences, and a 3' *ecfp* sequence fused via an *LGS-GGG* linker region.

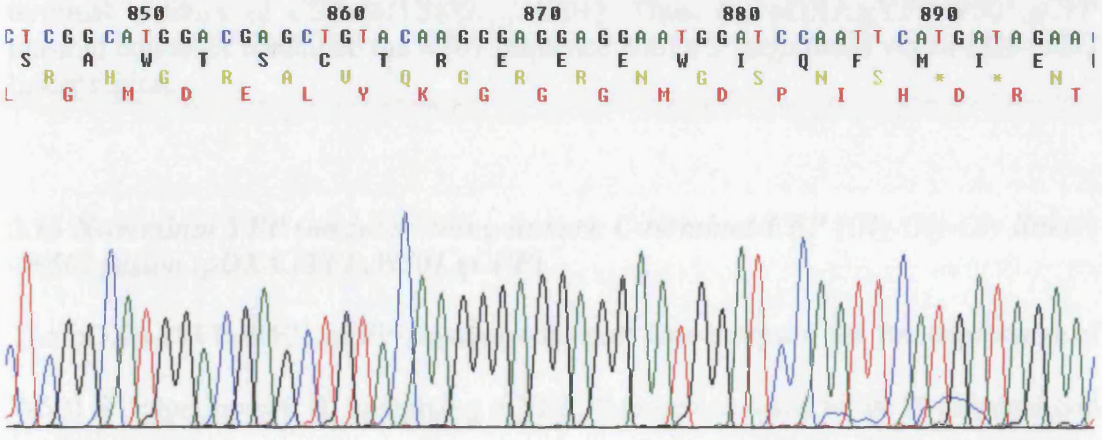


**Fig. 3.143** The final sequence analysis of the linker region between the W501 and YFP domains of pDXA.gYFP.W501.gCFP (3rd translation, shown in red). The final C-terminal residues of YFP (minus the final TSS sequence, *MDELYK**[TSS]***, 849-866) were followed immediately by triple-Gly linker region (867-875), and the beginning N-terminal residues of W501 (*MDPIHDR*..., 876+). Thus, the pDXA.gYFP.W501.gCFP plasmid construct containe the *w501* sequence with a 5' *gyfp* fused via a *GGG* linker region, with a 3 residue deletion from the native sequences.

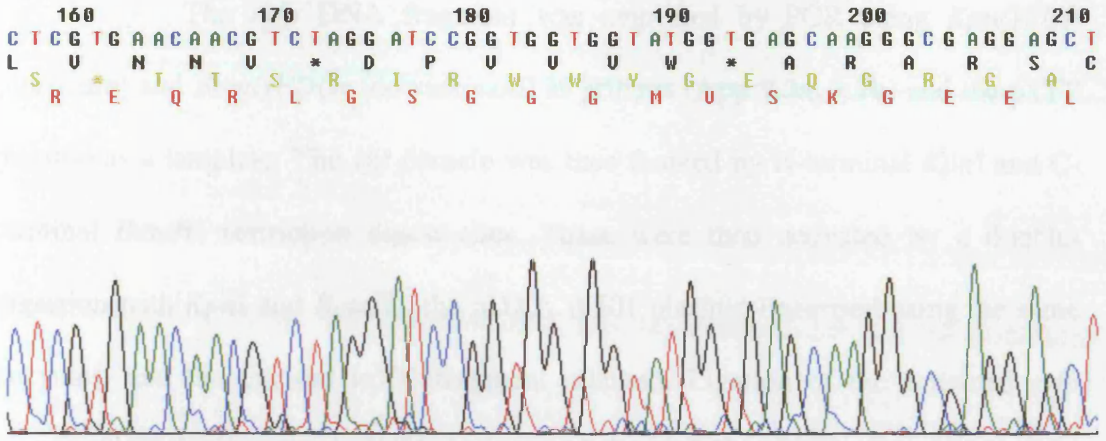


**Fig. 3.144** The final sequence analysis of the linker region between the W501 and CFP domains of pDXA.gYFP.W501.gCFP (3rd translation, shown in red). The final residues from the C-terminal end of W501 (**REQR{761}***LGS*, 159-179) were followed immediately by the triple-Gly linker region (180-188), and the beginning N-terminal residues of CFP (*MVSKG*..., 189+). Thus, the pDXA.gYFP.W501.gCFP plasmid construct contained the *w501* sequence with a 3' *gcfp* fused via an *LGS-GGG* linker region.

### *3.15 N-terminal YFP (no intervening linker), C-terminal CFP (Gly-Gly-Gly linker) -W501 fusion (pDXA.rYFP.W501.gCFP)*

The pDXA.rYFP.W501.gCFP plasmid construct was designed for the expression of W501 S1-type myosin II, containing a YFP fluorophore fused to the N-terminal end with no intervening linker region, and a CFP fluorophore fused to the C-terminal end via a triple-Gly linker (rYFP.W501.gCFP). The YFP and CFP fluorophores were the same variants as described in the previous section (GFP-10C YFP, eCFP, **3.14,** Cubitt *et al.*, 1999).

The rYFP.W501.gCFP protein itself was intended, as with gYFP.W501.gCFP, for use in FRET studies investigating the kinetics of physical movement of an S1-type myosin II in an actin-bound state, but also for control experiments relating to the functionality of novel myosin II double-fusion proteins with an N-terminal and a C-terminal FP-type moiety.

The *ryfp* DNA fragment was amplified by PCR using *KpnGFUP* (upstream) and *BamGFDOr* (downstream) as primers (**App 7.2a, 7.2b**) and the pYFP plasmid as a template. The *yfp* domain was thus flanked by N-terminal *Kpn*I and C-terminal *BamH*I restriction digest sites. These were then activated by a double-digestion with *Kpn*I and *BamH*I, the pDXA.W501 plasmid linearised using the same enzymes, and the excised *w501* fragment retained. Ligation of the activated *ryfp* fragment into the linearised pDXA vector yielded the pDXA.rYFP intermediate.

The *gcfp* DNA fragment was amplified by PCR using *GFPBa1* (upstream) and *NsiGF2* (downstream) as primers (**App. 7.2h, 7.2i**) and the pECFP plasmid as a template. The ECFP domain was thus flanked by N-terminal *BamH*I and C-terminal *Nsi*I restriction digest sites, with an additional triple-Gly linker region fused to the N-terminal end of ECFP. The digest sites were then activated by a double-digestion with *BamH*I and *Nsi*I, the pDXA.rYFP intermediate linearised using the same enzymes, and the secondary intermediate plasmid vector pDXA.rYFP.gCFP created by ligation of the activated *gcfp* fragment into the linearised pDXA.rYFP. The retained *w501* fragment was then ligated into *BamH*I linearised pDXA.rYFP.gCFP to create the desired pDXA.rYFP.W501.gCFP plasmid (**Fig. 3.151**).

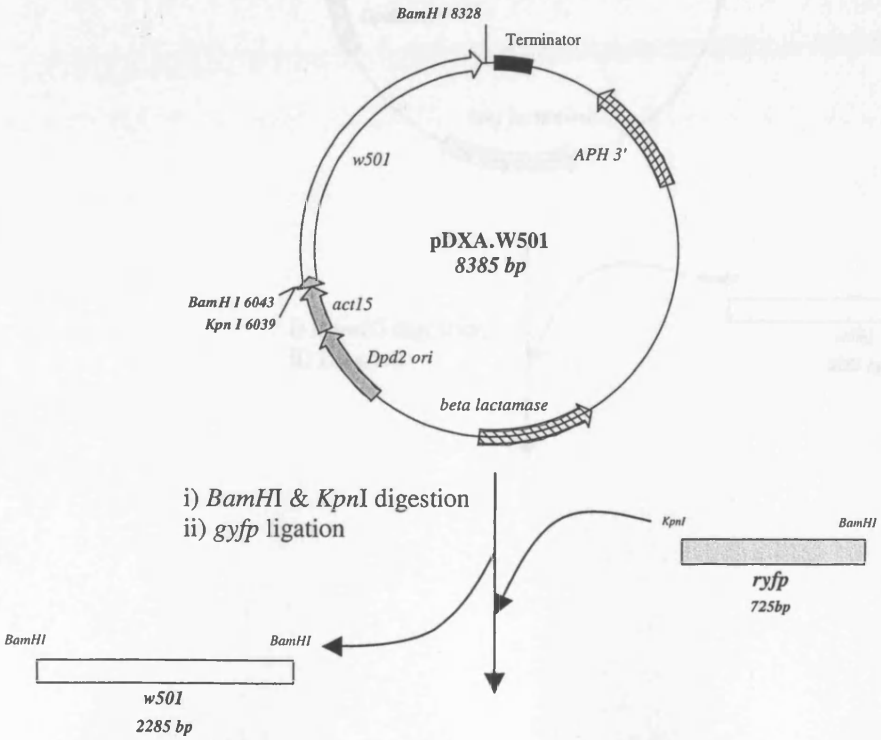

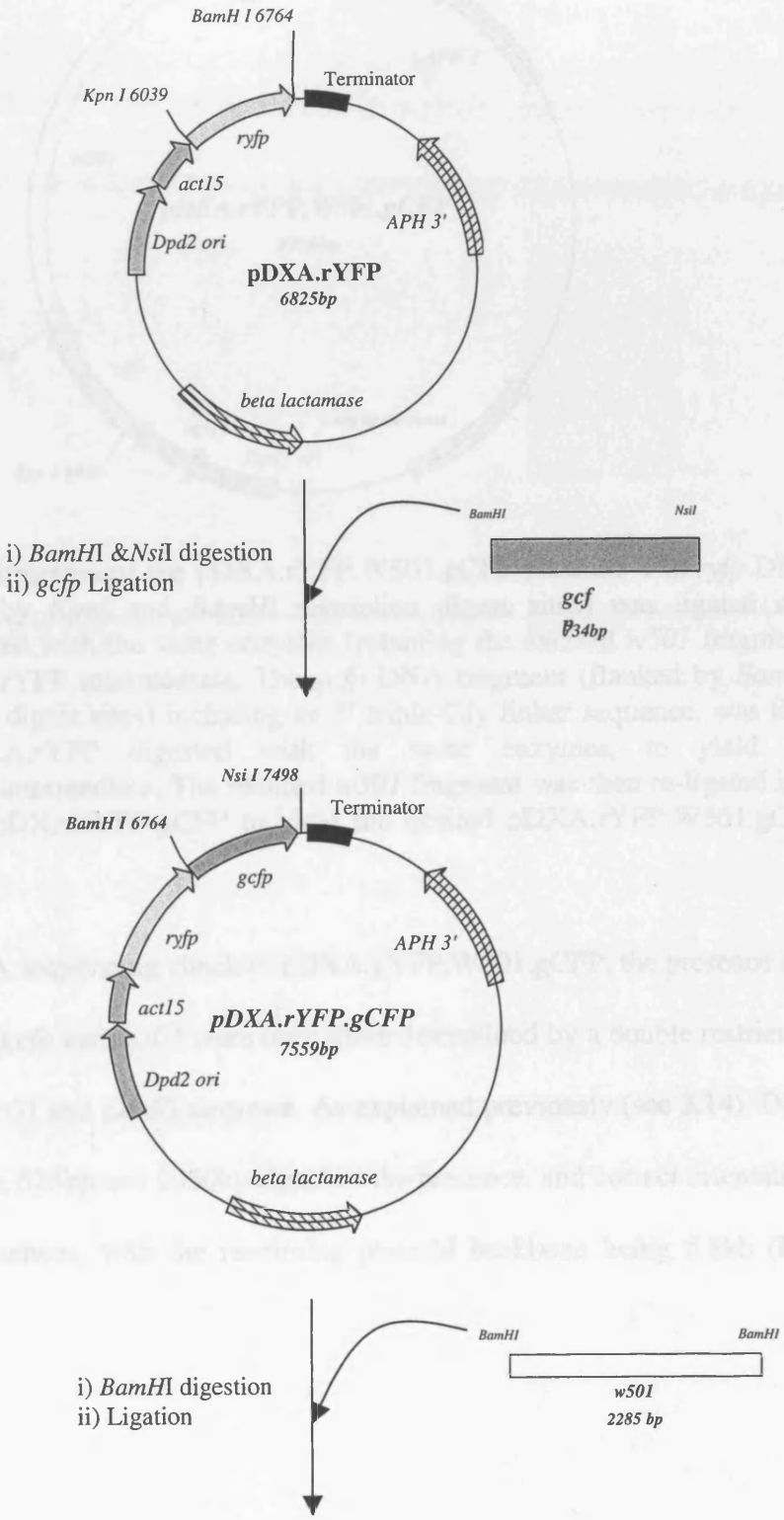
BamH I 6764
Terminator
Kpn I 6039
ryfp
act15
APH 3'
Dpd2 ori
pDXA.rYFP
6825bp
beta lactamase
i) BamHI &NsiI digestion
ii) gcfp Ligation
BamHI
NsiI
gcf
734bp
Nsi I 7498
Terminator
BamH I 6764
gcfp
ryfp
APH 3'
act15
pDXA.rYFP.gCFP
7559bp
Dpd2 ori
beta lactamase
i) BamHI digestion
ii) Ligation
BamHI
BamHI
w501
2285 bp

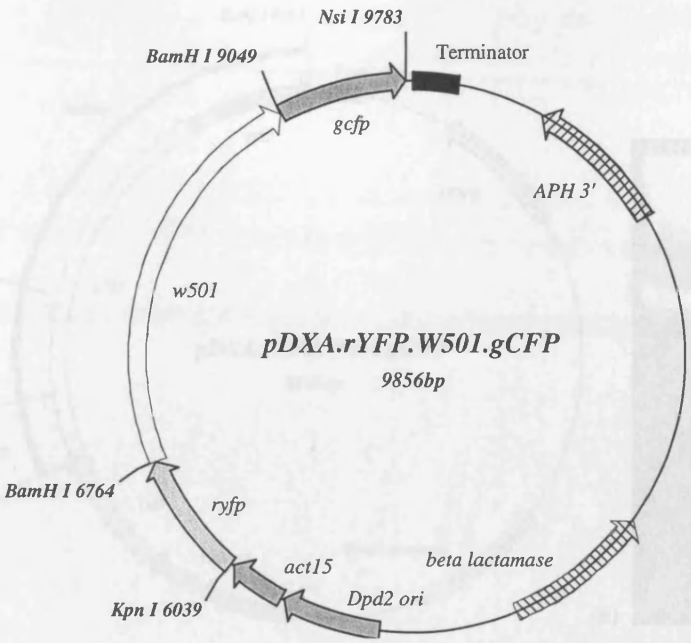


**Fig. 3.151** The construction of the pDXA.rYFP.W501.gCFP plasmid. The *ryfp* DNA fragment (flanked by *Kpn*I and *BamH*I restriction digest sites) was ligated into pDXA.W501 digested with the same enzymes (retaining the excised *w501* fragment) to yield the pDXA.rYFP intermediate. The *gcfp* DNA fragment (flanked by *BamH*I and *Nsi*I restriction digest sites) including an 3' triple-Gly linker sequence, was then ligated into pDXA.rYFP digested with the same enzymes, to yield the pDXA.rYFP.gCFP intermediate. The retained *w501* fragment was then re-ligated into *BamH*I linearised pDXA.rYFP.gCFP to yield the desired pDXA.rYFP.W501.gCFP plasmid vector.

Prior to a final DNA sequencing check of pDXA.gYFP.W501.gCFP, the presence and orientation of *ryfp*, *gcfp* and *w501* were once more determined by a double restriction digest using the *BsrG*I and *EcoR*I enzymes. As explained previously (**see 3.14**), DNA fragments of 414bp, 575bp and 2050bp signified the presence, and correct orientation, of these three sequences, with the remaining plasmid backbone being 6.8kb (**Fig. 3.152**).

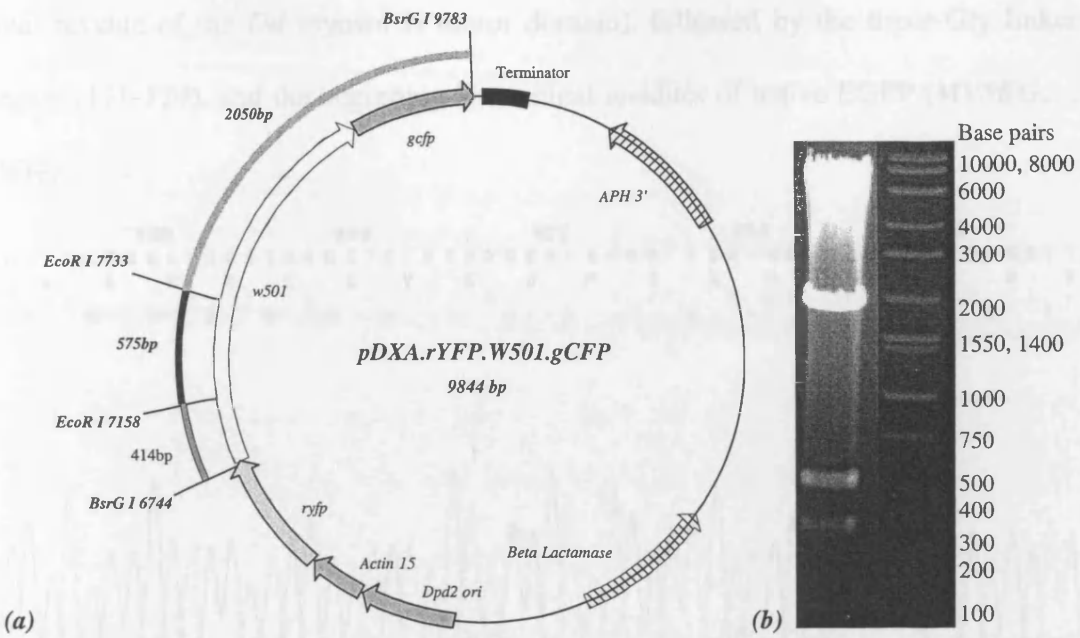


**Fig. 3.152** A DNA check prior to sequencing of the final plasmid contruct. The double restriction digest using the *BsrG*I and *EcoR*I enzymes yielded fragments of 414bp, 575bp and 2050bp if the construct contained *ryfp* and *gcfp* fused to the 5' and 3' ends of *w501* in the correct relative orientation ***(a)***. A standard 5% ethidium bromide agarose gel after double digestion of pDXA.gYFP.W501.gCFP gave the result shown in ***(b)***.

To determine that there was *(a)* no triple-Gly linker region between the N-terminal YFP and W501 domains of pDXA.gYFP.W501.gCFP, and *(b)* an *LGS-GGG* linker region between the C-terminal CFP and W501 domains, standard DNA sequencing was again employed utilising the oligonucleotides described previously (**3.14**) as primers.

The sequence analysis (**Fig. 3.153**, 1st translation; shown in black) clearly showed the final residues from the C-terminal end of native EGFP (once more minus the final TSS sequence, *MDELYK[TSS]*, 901-918) followed immediately by the beginning N-terminal residues of the original W501 domain (minus the very first M residue, *[M]DPIHDR*..., 919+). The sequence analysis of the W501-CFP linker region (**Fig. 3.154**, 3rd translation, shown in red) showed, as before (**3.14**), the final residues from the C-terminal end of W501 (**REQR{761}***LGS*, 150-170, R761 is the

final residue of the *Dd* myosin II motor domain), followed by the triple-Gly linker region (171-179), and the beginning N-terminal residues of native EGFP (*MVSKG*..., 180+).

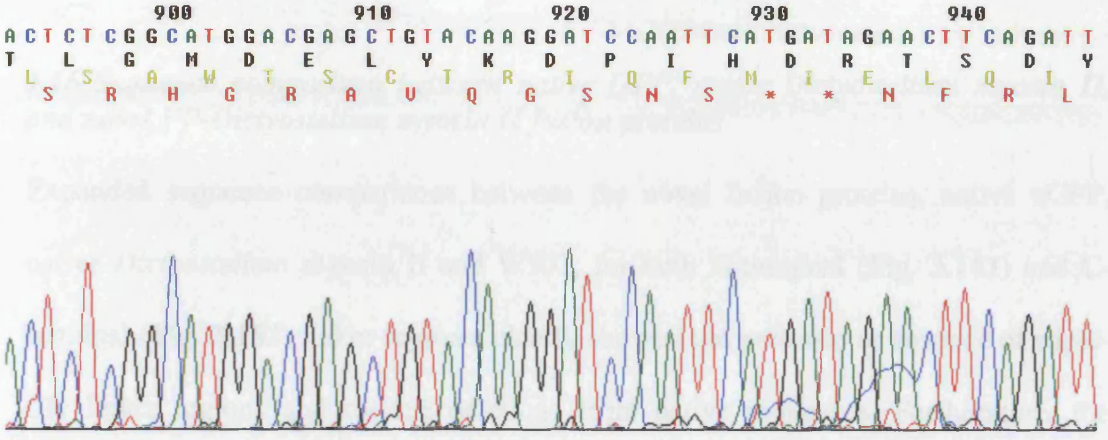

**Fig. 3.153** The final sequence analysis of the linker region between the W501 and YFP domains of pDXA.rYFP.W501.gCFP (1st translation, shown in black). The final C-terminal residues of YFP (minus the final TSS sequence, *MDELYK[TSS],* 901-918) were followed immediately by the beginning N-terminal residues of W501 (minus the very first M residue *[M]DPIHDR*..., 919+). Thus, the pDXA.rYFP.W501.gCFP plasmid construct contained the *w501* sequence with a 5' *ryfp* fused via a 4 residue deletion from the native sequences.

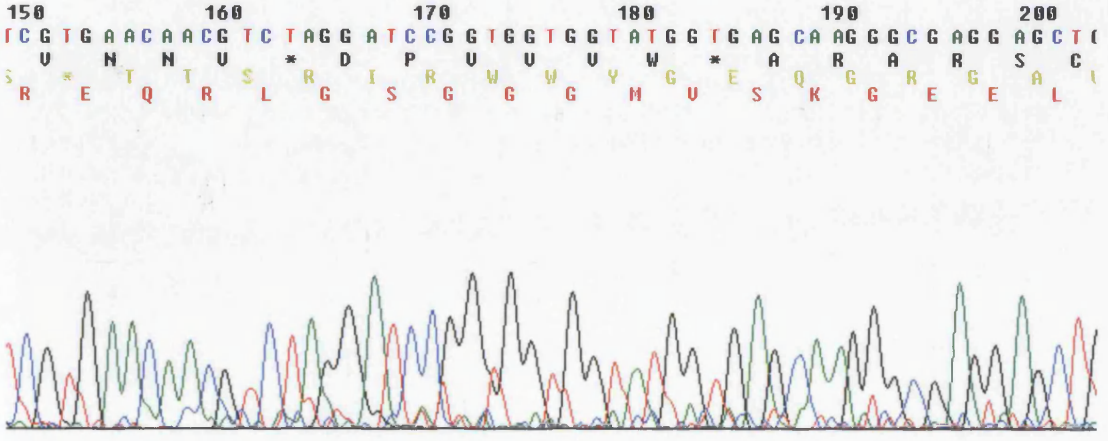

**Fig. 3.154** The final sequence analysis of the linker region between the W501 and CFP domains of pDXA.rYFP.W501.gCFP (3rd translation, shown in red). The final residues from the C-terminal end of W501 (**REQR{761}***LGS*, 150-170) were followed immediately by the triple-Gly linker region (171-179), and the beginning N-terminal residues of CFP (*MVSKG*..., 180+). Thus, the pDXA.rYFP.W501.gCFP plasmid construct contained the *w501* sequence with a 3' *gcfp* fused via an *LGS-GGG* linker region.

Therefore, the pDXA.rYFP.W501.gCFP plasmid construct contained *w501*, with a 5' *ryfp* fused via a 4 residue deletion from the native sequences, and a 3' *gcfp* fused via an *LGS-GGG* linker region.

### *3.16 Sequence comparison between native GFP, native Dictyostelium myosin II, and novel FP-Dictyostelium myosin II fusion proteins*

Expanded sequence comparisons between the novel fusion proteins, native eGFP, native *Dictyostelium* myosin II and W501, for both N-terminal (**Fig. 3.161**) and C-terminal (**Fig. 3.162**) linker regions, clearly showed the presence or absence of triple-*Gly* linker regions and residue deletions from native sequences. Furthermore, the comparisons also confirm the specific presence of *(a)* N-terminal YFP via the inherent T203Y mutation (-44), and *(b)* W501 via *i)* the original N2D cloning artefact and *ii)* the mutation of a tryptophan residue to phenylalanine (W36F).

```
                    -70         -60         -50         -40         -30
Original            ------------------------------------------------------
W501                ------------------------------------------------------
gYFP.W501.gCFP      HNIEDGSVQLADHYQQNTPIGDGPVLLPDNHYLSYQSALSKDPNEKRDHMV
W501.gGFP           ------------------------------------------------------
rYFP.W501.gCFP      HNIEDGSVQLADHYQQNTPIGDGPVXLPDNHYLSYQSALSKDPNEKRDHMV
rYFP.W501           HNIEDGSVQLADHYQQNTPIGDGPVLLPDNHYLSYQSALSKDPNEKRDHMV
eGFP                HNIEDGSVQLADHYQQNTPIGDGPVLLPDNHYLSTQSALSKDPNEKRDHMV

                          -20         -10          1          10          20
Original            ------------------------------MNPIHDRTSDYHKYLKVKQGDSD
W501                ------------------------------DPIHDRTSDYHKYLKVKQGDSD
gYFP.W501.gCFP      LLEFVTAAGITLGMDELYK---GGG--MDPIHDRTSDYHKYLKVKQGDSD
W501.gGFP           ------------------------------DPIHDRTSDYHKYLKVKQGDSD
rYFP.W501.gCFP      LLEFVTAAGITLGMDELYK----------DPIHDRTSDYHKYLKVKQGDSD
rYFP.W501           LLEFVTAAGITLGMDELYK----------DPIHDRTSDYHKYLKVKQGDSD
eGFP                LLEFVTAAGITLGMDELYKTSS-------------------------------

                          30          40
Original            LFKLTVSDKRYIWYNPDPKERD
W501                LFKLTVSDKRYIFYNPDPKERD
gYFP.W501.gCFP      LFKLTVSDKRYIFYNPDPKERD
W501.gGFP           LFKLTVSDKRYIFYNPDPKERD
rYFP.W501.gCFP      LFKLTVSDKRYIFYNPDPKERD
rYFP.W501           LFKLTVSDKRYIFYNPDPKERD
eGFP                ----------------------
```

**Fig. 3.161** A sequence comparison of the novel FP-*Dictyostelium* myosin II fusion proteins, the *Dictyostelium* S1-type myosin II head domain mutant W501, native EGFP and native *Dictyostelium* myosin, with respect to the N-terminal linker regions between the W501 and FP-type domains. Point mutations from native sequences are denoted in blue underscore, whereas null sequence data are denoted in red strikethrough.

```
                          740         750         760
Original            DPEQYRFGITKIFFRAGQLARIEEAREQR--------------------
W501                DPEQYRFGITKIFFRAGQLARIEXAREQR-LGS----------------
gYFP.W501.gCFP      DPEQYRFGITKIFFRAGQLARIEEAREQR-LGS---GGG-MVSKGEEL
W501.gGFP           DPEQYRFGITKIFFRAGQLARIEEAREQR-LGSTR-GGG-MVSKGEEL
rYFP.W501.gCFP      DPEQYRFGITKIFFRAGQLARIEEAREQR-LGS---GGG-MVSKGEEL
rYFP.W501           DPEQYRFGITKIFFRAGQLARIEEAREQR--------------------
eGFP                ------------------------------------------MVSKGEEL

Original            ----------------------------
W501                ----------------------------
gYFP.W501.gCFP      FTGVVPILVELDGDVNGHKFSVSGEGEGDA
W501.gGFP           FTGVVPILVELDGDVNGHKFSVSGEGEGDA
rYFP.W501.gCFP      FTGVVPILVELDGDVNGHXFSVSGEGXGDA
rYFP.W501           ----------------------------
eGFP                FTGVVPILVELDGDVNGHKFSVSGEGEGDA
```

**Fig. 3.162** A sequence comparison of the novel FP-*Dictyostelium* myosin II fusion proteins, the *Dictyostelium* S1-type myosin II head domain mutant W501, native EGFP and native *Dictyostelium* myosin, with respect to the C-terminal linker regions between the W501 and FP-type domains. Null sequence data are denoted in red strikethrough.

## *3.2 Basic characterisation of the novel fusion proteins*

### *3.21 Yields and purity of final purified proteins*

Following sequence analysis of the novel plasmid constructs, the plasmid DNA was transformed into *Dictyostelium discoideum*, grown to a specific size and density, typically 5 litres of $5x10^6$-$1x10^7$ cells/ml, and the novel proteins extracted and purified over a $Ni^{2+}$-NTA affinity column. The expression levels varied considerably depending on the efficiency of the transformation of plasmid DNA into *Dictyostelium*, the age of the culture which was to be harvested (the younger the culture, the greater the expression), the density of the culture at the time of harvesting (ideally $7.5x10^6$ cells/ml), and the type and size of the protein being expressed. Factors other than the expression level which affected the final yield were the age of the $Ni^{2+}$-NTA column and the stringency of the imidazole washes used to remove non-specifically (non-*His*-tagged) bound proteins.

Typically, the yield for the W501 protein was 0.3-0.4mg/g of cells, with the single FP fusion proteins (rYFP.W501, W501.gGFP) showing a slightly lower yield of 0.2-0.3mg/g of cells (**Fig. 3.211**), presumably due to the strain that expressing the extra FP moiety placed on the cell. Following this trend, the double FP fusion proteins (gYFP.W501.gCFP, rYFP.W501.gCFP) showed a still lower yield of 0.1-0.2mg/g of cells.

The purity of the fusion proteins in solution was approximated by comparison of the concentration as calculated by two separate methods. Firstly, a standard Bradford assay was used to determine the total protein concentration of the final purified solution. Secondly, via analysis of a standard absorption spectra and utilising the published extinction coefficients (Tsien, 1998, **see 3.22**), the concentration of the FP-myosin II fusion protein could be calculated. The discrepancy between these two

concentration calculations thus gave an indication to the purity of the protein solution. The purities themselves varied considerably, but were largely dependent on the age and quality of the $Ni^{2+}$-NTA column, and the stringency of the imidazole washes used. The W501 protein was reportedly obtained at a purity of between 80-90%, using graded imidazole washes of up to 85μM. The single FP-myosin II fusion proteins were washed at a lower imidazole concentration (60μM) in order to increase the overall yield, with the double FP-myosin II fusion proteins requiring a still lower imidazole wash (50μM) in order to obtain sufficient quantities of the protein. This affected the purity of the final protein solutions accordingly, yielding 75-90% and 60-80% purity variations respectively (**Fig. 3.211**). It is important to note, however, that due to the high dilution factors involved and the selective nature of the experiments carried out on the FP-myosin II fusion proteins, this lowering of the purity did not adversely affect the results of the majority of the key investigations. Furthermore, SDS-PAGE analysis of the purified proteins confirmed that there were no main contaminants present (**Fig. 3.212**).

These purities are only approximate values, due to *(a)* Bradford Reagent assays being <100% accurate, and *(b)* The pH dependence of fluorescence for FP-type proteins, especially in the case of YFP, which at pH7.0-7.5 may be ~10% lower than the extinction coefficient (given for pH8.0, Tsien, 1998).

| | *Yield (mls, μM)* | *Yield (mg/g of cells)* | *Purity (%) ε/B* |
|---|---|---|---|
| **W501** | 4-6, 15-20 | 0.3-0.4 | 80-90 |
| **rYFP.W501** | 5-7, 5-8 | 0.2-0.3 | 75-90 |
| **W501.gGFP** | 5-8, 5-8 | 0.2-0.3 | 75-90 |
| **gYFP.W501.gCFP** | 4-6, 3-5 | 0.1-0.2 | 60-80 |
| **rYFP.W501.gCFP** | 4-5, 3-5 | 0.1-0.2 | 60-80 |

**Fig. 3.211** A table showing the comparative typical yields and purities for the novel fusion proteins, with regard to the original W501 protein. Purity values were calculated from the ratio of the concentrations derived from absorbance spectra (using published extinction coefficients, ε) and Bradford Reagent assays (B).

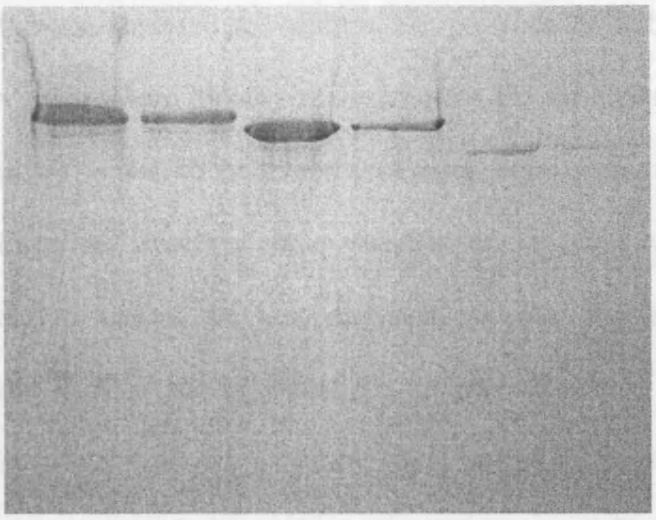

**Fig. 3.212** SDS-PAGE (8% acrylamide) analysis of the final purified proteins. The first two lanes (left to right) represent rYFP.W501.gCFP, the following two lanes rYFP.W501 and the final two W501. This type of result confirmed the absence of any single contaminant in the purified protein samples.

### *3.22 Absorbance, emission and excitation spectra for FP-myosin fusion proteins*

Standard assays to assess the absorption spectra of purified proteins were employed to determine; *(a)* the viability of the fluorophore, as the fluorescence from GFP is radically altered by incorrect folding of the protein, *(b)* the specific type of FP moiety present, and *(c)* the concentration of the purified protein by utilising the extinction coefficient for each particular fluorophore as published by (Tsien, 1998). With respect to the analysis of protein concentration, background corrections to compensate for impurities, and residual background gradients were consistently taken into consideration. Furthermore, due to the 1:1 stoichiometry of fluorophore to myosin ATPase unit, the protein concentration calculations were often combined with the results from standard Bradford assays to estimate the purity of the preparations.

Excitation and emission spectra were then obtained for full characterisation of the novel proteins, and for confirmation of the type and viability of the fluorophore by further comparison of the spectra with published data for the native FP proteins

(Tsien, 1998, **Fig 3.221**). Furthermore, the spectra for gYFP.W501.gCFP and rYFP.W501.gCFP were analysed to confirm the presence of a functional FRET pairing. Emission spectra were initially analysed using the main peak wavelength of the absorbance spectra as this, in the majority of cases, corresponds to the main peak of the excitation spectra. However some variation of excitation wavelengths was usually undertaken to ensure the best emission spectrum for a novel protein. Similarly, the main peak of the emission spectra was utilised to obtain the most accurate excitation trace, with both spectra being points of reference for further studies with regard to stopped-flow and fluorescence microscopy filter assignments.

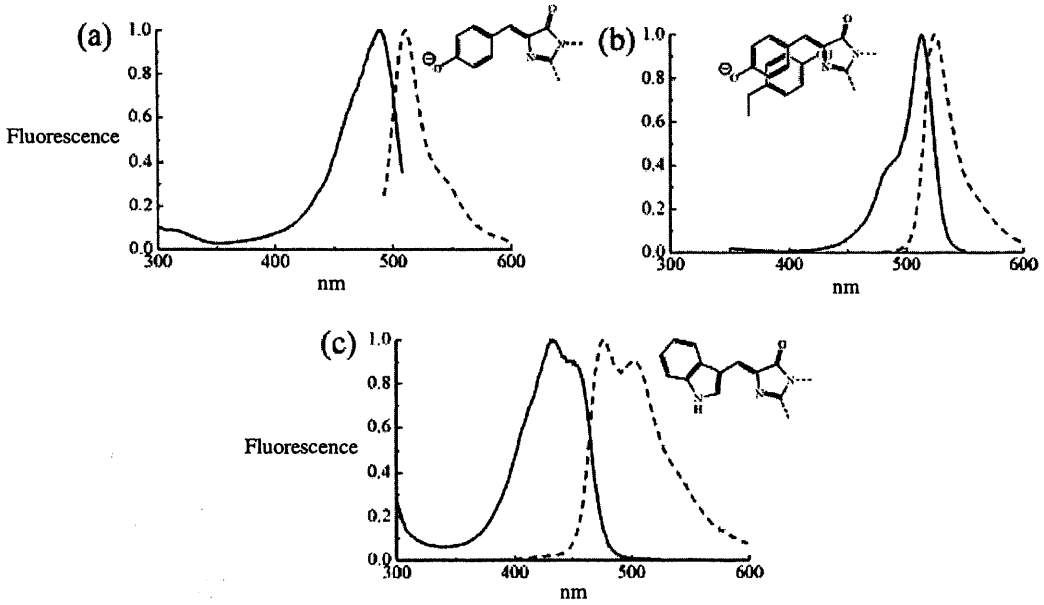


**Fig. 3.221** The published emission and excitation spectra (Tsien, 1998) for *(a)* eGFP ($\lambda_{exc}$=488nm, $\lambda_{em}$=507-509nm), *(b)* YFP (GFP-10C mutant, $\lambda_{exc}$=514nm, $\lambda_{em}$=527nm) and *(c)* eCFP ($\lambda_{exc}$=434 and 452nm, $\lambda_{em}$=476 and 505nm). The structures shown represent the chromophore believed to give rise to each set of spectra.

The absorbance spectrum for the single N-terminal YFP fusion protein rYFP.W501 (**Fig. 3.222**) was characterised by a strong, sharp single peak at 514nm, with a small, slightly broader shoulder, approximately 50% of the intensity of the main peak, from 480-495nm. The form and wavelength of these major peaks was characteristic with that of native YFP.

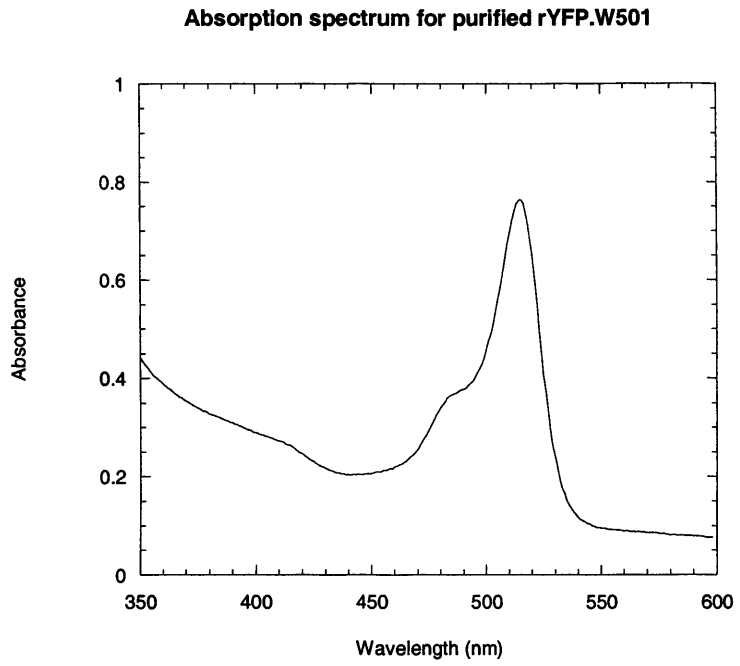


**Fig. 3.222** A typical absorption spectra for purified rYFP.W501. Measurements were taken using a Varian Cary 50 Probe UV visible spectrophotometer, a 1cm path length, with the purified protein in standard assay buffer (20mM HEPES, 40mM NaCl, 2mM $MgCl_2$, pH7.5, with freshly added 5mM βME, 0.01% w/v $NaN_3$). The main peak was 514nm, with a small shoulder approximately 50% of the main peak intensity from 480-495nm. The form and wavelength of the main peaks was characteristic of native YFP (GFP-10C mutant).

The excitation spectra ($\lambda_{em}$=530nm), strongly resembled that of the absorption spectra with a strong, sharp single peak at 514nm, plus a small, slightly broader shoulder approximately 50% of the main peak intensity from 480-495nm. The emission spectra ($\lambda_{ex}$=515nm), was characterised by a single sharp peak at 527nm, followed by a very broad shoulder, approximately 25% of the main peak intensity, from 555-580nm (**Fig. 3.223**). These spectra were indicative of a fully viable, correctly folded and active YFP protein (10C mutant, **Fig. 3.221**), thus the fusion to the N-terminal end of the W501 myosin-II domain did not adversely affect the function of the fluorophore and further studies could be undertaken.

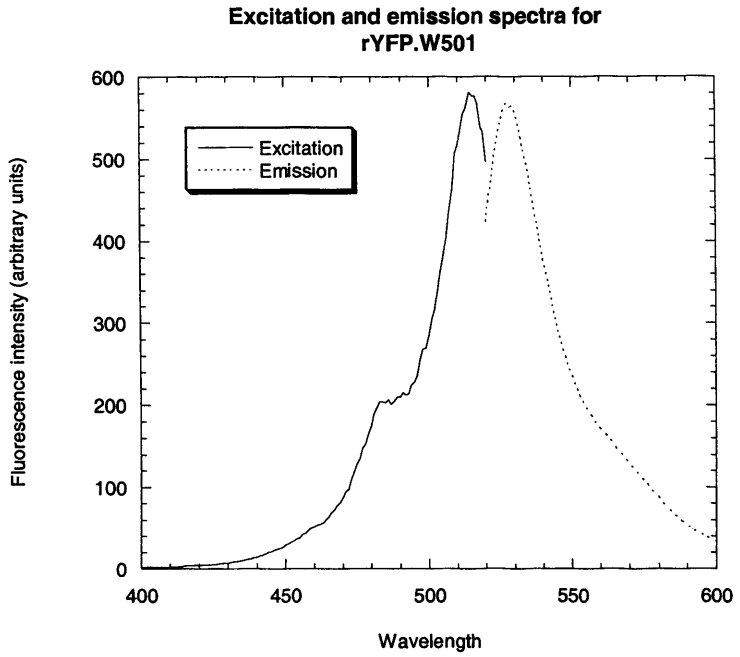


**Fig. 3.223** Typical excitation and emission spectra for rYFP.W501. Measurements were taken using a Varian Cary Eclipse fluorescence spectrophotomoter, a 1cm path length, $\lambda_{em}$=530nm, $\lambda_{ex}$=515nm, with a standard dilution of 1μM protein in standard assay buffer (20mM HEPES, 40mM NaCl, 2mM $MgCl_2$, pH7.5, with freshly added 5mM βME, 0.01% w/v $NaN_3$). The excitation spectra contained a sharp, single peak at 514nm, with a broad shoulder approximately 50% of the main peak intensity from 480-495nm. The emission spectra was characterised by a single sharp peak at 527nm, with a very broad shoulder, approximately 25% of the main peak intensity, from 555-580nm. These spectra were indicative of fully functional YFP.

The absorbance spectra for the single, C-terminal GFP fusion protein W501.gGFP (**Fig. 3.224**) was characterised by a single peak centred around 488-490nm, with a broad shoulder approximately 60-80% of the main peak intensity from 450-475nm. Due to the considerably lower extinction coefficient of GFP (EGFP, ε=55-57x$10^3M^{-1}cm^{-1}$) relative to YFP (GFP-10C, ε=83.4x$10^3M^{-1}cm^{-1}$) the background was usually considerably higher in GFP absorbance spectra relative to those of the other novel proteins. However, although the form of the peak could be difficult to distinguish with accuracy, the wavelength of the main peak was characteristic with that of native GFP.

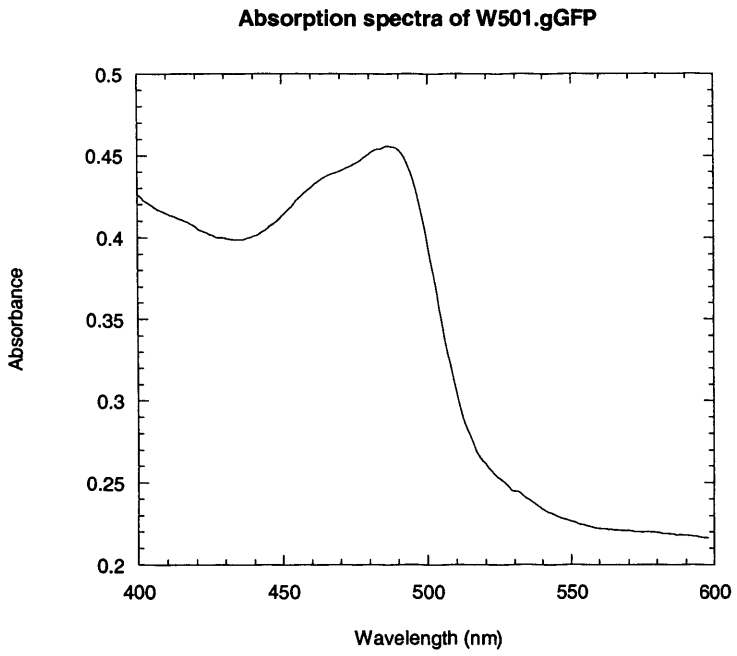


**Fig. 3.224** A typical absorption spectra for W501.gGFP. Measurements were taken using a Varian Cary 50 Probe UV visible spectrophotometer, a 1cm path length, with the purified protein in standard assay buffer (20mM HEPES, 40mM NaCl, 2mM $MgCl_2$, pH7.5, with freshly added 5mM βME, 0.01% w/v $NaN_3$). The main peak was centred around 488-490nm, with a broad shoulder approximately 60-80% of the main peak intensity from 450-475nm. The form and wavelength of the main peaks was characteristic of native GFP.

The excitation spectra ($\lambda_{em}$=510nm, **Fig. 3.225**) was similar to that of the absorbance spectra, albeit a considerably clearer trace with a negligible background. The main peak was again centred around 488-490nm, with a broad shoulder approximately 60-80% of the main peak intensity from 450-475nm. The emission spectra ($\lambda_{ex}$=490nm), however, was characterised by a single sharp peak at 508nm, followed by a very broad shoulder, approximately 30% of the main peak intensity, from 540-560nm. These spectra were indicative of a fully viable, correctly folded and active GFP protein (**Fig. 3.221**), thus the fusion to the C-terminal end of the W501 myosin-II domain did not aversely affect the function of the fluorophore and further studies could be undertaken.

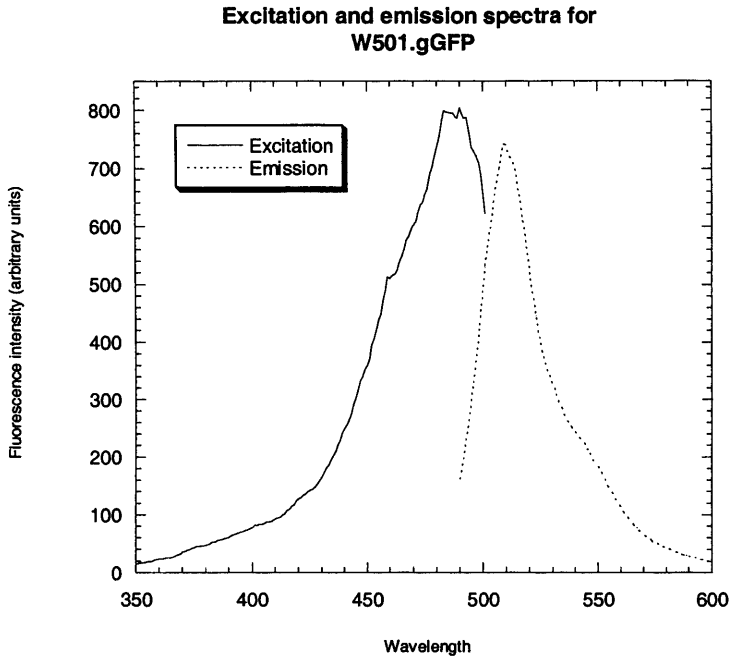


**Fig. 3.225** Typical excitation and emission spectra for W501.gGFP. Measurements were taken using a Varian Cary Eclipse fluorescence spectrophotomoter, a 1cm path length, $\lambda_{em}$=510nm, $\lambda_{ex}$=490nm, with a standard dilution of 1μM protein in standard assay buffer (20mM HEPES, 40mM NaCl, 2mM $MgCl_2$, pH7.5, with freshly added 5mM βME, 0.01% w/v $NaN_3$). The excitation spectra contained a single peak centred around 488-490nm, with a broad shoulder approximately 60-80% of the main peak intensity from 450-475nm. The emission spectra was characterised by a single sharp peak at 508nm, with a very broad shoulder, approximately 30% of the main peak intensity, from 540-560nm. These spectra were indicative of fully functional GFP.

The absorbance spectra for the double, N-terminal YFP, C-terminal CFP fusion proteins gYFP.W501.gCFP and rYFP.W501.gCFP (**Fig. 3.226**) were characterised by several main peaks. A sharp, single peak at 514nm, with a small, slightly broader shoulder from 480-495nm corresponded to the YFP absorbance peaks observed previously from rYFP.W501 (**Fig. 3.222**). However, two other minor peaks approximately 40-50% of the main peak intensity, at 435nm and 455nm respectively, denoted the presence of a CFP fluorophore. Although the form and wavelength of the major peaks corresponded very well to those of native YFP and the wavelength of the

two minor peaks were characteristic of native CFP, the two minor peaks were of an uneven intensity opposite to the characteristic form of native CFP. This was presumably a compound effect from the overlap of the YFP absorbance trace, thereby increasing the absorbance for 455nm.

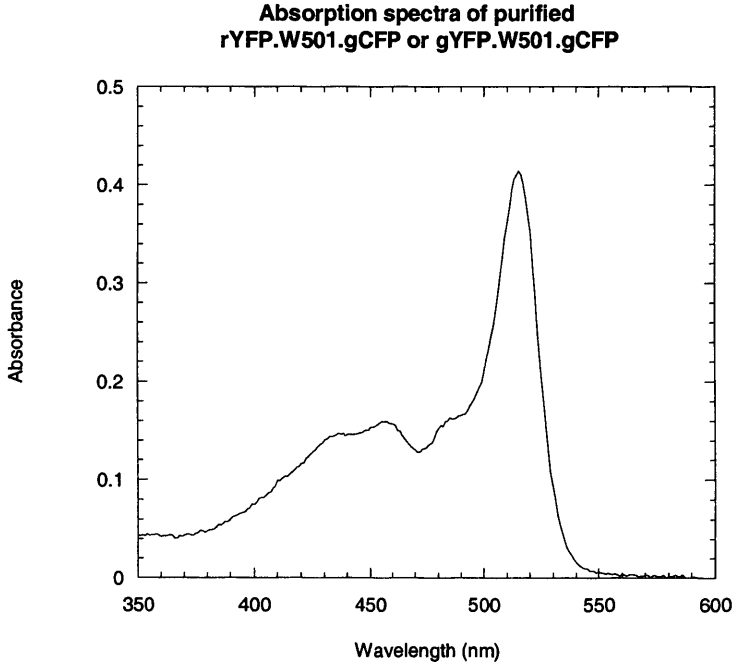


**Fig. 3.226** A typical absorption spectra for gYFP.W501.gCFP and rYFP.W501.gCFP. Measurements were taken using a Varian Cary 50 Probe UV visible spectrophotometer, a 1cm path length, with the purified protein in standard assay buffer (20mM HEPES, 40mM NaCl, 2mM $MgCl_2$, pH7.5, with freshly added 5mM βME, 0.01% w/v $NaN_3$). A sharp, single peak at 514nm, with a small, slightly broader shoulder from 480-495nm was characteristic in form and wavelength of native YFP. However, the two minor peaks, approximately 40-50% of the main peak intensity, at 435nm and 455nm, were characteristic of native CFP in wavelength, but not in form.

The excitation spectra for gYFP.W501.gCFP and rYFP.W501.gCFP were analysed using both the emission wavelength for YFP directly ($\lambda_{emYFP}$=535nm), and also the emission wavelength for CFP ($\lambda_{emCFP}$=510nm). The YFP emission wavelength yielded an excitation spectra containing a strong, sharp single peak at 516nm, plus a small, slightly broader shoulder approximately 50% of the main peak intensity from 480-495nm (**Fig. 3.227**) indicative of fully viable, correctly folded and active YFP (**Fig.**

**3.221**). However, fluorescence was noticeably increased in the 400-475nm range (*c.f.* **Fig. 3.223**).

The CFP emission wavelength yielded an excitation spectra of a very low intensity overall (~10% of YFP emission), but similar in form and wavelength to that of the absorption spectra (**Fig. 3.226**), with two minor peaks at 435nm and 456nm, plus a third minor peak at 485nm correlating to the shoulder peak of the YFP excitation spectra.

The increase in YFP emission due to excitation from 400-475nm (approximately the range of a CFP excitation peak), together with the very low intensity of CFP emission as a whole, gave evidence to suggest a working FRET pairing between the CFP and YFP fluorophores.

As with the excitation spectra, the emission spectra for gYFP.W501.gCFP and rYFP.W501.gCFP were also analysed using both YFP and CFP excitation wavelengths ($\lambda_{exYFP}$=480nm, $\lambda_{exCFP}$=420nm). Direct excitation of YFP yielded an emission spectra characterised by a single sharp peak at 527nm, followed by a very broad shoulder, approximately 25% of the main peak intensity, from 555-580nm (**Fig. 3.228**). This spectra was indicative of a fully viable, correctly folded and active YFP protein (GFP-10C mutant, **Fig. 3.221**). Excitation of CFP yielded an emission spectra characterised by two main peaks at 476nm and 527nm. The minor peak at 476nm, approximately 45% of the main peak intensity, correlated to the lower emission peak of native CFP. The major peak at 527nm, however, corresponded exactly to the major emission peak of YFP (10C mutant). Due to the fact that the YFP fluorophore could not be directly excited by the incident light used to excite CFP ($\lambda_{exCFP}$=420nm), it

follows that FRET must have occurred from the excited CFP, to the YFP, which subsequently emitted fluorescence at a wavelength of 527nm.

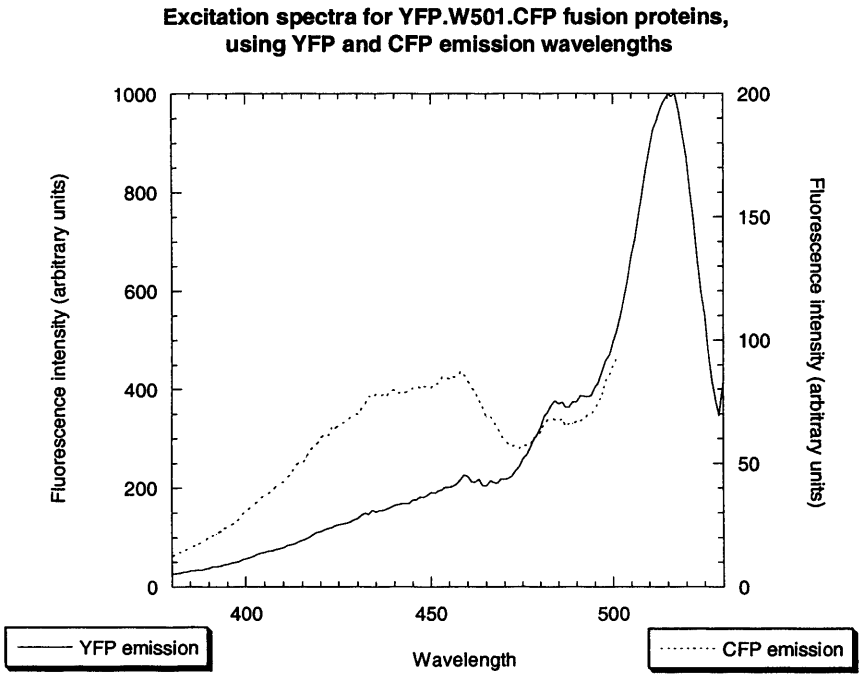


**Fig. 3.227** Typical excitation spectra for gYFP.W501.gCFP and rYFP.W501.gCFP using emission wavelengths for both CFP ($\lambda_{emCFP}$=510nm) and YFP ($\lambda_{emYFP}$=535nm). Measurements were taken using a Varian Cary Eclipse fluorescence spectrophotomoter, a 1cm path length, with a standard dilution of 1μM protein in standard assay buffer (20mM HEPES, 40mM NaCl, 2mM $MgCl_2$, pH7.5, with freshly added 5mM βME, 0.01% w/v $NaN_3$). Monitoring YFP emission yielded an excitation spectra indicative of native YFP, with a major peak at 516nm and a shoulder from 480-495nm, plus a significant increase in fluorescence with excitation from 400-475nm (CFP excitation range). Monitoring CFP emission yielded a very low intensity spectra (~10% of YFP emission intensity), with peaks at 435nm, 456nm, and 485nm. These results suggested that FRET was occurring between the two fluorophores.

In conclusion, the excitation and emission spectra for the double FP fusion proteins confirmed the presence of fully functional YFP and CFP fluorophores, existing in close enough proximity to form a viable FRET pairing.

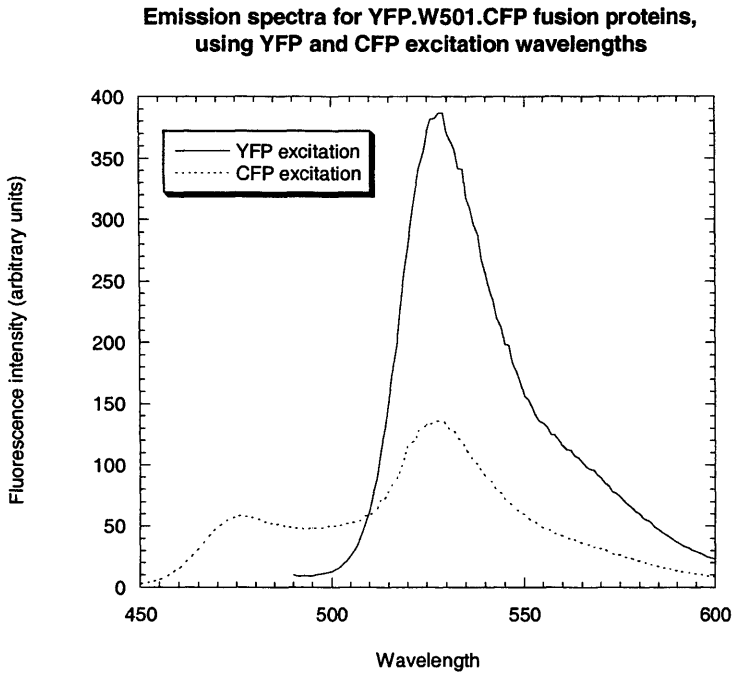


**Fig. 3.228** Typical emission spectra for gYFP.W501.gCFP and rYFP.W501.gCFP using excitation wavelengths for both CFP ($\lambda_{exCFP}$=420nm) and YFP ($\lambda_{exYFP}$=480nm). Measurements were taken using a Varian Cary Eclipse fluorescence spectrophotomoter, a 1cm path length, with a standard dilution of 1μM protein in standard assay buffer (20mM HEPES, 40mM NaCl, 2mM $MgCl_2$, pH7.5, with freshly added 5mM βME, 0.01% w/v $NaN_3$). Direct YFP excitation yielded an emission spectra indicative of native YFP, with single sharp peak at 527nm and a broad shoulder from 555-580nm. Direct excitation of CFP yielded an emission spectra characterised by two main peaks at 476nm (CFP emission) and 527nm (YFP emission). Thus, the two fluorophores formed a viable FRET pairing.

Therefore, to summarise, the fusion of a FP-type moiety to the N-terminal, C-terminal, or both termini of the W501 *Dictyostelium* myosin II domain did not unduly affect the folding or functionality of the fluorophore as a whole. Furthermore, the fusion of an eCFP and YFP (GFP-10C) to opposite termini of the W501 domain formed a viable FRET pairing. Thus, the fluorescence from these novel fusion proteins could be monitored to observe the movement and function of the W501 domain, provided that the fluorophores themselves did not alter the functionality of the W501 protein.

### *3.23 ATPase activity, actin binding, and subsequent ATP-induced dissociation of FP-myosin fusion proteins*

Having established the presence of functional fluorophores and a viable FRET pairing within the fusion proteins, the myosin II motor domain itself required basic characterisation. The binding, hydrolysis, and release of ATP is a strict requirement of a functional myosin motor, and thus the rate of turnover of ATP was monitored for each of the FP-myosin II fusion proteins.

The ATP turnover rate ($k_{cat}$) was determined in several different ways, including a steady-state NADH enzyme linked assay (**Fig. 3.231**), or more commonly by performing a limited turnover assay with a 3-5 fold excess of ATP. The latter of these studies were usually carried out under stopped-flow conditions by monitoring either *(a) Trp* fluorescence in the absence of F-actin (**Fig. 3.232**), as the W501 construct contained only a single *Trp* at the 501 position which has been shown to be sensitive to ATP binding and hydrolysis (Malnasi-Csizmadia *et al.*, 2001a, Malnasi-Csizmadia *et al.*, 2001b, Malnasi-Csizmadia *et al.*, 2000), or *(b)* light scattering at 365nm in the presence of F-actin (**Fig. 3.233**), as the increased mass of the actomyosin complex caused a significant increase in the degree of scattering relative to that of the dissociated proteins themselves. The effect of actin-activation of the myosin ATPase was negated in the light scattering analysis by using 40mM NaCl and low actin (1μM) concentrations.

The enzyme linked assay involved the regeneration of hydrolysed ATP via a reaction which converted NADH to NAD (**Fig. 3.231**). Therefore, as NADH absorbs strongly at 340nm, whereas NAD has virtually no absorbance at this particular wavelength, the production of ADP via hydrolysis of ATP by the FP-myosin II fusion proteins could be monitored by time-based spectroscopic analysis of the reduction rate of NADH.

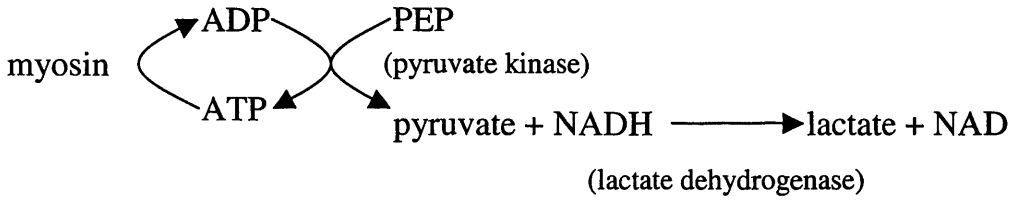


**Fig. 3.231** An enzyme-linked assay was used to determine the ATP turnover rate of novel *Dictyostelium* myosin-II fusion proteins. ATP, hydrolysed by myosin to ADP, is regenerated by the conversion of phosphoenolpyruvate (PEP) to pyruvate. Pyruvate and NADH are subsequently converted to lactate and NAD by lactate dehydrogenase. Thus, as NADH absorbs strongly at 340nm whereas NAD does not, the rate of ATP hydrolysis (thus the rate of ADP formation) can be monitored using spectrophotometric techniques, being directly proportional to NAD formation.

The $k_{cat}$ of W501.gGFP using an enzyme-linked assay usually proved to be between $0.035s^{-1}$ and $0.05s^{-1}$ following purity corrections (**Fig. 3.232**). This correlates well with the published $k_{cat}$ for W501 itself (~0.05s-1, Malnasi-Csizmadia *et al.*, 2000).

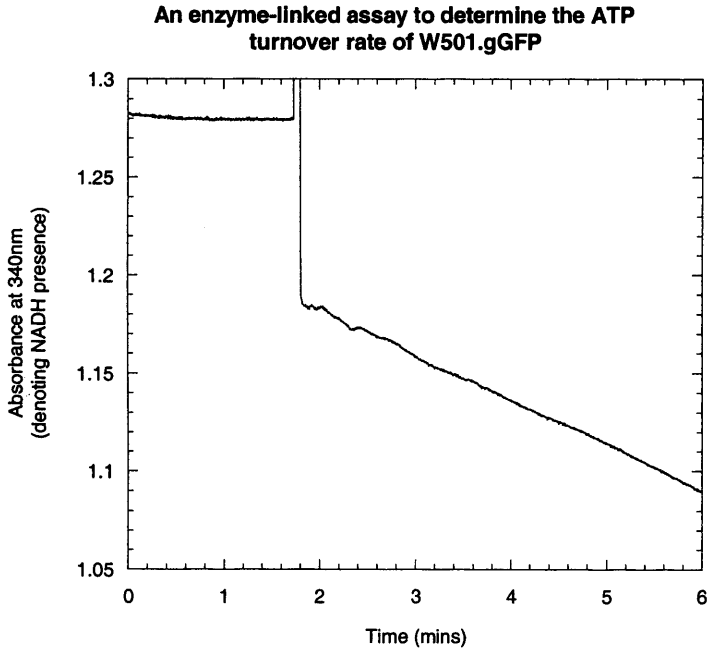


**Fig. 3.232** An enzyme linked assay to determine the $k_{cat}$ for W501.gGFP. Time based absorbance at 340nm was monitored using a Varian Cary 50 Probe UV visible spectrophotometer, using 1μM W501.gGFP diluted in standard assay buffer (20mM HEPES, 40mM NaCl, 2mM $MgCl_2$, pH7.5, with freshly added 5mM βME, 0.01% w/v $NaN_3$), 1mM ATP, 200μM NADH, 400μM PEP, 10U/μl pyruvate kinase, 20U/μl lactate dehydrogenase. The gradient of the slope (-0.0116 /min) yielded a $k_{cat}$ of $0.041s^{-1}$ following concentration corrections for purity.

Using *Trp* fluorescence or light scattering ($\lambda_{ex}$=365nm), under stopped flow conditions, to monitor the $k_{cat}$ for FP-myosin II fusion proteins yielded considerably more consistent results, varying between $k_{cat}$ of 0.042-0.062$s^{-1}$ for most proteins (**Figs 3.233, 3.234**). Typically, a 2.5–fold excess of ATP (2.5μM) was mixed with 1μM (reaction chamber concentrations) of the FP-myosin II fusion protein, yielding a half time of 40-60s.

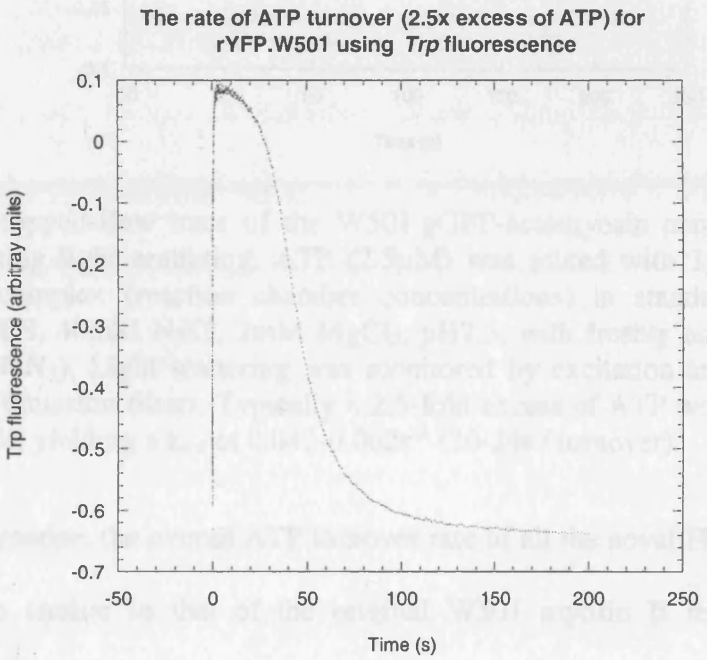


| *Protein* | *ATPase rate ($k_{cat}$)* |
|---|---|
| *W501.gGFP* | 0.050 ± 0.008 |
| *rYFP.W501* | 0.054 ± 0.008 |
| *rYFP.W501.gCFP* | 0.049 ± 0.007 |
| *gYFP.W501.gCFP* | 0.055 ± 0.004 |

**Fig. 3.233** *(top)* Stopped-flow trace of the rYFP.W501-actomyosin complex with ATP, monitored using tryptophan fluorescence. ATP (2.5μM) was mixed with 1μM rYFP.W501 actomyosin complex (reaction chamber concentrations) in standard assay buffer (20mM HEPES, 40mM NaCl, 2mM $MgCl_2$, pH7.5, with freshly added 5mM βME, 0.01% w/v $NaN_3$). Tryptophan fluorescence was monitored by excitation at 295nm and the emission selected with UG11 and WG320 filters. Typically a 2.5-fold excess of ATP would yield a half-time of 40-60s, yielding a $k_{cat}$ of 0.042-0.062$s^{-1}$ (20-24s / turnover). *(bottom)* A table comparison of $k_{cat}$ values for the novel fusion proteins.

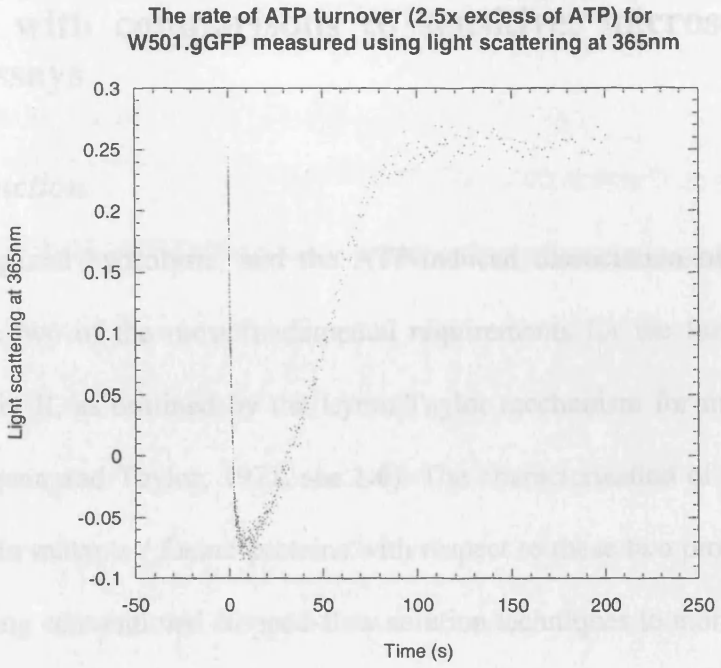


**Fig. 3.234** Stopped-flow trace of the W501.gGFP-actomyosin complex with ATP, monitored using light scattering. ATP (2.5μM) was mixed with 1μM W501.gGFP actomyosin complex (reaction chamber concentrations) in standard assay buffer (20mM HEPES, 40mM NaCl, 2mM $MgCl_2$, pH7.5, with freshly added 5mM βME, 0.01% w/v $NaN_3$). Light scattering was monitored by excitation at 365nm with no selection via emission filters. Typically a 2.5-fold excess of ATP would yield a half-time of 40-60s, yielding a $k_{cat}$ of 0.042-0.062$s^{-1}$ (20-24s / turnover).

Thus, to summarise, the overall ATP turnover rate of all the novel FP-fusion proteins proved to be similar to that of the original W501 myosin II mutant (~0.05$s^{-1}$). Therefore, the fusion of a FP moiety to either or both of the N- or C-termini of the W501 myosin II domain did not appear to adversely affect the function of the myosin motor with regards to ATP binding, hydrolysis, and release. Thus, further studies could be carried out on the FP-myosin II fusion proteins under the assumption that they were fully functional W501 myosin motors.

# 4 - Kinetic studies of the FP-myosin II fusion proteins in solution, with comparisons to sensitive, microscope based kinetic assays

## *4.1 Introduction*

ATP binding and hydrolysis, and the ATP-induced dissociation of an actomyosin complex are two of the most fundamental requirements for the functionality of an active myosin II, as outlined by the Lymn-Taylor mechanism for mechanochemical coupling (Lymn and Taylor, 1971, **see 1.6**). The characterisation of novel myosin II motor domain mutants / fusion proteins with respect to these two processes, has been achieved using conventional stopped-flow solution techniques to monitor *(a)* the light scattering transition corresponding to a turbidity decrease upon actomyosin dissociation, and *(b)* tryptophan fluorescence as an empirical probe for conformational transitions during ATP binding and hydrolysis (Bagshaw *et al.*, 1974, Bagshaw and Trentham, 1973, Kuhlman and Bagshaw, 1998). More recently, as discussed previously (**see 1.9**), these transient kinetic methods in conjunction with the W501 *Dictyostelium* myosin II motor domain mutant have yielded new kinetic and conformational information regarding the ATP-binding and hydrolysis mechanism of the myosin II motor (Malnasi-Csizmadia *et al.*, 2001a, Malnasi-Csizmadia *et al.*, 2001b, Malnasi-Csizmadia *et al.*, 2000). However, useful as these procedures are in elucidating kinetic and conformational features of myosin, actin, and nucleotide interactions, they traditionally require large amounts protein (>μg) and have thus been limited to muscle proteins purified from bulk muscle tissue or from organisms which allow their expression in relatively large amounts (*e.g. Dictyostelium discoideum*).

Previous research combining fluorescent microscopy with UV flash photolysis to cleave the nitro-benzyl group of an inert ATP precursor (caged-ATP, **Fig. 4.11**),

thus creating a localised burst of ATP in solution, has shown that the ATP-induced dissociation kinetics of fluorescently labelled actomyosin can be achieved using sub-microgram amounts of protein (Weiss *et al.*, 2000). However, the development of total internal reflection fluorescence microscopy (TIRFM), which enables the selective excitation of fluorophores within 150nm (the evanescent field) of a glass/water interface thus excluding those within the bulk solvent (Axelrod *et al.*, 1984, **see 1.13**), has paved the way for the development of even more sensitive, microscope-based kinetic assays. By combining TIRFM and UV flash photolysis of caged-ATP, the ATP-induced dissociation of novel fluorescent myosin II proteins from a single, fixed actin filament could be monitored in real-time. The kinetic information gained from the analysis of a single filament of actomyosin in this manner would require μl volumes of nM protein, and could thus be applied to proteins which are only available in «μg quantities.

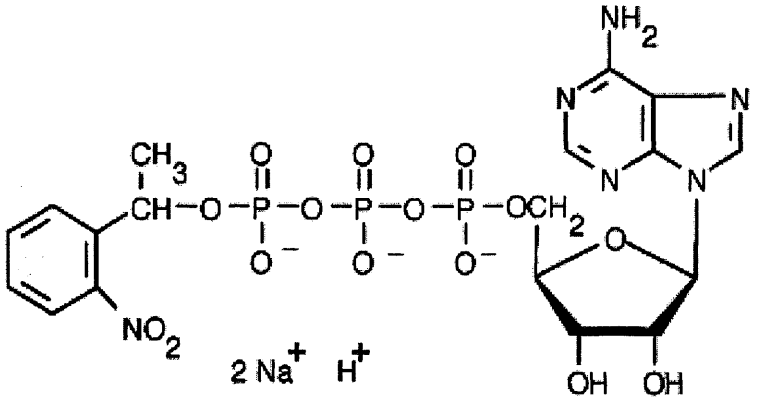


**Fig. 4.11** Caged-ATP (adenosine 5'-triphosphate, P3-1-(2-nitrophenyl)ethyl ester). This photolabile derivative of ATP can be selectively released by irradiation with short pulses of light of ~360nm, which cleave the nitro phenyl group creating a localised burst of ATP (Hibberd and Trentham, 1986).

The highly fluorescent nature of the *Dictyostelium* myosin II motor domain fusion proteins investigated during our research presented an excellent opportunity to develop these type of microscope-based kinetic assays, while characterising the

functionality of the proteins themselves using conventional transient kinetic methods such as stopped-flow. Further ways of improving the accuracy and sensitivity of the TIRFM flash-photolysis assays could then be investigated.

## *4.2 Solution kinetics of FP-myosin II fusion proteins*

### 4.21 ATP binding and hydrolysis; open-closed transition kinetics

As discussed previously (**see 1.9**), the single tryptophan at the 501 position of the 761 residue *Dictyostelium* myosin II motor domain W501 has been shown to exhibit a fluorescent enhancement upon ATP hydrolysis (Malnasi-Csizmadia *et al.*, 2001b, Malnasi-Csizmadia *et al.*, 2000), a step coupled to the open-closed transition (Malnasi-Csizmadia *et al.*, 2001a) of the myosin II motor. This transition can thus be easily monitored using conventional stopped-flow techniques.

All the novel fusion proteins, both single and double, exhibited a tryptophan enhancement upon ATP addition in a conventional stopped-flow environment (**Fig. 4.211a**). However, the fluorescence from the FP-type probes themselves proved insensitive to ATP binding and hydrolysis, presumably because the core of the fluorophore itself lies within a stable β-barrel structure, and is thus protected from local changes in environment. Furthermore, in the case of the GFP probe for W501.gGFP no change in any potential energy transfer from tryptophan to GFP could be detected upon ATP binding (**Fig. 4.211b**), therefore it is likely that this effect is dominated by tryptophans within the GFP protein itself (van Thor *et al.*, 2002).

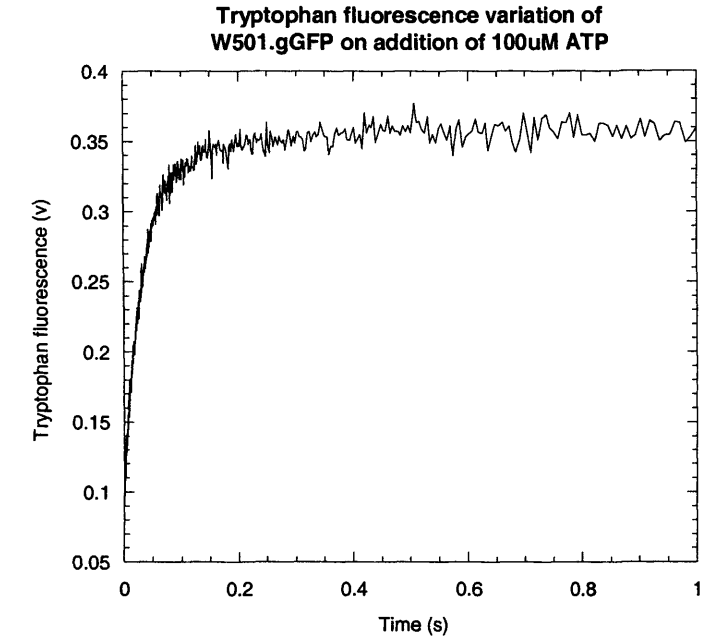


*(a)*

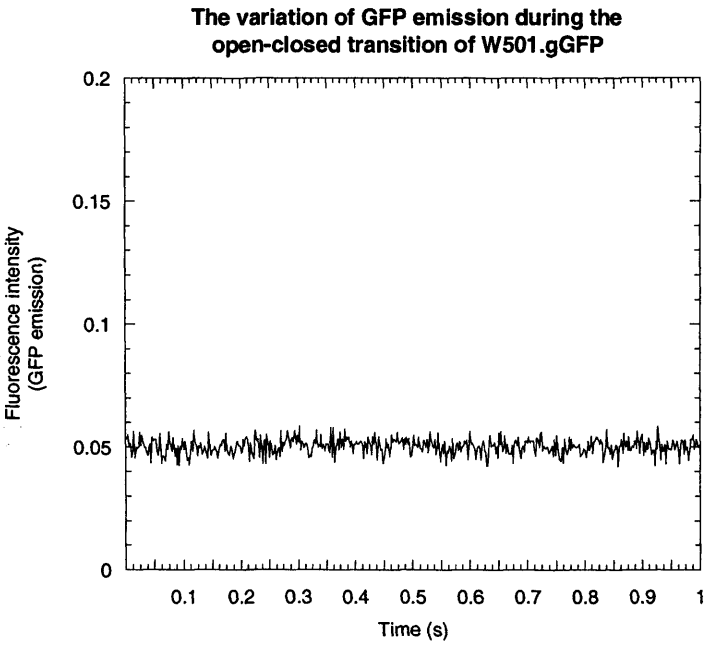


*(b)*

**Fig. 4.211** Stopped-flow traces of W501.gGFP interaction with ATP, monitored by *(a)* tryptophan fluorescence and *(b)* GFP fluorescence. ATP (100μM in *(a)*, 25μM in *(b)*) was mixed with 0.5μM W501.gGFP (reaction chamber concentrations) in standard assay buffer (20mM HEPES, 40mM NaCl, 2mM $MgCl_2$, pH7.5, with freshly added 5mM βME, 0.01% w/v $NaN_3$). Tryptophan fluorescence was monitored by excitation at 295nm and the emission selected using UG11 and WG320 filters. The tryptophan record was fit to a single phase exponential with a rate constant ($k_{obs}$) of $26.7s^{-1}$ (± 0.22). GFP fluorescence was monitored using excitation at 490nm and the emission selected with an OG515 cut-off filter.

By fitting single-phase exponentials to the tryptophan fluorescence changes, ATP binding kinetics for various nucleotide concentrations ($k_{obs}$) were determined. These in turn were then plotted against [ATP] to determine the maximum rate of change upon ATP binding (**Fig. 4.212**), which is defined in terms of the isomerisation equilibrium ($K_{3a}$=0.4) and hydrolysis rate ($k_{3b}$=100$s^{-1}$, $k_{-3b}$≈2$s^{-1}$) constants (steps 3a, 3b, $k_{max}$=30$s^{-1}$ for wildtype, **see 1.7**);

$$k_{\max} = \left( \frac{K_{3a}}{1 + K_{3a}} \right) k_{3b} + k_{-3b}$$

All the single fusion proteins and rYFP.W501.gCFP proved to have ATP-binding kinetics similar to the W501 protein alone (**Fig. 4.213**), and thus the *Dictyostelium* myosin II motor domain appeared to retain a conventional ATP-binding and hydrolysis functionality when a FP-type moiety was fused to either or both of the N- and C-termini.

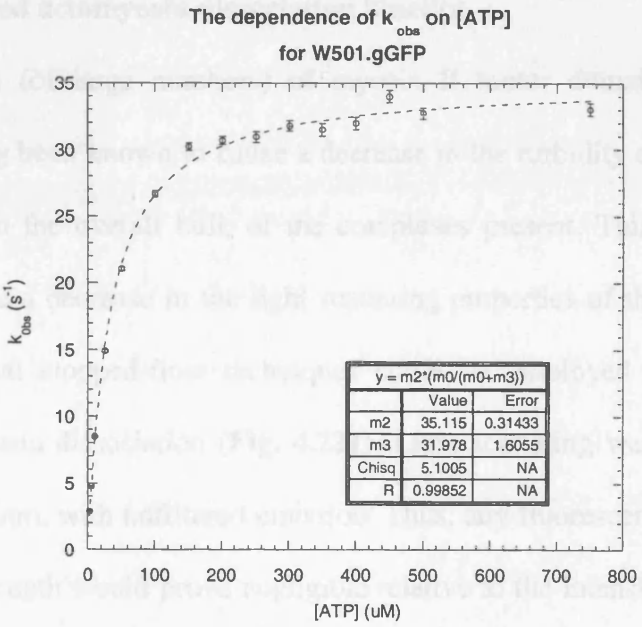


**Fig. 4.212** The determination of the maximum rate of ATP binding and hydrolysis for W501.gGFP. A hyperbolic fit was assigned to the variation of $k_{obs}$ with [ATP], yielding a $k_{max}$ of 35.1$s^{-1}$, similar to that of W501 alone.

Therefore, ATP-induced actomyosin dissociation kinetics could now be investigated to determine if the introduction of these fluorescent probes disrupted the interaction between the myosin motor and actin, prior to *(a)* investigations into the kinetics and conformational changes which occur during the actin-bound stages of the crossbridge cycle, and *(b)* the development of sensitive kinetic microscopy assays.

| *Protein* | $k_{max}$ ($s^{-1}$) | |
|---|---|---|
| W501 | 30 | (*Malnasi et al, 2000*) |
| rYFP.W501 | 32.46 ± 1.09 | |
| W501.gGFP | 35.12 ± 0.31 | |
| rYFP.W501.gCFP | 33.99 ± 1.59 | |

**Fig. 4.213** Comparison of the maximum rates for ATP binding and hydrolysis ($k_{max}$) for the novel fusion proteins and the original *Dictyostelium* myosin II motor domain mutant W501. NOTE: Due to the similarity in structure of gYFP.W501.gCFP to rYFP.W501.gCFP, and the limited availability of the former relative to the latter, a full, stopped-flow ATP-binding and hydrolysis curve to determine $k_{max}$ was not attempted. However, a single $k_{obs}$ was determined for 500μM [ATP] mixed with 0.5μM gYFP.W501.gCFP (reaction chamber concentrations) to confirm an approximate $k_{max}$ of $32s^{-1}$.

## 4.22 ATP-induced actomyosin dissociation kinetics

The dissociation (of large numbers) of myosin II motor domains from an actin filament has long been known to cause a decrease in the turbidity of the solution due to a reduction in the overall bulk of the complexes present. This turbidity change would thus cause a decrease in the light scattering properties of the solution, and as such conventional stopped-flow techniques could be employed to monitor ATP-induced actomyosin dissociation (**Fig. 4.221**). Light scattering was monitored using excitation at 365nm, with unfiltered emission. Thus, any fluorescence changes at this particular wavelength would prove negligible relative to the intensity of the scattered light.

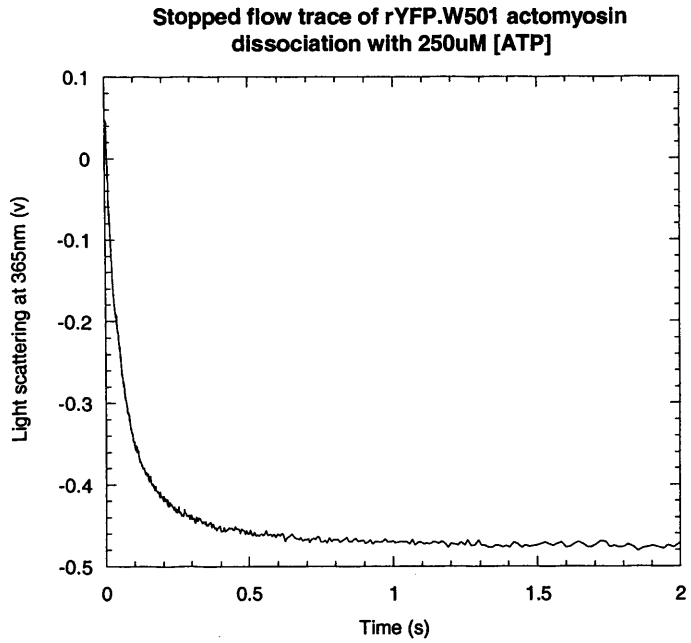


**Fig. 4.221** Stopped flow trace of ATP-induced rYFP.W501 actomyosin dissociation monitored by light scattering at 365nm. ATP (250μM) was mixed with 1μM rYFP.W501 actomyosin (reaction chamber concentrations, stoichiometrically labelled actin) in standard assay buffer (20mM HEPES, 40mM NaCl, 2mM $MgCl_2$, pH7.5, with freshly added 5mM βME, 0.01% w/v $NaN_3$). The record was fit to a biphasic exponential with rate constants ($k_{obs}$ (amplitude)) of $27.4s^{-1}$ (0.38) and $5.0s^{-1}$ (0.17).

Although the dissociation of myosin from actin is reported to be a single-step reaction (A.M → A + M.ATP), requiring single phase exponential analysis of the observed rate ($k_{obs}$), the stopped-flow traces appeared to be partially biphasic, with an initial fast phase followed by a separate slower phase. Analysis of $k_{obs}$ using a biphasic exponential fit yielded similar amplitudes for the fast and slow phases, suggesting that there were indeed two separate effects with differing rates acting upon the turbidity of the solution. It was assumed that the fast phase corresponded to ATP-induced actomyosin dissociation, as the wildtype *Dictyostelium* myosin II motor has been reported to have a $k_{max}$ of $150s^{-1}$ (Kuhlman and Bagshaw, 1998). The slow phase was presumably due to some sort of de-bundling effect, which can often cause slow drifts in fluorescence experiments containing filamentous actin in solution (Kuhlman and Bagshaw, 1998).

Analysis of the maximum rate of ATP-induced dissociation ($k_{max}$), by a hyperbolic fit of $k_{obs}$ vs [ATP], highlighted the difference between the single phase and biphasic exponential analyses of $k_{obs}$ (**Fig. 4.222**). Comparisons of $k_{max}$ (fast phase) to that of W501 (~100$s^{-1}$, Conibear, 2004) showed rYFP.W501 to have similar ATP-induced dissociation kinetics to those of W501, with W501.gGFP yielding a slightly slower $k_{max}$, but still within the expected experimental range (**Fig. 4.223**). The double fusion protein rYFP.W501.gCFP, however, proved to have considerably slower dissociation kinetics to those of W501 ($k_{max}$ (fast phase) =~23$s^{-1}$ ± 9, 6-fold decrease). Furthermore, comparisons of observed dissociation rates for a specific ATP concentration (100μM) yielded fast-phase $k_{obs}$ for rYFP.W501 and W501.gGFP that were ~4-fold slower than those of W501, and ~13 fold slower for rYFP.W501.gCFP.

Therefore, in summary, the presence of FP-type fluorescent probes at the N- or C- termini of W501 caused a decrease in the dissociation rate from actin, with the N-terminal probe causing an effect of less significance than the C-terminal probe, and maximal disruption of dissociation caused by the presence of probes at both termini. As the N- and C-termini exist on the opposite side of the myosin motor domain from the actin-binding site, it seemed unlikely that the probes were altering the binding capacity of the motor itself via steric interference. Furthermore, given GFP's reported propensity to dimerise at high concentrations (Tsien, 1998), and that the disruption by fusion to both termini was considerably greater than the compound disruption from fusion to each terminal individually, it was concluded that interactions between the probes, when forced into close proximity by binding of the myosin motor to actin, was affecting the ATP-induced actomyosin dissociation kinetics. Whether this was due to *(a) intra*filament interactions between neighbouring fusion proteins, *(b) inter*filament interactions causing increased bundling of filamentous actin, thus

increasing turbidity and potentially the freedom of ATP to perfuse through the solution, or *(c)* a combination of both, was something that could presumably be determined by monitoring the dissociation from a single, fixed filament using TIRFM.

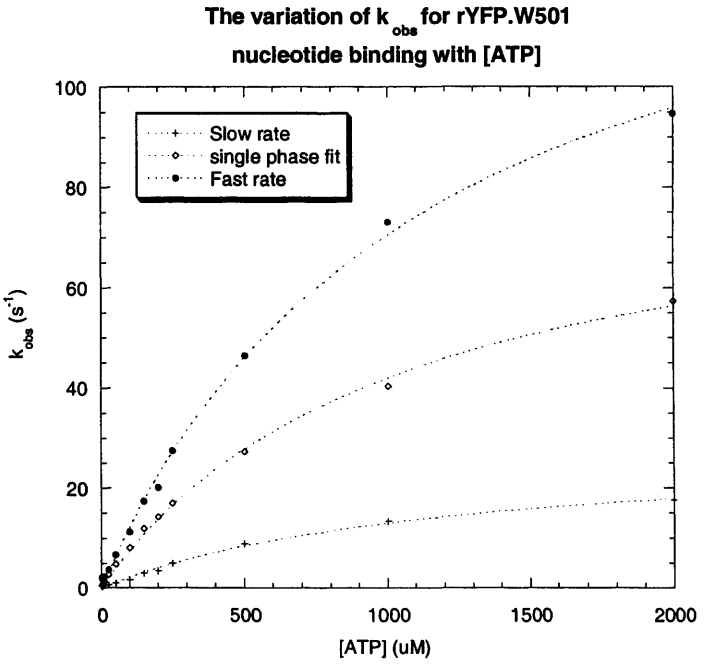


**Fig. 4.222** The determination of the maximum rate of ATP-induced actomyosin dissociation for rYFP.W501. Both single phase and biphasic exponential fits were assigned to the original stopped-flow traces to obtain the observed rate constants ($k_{obs}$), and subsequent hyperbolic fits assigned to the variation of $k_{obs}$ with [ATP] to determine the maximum dissociation rate constants ($k_{max}$). For rYFP.W501 the fast phase of a biphasic exponential fit yielded a $k_{max}$(149.5$s^{-1}$) which correlated well with that of the wildtype *Dictyostelium* myosin II motor (~150$s^{-1}$). The single phase fit, however, yielded a considerably slower rate constant ($k_{max}$≈86$s^{-1}$).

| Protein | $k_{max}$ ($s^{-1}$) | | | $k_{obs}$ ($s^{-1}$) at 100μM [ATP] | | |
|---|---|---|---|---|---|---|
| | *Fast phase* | *Slow phase* | *Single phase* | *Fast phase* | *Slow phase* | *Single phase* |
| Wildtype *Dd* myosin II motor domain | - | - | 150 | - | - | 50 |
| rYFP.W501 | 149.5 ± 5.2 | 28.5 ± 1.5 | 85.5 ± 2.78 | 11.15 | 1.72 | 8.07 |
| W501.gGFP | 123.4 ± 29.5 | 5.8 ± 2.4 | 17.6 ± 2.48 | 8.91 | 0.81 | 4.42 |
| rYFP.W501.gCFP | 23.24 ± 8.9 | 2.45 ± 0.6 | 11.6 ± 0.81 | 3.08 | 0.43 | 1.57 |

**Fig. 4.223** A comparison of the extrapolated maximum rate constants ($k_{max}$) and observed rate constants ($k_{obs}$, for 100μM [ATP]) for ATP-induced actomyosin dissociation, as determined by single phase and biphasic exponential fits, for the novel fusion proteins and the original *Dictyostelium* myosin II motor domain mutant W501.

## *4.3 Comparison of solution kinetics with sensitive, caged-ATP flash photolysis TIRFM assays*

### *4.31 Sensitive kinetic assays of single FP-myosin II fusion proteins utilising caged-ATP flash photolysis under TIRFM*

The production of a localised burst of ATP upon hydrolysis of caged-ATP by a UV flash of 350nm (Conibear and Bagshaw, 1996, Conibear and Bagshaw, 2000), and the clear visualisation of coverslip-bound actin filaments fully labelled with W501 fusion proteins under TIRFM, provided a very sensitive potential method for determining the kinetics of ATP-induced dissociation (Weiss *et al.*, 2000). Furthermore, should the disruption of ATP-induced dissociation kinetics reported for the novel fusion proteins in solution prove to be a direct result of increased bundling due to interactions between fluorescent probes bound to separate filaments in a rigor state, then this technique, if successful, would overcome this problem and yield conventional W501 kinetics.

The perfusion of caged-ATP at mM concentrations into a flow cell containing fixed actin filaments fully labelled with fusion protein caused no loss in the fluorescent intensity of the visualised filaments. However, on flash photolysis at 350nm, the fusion proteins quickly dissociated from the fixed actin filaments and diffused out of the evanescent field. This process was recorded via image enhancing cameras and videotape, and the fluorescence intensity change over time analysed for specific filaments using NIH imaging software (**Fig. 4.311**). A control experiment (data not shown) where a UV flash was conducted in the absence of caged-ATP showed no significant photobleaching of the labelled actin filaments by the strong burst of 350nm incident light. Interestingly, as shown in **Fig. 4.311,** when YFP was the observed fluorescent probe a small enhancement in fluorescence was detected immediately after the UV flash, which was eventually deduced to be photoactivation

of the dark state of the fluorophore (Miyawaki and Tsien, 2000), discussed in more detail in **4.32 & 6.3**).

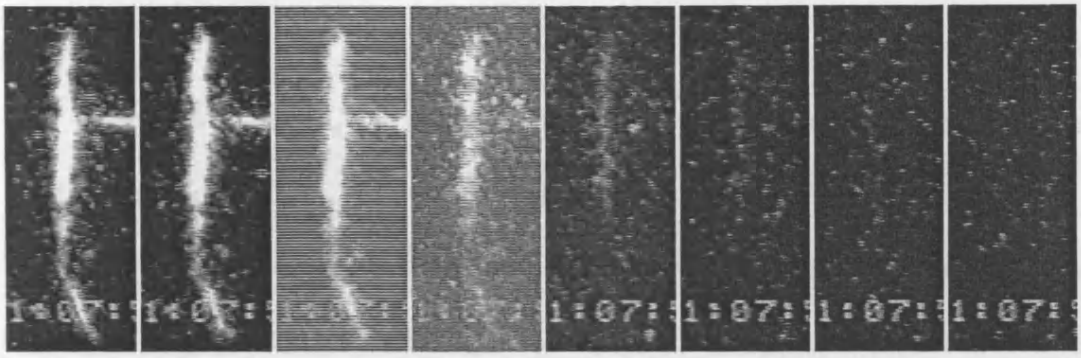

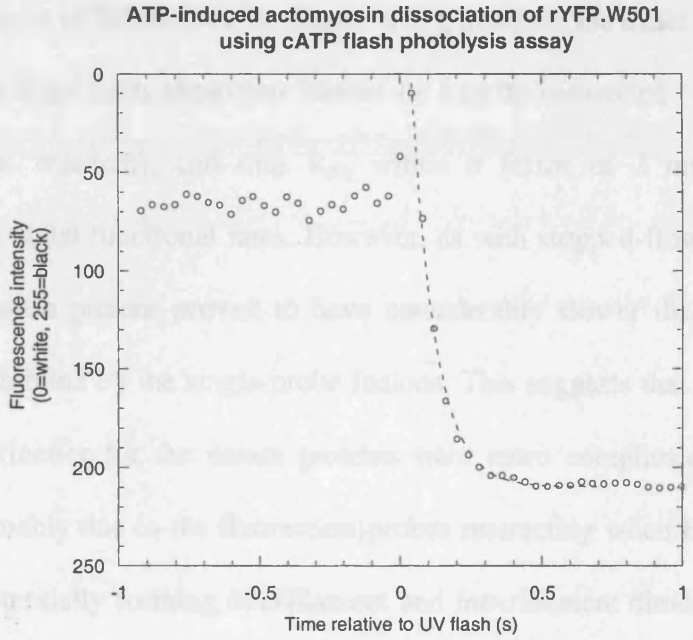


**Fig. 4.311** ATP-induced dissociation of rYFP.W501 from actin filaments on flash photolysis of caged-ATP monitored using TIRFM. F-actin filaments were immobilised on a surface of aged rabbit heavy meromyosin (HMM) which formed a significant number of ATP resistant *rigor* bonds in a flow cell. The actin was perfused with rYFP.W501 (10-40nM) and visualised using TIRFM with excitation at 514nm from an argon ion laser and excitation/emission selected with 500AF25/545AF35 filters. Caged-ATP (500μM in this case) in microscopy buffer (20mM HEPES, 40mM NaCl, 2mM $MgCl_2$, 0.1mM EGTA, 10mM DTT, 0.01% w/v $NaN_3$, at 20°C) was added, and flash photolysis used to release ~50μM ATP (Conibear and Bagshaw, 1996, Conibear and Bagshaw, 2000). *(top)* A montage of images taken at 0.08s intervals, with the first image 0.12s before the 350nm UV flash. *(bottom)* The decay of YFP fluorescence intensity measured from the averaged grey-scale value of an individual actin filament. An exponential fit of the record yielded a rate constant of $12.1s^{-1}$. This method was limited to a maximum resolution of $25s^{-1}$ by the video acquisition frame rate.

This phenomenon did not affect the analysis of the ATP-induced actomyosin dissociation, which remained the dominant transient with respect to fluorescence intensity.

Analysis of the $k_{obs}$ by fitting exponentials to the resultant fluorescent changes yielded consistently faster actomyosin dissociation rates (~2-fold) for various caged-ATP concentrations, relative to those observed using conventional stopped-flow techniques (**Fig. 4.312**). At saturating ATP concentrations dissociation was observed within 1 frame, thus the $k_{obs}$ was $>25s^{-1}$. The single fusion proteins' $k_{obs}$ were still slower than those of W501 ($20s^{-1}$ at 50μM ATP), however the exact amount of caged-ATP released from flash photolysis cannot be exactly controlled (~10% is assumed from previous research), and thus $k_{obs}$ within a factor of 2 may be tentatively interpreted as equal functional rates. However, as with stopped-flow kinetic analysis, the double-fusion protein proved to have considerably slower dissociation kinetics than those exhibited by the single-probe fusions. This suggests that the ATP-induced dissociation kinetics for the fusion proteins were more complicated than those for W501, presumably due to the fluorescent probes interacting when brought into close proximity; potentially forming *inter*filament and *intra*filament dimers when bound to actin. Thus the fusion proteins could not be utilised to accurately resolve actin-bound kinetics of the W501 *Dictyostelium* myosin II motor using these standard analytical techniques. However, the highly sensitive distance dependence of FRET may still have yielded information which could be used to resolve certain conformational changes and kinetic states within the actin-bound stages of the crossbridge cycle, thus this line of research was continued. Furthermore, studies to confirm the proposed dimerisation of the novel fusion proteins were also undertaken.

| *Protein* | *[cATP] / ~[ATP] (μM)* | *Stopped-flow actomyosin dissociation rate ($s^{-1}$)* | *Flash photolysis actomyosin dissociation rate ($s^{-1}$)* |
|---|---|---|---|
| rYFP.W501 | 500 / 50 | 6.63 | 12.1 |
| W501.gGFP | 100 / 10 | 1.85 | 3.13 |
| rYFP.W501.gCFP | 200 / 20 | 0.26 | 0.56 |

**Fig. 4.312** A comparison of some ATP-induced actomyosin dissociation rates obtained from stopped-flow and flash photolysis TIRFM methods. The $k_{obs}$ obtained via flash photolysis TIRFM assays, although consistently 2-fold faster than those obtained using stopped-flow techniques, still remained slower than those obtained for native W501 (*e.g.* $20s^{-1}$ for 50μM ATP).

The technique itself yielded transient kinetic information, while avoiding the common problem of actin-bundling in solution, using only 50μl of 10-40nM fusion proteins, (~50-200ng). Furthermore, the high loading of fully labelled actin filaments presented here could easily be reduced by lowering the actin and protein concentrations, potentially by up to 10-fold. This, combined with the production of 10μl flow cells instead of the 50μl cells typically used during this research, results in the potential to gain transient kinetic information using only 10μl of 1nM (~1ng) protein. This extremely sensitive method may therefore open the way for the kinetic resolution of proteins only available in microgram quantities. However, it must be noted that by using video capture the maximum resolution is limited to the frame rate (0.04s), thus the maximum $k_{obs}$ for ATP-induced dissociation detectable using this method is $25s^{-1}$. This resolution may be improved by employing photon-counting apparatus to directly observe the fluorescence intensity changes down to the 4ms level (limited by the UV flash).

## 4.32 Photoexcitation of YFP

During the course of the caged-ATP flash photolysis assays into the ATP-induced dissociation kinetics of rYFP.W501 (**see 4.31**), a curious phenomenon was observed.

Immediately following the 350nm UV flash used to create a localised ATP burst in solution, a bright, screen-wide flash of fluorescence was observed via the image-enhancing cameras and NIH imaging software (**Fig. 4.321**). Theoretically, this could not have been due to UV itself, as an electronically timed shutter should have closed off the cameras to protect them from the 350nm burst of incident light (Conibear *et al.*, 1998).

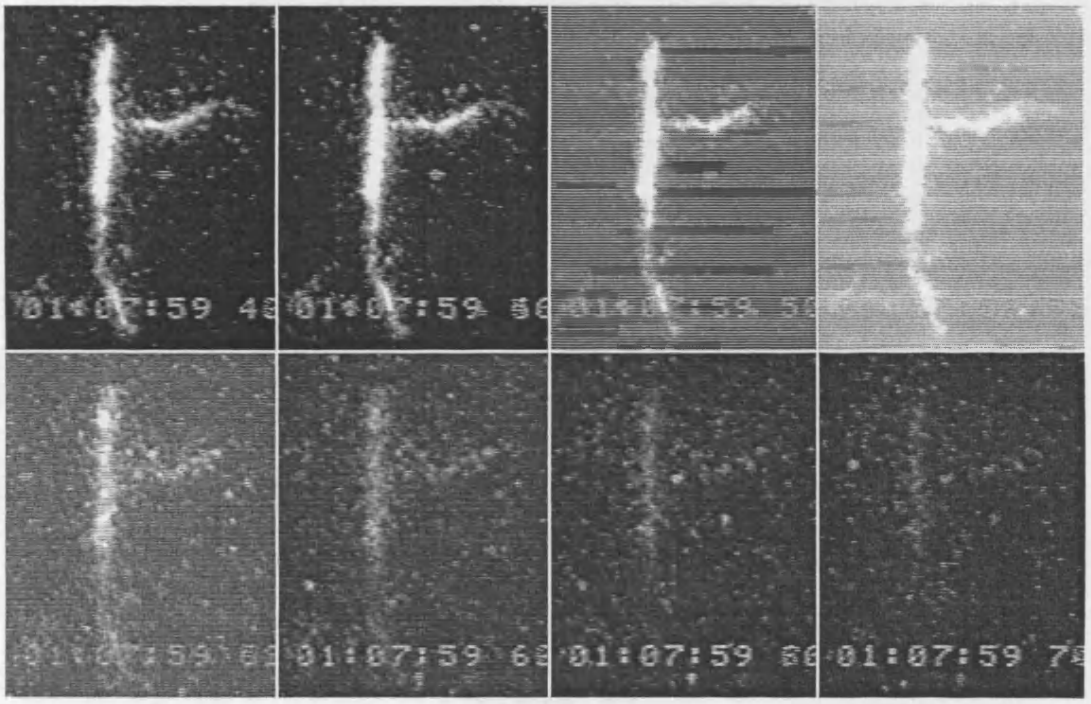


**Fig. 4.321** An example of the short-lived, global fluorescence observed during caged-ATP flash photolysis TIRFM assays into the kinetics of rYFP.W501 ATP-induced actomyosin dissociation (**see 4.21**). The images were taken at 0.04s intervals, with the first image 0.04s prior to the 350nm UV flash. The fluorescence lasted considerably longer than the lifetime of the flash itself (4ms) and was thus deduced to be an example of photoactivation of the dark state of YFP (Miyawaki and Tsien, 2000), existing in solution as rYFP.W501.

Initially, however, this short-lived global fluorescence *was* put down to some small breakthrough of UV light due to either *(a)* a misalignment of the shutter, or *(b)* mis-timing of the open-close mechanism of the shutter itself. However, when time-based fluorescence intensity measurements were carried out on specific rYFP.W501 labelled actin filaments, in order to calculate rate constants for dissociation kinetics, not only

was the global fluorescence visible for considerably longer (0.2s) than the 4ms of the UV flash, but the overall fluorescent intensity of the filament itself increased for 0.08s before dissociation became the dominant transient (**Fig. 4.322**). Therefore, it was theorised that we were observing photoactivation of the dark state of the YFP fluorophore (Miyawaki and Tsien, 2000), with the global fluorescence arising from photoactivation of rYFP.W501 remaining in solution following flow-cell washes.

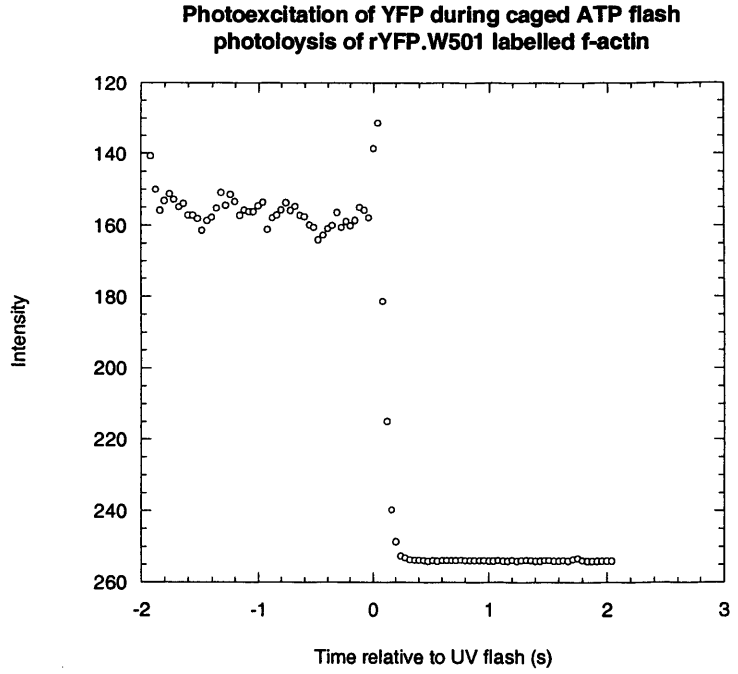


**Fig. 4.322** Evidence of photoexcitation of YFP during a caged-ATP TIRFM assay of the ATP-induced actomyosin kinetics of rYFP.W501. The protocol was exactly as described in **Fig. 4.311**. A short-lived increase in filament intensity was observed (0.08s) before dissociation became the dominant transient.

To address this hypothesis, a fixed actin filament fully decorated with rYFP.W501 was viewed under high power argon ion laser intensity (200mW, 514nm) until it appeared completely photobleached. The localised field was then exposed to a standard 350nm UV flash, whereupon the decorated filament recovered ~25% of its original fluorescence intensity over a period of 2s before gradually decaying once more as a result of photobleaching (**Fig. 4.323**). This process could be repeated

several times, each iteration yielding a smaller fluorescence recovery, until all the bound rYFP.W501 was irreversibly photobleached. Thus it was concluded that we were indeed observing photoactivation of the YFP fluorophore.

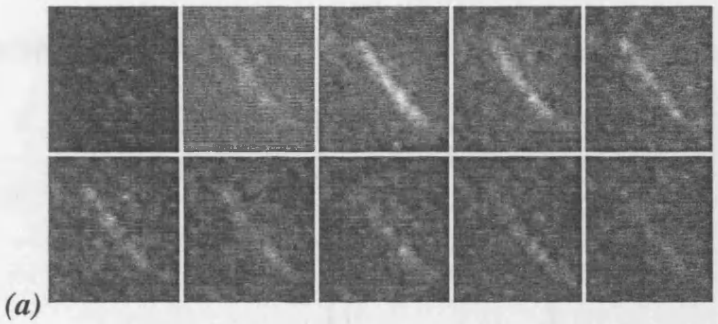

*(a)*

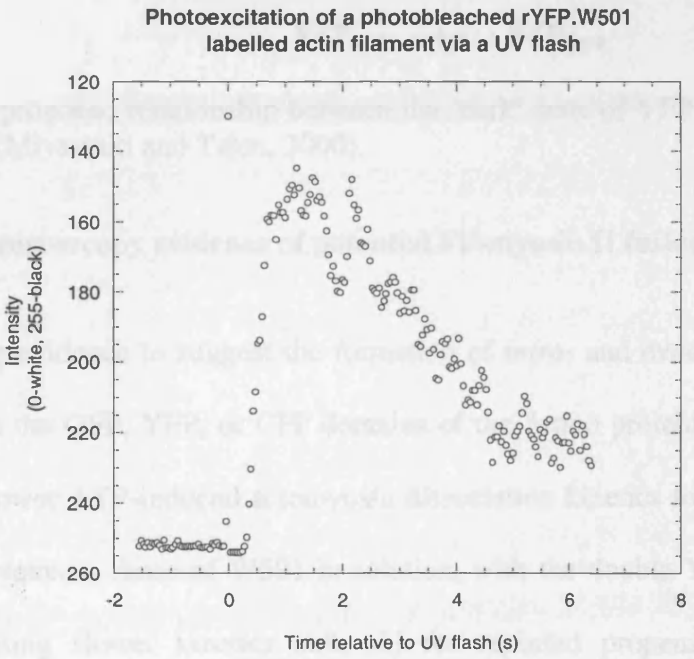


*(b)*

**Fig. 4.323** Photoactivation of the dark state of YFP monitored using TIRFM. An F-actin filament immobilised on a surface of aged heavy rabbit meromyosin was fully labelled by perfusion of 40nM rYFP.W501 into the flow cell, and visualised using TIRFM with excitation at 514nm with an argon ion laser. Following apparent full photobleaching of the labelled filament at high laser power (~200mW), a single UV flash of 350nm incident light caused the recovery of ~25% of the original signal intensity. *(a)* A montage of images taken at 1.6s intervals, with the first image occurring 0.5s prior to the flash. *(b)* The recovery and subsequent decay due to photobleaching of YFP fluorescence intensity measured from the averaged grey-scale value of an individual filament.

Photoactivation of this dark state, whereby an excited fluorophore does not return to the ground state or a final photobleached state, but returns to a dormant (dark) state until activated again by incident light of 350nm (**Fig. 4.324**), opens up many future possibilities to utilise localised photoexcitation as a analytical tool, particularly towards cells *in vivo*.

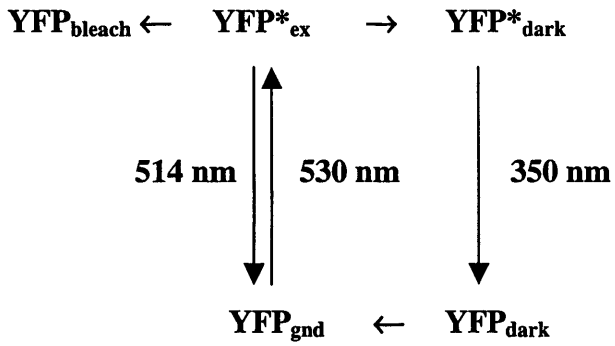


**Fig. 4.324** The proposed relationship between the 'dark' state of YFP and the excited / ground states (Miyawaki and Tsien, 2000).

### 4.33 Electron microscopy evidence of potential FP-myosin II fusion protein dimers

With increasing evidence to suggest the formation of *intra-* and even *inter*molecular dimers between the GFP, YFP, or CFP domains of the fusion proteins, including *(a)* considerably slower ATP-induced actomyosin dissociation kinetics for single GFP or YFP fusion proteins to those of W501 in solution, with the double YFP/CFP fusion proteins exhibiting slower kinetics still, *(b)* the reported propensity of FP-type molecules to form dimers at high concentrations (Tsien, 1998), *(c)* a decrease in the level of FRET between the YFP and CFP probes of *apo* YFP.W501.CFP fusion proteins, when subjected to a high ionic environment (**see 5.2**), and *(d)* the observation that rYFP.W501 molecules on a fixed, fully decorated actin filament under TIRFM conditions, do not exist in equilibrium with those in solution, neither would they be replaced by HMM, led to a collaboration with Dr. P. Knight & K.

Thirumurugan of Leeds University, to observe these proteins using electron microscopy (EM) techniques.

W501 bound to actin under EM showed small globular domains in solution, presumably single molecules of W501, but also what appears to be some dimers present (**Fig. 4.331a**), although the images are open to interpretation. It is plausible that dimerisation of W501 molecules may occur via the poly-histidine tag in solution, and this may explain the high level of actin filament bundling which is evident from the images (**Fig. 4.331b**). Furthermore, this bundling was significantly reduced when actin filaments were labelled with sub-stoichiometric amounts (1:10 ratio) of W501 (**Fig. 4.332**). However, filamentous actin bundling has been reported to often occur in these conditions, and thus the preparation of EM images may be a factor. The selection of the images themselves may give erroneous conclusions with respect to macromolecular structures, thus the appearance of the fusion proteins was weighted above actin filament aggregation in concluding the propensity for dimer formation for any of the considered proteins.

The images for rYFP.W501 show a much greater degree of molecules containing two approximately equally sized globular domains in solution (**Fig. 4.333**). Given the lower magnification of this image relative to those for W501, and the fact that the *Dictyostelium* myosin motor domain is considerably larger than the FP domain, we logically interpreted these double-globular molecules to be rYFP.W501 dimers in solution. Furthermore, the greater number of these potential dimers compared to the W501 images led to the conclusion that the increased binding affinity was directly due to the presence of the YFP domains.

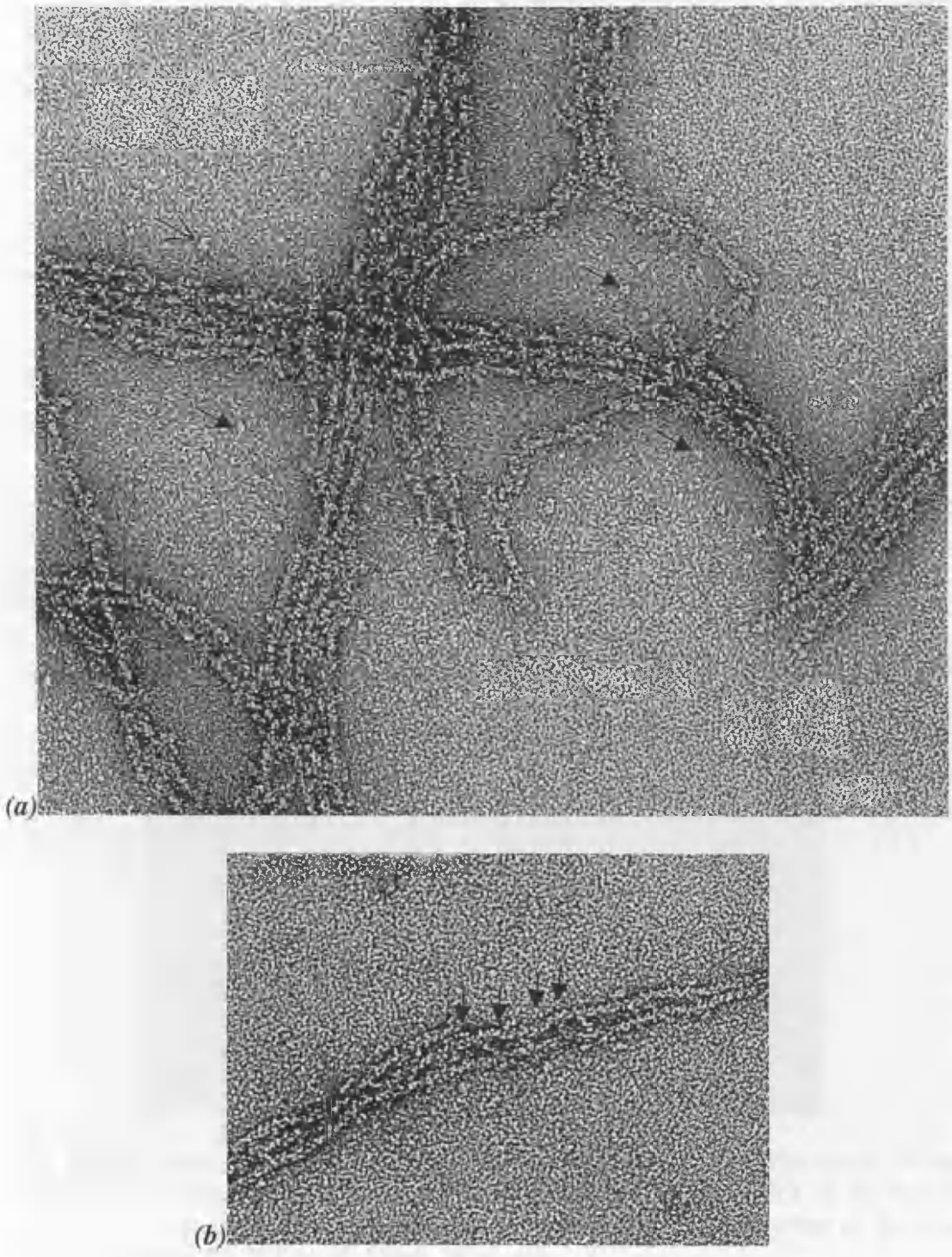


**Fig. 4.331** Potential dimer formation of W501 in solution, with increased bundling of filamentous actin labelled with stoichiometric amounts of W501, viewed under electron microscopy (EM). *(a)* Single molecules of W501 in solution (arrowed), with potentially a W501 dimer (hollow arrow). *(b)* potential inter-filament W501 dimers (arrowed) may be contributing to actin bundling in solution. Images courtesy of Kavitha Thirumurugan & Dr. P. Knight, *Leeds University*

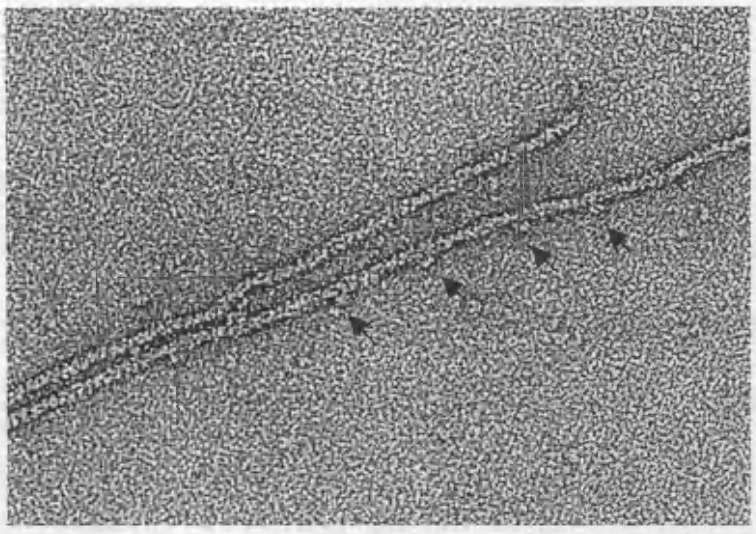

**Fig. 4.332** Filamentous actin labelled with sub-stoichiometric amounts (1:10 ratio) of W501, visualised using EM. Considerably less evidence of *inter*filament dimerisation between actin-bound W501 molecules (arrowed) was present. Image courtesy of Kavitha Thirumurugan & Dr. P. Knight, *Leeds University*

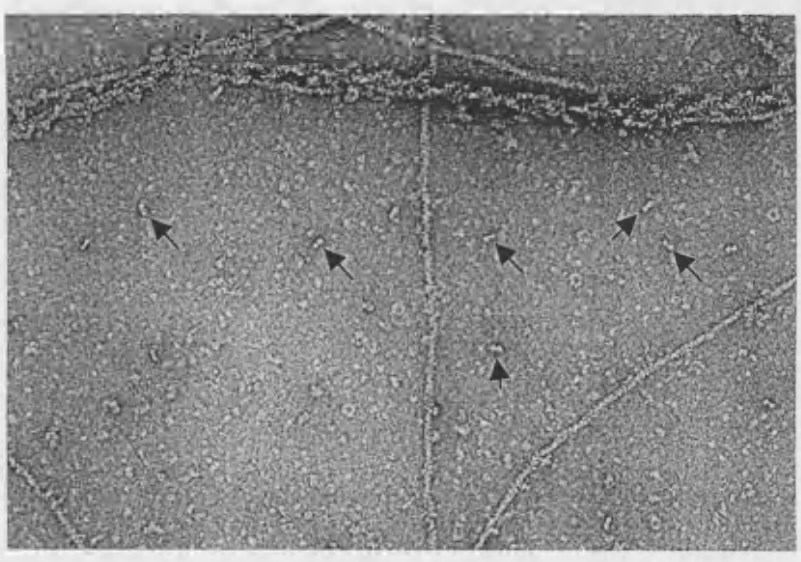

**Fig. 4.333** Potential dimer formation of rYFP.W501 in solution (arrowed). Actin filaments were labelled with sub-stoichiometric amounts (1:10 ratio) of the fusion protein, then visualised using electron microscopy (EM). Image courtesy of Kavitha Thirumurugan & Dr. P. Knight, *Leeds University*

The images for rYFP.W501.gCFP, of a similar magnification to that of the W501 images, clearly show fully labelled actin filaments, together with a large number of what appears to be double-globular proteins which have dimerised to form a 'ring' structure (**Fig. 4.334**). Given *(a)* that the CFP and YFP probes are bound to the N- and C- terminal ends of the *Dictyostelium* myosin II motor domain, *(b)* that these domains

exists close to each other on the lever-arm edge of the myosin motor (**see 1.12, Fig. 1.121**), and *(c)* the combined molecular volume of these two fluorescent probes is approximately equal to that of the motor domain, we concluded that these 'ring' structures were evidence of rYFP.W501.gCFP dimers in solution. There appear to be considerably more of these relative to W501 and rYFP.W501, giving evidence to suggest that the increased propensity to form dimers is directly linked to the extra presence of another FP-type moiety.

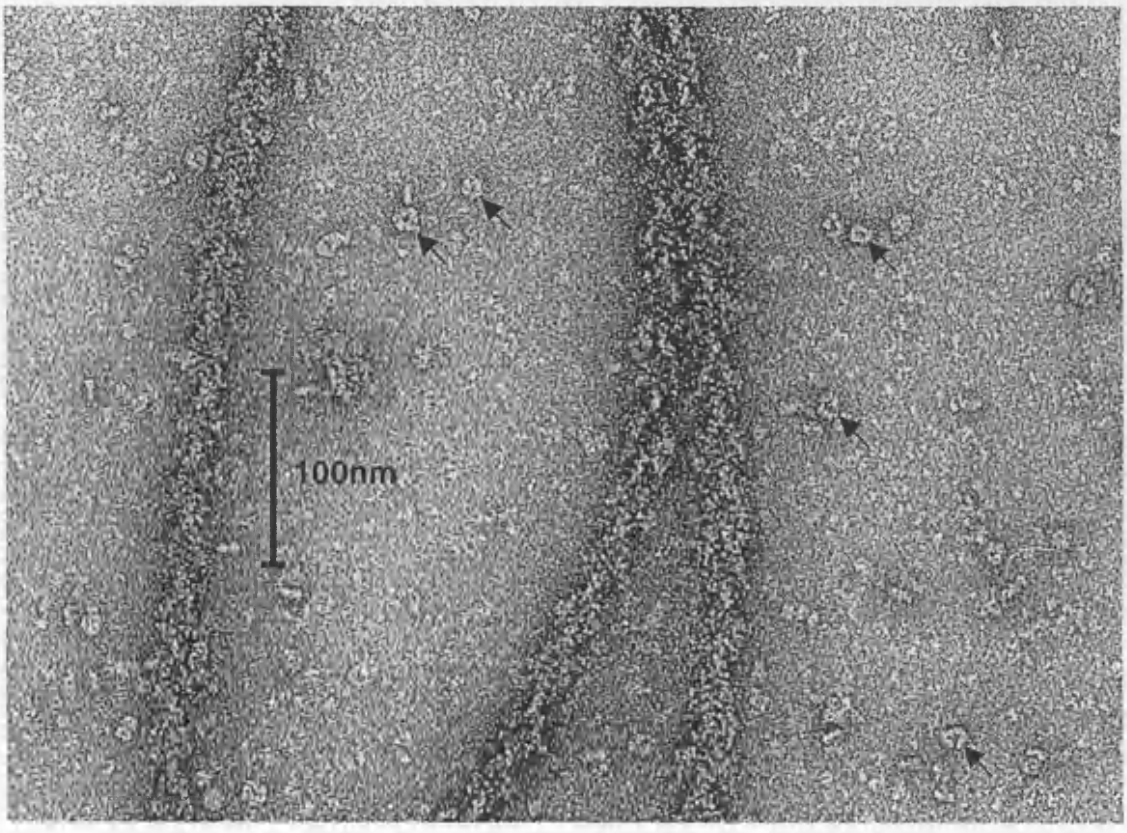


**Fig. 4.334** Potential dimer formation of rYFP.W501.gCFP in solution (arrowed). Filamentous actin was labelled with stoichiometric amounts of rYFP.W501.gCFP, then visualised using EM. Image courtesy of Kavitha Thirumurugan & Dr. P. Knight, *Leeds University*

Furthermore, when the actin filaments were labelled with sub-stoichiometric amounts (1:10 ratio) of rYFP.W501.gCFP it appears than dimers could form not only between fusion protein molecules in solution, but also between molecules bound to actin, causing interfilamental links (**Fig. 4.335**). This observation gives further evidence to

suggest dimer formation via FP-type domain interaction, and not other, non-specific protein interactions, as the actin-binding domain of the *Dictyostelium* myosin II motor lies on the opposite site of the protein relative to the N- and C-temini.

To summarise, the EM images gave evidence, if not conclusive due to their interpretational nature, of increased dimer formation due to YFP and CFP's affinity to bind at high concentrations (Tsien, 1998). The fact that binding to actin would produce a localised high concentration of these probes even at low concentrations in solution, suggests that the disruption of ATP-induced dissociation observed may have been directly related to the fluorescent probes propensity for dimerisation.

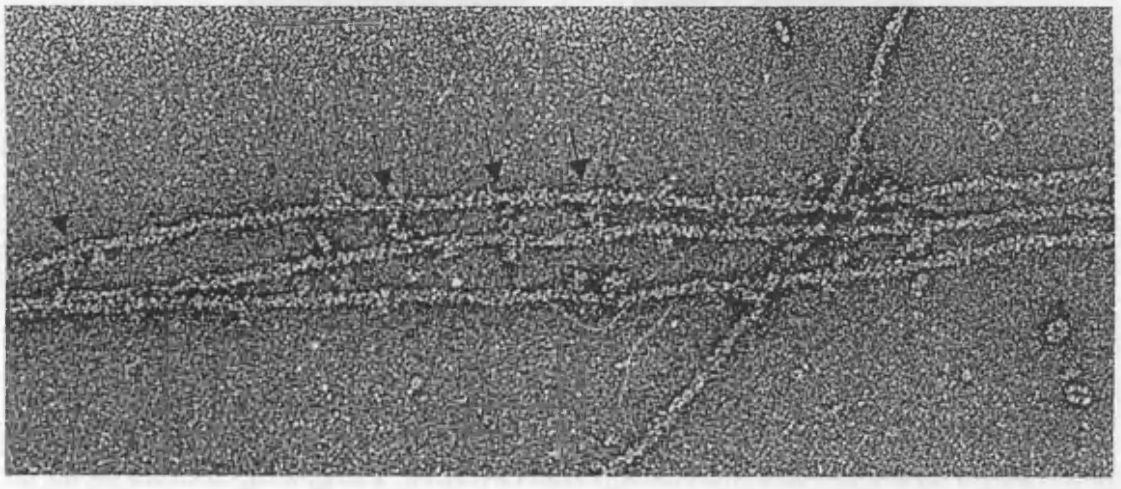

**Fig. 4.335** Potential evidence of *inter*filament dimerisation of actin-bound rYFP.W501.gCFP (arrowed). Filamentous actin was labelled with sub-stoichiometric amounts (1:10 ratio) of rYFP.W501.gCFP, then visualised using EM. Image courtesy of Kavitha Thirumurugan & Dr. P. Knight, *Leeds University*

### 4.34 Actin binding kinetics of a single fusion proteins under TIRFM

To observe the binding kinetics of the fusion proteins in the absence of ATP, a sample of fixed actin filaments fully decorated with rYFP.W501 or W501.gGFP was given repeated flow-cell washes over a period of 1hr, to ensure that no rYFP.W501/W501.gGFP remained in solution. At regular intervals over this time images were captured under TIRFM, while ensuring minimum exposure to excitation

light to nullify the effect of photobleaching. Theoretically, the fluorescent intensity of one of these fully labelled filaments should decrease over time as molecules of the fusion protein detach from actin and are not replaced by those existing in the surrounding solution. Previous studies (Kuhlman and Bagshaw, 1998) have shown that single molecules of the *Dictyostelium* myosin II motor have a dissociation rate of ~0.036$s^{-1}$ ($t_{½}$=~20s) in the absence of ATP. However, with rYFP.W501 and W501.gGFP, fully labelled filaments were still clearly visible under TIRFM after 1hr (**Fig. 4.341**).

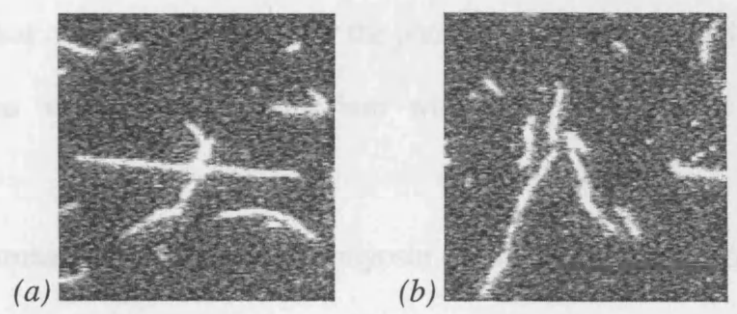


**Fig. 4.341** Actin filaments fully decorated with W501.gGFP viewed directly after production *(a)* and after 1hr *(b)*. F-actin filaments were immobilised on a surface of aged rabbit heavy meromyosin (HMM) which formed a significant number of ATP resistant *rigor* bonds in a flow cell. The actin was perfused with W501.gGFP (40nM), allowed to stand for 1-2min, washed repeatedly with microscopy buffer (20mM HEPES, 40mM NaCl, 2mM $MgCl_2$, 0.1mM EGTA, 10mM DTT, 0.01% w/v $NaN_3$, at 20°C) to remove W501.gGFP within the flow-cell, and visualised using TIRFM with excitation at 488nm from an argon ion laser at regular intervals up to 1hr. Excitation/emission was selected using Omega 455DF70/510AF23 filters. No significant decrease in filament intensity was observed over this period.

Further 'chase' experiments involving the perfusion of relatively high concentrations (50nM) of HMM into a flow-cell containing fixed actin filaments fully labelled with rYFP.W501/W501.gGFP also showed no decrease in fluorescence intensity over time (data not shown). Thus, as HMM should displace *Dictyostelium* myosin II motor domains from actin due to its higher binding affinity, we concluded that the presence of FP-type moieties at the N- or C-termini either *(a)* disrupted the binding kinetics of the myosin motor, yielding a much higher binding affinity in an ATP free

environment, or *(b)* created a multilateral 'string' of single FP fusion proteins along the actin filament connected via FP-type dimers, thus holding a recently detached myosin motor in place until binding to the actin monomer occurred once more, effectively giving the appearance of permanently bound proteins under TIRFM.

Further evidence of the high binding affinity and slow binding kinetics of single FP-myosin fusion proteins was obtained by Prof. C. Bagshaw and Dr. W. Zeng, whereby a focussed beam of incident laser light was employed to photobleach a small section of an actin filament fully labelled with W501.gGFP. No recovery of fluorescence was observed over time for the photobleached section, indicating that the bound proteins were not in equilibrium with non-photobleached molecules in solution.

In summary, the single-FP myosin fusion proteins W501.gGFP and rYFP.W501 did not exhibit typical actin-binding kinetics in the absence of ATP, and thus, with the proteins also exhibiting atypical ATP-induced actin dissociation kinetics in solution, it did not seem likely that these systems and techniques could be employed to investigate actin-bound kinetics of the *Dictyostelium* myosin II motor domain.

Interestingly, when investigating the photoexcitation of YFP (**see 4.32**) an actin filament fully labelled with rYFP.W501, and completely photobleached, still exhibited regular single flashes of fluorescence similar in size and appearance to single molecules of GFP, which lasted approximately 0.5-1s. Following the previous experiments it was concluded that these flashes were not due to non-photobleached molecules of rYFP.W501 in solution replacing those that had detached from the filament itself, but were YFP probes returning to a ground state and then excited state from the reported 'dark state' under the increased power of the incident laser light

used to bleach the filament (~200mW). This gives further evidence to support the 'blinking' effect of YFP molecules reported in previous studies (Dickson *et al.*, 1997).

## *4.4 Conclusion*

All the novel fusion proteins exhibited a well-defined tryptophan peak which responded (with a slight enhancement) to ATP binding and hydrolysis with solution kinetics similar to those of W501 alone. Thus, the *Dictyostelium* myosin II motor domain appeared to retain a conventional ATP-binding and hydrolysis functionality when a FP-type moiety was fused to either or both of the N- and C-termini. The FP fluorescent probes proved insensitive to ATP binding and hydrolysis, presumably because the core of the fluorophore itself lies protected within a stable β-barrel structure. Furthermore, no change in energy transfer from tryptophan to GFP could be detected upon ATP binding, however it is likely that this effect is dominated by the tryptophans within the GFP protein itself (van Thor *et al.*, 2002).

Transient solution kinetic analysis combined with sensitive, TIRFM caged-ATP flash photolysis assays, showed the presence of a slow phase and a fast phase for the ATP-induced actomyosin dissociation of the novel fusion proteins. The slow phase proved considerably more dominant in solution, therefore was likely the result of increased actin bundling caused by FP-type proteins propensity to dimerise at high concentrations (Tsien, 1998). This effect was nullified under TIRFM as single fixed actin filaments were analysed separately. The fast phase, presumably a measure of ATP-induced actomyosin dissociation, showed rYFP.W501 and W501.gGFP to have maximum dissociation rate constants ($150s^{-1}$ and $123s^{-1}$ respectively) similar to those of W501 and wildtype *Dictyostelium* myosin II motor in solution ($100\text{-}150s^{-1}$). However the rate constants for specific ATP concentrations below the maximal level proved to be slower for both single fusion proteins. Furthermore, the binding of the

single fusion proteins to actin filaments was not competitively inhibited by HMM, nor did actin-bound fusion proteins (in the absence of ATP) appear to be in a slow equilibrium with those in solution, but rather permanently (1hr+) fixed in a *rigor* state. Thus, the presence of FP fluorescent probes at the N- or C- termini of W501 caused an increase in the apparent binding affinity to actin.

Similarly, analysis of the fast phase kinetics for the double fusion protein rYFP.W501.gCFP yielded rate constants considerably slower than those of W501 *or* the single fusion proteins, for both the extrapolated maximum rate constant in solution ($23s^{-1}$), and for rate constants at specific ATP concentrations under TIRFM. Thus the binding affinity for actin seemed to be further increased when FP fluorescent probes were fused to *both* terminal ends of W501. As the N- and C-termini exist on the opposite side of the myosin motor domain from the actin-binding site, it was unlikely that the probes were altering the binding capacity of the motor itself via steric interference. Thus, given the reported propensity of FP-type proteins to dimerise at high concentrations, it was concluded that non-specific electrostatic interactions between the probes when forced into close proximity, *e.g.* by binding of the myosin motor to actin, was affecting the actin-binding and ATP-induced actomyosin dissociation kinetics of the fusion proteins. EM images of the fusion proteins bound to actin, although not conclusive proof due to their interpretational nature, gave strong evidence to support the formation of fusion protein dimers (increasing in frequency for double-fusion proteins) both *(a)* in solution and *(b)* between separate actin filaments. Thus we can assume that fusion proteins bound to adjacent actin monomers are likely to exhibit these same interactions when in such close proximity.

The formation of these *intra*filamental and *inter*filamental dimers meant that that the ATP-induced dissociation kinetics for the fusion proteins were more

complicated than those for W501, and meant that the fusion proteins could not be utilised to accurately resolve actin-bound kinetics of the W501 *Dictyostelium* myosin II motor using these standard analytical techniques. However, despite these negative results, information about conformational changes and kinetics of the actin bound stages of the crossbridge cycle could still potentially be gleaned by utilising the extremely sensitive distance dependence of FRET in concert with the double fusion proteins.

Also on the *pro* side, the monitoring of fusion-protein ATP-induced actomyosin dissociation kinetics via TIRFM using caged-ATP flash photolysis yielded fairly accurate transient kinetic information, while avoiding the common problem of actin-bundling in solution. This extremely sensitive technique has the potential to be carried out using only 10µl of 1nM protein (~1ng of fusion protein), and may therefore open the way for the kinetic resolution of proteins only available in «µg quantities. Improvement of the maximum resolution ($k_{obs}$=25$s^{-1}$), limited by the video capture frame rate (0.04s), may be achieved by employing photon-counting apparatus to directly observe the fluorescence intensity changes down to the 4ms level.

Evidence to support the reported photoexcitation of the 'dark-state' of the YFP fluorophore (Miyawaki and Tsien, 2000) was also gained during the caged-ATP flash photolysis investigations. A fully rYFP.W501 labelled, completely photobleached, fixed actin filament, when exposed to a brief flash of 350nm light, regained ~25% of its original signal intensity for a brief period. This phenomenon opens up many future possibilities to utilise localised photoexcitation as a analytical tool, particularly towards cells *in vivo*.

# 5 - FRET studies on double FP-myosin II fusion proteins

## *5.1 Introduction*

As discussed previously (**see 1.12**), fluorescence resonance energy transfer (FRET) is the transfer of energy from the excited state of a donor to an acceptor fluorophore, without the appearance of a photon, and is primarily due to dipole-dipole interactions between the two fluorophores themselves. The rate of this energy transfer depends upon *(a)* the extent of the overlap between the donor emission spectrum and the acceptor excitation spectrum, *(b)* the relative orientation of the donor and acceptor dipoles, and *(c)* the distance between the two fluorophores, as related by equations ***(i)*** and ***(ii)*** (**Fig. 5.11**). It is this sensitive distance dependence that has made this phenomenon such a useful tool for observing small steady-state and real-time conformational changes within biological systems.

*(i)* $$Ro = 8.8\times10^{-25}\left(\kappa^2 n^{-4}\phi_d J\right)$$

*(ii)* $$E = \frac{R_o}{R_o + r^6}$$

**Fig. 5.11** The equations relating the efficiency of FRET ($E$) to the distance separating the donor and acceptor ($r$), and the relative orientations of the donor and acceptor dipoles ($\kappa^2$). $J$ is the overlap integral expressing the degree of spectral overlap between donor emission and acceptor absorption ($M^{-1}cm^3$), $\phi_d$ is the quantum yield of the donor in the absence of the acceptor, and $n$ is the refractive index of the medium. By definition, $R_o$ is the distance at which 50% energy transfer occurs from the donor to the acceptor (the Förster distance).

The introduction of site-specific fluorophores within biological proteins generally involves one of three routes, *(a)* the introduction of a tryptophan residue (and/or removal of prominent native tryptophans) to yield a single tryptophan mutant, *(b)* the introduction of a cysteine residue (and/or removal of native cysteines) followed by

directed covalent modification, and *(c)* the genetic construction of a fusion protein with GFP or another related fluorescent molecule. The approach adopted by Suzuki *et al.* (1998) utilised the latter of the three routes, whereby the lever arm domain of the myosin head was replaced with either GFP or blue fluorescent protein (BFP, Heim and Tsien, 1996) by fusion of the fluorophore to the C-terminus of the motor domain (residues 1-761, S1dC) of *Dictyostelium discoideum* myosin II, via a flexible triple-Gly linker region. Subsequent fusion of the second GFP or BFP to the N-terminus of the motor domain, again by a triple-Gly linker region, yielded a potential FRET pairing sensitive to conformational changes within the lever arm of *Dictyostelium* myosin II (**Fig. 5.12**). Therefore, should the lever arm tilt against the motor domain during the actin-bound working stroke of the crossbridge-cycle, as predicted by the 'lever arm hypothesis' (Holmes, 1997, Spudich, 1994), these conformational changes could be observed and quantified by analysis of the FRET changes. Suzuki *et al.* (1998), demonstrated a significant FRET change in several nucleotide-bound states representing conformational changes during the recovery stroke (ATP bound state) and after the 'reverse stroke' and $P_i$ release (ADP bound state, **Fig. 5.12**). However, quantification of movement was dependent upon the assumption that the pairs of fluorophores were rapidly rotating in solution, thus yielding a deduced $\kappa^2$ value of 0.67, which is unlikely to be the case for such large and bulky molecules.

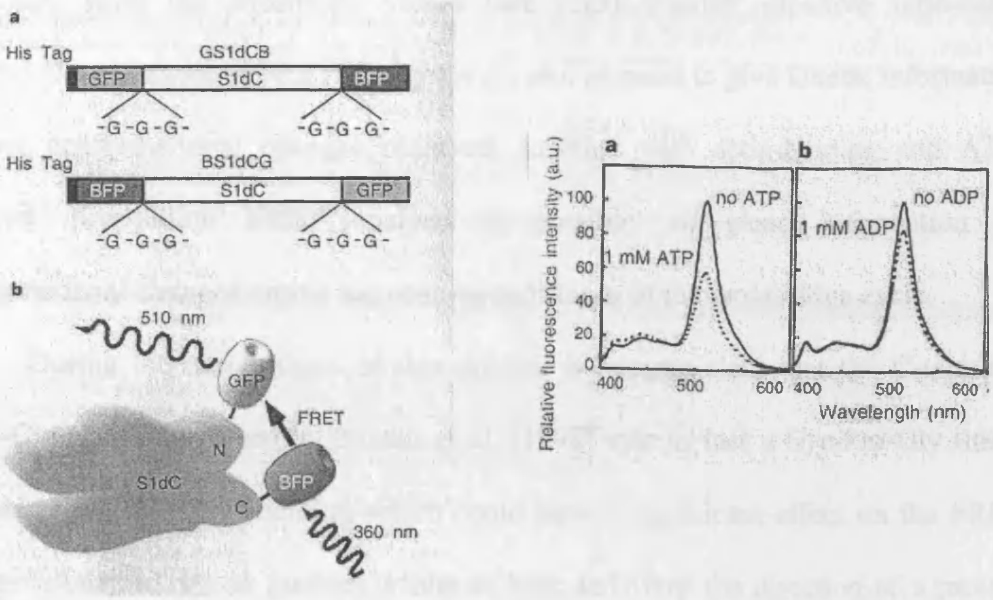


**Fig. 5.12** The structure of the *Dictyostelium discoideum* myosin II motor domain (S1dC) fusion proteins containing C-terminal and N-terminal BFP or GFP fluorophores, linked via a flexible triple-Gly region, to form a FRET pairing (left, taken from Suzuki *et al.* (1998). Also shown (right) are the FRET changes observed for these chimaeras upon ATP (40% decrease in GFP emission via FRET) and ADP (15% decrease in FRET) binding.

My main project aim related to this research was to create a similar chimera to the BS1dCG fusion protein, using YFP and CFP fluorophores due to *(a)* the unavailability to us of BFP or the original BS1dCG DNA, *(b)* the better spectral overlap for the YFP/CFP FRET pair, *(c)* the longer wavelength of the FRET pair rendering the system, in principle, more suited to light microscopy, and *(d)* the increased resistance of the CFP donor to photobleaching (BFP is very photolabile). Following the successful cloning and functional characterisation of this fusion protein, attempts to emulate the FRET changes upon ADP and ATP binding were planned, followed by anisotropy studies to determine the speed of rotation of the fluorophore pairs in solution. Should the assumed $\kappa^2$ value of 0.67 in the Förster equation prove unsuitable in quantifying FRET changes into absolute distances, studies to determine the rotational and/or orientational properties of the fluorophores would have to be undertaken, although a range of possible values for $\kappa^2$ may be

calculated from the anisotropy values (**see 1.13**). Further sensitive time-based stopped-flow analysis of FRET changes were also planned to give kinetic information on any conformational changes observed, together with actin-binding and ATP-induced dissociation FRET analysis if possible, to glean information on conformational changes during the actin-bound stages of the crossbridge cycle.

During the early stages of this project, it became clear that the C-terminal triple-Gly linker discussed by Suzuki *et al.* (1998) was in fact a Gly-Pro-Gly linker (Sasaki *et al.*, 2003), something which could have a significant effect on the FRET changes observed due to prolines nature to kink and warp the direction of a protein chain. Continuation with a triple-Gly linker was favoured to avoid this possibility, with a view to varying the linker region should any FRET changes show considerable discrepancy from the published findings.

## *5.2 Spectral changes of FRET in the presence of ATP, ADP, filamentous actin and guanidine HCl*

Following the successful cloning, purification and basic characterisation of the double fusion proteins rYFP.W501.gCFP and gYFP.W501.gCFP, and after establishing the presence of a functional FRET pairing between the N-terminal YFP and C-terminal CFP in both cases, analysis of the FRET emission spectra was carried out in several different ligand bound states to determine whether the FRET system was sensitive to small conformational changes within the W501 myosin II domain. Should this be the case, as with the BS1dCG chimera previously discussed (Suzuki *et al.*, 1998), then further studies monitoring time-based FRET changes both in the actin-free and actin-bound stages of the crossbridge cycle could be attempted. This would give an indication of the type and size of the conformational changes undergone by the lever-

arm domain during the 'reverse' tail-swing stage of the crossbridge cycle (**see 1.6 & 1.7**).

The spectral traces for rYFP.W501.gCFP and gYFP.W501.gCFP were identical within the confines of experimental error (data not shown), and thus the results presented here are generalised to cover both double-fusion proteins. Direct and exclusive excitation of the CFP fluorophore to obtain the FRET emission spectra was always obtained by using incident light of 420nm.

FRET efficiency may be calculated by monitoring *(a)* quenching of the donor emission, *(b)* enhancement of the acceptor emission, or *(c)* shortening of the fluorescent lifetime of the donor. Of the two methods readily available to us (*a* & *b*), the most reliable was quenching of the donor emission. In order to accurately calculate changes in the FRET via this method, the emission intensity of the donor (CFP) in the absence of the acceptor needed to be established. Therefore, as a single CFP intermediate was not produced during the cloning of the double fusion protein, the addition of 1M guanidine hydrochloride was employed to denature the W501 protein, while the stable β-barrel structure of the YFP and CFP probes was maintained. The two fluorophores would thus be connected by a long, denatured protein chain and no FRET would be theoretically possible.

The presence of 1M guanidine hydrochloride gave rise to a typical CFP emission spectrum (**see 1.10, Fig. 1.101**) with no visible peak from any YFP emission (**Fig. 5.21**). Therefore, no FRET was taking place between the two fluorophores. By taking the intensity of the 476nm CFP (donor) peak of the denatured protein to be the indicator of 0% FRET, the *apo* protein was shown to exhibit 38% FRET efficiency

via donor quenching. All subsequent FRET efficiency values were calulated in this way.

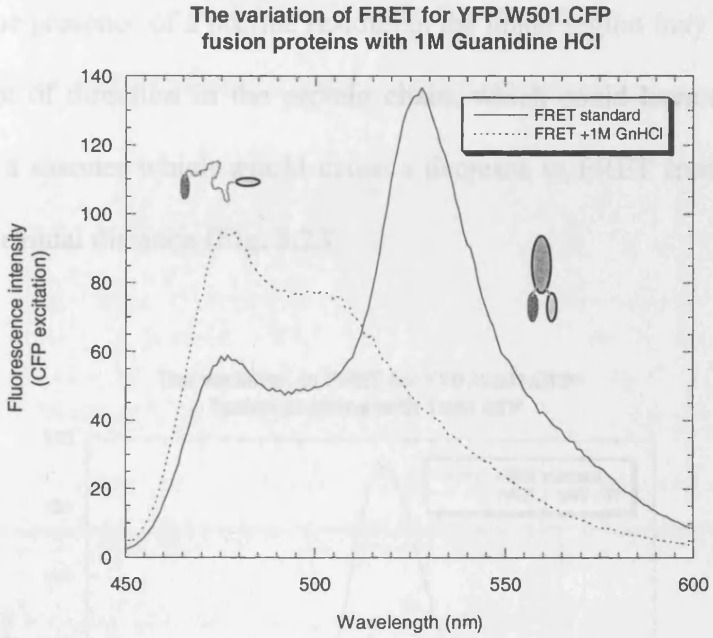


**Fig. 5.21** The variation of FRET in YFP.W501.CFP fusion proteins in the presence of 1M guanidine hydrochloride. The emission spectrum was recorded using a Varian Cary Eclipse fluorescence spectrophotometer, 1cm path length, $\lambda_{ex}$=420nm, with 1μM YFP.W501.CFP diluted in standard assay buffer (20mM HEPES, 40mM NaCl, 2mM $MgCl_2$, pH7.5, with freshly added 5mM βME, 0.01% w/v $NaN_3$). A typical CFP emission spectra was obtained, with a 60.7% increase in CFP (476nm) emission, and no YFP emission peak (76% reduction at 527nm). This indicated that no FRET was occurring, enabling the FRET efficiency of the *apo* protein (38%) to be calculated.

In a repeat of the experiment published by Suzuki *et al.* (1998), FRET was analysed upon ATP binding to YFP.W501.CFP (**Fig. 5.22**). The presence of 1mM ATP resulted in a 5.0% decrease in CFP fluorescence with a corresponding 1.1% *increase* in YFP fluorescence, indicative of a FRET change (+3.2%). These changes were considerably smaller than the published data (10% increase in BFP emission, 40% decrease in GFP emission, **Fig. 5.12, 2a**), and also in the opposite direction. This suggested that the N- and C- terminal ends of the myosin II head domain were moving closer together, thus the angle between the lever-arm and the motor domain was decreasing. This observation was in line with analysis of the crystal structures of

various ligand-bound states. After correspondence with the laboratory concerned, this discrepancy could have been attributed to the presence of a GPG linker between the N-terminal probe and the *Dictyostelium* myosin II head domain, and not a GGG linker as published. The presence of a proline residue in the linker region may have caused a 'kink' or change of direction in the protein chain, which could have re-aligned the fluorophores in a manner which would cause a decrease in FRET from a closing of the N- and C- terminal distance (**Fig. 5.23**).

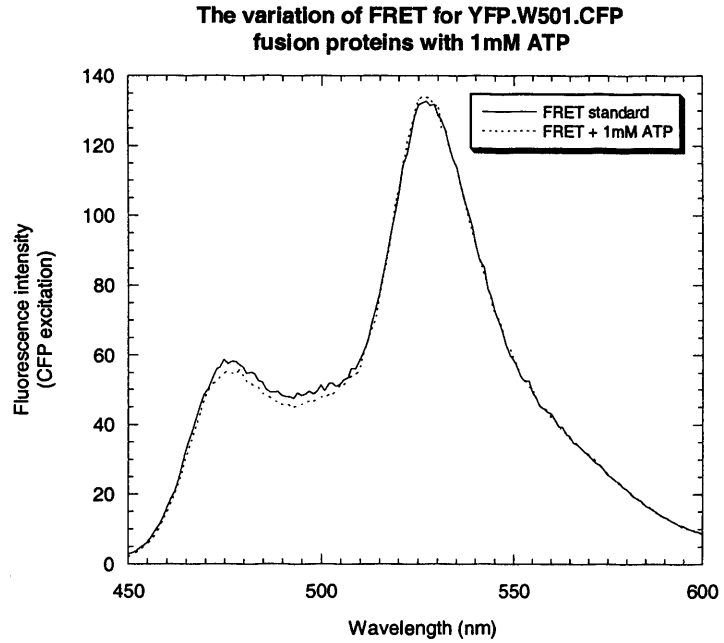


**Fig. 5.22** The variation of FRET in YFP.W501.CFP fusion proteins on addition of 1mM ATP. The emission spectrum was recorded using a 1cm path length, $\lambda_{ex}$=420nm, with 1μM YFP.W501.CFP diluted in standard assay buffer (20mM HEPES, 40mM NaCl, 2mM $MgCl_2$, pH7.5, with freshly added 5mM βME, 0.01% w/v $NaN_3$). A 5.0% decrease in CFP (476nm) emission and 1.1% increase in YFP (527nm) emission indicated a slight increase in FRET, in direct contrast to the published data (Suzuki *et al.*, 1998).

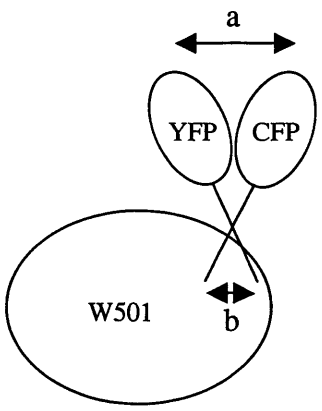


**Fig. 5.23** A potential 'scissor' alignment of the N- and C-terminal fluorescent probes which could result in a decrease in FRET from a decrease of the distance between the termini (a). The distance (b) would thus increase on shortening of the distance (a), giving rise to a decrease in FRET.

This FRET change in the presence of ATP was very small, suggesting *(a)* that the probes had moved a small distance, perhaps not at all, with simply an orientational twist of the fluorophores yielding a more favourable dipole-dipole alignment, or *(b)* that there was some factor restricting their relative movement. It was considered possible that the probes were forming dimers through non-specific electrostatic interactions. In order to account for this hypothesis, we changed the assay solution to that of a much higher ionic strength (1M NaCl) in order to disrupt these interactions.

This environmental change from low (40mM NaCl) to high (1M NaCl) ionic strength yielded a considerable decrease in FRET efficiency of the *apo* protein (to 1.8%, **Fig. 5.24**). It was concluded that this was a combination of *(a)* a disruption between the potential affinities of the fluorescent probes, a subsequent separation and decrease in FRET efficiency, and *(b)* the increased binding of chloride ions by YFP, resulting in an increase its pK and a decrease of its absorbance rendering it a weaker acceptor (Wachter and Remington, 1999).

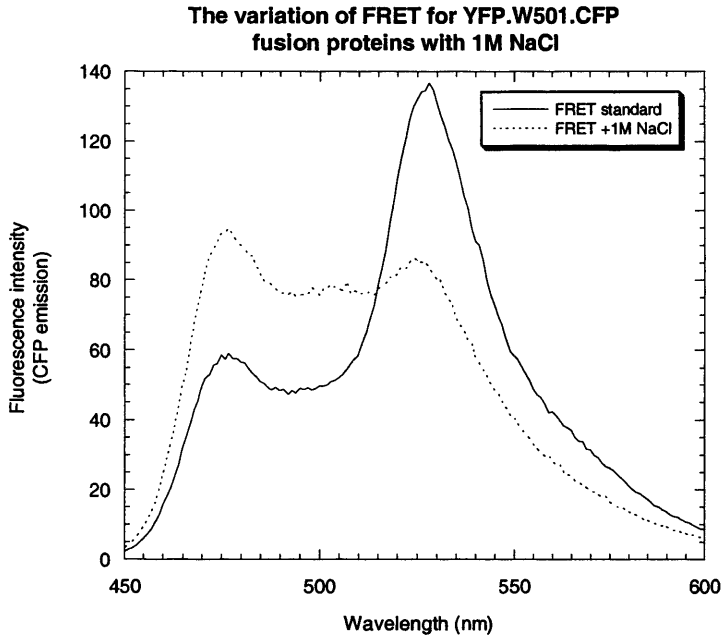


**Fig. 5.24** The variation of FRET efficiency in YFP.W501.CFP fusion proteins in high ionic conditions (1M NaCl). The emission spectrum was recorded using a 1cm path length, $\lambda_{ex}$=420nm, with 1μM YFP.W501.CFP diluted in high salt assay buffer (20mM HEPES, 1M NaCl, 2mM $MgCl_2$, with freshly added 5mM βME, 0.01% w/v $NaN_3$). A 60.7% increase in CFP (476nm) emission and a 43.3% decrease in YFP (527nm) emission indicated a substantial decrease in FRET, potentially due to YFP-CFP dimer interaction being disrupted by a high ionic strength environment, and the binding of chloride ions by YFP rendering it a weaker acceptor.

The presence of 1mM ATP in a high ionic environment yielded a 5.0% increase in FRET efficiency (**Fig. 5.25**). This was still a small change, thus more sensitive, time-based resolution using stopped-flow techniques were employed to enable a more accurate analysis of the fluorescence variations.

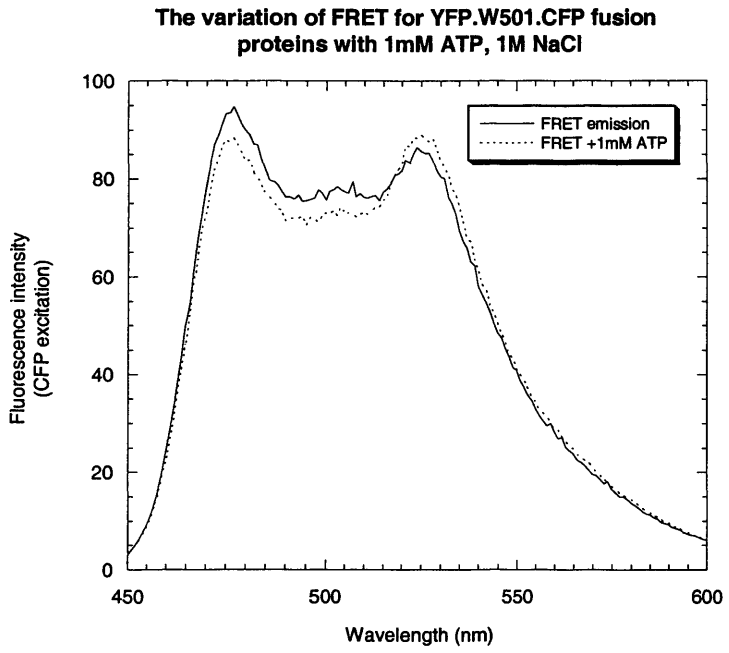


**Fig. 5.25** The variation of FRET efficiency in YFP.W501.CFP fusion proteins in high ionic conditions (1M NaCl) on addition of 1mM ATP. The emission spectrum was recorded using a 1cm path length, $\lambda_{ex}$=420nm, with 1μM YFP.W501.CFP diluted in high salt assay buffer (20mM HEPES, 1M NaCl, 2mM $MgCl_2$, with freshly added 5mM βME, 0.01% w/v $NaN_3$). An 8.1% decrease and 1.9% increase in CFP (476nm) and YFP (527nm) emission respectively (relative to *apo* intensities) indicated an increase in FRET efficiency (5.0%), again in direct contrast to previously published data (Suzuki *et al.*, 1998).

The presence of 1mM ADP resulted in a small quench emission for both probes (**Fig. 5.26**), similar to the findings of Suzuki *et al.* (1998) who observed a 20% quench in the acceptor emission, with the stability of the donor emission suggested a quench, not a variation in FRET efficiency.

In the presence of 2μM filamentous actin a slight quench in both CFP and YFP emission (10.5 and 5.5% respectively, data not shown) was observed, with a small (1-2%) further quench on addition of 1mM ATP. The presence of a 10-fold increase in filamentous actin, ensuring a large excess of available binding sites, resulted in a large quench in both CFP and YFP emission (**Fig. 5.27**). Furthermore, on subsequent addition of 1mM ATP a small (1.2%) decrease in FRET efficiency was observed. As the fluorescence emission intensities do not return to ~*apo* levels on

1mM ATP addition, but we still observe a decrease in FRET efficiency, we hypothesised that *(a)* The changes were artefactual due to the high turbidity of the solution, or *(b)* the fluorophores were forming dimers which allowed one molecule to dissociate from the actin filament while being held in place by its adjacent neighbour, turn over ATP and then reassociate with the actin filament, as mentioned previously. The strain this would place on the probes may slightly increase the separating distance or the relative orientation of their dipoles, to yield an overall decrease in FRET efficiency.

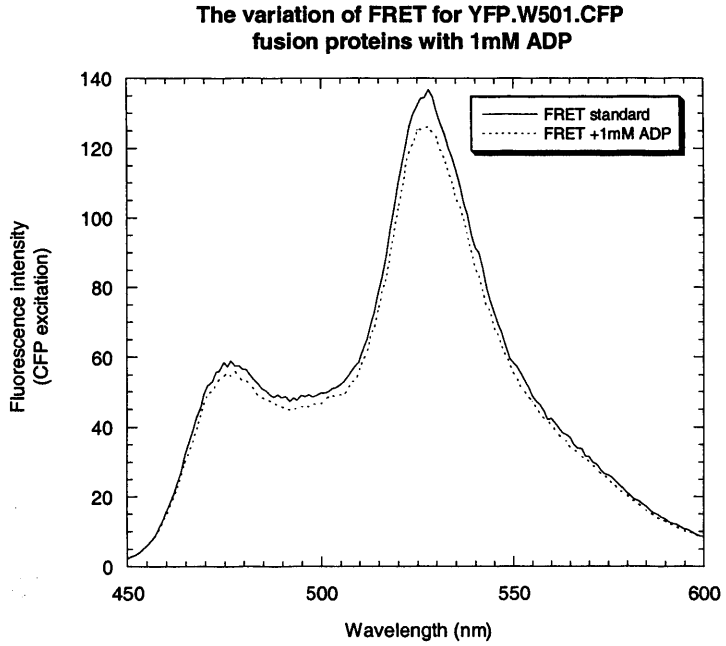


**Fig. 5.26** The variation of FRET in YFP.W501.CFP fusion proteins on addition of 1mM ADP. The emission spectrum was recorded using a 1cm path length, $\lambda_{ex}$=420nm, with 1μM YFP.W501.CFP diluted in standard assay buffer (20mM HEPES, 40mM NaCl, 2mM $MgCl_2$, pH7.5, with freshly added 5mM βME, 0.01% w/v $NaN_3$). A 5.1% and 7.9% quench in CFP (476nm) and YFP (527nm) fluorescence respectively was similar to previously published data (Suzuki *et al.*, 1998).

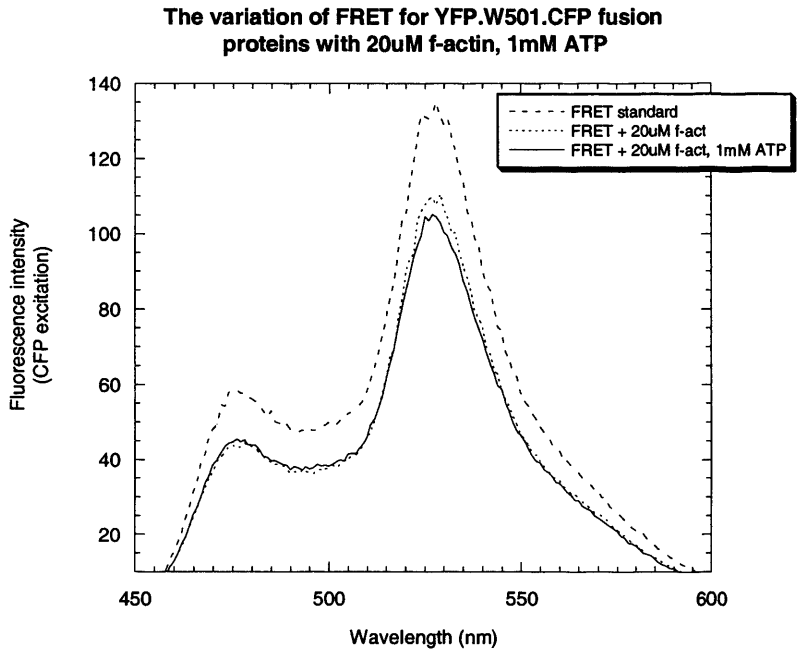


**Fig. 5.27** The variation of FRET in YFP.W501.CFP fusion proteins on addition of 20μM f-actin and 1mM ATP. The emission spectrum was recorded using a 1cm path length, $\lambda_{ex}$=420nm, with 1μM YFP.W501.CFP diluted in high salt assay buffer (20mM HEPES, 1M NaCl, 2mM $MgCl_2$, pH7.5, with freshly added 5mM βME, 0.01% w/v $NaN_3$). On addition of actin a 14.4% and 11.0% quench was observed for CFP and YFP emission respectively. Subsequent addition of ATP yielded a 1.2% decrease in FRET efficiency.

In conclusion, the YFP.W501.CFP fusion proteins contained a functional FRET pairing, which proved to be sensitive to ATP binding, both in low salt (40mM) and high salt (1M) concentrations. The FRET changes themselves indicated that the N- and C-termini of the W501 *Dictyostelium* myosin II domain move closer together upon ATP binding, although the absolute distance required further studies on the oritentational properties of the fluorophores to calculate accurately. This conformational change agrees with the analysis of the crystal structures of various ligand-bound states, but is in direct contrast to the FRET studies published by Suzuki *et al.* (1998). The presence of a proline residue in the N-terminal linker region of Sutoh and ceolleagues' (Suzuki *et al.*, 1998) BS1dCG chimera may explain this discrepancy. ADP binding to YFP.W501.CFP fusion proteins yielded a small quench

in both YFP and CFP fluorescence, as did binding to filamentous actin. Interestingly, when bound to filamentous actin the presence of ATP yielded a FRET change indicating that the N- and C-termini of the W501 myosin domain move further apart, however more evidence from sensitive time-based stopped-flow studies would be needed to distinguish this result from artefact.

| *State* | *FRET efficiency (E)* | *CFP peak (476nm) change (%)* | *YFP peak (527nm) change (%)* |
|---|---|---|---|
| *apo* | 37.7% | - | - |
| 1mM ATP | 41.0% | -5.0 | 1.1 |
| 1mM ADP | - | -5.1 | -7.9 |
| 1M NaCl (+1mM ATP) | 1.8% (6.8%) | 57.8 (49.8, [-8.0]) | -36.9 (-35.0, [+1.9]) |
| 20uM f-act (+1mM ATP) | - | -14.4 (-12.5, [+1.9]) | -11.0 (-15.5, [-4.5]) |

**Fig. 5.28** A summary of the emission intensity changes observed for both fluorescent probes of YFP.W501.CFP in various ligand bound states. The percentage change is calculated against the fluorescent intensity of the apo protein in standard assay buffer (20mM HEPES, 40mM NaCl, 2mM $MgCl_2$, pH 7.5, with freshly added 5mM βME, 0.01% w/v $NaN_3$)

## *5.3 Stopped-flow FRET changes on ATP addition, and actomyosin dissociation.*

Following the successful spectral analysis of FRET changes for various ligand-bound states of YFP.W501.CFP fusion proteins, more sensitive time-based stopped-flow analysis was employed to fully characterise the FRET efficiency change upon ATP and (potentially) actin binding. Again, only data for one of the double fusion proteins has been included when the results were identical within the confines of experimental error.

Utilising dual-detection to monitor YFP and CFP emission simultaneously, a distinct but small FRET efficiency increase on mixing with 0.5mM ATP was again recorded in both high salt (1M NaCl, 5.0%) and low salt (40mM NaCl, 3.2%) conditions (**Figs. 5.31**, **Fig. 5.32**). These changes were calculated by analysis of donor

quenching, with the donor emission of the *apo* protein assumed to be equivalent to 38% FRET efficiency based on guanidine hydrochloride denaturation studies (**see 5.2, Fig. 5.21**). At high ionic strength both fluorescence changes had a $k_{obs}$ of ~$1s^{-1}$ (single exponential fit). At low ionic strength the YFP emission change appeared faster that that of CFP ($k_{obs}$=$10s^{-1}$ and $3s^{-1}$ respectively), however this was probably due to the reduced amplitude of the changes yielding a more prominent contribution from background noise, manifesting as a waveform upon the signal itself and thus distorting the trace.

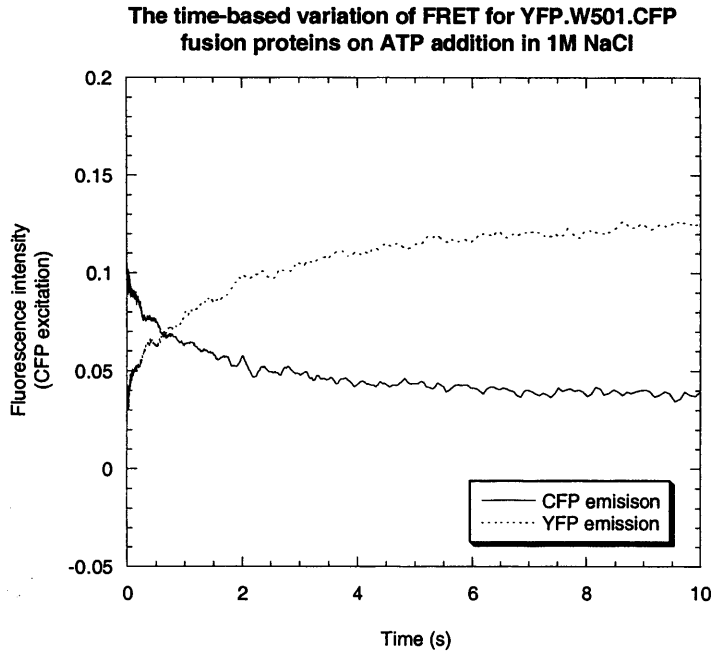


**Fig. 5.31** Stopped-flow trace of ATP interaction with YFP.W501.CFP double fusion proteins, monitored using simultaneous YFP and CFP fluorescence under exclusive CFP excitation, i.e. monitoring FRET, in a high salt environment. ATP (0.5mM, reaction chamber concentrations) was mixed with 0.5μM rYFP.W501.gCFP (in this example) in high salt assay buffer (20mM HEPES, 1M NaCl, 2mM $MgCl_2$, with freshly added 5mM βME, 0.01% w/v $NaN_3$). YFP and CFP fluorescence were monitored by excitation at 438nm and the emission selected with an OG530 cutoff filter (YFP) and GK450 & IK405 filters (CFP, Comar Ins truments, Cambridge U.K., giving 485 ± 25 nm bandpass). The traces show a 10% increase and an 8% decrease in YFP and CFP emission respectively, both with a $k_{obs}$ of ~$1s^{-1}$.

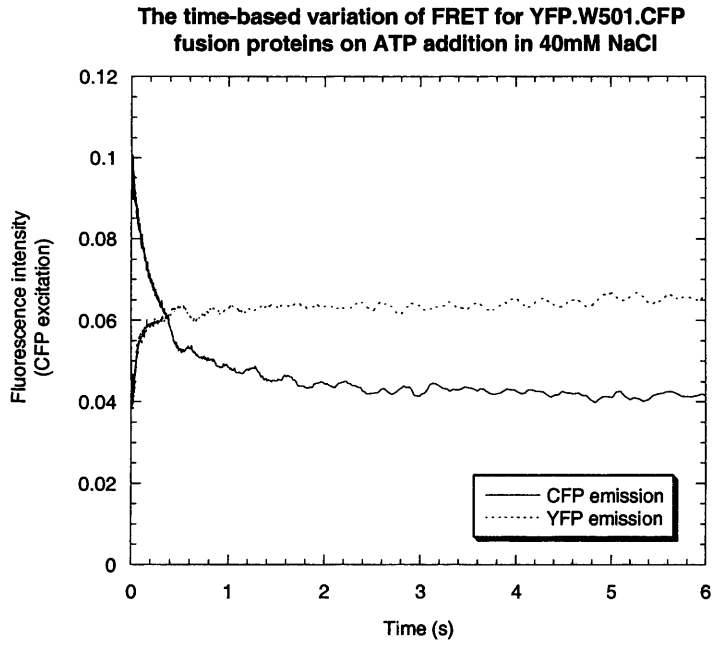


**Fig. 5.32** Stopped-flow trace of ATP interaction with YFP.W501.CFP double fusion proteins, monitored using simultaneous YFP and CFP fluorescence under exclusive CFP excitation, *i.e.* monitoring FRET, in a low salt environment. ATP (0.5mM, reaction chamber concentrations) was mixed with 0.5μM rYFP.W501.gCFP (in this example) in standard assay buffer (20mM HEPES, 40mM NaCl, 2mM $MgCl_2$, pH7.5, with freshly added 5mM βME, 0.01% w/v $NaN_3$). YFP and CFP fluorescence were monitored by excitation at 438nm. The traces showed a 2% increase and a 5% decrease in YFP and CFP emission, with $k_{obs}$ of ~$10s^{-1}$ and $3s^{-1}$ respectively. It is important to note, however, that the decreased amplitude of the signal, thus more prominent background noise, may have distorted the traces to produce the significant difference in $k_{obs}$.

Time-based monitoring of ATP turnover using dual detection of YFP and CFP fluorescence (**Fig. 5.32**) showed that the protein was functional and active with regards to ATP binding and hydrolysis with a turnover rate of $0.056s^{-1}$, and also highlighted the effect of photobleaching with prolonged exposure to incident light (slow drift from 200-300s). Thus we concluded from these observations, plus those obtained from steady-state spectra, that the FRET efficiency variations between fluorescent probes bound to the N- and C-termini of the myosin motor domain corresponded to lever arm movement in response to the presence of a nucleotide bound to the active site.

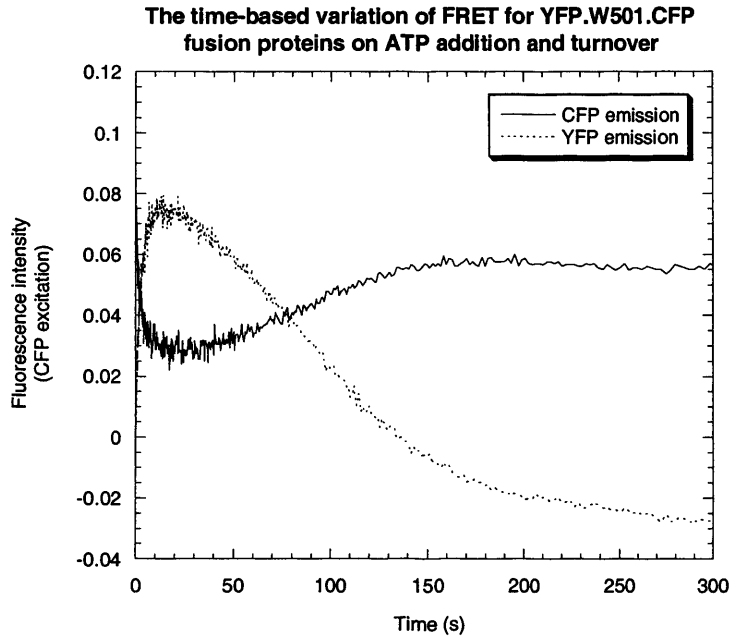


**Fig. 5.33** Stopped-flow trace of ATP interaction with YFP.W501.CFP double fusion proteins, monitored using simultaneous YFP and CFP fluorescence under exclusive CFP excitation, i.e. monitoring FRET, in a low salt environment. ATP (2.5μM, reaction chamber concentrations) was mixed with 0.5μM rYFP.W501.gCFP (in this example) in standard assay buffer (20mM HEPES, 40mM NaCl, 2mM $MgCl_2$, pH7.5, with freshly added 5mM βME, 0.01% w/v $NaN_3$). YFP and CFP fluorescence was monitored by excitation at 438nm. In this typical example, a 5x excess of ATP yielded a total turnover time of 90s and a turnover rate of $0.056s^{-1}$.

This approach was then applied to the formation and ATP-induced dissociation of the *rigor* actomyosin complex, in an attempt to monitor conformational changes which occur during the actin-bound stages of the crossbridge cycle.

Simultaneous stopped-flow monitoring of YFP and CFP emission showed no FRET efficiency change upon YFP.W501.CFP binding to F-actin (**Fig. 5.34**). YFP emission, however, showed a rapid, short-lived initial increase followed by a very slow exponential increase which had not reached a plateaux after 100s (**Fig. 5.34**). Given the extremely small nature of the initial change (2-3%), and the fact that it exists only for the first 0.1s; within the timescale of the CFP emission background noise created by the push of the stopped-flow apparatus, this change could not be resolved from artefact. As the formation of a *Dictyostelium* myosin II motor domain

actomyosin complex in solution is complete after ~5s (Kuhlman and Bagshaw, 1998) it was concluded that the slow increase in YFP emission was an artefact derived from increased bundling of actin filaments in solution, presumably facilitated by the propensity of YFP and CFP to dimerise, as discussed previously. These results argue that the lever arm does not undergo a conformational change when *Dictyostelium* myosin II binds to actin in the *rigor* state, something which is in line with data collected from crystallographic and electron microscopy studies (Holmes and Schroeder, 2003).

Simultaneous stopped-flow monitoring of YFP and CFP emission upon ATP-induced dissociation of YFP.W501.CFP actomyosin unfortunately showed no initial change in CFP emission discernable above the initial background noise. YFP emission, however, showed a fast initial increase (3%) similar to that observed as a result of increased FRET efficiency when the *apo* fusion protein bound to ATP (low salt conditions, **Fig. 5.32**). This was followed by a gradual decrease in emission (**Fig. 5.35**), presumably a de-bundling artefact.

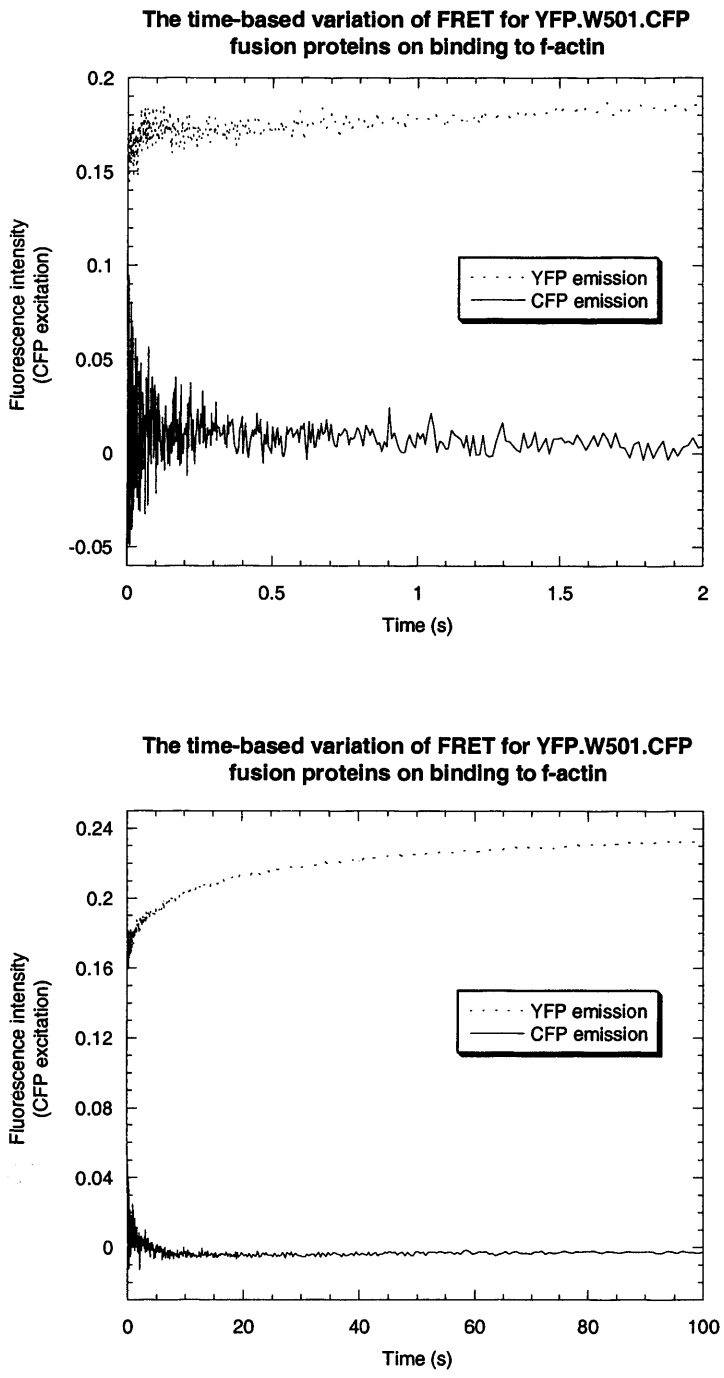


**Fig. 5.34** Stopped-flow traces of YFP.W501.CFP binding to filamentous actin, monitored using simultaneous YFP and CFP fluorescence under exclusive CFP excitation, i.e. monitoring FRET, in a low salt environment. F-actin (1μM, reaction chamber concentrations) was mixed with 0.5μM rYFP.W501.gCFP (in this example) in standard assay buffer (20mM HEPES, 40mM NaCl, 2mM $MgCl_2$, pH7.5, with freshly added 5mM βME, 0.01% w/v $NaN_3$). YFP and CFP fluorescence was monitored by excitation at 438nm. The only significant change discernable above the background noise was a slow increase in YFP emission lasting >100s, presumably due to F-actin bundling in solution and therefore artefactual.

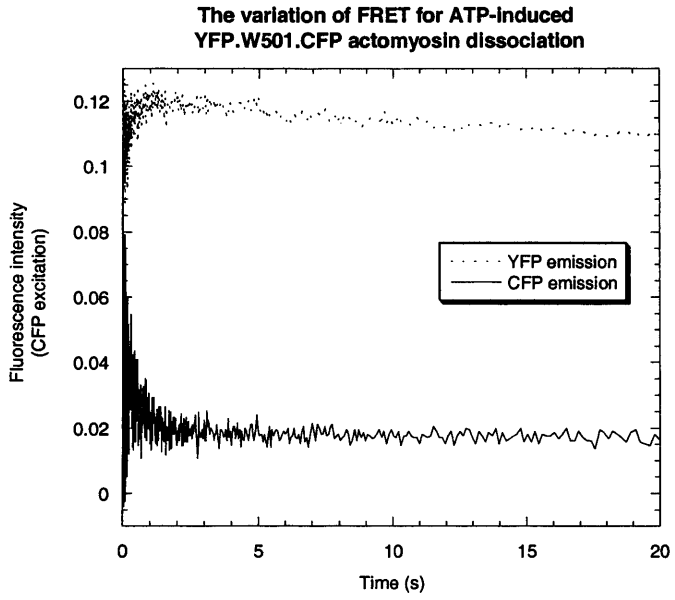


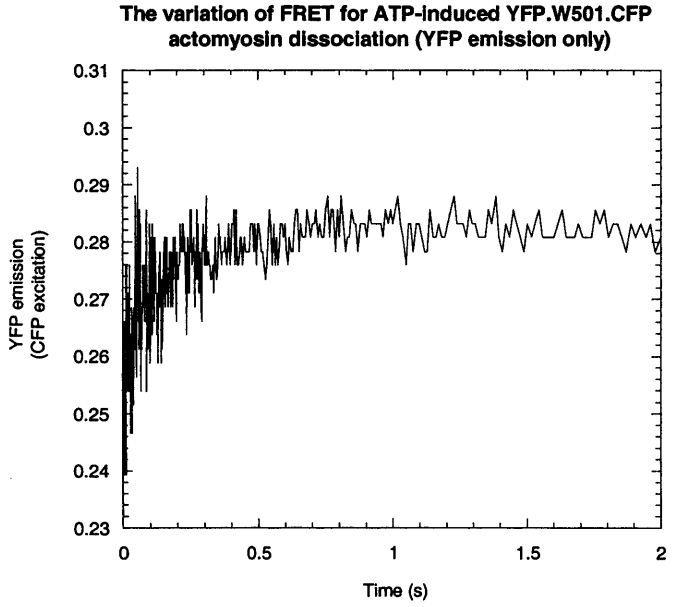


**Fig. 5.35** Stopped-flow traces of ATP-induced dissociation of YFP.W501.CFP actomyosin, monitored using simultaneous YFP and CFP fluorescence under exclusive CFP excitation, i.e. monitoring FRET, in a low salt environment. ATP (0.5mM, reaction chamber concentrations) was mixed with 0.5μM rYFP.W501.gCFP actomyosin (in this example) in standard assay buffer (20mM HEPES, 40mM NaCl, 2mM $MgCl_2$, pH7.5, with freshly added 5mM βME, 0.01% w/v $NaN_3$). YFP and CFP fluorescence was monitored by excitation at 438nm. The shorter timebase trace utilised a 1ms filter to clean up background noise. A fast <1s increase in YFP emission correlates to the FRET increase observed upon ATP binding, with the slower (>20s) decrease in YFP emission presumably a de-bundling artefact.

In conclusion, a small increase in FRET was again observed, as with the steady-state spectral analysis, on binding of ATP to the active site of the myosin motor domain of YFP.W501.CFP fusion proteins, in direct contrast to the decrease in FRET efficiency reported in previous studies (Suzuki *et al.*, 1998). This increase was again more significant in high salt (1M NaCl) conditions than in a conventional assay buffer environment (40mM NaCl), suggesting that electrostatic interactions between the fluorescent probes may have been affecting their freedom of movement although the activity of the myosin motor was retained. These findings provided evidence of lever arm movement in response to nucleotide occupation of the active site of the myosin motor, although quantification of the absolute distances required further anisotropy and/or studies into the relative orientations of the probes. The addition of F-actin to YFP.W501.CFP fusion proteins gave no significant intial change in FRET, however a slow increase in YFP emission over a period of >100s was presumably an artefact due to filamentous bundling of actin in solution being facilitated by the propensity of YFP and CFP to dimerise. ATP-induced dissociation of YFP.W501.CFP actomyosin yielded a small increase in YFP over a 1s timescale corresponding to an increase in FRET efficiency due to the conformational change caused by ATP-binding. This was followed by a slow decrease in YFP emission over >20s, presumably a de-bundling artefact arising from actomyosin dissociation.

## *5.4 Anisotropy studies on FP myosin II fusion proteins*

Quantification of physical movement from FRET efficiency variations requires the implementation of the Förster equation, as mentioned previously (**1.12**). The orientation factor $\kappa^2$ within this equation can be deduced to be 0.67 for pairs of rapidly rotating fluorophores. Therefore, fluorophores that display an anisotropy of $\approx 0$, thus

indicating a rapid rotation on the nanoseconds timescale, require no further studies for quantification of movement. However, those that exhibit an anisotropy approaching that of the theoretical maximum for totally immobilised fluorophores randomly distributed in solution (0.4) require specific determination of the orientation factor via polarisation studies.

Steady-state anisotropy measurements on isolated eGFP, W501.gGFP and rYFP.W501 showed that the fluorophores were virtually immobile on the timescale of their fluorescent lifetime (~3ns, **Fig. 5.41**), an observation which was in line with previous studies (Chattoraj *et al.*, 1996). Given that the molecular volume of GFP itself yields a slowly rotating fluorophore with an anisotropy of 0.295, it was expected that tethering the fluorophore to a myosin domain would cause only a little additional restriction. These readings also proved useful in the subsequent development of isotropic excitation prisms for use in TIRFM (Wakelin and Bagshaw, 2002).

| Protein | *Ligand* | *Anisotropy* |
|---|---|---|
| **GFP** | - | 0.295 ± 0.008 |
| **W501.gGFP** | - | 0.311 ± 0.002 |
| **W501.gGFP** | F-actin | 0.311 ± 0.003 |
| **W501.gGFP** | ATP | 0.311 ± 0.003 |
| **rYFP.W501** | - | 0.311 ± 0.002 |
| **Fluorescein** | - | 0.046 ± 0.002 |

**Fig. 5.41** Comparison of anisotropy values for GFP (λex=490nm, λem=510nm), courtesy of Mohammed Kahir, W501.gGFP (λex=490nm, λem=510nm) in *apo*, ATP, and F-actin bound states, rYFP.W501 (λex=480nm, λem=535nm) and fluorescein (λex=490nm, λem=520nm). Measurements were recorded on an SLM 48000S fluorescence spectrophotometer, using 1μM of each protein diluted in standard assay buffer (20mM HEPES, 40mM NaCl, 2mM $MgCl_2$, pH7.5, with freshly added 5mM βME, 0.01% w/v $NaN_3$), with Glans-Thompson polarising quartz prisms.

The anisotropy of the fusion proteins was insensitive to ATP binding in steady-state and polarisation resolved stopped-flow studies, and even binding to bulky filamentous actin yielded no anisotropy change. Therefore, the difference from the theoretical maximum (0.4) probably arose from a small difference between the absorption and

emission dipoles of the GFP and YFP fluorophores (Lacowicz, 1999, Rosell and Boxer, 2003).

Steady-state anisotropy measurements on the gYFP.W501.gCFP double fusion protein similarly showed that it was virtually immobile (0.375 anisotropy) on the nanoseconds timescale when CFP fluorescence was excited directly (**Fig. 5.42**). These anisotropy values proved insensitive to ATP binding and remained relatively unchanged in low salt (40mM NaCl) or high salt (1M NaCl) conditions. The higher anisotropy reading relative to that of a single W501-bound YFP or GFP was attributed to a more favourable alignment of the absorption and emission dipoles within the CFP fluorophore itself.

Furthermore, the anisotropy values for gYFP.W501.gCFP FRET emission, were decreased by a factor of 3 ($a$=0.103) in low salt conditions, and a factor of 2 in high salt conditions ($a$=0.187). As we could assume that the rotational mobility of the protein was not affected by the wavelength at which the emitted light was observed, the decrease in anisotropy was most probably due to different alignments of the donor and acceptor dipoles. This depolarisation by FRET was confirmed by comparisons between a FRET anisotropy spectrum and a FRET emission spectrum for gYFP.W501.gCFP (**Fig. 5.43**). The anisotropy for direct CFP emission (460-510nm) remains close to the theoretical maximum of 0.4, whereupon a sharp drop in anisotropy is observed for YFP emission as a direct result of FRET (510-560nm).

The increase in gYFP.W501.gCFP FRET anisotropy from 0.10-0.19 in high salt conditions (1M NaCl) presumably arises from the decrease in FRET efficiency that occurs in this environment (**see 5.2, Fig, 5.24**). A decrease in FRET efficiency would result in an increase in highly polarised CFP emission, which would contribute to the overall anisotropy to a greater degree thereby increasing the final result.

Alternatively, the increase in anisotropy could arise from disruption of electrostatic interactions between the probes, allowing the separating distance to increase, while the dipoles themselves attain a more favourable alignment.

| | | *40mM NaCl buffer* | | *1M NaCl buffer* | |
|---|---|---|---|---|---|
| ***Protein*** | $\lambda_{ex}$ $\lambda_{em}$ | ***Ligand*** | ***Anisotropy*** | ***Ligand*** | ***Anisotropy*** |
| gYFP.W501.gCFP | CFP | - | 0.375 ± 0.010 | - | 0.368 ± 0.002 |
| gYFP.W501.gCFP | CFP | ATP | 0.366 ± 0.002 | ATP | 0.349 ± 0.006 |
| gYFP.W501.gCFP | FRET | - | 0.103 ± 0.003 | - | 0.187 ± 0.009 |
| gYFP.W501.gCFP | FRET | ATP | 0.108 ± 0.006 | ATP | 0.187 ± 0.009 |
| gYFP.W501.gCFP | YFP | - | 0.267 ± 0.001 | - | 0.309 ± 0.004 |
| gYFP.W501.gCFP | YFP | ATP | 0.268 ± 0.002 | ATP | 0.303 ± 0.010 |

**Fig. 5.42** Comparisons of anisotropy values for gYFP.W501.gCFP in the *apo* and ATP bound states, in low salt (40mM NaCl) and high salt (1M NaCl) conditions, for direct CFP excitation / emission (λex=420nm, λex=510nm), direct YFP excitation / emission (λex=480nm, λem=535nm), and for FRET emission (λex=420nm, λem=535nm). Measurements were recorded using 1μM protein diluted in standard assay buffer (20mM HEPES, 40mM NaCl, 2mM $MgCl_2$, pH7.5, with freshly added 5mM βME, 0.01% w/v $NaN_3$), with Glans-Thompson polarising quartz prisms. Courtesy of Rob Woolley, Leicester University.

Steady-state anisotropy measurements on gYFP.W501.gCFP via the direct analysis of YFP fluorescence again showed *(a)* the fluorophore to be relatively immobile on the nanoseconds timescale, and *(b)* that the anisotropy values were insensitive to ATP binding. The lower anisotropy relative to rYFP.W501 observed in low salt conditions was presumably due to a small excitation of CFP, thus a small degree of FRET, occurring at the YFP excitation wavelength. At high salt concentrations, as alluded to previously, the decrease in affinity for interactions between the fluorescent probes yielded a decrease in FRET efficiency, thereby increasing the anisotropy almost to the value of a single W501-bound YFP fluorophore.

Due to the restricted availability of the double-fusion proteins and considering the similarly large bulk of gYFP.W501.gCFP and rYFP.W501.gCFP it was assumed that the rYFP.W501.gCFP protein would also be virtually immobile on the timescale of its fluorescent lifetime (~3ns).

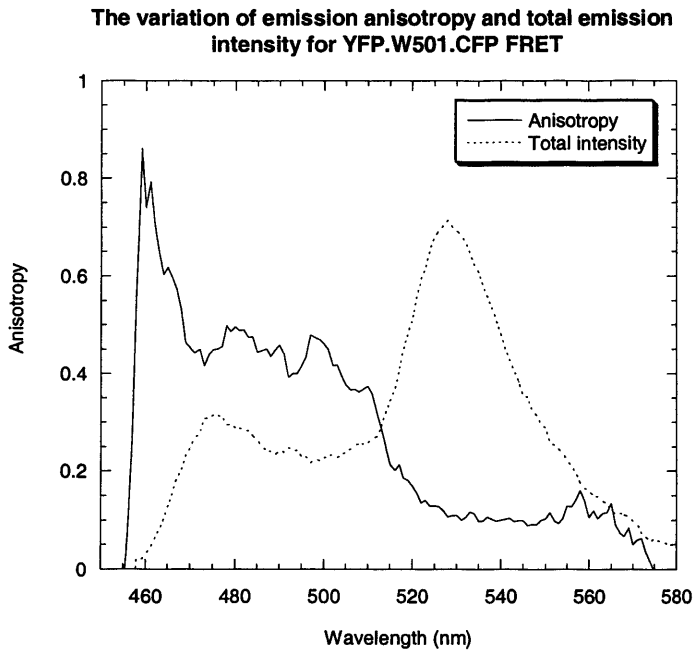


**Fig. 5.43** Depolarisation by FRET, as demonstrated by a comparison of anisotropy and emission spectra for gYFP.W501.gCFP. Measurements were recorded on an SLM 48000S fluorescence spectrophotometer, $\lambda_{ex}$=420nm, using 1μM protein diluted in standard assay buffer (20mM HEPES, 40mM NaCl, 2mM $MgCl_2$, pH7.5, with freshly added 5mM βME, 0.01% w/v $NaN_3$). Direct CFP emission heralded a high anisotropy of ~0.4 from 460-510nm, whereupon a sharp drop in anisotropy accompanied YFP emission via FRET from 510-560nm. Anisotropy values of >0.4 were due to a light scattering contribution.

In conclusion, the W501.gGFP and rYFP.W501 single fusion proteins, and the gYFP.W501.gCFP double fusion protein were relatively immobile on the nanoseconds timescale and as such required further studies to determine a suitable value for $\kappa^2$ in the Förster equation before quantification of movement from the previous FRET changes could be accurately achieved. Fluorescent emission from YFP as a direct result of FRET was depolarised due to a difference in the alignment of the donor and acceptor dipoles, resulting in a lower anisotropy reading than a perfectly aligned YFP fluorophore would be expected to produce. Direct CFP emission yielded a higher anisotropy reading than that of a single W501-bound YFP or GFP, presumably due to a more favourable alignment of the absorption and emission dipoles within the CFP fluorophore itself.

## *5.5 Conclusion*

To conclude, the YFP.W501.CFP fusion proteins contained a functional FRET pairing consisting of YFP and CFP fluorescent probes fused to the N and C-termini of the W501 *Dictyostelium* myosin II motor domain, similar to systems used to study conformational changes of the lever arm in previous studies (Shih *et al.*, 2000, Suzuki *et al.*, 1998, Xiao *et al.*, 2003). Considerable FRET between these two probes was observed in the fusion proteins *apo* state (38% efficiency), with a small increase in FRET efficiency occurring upon ATP occupancy of the active site in both steady-state spectral analysis and time-based stopped-flow studies. This FRET increase is supported by evidence from the analysis of various ligand-bound crystal structures, but was in direct contrast to the significant decrease in FRET reported by Suzuki *et al.* (1998) using the BS1dCG chimera. However, this discrepancy may well be due to the presence of an unreported proline residue in the linker region between the fluorescent probes and the myosin motor domain of the chimera (Sasaki *et al.*, 2003), thus potentially altering the orientations of the probes relative to each other. Nevertheless, this FRET change provides evidence of lever arm movement upon ATP binding to the active site, although quantification into absolute distances cannot be accurately achieved due to the relative immobility of the proteins on the timescale of their fluorescent lifetimes (~3ns), as shown by anisotropy values of ~0.3. Therefore the $\kappa^2$ value of 0.67 used for rapidly rotating fluorophores in solution cannot be applied to the Förster equation. Thus, although a closing of the distance between the N and C-termini can be assumed upon ATP binding to the active site (thus a FRET efficiency increase), further studies into the relative orientations of the YFP and CFP probes

need to be carried out before definite claims and absolute distances may be accurately calculated.

However, YFP emission as a direct result of FRET was depolarised due to a difference in the alignment of the donor and acceptor dipoles, resulting in a lower anisotropy despite being virtually immobile on the nanoseconds timescale. This observation enabled a range of values for $\kappa^2$ to be obtained via the use of a family of curves, calculated by Dale *et al*, (1979), relating the upper and lower limits of $\kappa^2$ for FRET pairs where the donor, acceptor and FRET anisotropies are defined. The myosin contructs yielded CFP donor and YFP acceptor anisotropies of 0.368 and 0.309 respectively, while the FRET anisotropy was 0.187 (**Fig. 5.42**). These values were normalised to 0.4 (The theoretical maximum anisotropy) to give $CFP_{don}$ = 0.92, $YFP_{acc}$ = 0.77, FRET = 0.47, from which the range of $\kappa^2$ (0.17-2.9) was read from the published contour plots. This enabled a range of potential values to be calculated for $R_o$ and $r$ (**Fig. 5.51**) using the following equations;

$$\kappa^2 = \left(\cos\theta_T - 3\cos\theta_D \cos\theta_A\right)^2$$

$$R_0^6 = 8.8\times10^{-25}\left(\kappa^2 n^{-4} \phi_d J\right)$$

$$r = \sqrt[6]{\frac{R_0^6(1-E)}{E}}$$

| *Variable* | *YFP.W501.CFP in the apo state* | *YFP.W501.CFP in the presence of ATP* |
|---|---|---|
| $a$ | 0.187 | 0.187 |
| $\theta_T$ | 36.57 | 36.57 |
| $\kappa^2$ | 0.17-2.9 | 0.17-2.9 |
| $R_o$ | 3.92-6.28 | 3.92-6.28 |
| $E$ | 0.38 | 0.43 |
| *r (nm)* | 4.25 – 6.82 | 4.10 – 6.58 |

**Fig. 5.51** The range of possible values for $\kappa^2$ (the orientation factor relating the donor and acceptor dipoles), $R_o$ (the Förster distance) and $r$ (the donor and acceptor

distance), as derived from the FRET anisotropy *a*. This value allows the calculation of $\theta$, which is equivalent to the angle $\theta_T$ for the calculation of $\kappa^2$. The relevant equations are listed above, where $\theta_T$, $\theta_A$ *and* $\theta_D$ represent the angles relating the donor and acceptor dipoles in the x, y and z-planes (note: when calculating the range of $\kappa^2$, if $\theta_A=0^\circ$, $\theta_D$ must be equal or greater than $\theta_T$ to a maximum of $90^\circ$, and *vice versa*), *E* represents the FRET efficiency, $\Phi_d$ the quantum yield of the donor and *J* the overlap integral of the donor emission and acceptor absorption.

Thus, as the range of fluorescent probe separation distances (*r*) share an ~90% overlap between the *apo* and ATP bound states, it is not possible to determine whether the changes in FRET efficiency are a result of changes in *r*, or a result of orientational variations altering $\kappa^2$. Therefore the result is qualitative rather than quantitative.

Increasing the ionic strength of the environment yielded a decrease in FRET efficiency for the *apo* protein, presumably due to either *(a)* the disruption of non-specific electrostatic interactions between the fluorescent probes (potential dimer formation), or *(b)* a reduction in the absorbance of YFP upon binding to chloride ions which make it a weaker acceptor (Wachter and Remington, 1999). Furthermore, the change in FRET efficiency upon ATP binding was considerably greater in a high ionic strength environment, lending support to the hypothesis that electrostatic interactions between the fluorescent probes may be restricting their freedom of movement, although the activity of the myosin motor was retained.

ADP binding to the active site of the myosin motor domain yielded a small quench in both YFP and CFP emission, but no discernable change in FRET. Similarly, binding to F-actin gave rise to a quench in both fluorophores, but gave no significant initial change in FRET. This suggests that the lever arm does not undergo any conformational change upon binding of the *apo* myosin motor to actin in the *rigor* state, something which crystallographic and electron microscopy studies have reported, as no change in the myosin head/light chain binding domain angle was necessary when docking molecular structures into the electron density patterns of

decorated filaments (Holmes and Schroeder, 2003). However, upon actin binding in solution a slow increase in YFP emission was observed over a 100s+ timescale. This was presumably an artefact due to filamentous bundling of actin in solution being facilitated by the propensity of YFP and CFP to dimerise. ATP-induced dissociation of YFP.W501.CFP actomyosin yielded a small increase in FRET efficiency due to the conformational change caused by ATP-binding, followed by a slow decrease in YFP emission over >20s. The latter was presumably a de-bundling artefact arising from actomyosin dissociation.

Furthermore, with respect to the N-terminal linker region, no significant difference was observed between the triple-Gly and rigid linker proteins for any of the above studies.

# 6 - Discussion

Within this section the overall conclusions from the work undertaken during this thesis will be collated, reviewed, and further hypotheses drawn. As with any active field within scientific research, there is a large amount of recent literature which complements the approaches used, and as such will be reviewed and relevant implications drawn. Furthermore, since the cessation of my laboratory work in August 2003, subsequent experiments into areas pertaining to my thesis (particularly into the non-fluorescent states of YFP) have extended or clarified some of my initial findings, and thus will be included as part of this discussion. The potential practical uses for some of the techniques developed, and suggestions for the direction of future research will also be given.

The fusion of *gfp*, *yfp*, or *cfp* genes to the N- or C-termini of the *Dictyostelium* myosin II mutant *w501* produced viable proteins in *Dictyostelium discoideum,* which exhibited conventional fluorescence with respect to the fluorophores used (YFP [$\lambda_{ex}$=514nm, $\lambda_{ex}$=527nm]; CFP [$\lambda_{ex}$=434, 452nm, $\lambda_{em}$=476, 505nm]; GFP [$\lambda_{ex}$=488nm, $\lambda_{em}$=507-508nm]). All the novel fusion proteins also exhibited a well-defined tryptophan peak which responded to ATP-binding and hydrolysis (more specifically to the OPEN-CLOSED transition) with kinetics similar to those of W501 alone (~30$s^{-1}$, overall ATPase 0.05$s^{-1}$). Thus, the W501 myosin motor retained its ATPase functionality when a FP-type moiety was fused to either or both termini.

### *6.1 Disruption of ATP-induced actomyosin dissociation kinetics*

Transient solution kinetic analysis showed a slow phase and fast phase for the ATP-induced actomyosin dissociation of the novel fusion proteins. A comparison with TIRFM caged-ATP flash photolysis assays of single fixed actomyosin filaments

showed the slow phase to be more dominant in solution, therefore this was likely to be a result of increased actin-bundling, presumably caused by FP-type proteins propensity to dimerise when brought into close proximity (Tsien, 1998). Further evidence of this bundling effect was provided by EM images of actin filaments fully decorated with single or double fusion protein (**see 4.23**).

Transient kinetic analysis of the fast phase, assumed to be a measure of the ATP-induced actomyosin dissociation, showed the single fusion proteins to have maximum dissociation rate constants ($k_{max}$=150$s^{-1}$, 123$s^{-1}$ for rYFP.W501 and W501.gGFP respectively) similar to those of W501. However, the $k_{obs}$ for specific [ATP] below the maximal level were slower than those of W501, indicating that a higher [ATP] was required to achieve $k_{max}$.

TIRFM caged-ATP flash photolysis assays for the single fusion proteins showed faster kinetics at less than maximal [ATP] than those obtained in solution, which suggests an artefactual bundling component within the fast phase analysis of the latter. However the dissociation rate constants for the former ($k_{obs}$) were still slower than those expected for W501. Thus, the fusion of an FP fluorescent probe to either the N- or C-terminus of the W501 protein increased the apparent binding affinity for actin.

This observation was compounded by the fact that single fusion proteins bound to actin (fully decorated) were not competitively inhibited by HMM, nor did they appear to be in dynamic equilibrium with fusion proteins in solution, but rather permanently fixed (1hr+) in a *rigor* state. Considering that the N- and C-termini exist on the opposite side of the myosin motor domain to the actin-binding site, it seems unlikely that the probes were directly affecting the binding affinity via steric interference. Therefore, once again the reported propensity for FP-type molecules to

dimerise at high concentrations needs to be addressed. At high loadings fusion proteins bound to actin would be forced into close proximity, thus it is likely that electrostatic interactions may occur between the FP-moieties of proteins bound to adjacent actin monomers. Therefore it is conceivable that one molecule could detach from actin, but be held in place via FP-FP interactions, before reassociating while the adjacent protein is still bound. If this were the case then the double-fusion proteins would show a much greater binding affinity to actin as they have the potential to form an interconnected chain of myosin domains, held together by YFP-CFP dimers, along the length of a fully decorated filament. Transient kinetic analysis and TIRFM flash photolysis assays subsequently showed the kinetics of the YFP.W501.CFP fusion proteins to be extremely slow compared to W501 and the single fusion proteins, both for $k_{obs}$ and $k_{max}$ ($23s^{-1}$), giving evidence to support the hypothesis that ATP-induced actomyosin dissociation kinetics were disrupted by the non-specific electrostatic interactions between the fluorescent probes themselves.

Subsequent research by Dr. Zeng & Prof. Bagshaw, involving the reduction the fluorophores' propensity to dimerise by the point mutation of specific hydrophobic residues within the β-barrel (A206K, L221K, F223R, Zacharias *et al.*, 2002), yielded no apparent increase in the single fusion proteins' ATP-dissociation kinetics ($k_{obs}$), thus the exact reason for their disruption still remains ambiguous. Further work to investigate and/or solve this problem could involve *(a)* FPLC to determine if fusion protein dimers exist in solution, and *(b)* the kinetic analysis of ATP-induced dissociation, using TIRFM caged-ATP flash photolysis, of single molecules of fusion protein bound to actin. This could be achieved via sub-stoichiometric loadings, and should negate the potential effect of FP-FP interactions, provided that the molecules do not bind exclusively in dimer pairs.

In summary, although the myosin ATPase appears unaffected by fusion of an FP fluorescent probe to W501, the ATP-induced actomyosin dissociation kinetics appear to be disrupted. Therefore, these systems cannot be realistically employed to investigate the actomyosin ATPase using current transient techniques, although FRET studies on the double fusion proteins still have the potential to impart useful kinetic and conformational information.

However, on a more positive note, it has been shown that transient kinetic information can be obtained for fluorescently labelled myosin constructs using a combination of TIRFM and caged-ATP flash photolysis. Unlike previous studies which photolysed the entire sample (Weiss *et al.*, 2000), this technique selectively photolyses the caged-ATP contained within the volume of one field of view of a flow-cell. Diffusion of the localised ATP burst only becomes a problem at high caged-ATP concentrations, and thus multiple flashes may be applied to a single sample. Thus, this technique has the potential to yield transient kinetic information using only 10µl of 1nM protein (~1ng of fusion protein), and may therefore allow the kinetic resolution of myosin proteins only available in «µg quantities. The maximum resolution of this technique ($k_{obs}$=25$s^{-1}$) is limited by the video-capture frame-rate (0.04s), however this may be increased to the limit of flash photolysis itself (0.004s, max. $k_{obs}$=250$s^{-1}$) by employing photon-counting apparatus instead of video-capture. Furthermore, the successful visualisation using TIRFM of single molecules of fluorescently labelled W501, achieved via sub-stoichiometric labelling of fixed actin filaments (**Fig. 6.11**), opens up opportunities for the development of this technique to investigate the processivity of fluorescently labelled non-classical (non-myosin II) myosins (discussed later).

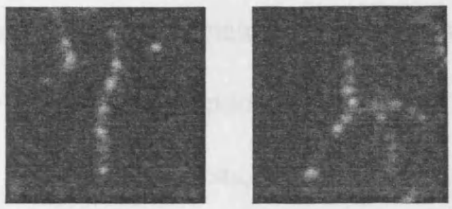

**Fig 6.11** Single molecule visualisation of W501.gGFP using TIRFM. Aged HMM-fixed actin filaments were decorated (via perfusion through a flow-cell) with sub-stoichiometric (1:10 ratio) amounts of W501.gGFP. Excitation was achieved with 488nm laser light from and argon-ion laser, and the excitation/emission selected with 455DF70/510AF23 filters.

### *6.2 FRET studies of the YFP.W501.CFP fusion proteins*

The fusion of YFP and CFP fluorescent probes to the N- and C-termini of W501 produced a functional FRET pairing, which proved to be sensitive (~3-6% increase) to ATP binding both in low salt (40mM) and high salt (1M) conditions. The increase in FRET was not affected by the absence of the N-terminal linker (GGG), and was observed both in steady-state spectral analysis and time-resolved solution kinetics. This result has proven to be more qualitative than quantitative due to *(a)* The relative immobility of the protein on the timescale of their fluorescent lifetime (~3ns, anisotropy ~0.35) negating the assumption that $\kappa^2$=0.67 for the Förster equation, and thus *(b)* two angles ($\theta_D$, $\theta_A$) relating the orientations of the fluorescent dipoles are unknown, leading to a range of possible $\kappa^2$ values, therefore a range of possible absolute distances (*r*). Despite this, these data suggest a *decrease* in the distance between the N- and C-termini of W501, thus a lever arm movement towards the myosin motor, on nucleotide occupancy of the active site. This observation is in line with evidence from the analysis of various ligand-bound crystal structures, but is in direct contrast to the similar FRET work published by Suzuki *et al.* (1998). Initial collaborative efforts to reproduce the results reported by Suzuki *et al.* (1998) were thwarted by the wrong construct being supplied.

At high ionic strength the *apo* protein showed a considerably lower degree of FRET. This could be due to *(a)* the disruption of (potential) non-specific electrostatic interactions between the fluorescent probes, or *(b)* a reduction in the absorbance of YFP upon binding to chloride ions, thus making it a weaker acceptor (Wachter and Remington, 1999). The greater FRET change observed at high ionic strength lends support to *(a)*. ADP binding to the YFP.W501.CFP fusion proteins yielded a small quench in both YFP and CFP emission, as did binding to filamentous actin. This suggests that the lever arm does not undergo any conformational change when binding to actin in the *rigor* state. This finding is supported by the fact that no change in the angle between the myosin head and light-chain binding domain was required when docking molecular structures (from crystallography) into the electron density patterns of decorated filaments (from EM, Holmes and Schroeder, 2003).

Subsequent research by Dr. Zeng and Prof. Bagshaw has shown that the absence of both GGG linker regions has no effect upon the FRET changes observed. Also, collaborative work with Sutoh and colleagues has resulted in the reproduction of their published findings (Suzuki *et al.*, 1998). However, sequence analysis has shown the presence of a proline in the N-terminal linker region (GPG, also reported by Sasaki *et al.*, 2003), and a two residue deletion at the C-terminal region of the myosin motor domain (EARE**QR***761* → EARE*759*). Thus the contradictory results from the YFP.W501.CFP and BS1dCG proteins may be due to differing relative alignments/orientations of the fluorescent probes resulting from *(a)* a kink in the protein chain caused by the proline residue, or *(b)* the fluorescent probe being fused 2-residues earlier along the C-terminal α-helix, thus projecting out at a radically different angle. Furthermore, anisotropy spectra have shown the *Sutoh* clone (BS1dCG) to undergo a distinct anisotropy increase in the presence of ATP, unlike

the YFP.W501.CFP fusion proteins. This suggests that the reported FRET *decrease* (Suzuki *et al.*, 1998) contains a considerable orientational element, and as such cannot accurately be quantified.

Due to the small FRET changes observed during these studies, further research (using this system) into the nature of the myosin motor during actin-bound stages of the crossbridge cycle hinges on the improvement of FRET between the CFP and YFP probes. Recent studies by Miyawaki and colleagues (Nagai *et al.*, 2004) have shown a distinct increase in the dynamic range of a CFP-YFP FRET pairing, by the development of a circularly permuted YFP (cpYFP). The creation of a cpYFP.W501.CFP fusion protein may yield better resolution of FRET changes, from which further kinetic and conformational information may be gleaned.

### *6.3 Recent research into the photoexcitation of YFP*

The observation that a fixed actin filament, fully decorated with rYFP.W501 and fully photobleached, regained ~25% of its fluorescent intensity over ~1s when exposed to a 4ms UV flash (350nm), led to the conclusion that this was a direct observation of the transition from the proposed dormant 'dark-state' of YFP (Miyawaki and Tsien, 2000) back to the conventional excited state of the fluorophore (photoexcitation, **see 4.32**). The potential applications for this technique as an analytical tool, particularly towards cells *in vivo*, led to further investigations by Prof. Bagshaw & Dr. Zeng into the mechanism by which this process takes place. The current scheme (**Fig. 6.31**) shows that the chromophore of YFP is constantly in a dynamic equilibrium between a protonated and non-protonated state ($YFP^-$ and YFPH respectively). It has been suggested that protonation (<1ms) of the excited state ($YFP^{-*}$) leads to a redistribution of $\pi$–bonds within the chromophore, resulting in a rotational axis which could then

easily undergo isomerisation (**Fig. 6.32**). This excited isomerised form (YFPH*) does not exhibit fluorescence at 514nm excitation, and can either return to the original ground state ($YFP^-$) via deprotonation and reverse isomerisation (thought to be the cause of the reported 'blinking' of the YFP fluorophore, ~0.5-1s timescale, Dickson *et al.*, 1997, **see 4.32**), or form the so-called 'dark state' (YFPHd*). Should this excited state return to the long-lived dark state (YFPHd) the fluorophore can be regarded as dormant, as without excitation via 350nm light the half-time of the reverse reaction (YFHd→YFPH) is ~1hr. The stability of this dark-state is presumably due to some H-bonding, ionic interactions, or even the formation of a covalent bond similar to the ethyl ester bond cleaved in the flash photolysis of caged-ATP (also at 350nm), consolidating the isomerised form of the chromophore.

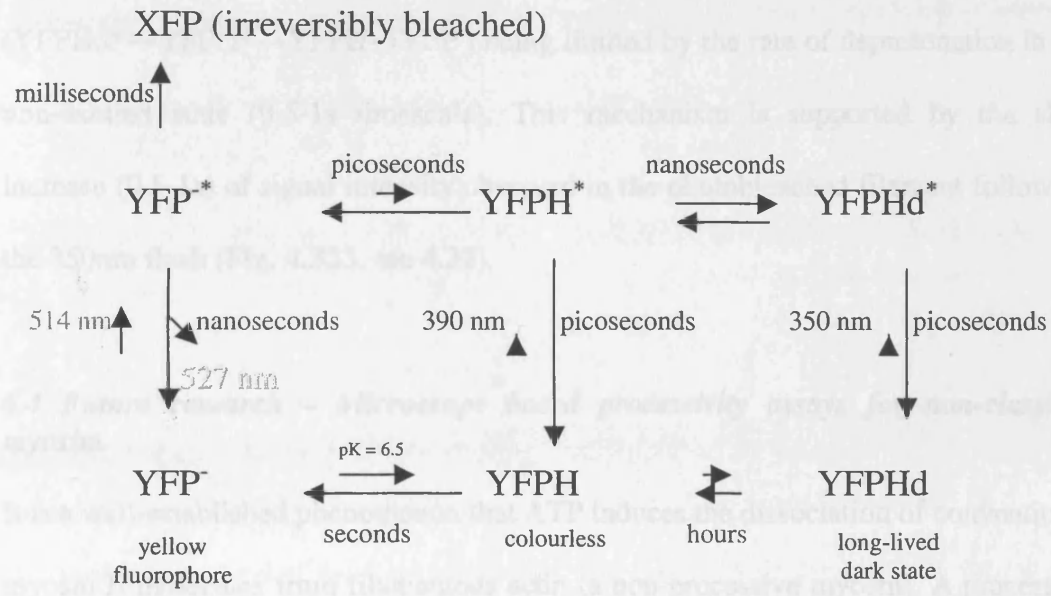


**Fig. 6.31** The current proposed relationships between fluorescent, protonated (colourless) and so-called 'dark states' of YFP.

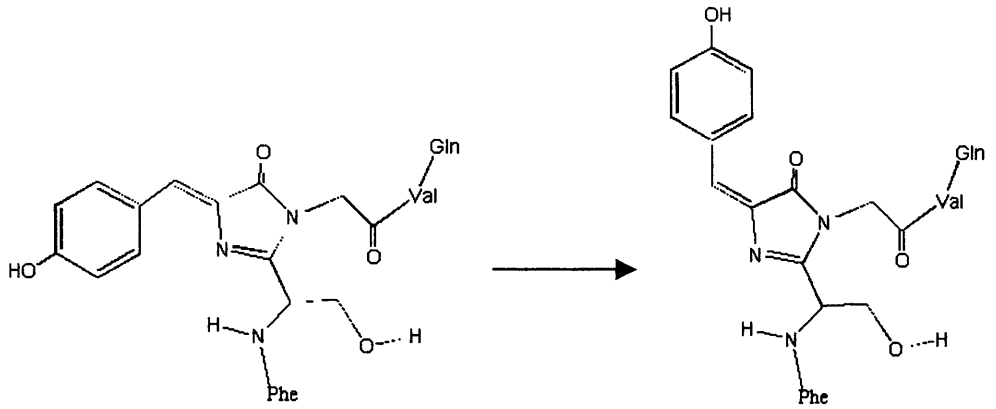


*cis* *trans*

**Fig. 6.32** The potential rotational (*cis-trans*) isomerisation which may be caused by protonation of the YFP chromophore.

Therefore, photolysis of these interactions with 350nm incident light would therefore set the chromophore back into dynamic equilibrium, whereby it can achieve the original ground state with the most favourable pathway (YFPHd*→YFPH*→YFPH→$YFP^-$) being limited by the rate of deprotonation in the non-excited state (0.5-1s timescale). This mechanism is supported by the slow increase (0.5-1s) of signal intensity observed in the photobleached filament following the 350nm flash (**Fig. 4.323, see 4.32**).

### *6.4 Future research – Microscope based processivity assays for non-classical myosins*

It is a well-established phenomenon that ATP induces the dissociation of conventional myosin II molecules from filamentous actin (a non-processive myosin). A processive myosin type, however, would exhibit independent movement along an actin filament in the presence of ATP, analogous to kinesin movement along microtubules, before eventual dissociation. A great deal of studies have been conducted upon the proposed processivity of myosin V (Mehta *et al.*, 1999), ranging from the studies of Sakamoto *et al.* (2000), where visualisation of their movement along fixed actin filaments was

achieved using Cy3-labelled calmodulin, which binds to the 'neck' (IQ motif) of chick brain myosin V (BMV), to kinetic studies which have shown myosin V to spend most of its kinetic cycle bound to actin (Sweeney, 1999), with A.M.ADP clearly resolved as the rate determining step. Recently, the processive step size of mouse myosin V has been resolved (74.1nm) by direct observation (using TIRFM) of the movement of GFP-labelled mouse myosin V HMM, confirming the hand-over-hand model of myosin V processivity (**Fig. 6.41**, Snyder *et al.*, 2004).

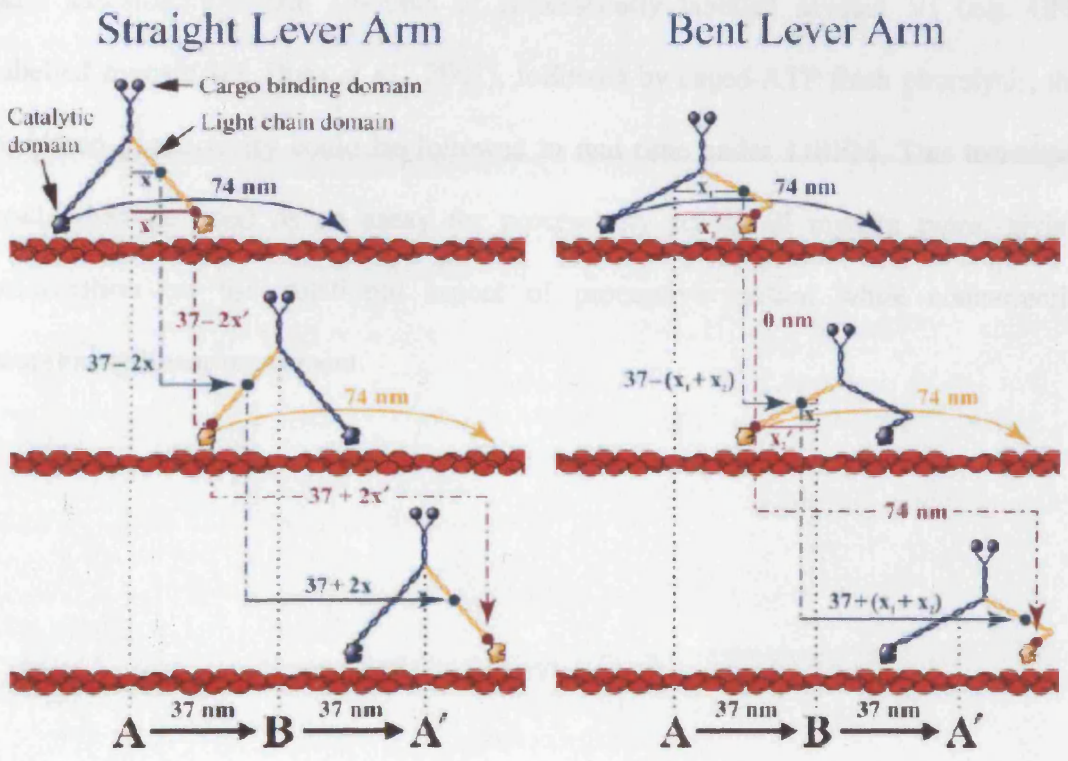


**Fig. 6.41** The proposed mechanisms (straight and bent lever arm) for the processive hand-over-hand motion of myosin V along an actin filament, taken from Snyder *et al.* (2004).

Mammalian myosin VI, of particular interest as it is the only myosin known to exhibit movement towards the –ve end of actin filaments (Wells *et al.*, 1999), exhibits kinetics similar to those of myosin V (slow A.M.ADP and A.M dissociation, (De La Cruz *et al.*, 2001), thus fuelling speculation about its' potentially processive nature. A

dissociation event has been previously observed when fixed actin-filaments sparsely decorated with fluorescently labelled myosin VI were exposed to ATP. However due to its' short neck region, it has been proposed that myosin VI may move along the actin filament one monomer at a time, thereby following the turn of the actin helix.

Further research into this area could be achieved by a simple adaptation of the TIRFM caged-ATP flash photolysis assays developed during this thesis. By forming an actin filament 'lattice' over aged thick molluscan myosin filaments, the actin could be suspended from the glass surface. Thus, by subsequent decoration of the filaments with sub-stoichiometric amounts of fluorescently labelled myosin VI (*e.g.* GFP labelled myosin VI, Buss *et al.*, 2001), followed by caged-ATP flash photolysis, the proposed processivity could be followed in real time under TIRFM. This technique could thus be used as an assay for processivity across all myosin types, giving information on the rotational aspect of processive motion while concurrently monitoring linear movement.

# 7 - Appendices

## *7.1 Commonly used abbreviations*

| | |
|---|---|
| β-ME | β mercaptoethanol |
| ACC | Anti-parallel coiled coil |
| ADP | Adenosine 5' diphosphate |
| ATP | Adenosine 5' triphosphate |
| BMV | Chick brain myosin V |
| BSA | Bovine serum albumin |
| C-terminal | Carboxy terminal |
| CIAP | Calf intestinal alkaline phosphatase |
| *Dd* | *Dictyostelium discoideum* |
| $DIH_2O$ | De-ionised water |
| DNA | Deoxyribonucleic acid |
| DTT | Dithiothreitol |
| DMSO | Dimethylsulfoxide |
| EDTA | Ethylenediaminacetic acid |
| EGFP | Enhanced GFP |
| EGTA | Ethylene glycol-bis(β-aminoethyl ether) tetraacetic acid |
| EM | Electron microscopy |
| FRET | Fluorescence resonance energy transfer |
| gYFP.W501.gCFP | W501 with an N-terminal YFP, and C-terminal CFP, both fused via triple-glycine linker regions (g) |
| GFP/BFP/CFP/YFP | Green/Blue/Cyan/Yellow fluorescent protein |
| HEPES | (N-[2-hydroxyethyl]piperazine-N'-[2-ethanesulfonic acid]) |
| HMM | Heavy meromyosin (myosin with light meromyosin cleaved) |
| His-tag | Multiple histidine residues used for $Ni^{2+}$ column purification |
| ICCD | Intensified charge coupled device |
| IQ | Light-chain binding motifs in the neck region of myosin |
| KAc | Potassium acetate |
| MgAc | Magnesium acetate |
| MOPS | (3-[N-Morpholino]propanesulfonic acid) |
| N-terminal | Amino terminal |
| NEB | New England Biolabs |
| $Ni^{2+}$-NTA | Nitriloacetic acid with a nickel chelate |
| $P_i$ | Inorganic phosphate molecule |
| PCR | Polymerase chain reaction |
| PMSF | Phenylmethylsulfonylfluoride |
| rYFP.W501 | W501 with an N-terminal YFP fused without an intermediate triple-glycine linker region (r) |
| rYFP.W501.gGFP | W501 with an N-terminal YFP fused without an intermediate triple-glycine linker region (r), and a C terminal CFP fused via this linker (g) |
| TAME | Proteolytic enzyme |
| TIRFM | Total internal reflectance fluorescence microscopy |
| TLCK | Protease inhibitor |
| W501 | A 761 residue *Dictyostelium discoideum* myosin II motor domain, with all native tryptophan residues mutated to phenylalanine save that at the 501 position |

| | |
|---|---|
| W501.gGFP | W501 with a C-terminal GFP fused via an intermediate triple-glycine linker region (g) |

### *7.2 Oligonucleotides*

All oligonucleotides are given 5'-3'.

7.2a *KpnGFUP* (upstream)

CGG GGT ACC ATG GTG AGC AAG GGC GAG GAG CTG

7.2b *BamGFDOr* (downstream)

CGG GGA TCC CTT GTA CAG CTC GTC CAT GCC GAG AGT GAT CCC G

7.2c *Seq3* (downstream)

CTG TCT TGA CCA TCA ACG G

7.2d *XhoGFUP* (upstream)

CC GCT CGA GGT GGT GGT ATG GTG AGC AAG GGC GAG GAG CTG

7.2e *XhoGFDO* (downstream)

CC GCT CGA GGT CTT GTA CAG CTC GTC CAT GCC GAG AGT GAT CCC G

7.2f *T706W* (upstream)

GCC GAT TTC GTC AAA CGT TGG TAT TTA TTA GCT CCA AAC GTT CCA AGA GAC GC

7.2g *BamGFDOg* (downstream)

CGG GGA TCC GGT CTT GTA CAG CTC GTC CAT GCC GAG AGT GAT CCC G

7.2h *GFPBa1* (upstream)

ACGC GGA TCC GGT GGT GGT ATG GTG AGC AAG GGC GAG GAG CTG TTC ACC

7.2i *NsiGF2* (downstream)

AA CCA A TGC ATG CTT GTA CAG CTC GTC CAT GCC GAG AGT GAT CCC

### *7.3 Publications*

Wakelin S, Conibear PB, Woolley RJ, Floyd DN, Bagshaw CR, Kovacs M, Malnasi-Csizmadia A (2002) Engineering Dictyostelium discoideum myosin II for the introduction of site-specific fluorescence probes. *Journal of Muscle Research and Cell Motility* **23:** 673-683.

Wakelin S, Bagshaw CR, (2002) A prism combination for near isotropic fluorescence excitation by total internal reflection. *Journal of Microscopy* **209:** 143-148

Wei Z, Conibear PB, Dickens JL, Cowie RA, Wakelin S, Málnási-Csizmadia A, and Bagshaw CR (2004) Dynamics of actomyosin interactions in relation to the crossbridge cycle. *Phil. Trans. Royal Soc.* **in press.**

# 8 – References

Arata T (1990) Orientation of spin-labeled light chain 2 of myosin heads in muscle fibers. *J Mol Biol* **214**: 471-8.

Axelrod D (1999) *Light microscopy in biology: A practical approach.*

Axelrod D, Burghardt TP and Thompson NL (1984) Total internal reflection fluorescence. *Annu Rev Biophys Bioeng* **13**: 247-68.

Bagshaw CR (1987) Muscle contraction. Are two heads better than one? *Nature* **326**: 746-7.

Bagshaw CR (1993) *Muscle contraction.* Second edit, London.

Bagshaw CR, Eccleston JF, Eckstein F, Goody RS, Gutfreund H and Trentham DR (1974) The magnesium ion-dependent adenosine triphosphatase of myosin. Two-step processes of adenosine triphosphate association and adenosine diphosphate dissociation. *Biochem J* **141**: 351-64.

Bagshaw CR and Trentham DR (1973) The reversibility of adenosine triphosphate cleavage by myosin. *Biochem J* **133**: 323-8.

Becker WM, Kleinsmith, L. J., Hardin, J. (2001) *The world of the cell*, Addison Wesley Longman.

Bertrand R, Chaussepied P, Kassab R, Boyer M, Roustan C and Benyamin Y (1988) Cross-linking of the skeletal myosin subfragment 1 heavy chain to the N-terminal actin segment of residues 40-113. *Biochemistry* **27**: 5728-36.

Brefeld (1869) Dictyostelium mucoroides. Ein neuer organismus aus der Verwandtschaft der Myxomyceten. *Abhandlungen der Senckenbergischen Naturforschenden Gesellschaft Frankfurt* **7**: 85-107.

Buss F, Arden SD, Lindsay M, Luzio JP and Kendrick-Jones J (2001) Myosin VI isoform localized to clathrin-coated vesicles with a role in clathrin-mediated endocytosis. *Embo J* **20**: 3676-84.

Carlier MF (1991) Actin: protein structure and filament dynamics. *J Biol Chem* **266**: 1-4.

Chalfie M, Tu Y, Euskirchen G, Ward WW and Prasher DC (1994) Green fluorescent protein as a marker for gene expression. *Science* **263**: 802-5.

Chang AC, Slade MB and Williams KL (1990) Identification of the origin of replication of the eukaryote Dictyostelium discoideum nuclear plasmid Ddp2. *Plasmid* **24**: 208-17.

Chattoraj M, King BA, Bublitz GU and Boxer SG (1996) Ultra-fast excited state dynamics in green fluorescent protein: multiple states and proton transfer. *Proc Natl Acad Sci U S A* **93**: 8362-7.

Cheng L, Fu J, Tsukamoto A and Hawley RG (1996) Use of green fluorescent protein variants to monitor gene transfer and expression in mammalian cells. *Nat Biotechnol* **14**: 606-9.

Cody CW, Prasher DC, Westler WM, Prendergast FG and Ward WW (1993) Chemical structure of the hexapeptide chromophore of the Aequorea green-fluorescent protein. *Biochemistry* **32**: 1212-8.

Conibear PB and Bagshaw CR (1996) Measurement of nucleotide exchange kinetics with isolated synthetic myosin filaments using flash photolysis. *FEBS Lett* **380**: 13-6.

Conibear PB and Bagshaw CR (2000) A comparison of optical geometries for combined flash photolysis and total internal reflection fluorescence microscopy. *J Microsc* **200 Pt 3**: 218-29.

Conibear PB, Kuhlman PA and Bagshaw CR (1998) Measurement of ATPase activities of myosin at the level of tracks and single molecules. *Adv Exp Med Biol* **453**: 15-26; discussion 26-7.

Conibear PB, Malnasi-Csizmadia, A., Bagshaw, C. R. (2004) The effect of F-actin on the relay position of myosin II, as revealed by tryptophan fluorescence, and its implications for mechanochemical coupling. **in press**.

Cooke R (1986) The mechanism of muscle contraction. *CRC Crit Rev Biochem* **21**: 53-118.

Cope MJ, Whisstock J, Rayment I and Kendrick-Jones J (1996) Conservation within the myosin motor domain: implications for structure and function. *Structure* **4**: 969-87.

Cowles CR, Odorizzi G, Payne GS and Emr SD (1997) The AP-3 adaptor complex is essential for cargo-selective transport to the yeast vacuole. *Cell* **91**: 109-18.

Cubitt AB, Woollenweber LA and Heim R (1999) Understanding structure-function relationships in the Aequorea victoria green fluorescent protein. *Methods Cell Biol* **58**: 19-30.

Dale RE, Eisinger J and Blumberg WE (1979) The orientational freedom of molecular probes. *Biophys J* **26**: 161-194

De La Cruz EM, Ostap EM and Sweeney HL (2001) Kinetic mechanism and regulation of myosin VI. *J Biol Chem* **276**: 32373-81.

Dickson RM, Cubitt AB, Tsien RY and Moerner WE (1997) On/off blinking and switching behaviour of single molecules of green fluorescent protein. *Nature* **388**: 355-8.

Egelman EH (1985) The structure of F-actin. *J Muscle Res Cell Motil* **6**: 129-51.

Eisenberg E and Moos C (1968) The adenosine triphosphatase activity of acto-heavy meromyosin. A kinetic analysis of actin activation. *Biochemistry* **7**: 1486-9.

Eisenberg E, Zobel CR and Moos C (1968) Subfragment 1 of myosin: adenosine triphophatase activation by actin. *Biochemistry* **7**: 3186-94.

Engelhardt WA, Ljubimowa, M. N. (1939) Myosine adeosinetriphosphatase. *Nature* **144**.

Firtel RA, Silan C, Ward TE, Howard P, Metz BA, Nellen W and Jacobson A (1985) Extrachromosomal replication of shuttle vectors in Dictyostelium discoideum. *Mol Cell Biol* **5**: 3241-50.

Fisher AJ, Smith CA, Thoden JB, Smith R, Sutoh K, Holden HM and Rayment I (1995) X-ray structures of the myosin motor domain of Dictyostelium discoideum complexed with MgADP.BeFx and MgADP.AlF4. *Biochemistry* **34**: 8960-72.

Forster VT (1948) Zwischenmolekulare energiewanderung und fluoreszenz. *Ann Phys* **6**.

Funatsu T, Harada Y, Tokunaga M, Saito K and Yanagida T (1995) Imaging of single fluorescent molecules and individual ATP turnovers by single myosin molecules in aqueous solution. *Nature* **374**: 555-9.

Geeves MA and Holmes KC (1999) Structural mechanism of muscle contraction. *Annu Rev Biochem* **68**: 687-728.

Gingell D, Todd I and Bailey J (1985) Topography of cell-glass apposition revealed by total internal reflection fluorescence of volume markers. *J Cell Biol* **100**: 1334-8.

Gonzales CM, Spencer TD, Pendley SS and Welker DL (1999) Dgp1 and Dfp1 are closely related plasmids in the Dictyostelium Ddp2 plasmid family. *Plasmid* **41**: 89-96.

Gulick AM, Bauer CB, Thoden JB and Rayment I (1997) X-ray structures of the MgADP, MgATPgammaS, and MgAMPPNP complexes of the Dictyostelium discoideum myosin motor domain. *Biochemistry* **36**: 11619-28.

Gutfreund H (1972) *Enzymes-physical principles* (ltd WI, Ed.), London.

Harada Y, Noguchi A, Kishino A and Yanagida T (1987) Sliding movement of single actin filaments on one-headed myosin filaments. *Nature* **326**: 805-8.

Heim R, Prasher DC and Tsien RY (1994) Wavelength mutations and posttranslational autoxidation of green fluorescent protein. *Proc Natl Acad Sci U S A* **91**: 12501-4.

Heim R and Tsien RY (1996) Engineering green fluorescent protein for improved brightness, longer wavelengths and fluorescence resonance energy transfer. *Curr Biol* **6**: 178-82.

Hibberd MG and Trentham DR (1986) Relationships between chemical and mechanical events during muscular contraction. *Annu Rev Biophys Biophys Chem* **15**: 119-61.

Holmes KC (1997) The swinging lever-arm hypothesis of muscle contraction. *Curr Biol* **7**: R112-8.

Holmes KC, Popp D, Gebhard W and Kabsch W (1990) Atomic model of the actin filament. *Nature* **347**: 44-9.

Holmes KC and Schroeder RR (2003) Switch 1 opens on strong binding to actin. *Adv Exp Med Biol* **in press**.

Houdusse A and Cohen C (1996) Structure of the regulatory domain of scallop myosin at 2 A resolution: implications for regulation. *Structure* **4**: 21-32.

Houdusse A and Sweeney HL (2001) Myosin motors: missing structures and hidden springs. *Curr Opin Struct Biol* **11**: 182-94.

Huxley AF and Niedergerke R (1954) Structural changes in muscle during contraction; interference microscopy of living muscle fibres. *Nature* **173**: 971-3.

Huxley AF and Simmons RM (1971) Proposed mechanism of force generation in striated muscle. *Nature* **233**: 533-8.

Huxley H and Hanson J (1954) Changes in the cross-striations of muscle during contraction and stretch and their structural interpretation. *Nature* **173**: 973-6.

Huxley HE (1957) The double array of filaments in cross-striated muscle. *J Biophys Biochem Cytol* **3**: 631-48.

Huxley HE (1963) Electron Microscope Studies on the Structure of Natural and Synthetic Protein Filaments from Striated Muscle. *J Mol Biol* **77**: 281-308.

Inouye S and Tsuji FI (1994) Evidence for redox forms of the Aequorea green fluorescent protein. *FEBS Lett* **351**: 211-4.

Irving M (1987) *Muscle mechanics and probes of the crossbridge cycle.*

Janknecht R, de Martynoff G, Lou J, Hipskind RA, Nordheim A and Stunnenberg HG (1991) Rapid and efficient purification of native histidine-tagged protein expressed by recombinant vaccinia virus. *Proc Natl Acad Sci U S A* **88**: 8972-6.

Johnson FH, Shimomura O and Saiga Y (1962) Action of cyanide on Cypridina luciferin. *J Cell Comp Physiol* **59**: 265-72.

Jontes JD and Milligan RA (1997) Brush border myosin-I structure and ADP-dependent conformational changes revealed by cryoelectron microscopy and image analysis. *J Cell Biol* **139**: 683-93.

Kabsch W, Mannherz HG, Suck D, Pai EF and Holmes KC (1990) Atomic structure of the actin:DNase I complex. *Nature* **347**: 37-44.

Kaether C and Gerdes HH (1995) Visualization of protein transport along the secretory pathway using green fluorescent protein. *FEBS Lett* **369**: 267-71.

Kishino A and Yanagida T (1988) Force measurements by micromanipulation of a single actin filament by glass needles. *Nature* **334**: 74-6.

Kiyosawa H, Hughes JE, Podgorski GJ and Welker DL (1993) Small circular plasmids of the eukaryote Dictyostelium purpureum define two novel plasmid families. *Plasmid* **30**: 106-18.

Knight P and Trinick J (1984) Structure of the myosin projections on native thick filaments from vertebrate skeletal muscle. *J Mol Biol* **177**: 461-82.

Kron SJ and Spudich JA (1986) Fluorescent actin filaments move on myosin fixed to a glass surface. *Proc Natl Acad Sci U S A* **83**: 6272-6.

Kuhlman PA and Bagshaw CR (1998) ATPase kinetics of the Dictyostelium discoideum myosin II motor domain. *J Muscle Res Cell Motil* **19**: 491-504.

Lacowicz J (1999) *Principles of fluorescence spectroscopy*. Second edit, Kluwer Academic / Plenum Press, New York.

Leiting B, Lindner IJ and Noegel AA (1990) The extrachromosomal replication of Dictyostelium plasmid Ddp2 requires a cis-acting element and a plasmid-encoded trans-acting factor. *Mol Cell Biol* **10**: 3727-36.

Lorenz M, Popp D and Holmes KC (1993) Refinement of the F-actin model against X-ray fiber diffraction data by the use of a directed mutation algorithm. *J Mol Biol* **234**: 826-36.

Lowey S and Luck SM (1969) Equilibrium binding of adenosine diphosphate to myosin. *Biochemistry* **8**: 3195-9.

Lymn RW and Taylor EW (1971) Mechanism of adenosine triphosphate hydrolysis by actomyosin. *Biochemistry* **10**: 4617-24.

Mahmood R, Cremo C, Nakamaye KL and Yount RG (1987) The interaction and photolabeling of myosin subfragment 1 with 3'(2')-O-(4-benzoyl)benzoyladenosine 5'-triphosphate. *J Biol Chem* **262**: 14479-86.

Malnasi-Csizmadia A, Kovacs M, Woolley RJ, Botchway SW and Bagshaw CR (2001a) The dynamics of the relay loop tryptophan residue in the Dictyostelium myosin motor domain and the origin of spectroscopic signals. *J Biol Chem* **276**: 19483-90.

Malnasi-Csizmadia A, Pearson DS, Kovacs M, Woolley RJ, Geeves MA and Bagshaw CR (2001b) Kinetic resolution of a conformational transition and the ATP hydrolysis step using relaxation methods with a Dictyostelium myosin II mutant containing a single tryptophan residue. *Biochemistry* **40**: 12727-37.

Malnasi-Csizmadia A, Woolley RJ and Bagshaw CR (2000) Resolution of conformational states of Dictyostelium myosin II motor domain using tryptophan (W501) mutants: implications for the open-closed transition identified by crystallography. *Biochemistry* **39**: 16135-46.

Maniak M, Rauchenberger R, Albrecht R, Murphy J and Gerisch G (1995) Coronin involved in phagocytosis: dynamics of particle-induced relocalization visualized by a green fluorescent protein Tag. *Cell* **83**: 915-24.

Manstein DJ, Schuster HP, Morandini P and Hunt DM (1995) Cloning vectors for the production of proteins in Dictyostelium discoideum. *Gene* **162**: 129-34.

Margossian SS and Lowey S (1973a):Substructure of the myosin molecule. 3. Preparation of single-headed derivatives of myosin. *J Mol Biol* **74**: 301-11.

Margossian SS and Lowey S (1973b) Substructure of the myosin molecule. IV. Interactions of myosin and its subfragments with adenosine triphosphate and F-actin. *J Mol Biol* **74**: 313-30.

Margossian SS and Lowey S (1982) Preparation of myosin and its subfragments from rabbit skeletal muscle. *Methods Enzymol* **85 Pt B**: 55-71.

Marston SB and Taylor EW (1980) Comparison of the myosin and actomyosin ATPase mechanisms of the four types of vertebrate muscles. *J Mol Biol* **139**: 573-600.

McCray JA and Trentham DR (1989) Properties and uses of photoreactive caged compounds. *Annu Rev Biophys Biophys Chem* **18**: 239-70.

McLachlan AD (1984) Structural implications of the myosin amino acid sequence. *Annu Rev Biophys Bioeng* **13**: 167-89.

Mehta AD, Rock RS, Rief M, Spudich JA, Mooseker MS and Cheney RE (1999) Myosin-V is a processive actin-based motor. *Nature* **400**: 590-3.

Milligan RA, Whittaker M and Safer D (1990) Molecular structure of F-actin and location of surface binding sites. *Nature* **348**: 217-21.

Miyawaki A, Llopis J, Heim R, McCaffery JM, Adams JA, Ikura M and Tsien RY (1997) Fluorescent indicators for Ca2+ based on green fluorescent proteins and calmodulin. *Nature* **388**: 882-7.

Miyawaki A and Tsien RY (2000) Monitoring protein conformations and interactions by fluorescence resonance energy transfer between mutants of green fluorescent protein. *Methods Enzymol* **327**: 472-500.

Morin JG and Hastings JW (1971) Energy transfer in a bioluminescent system. *J Cell Physiol* **77**: 313-8.

Morise H, Shimomura O, Johnson FH and Winant J (1974) Intermolecular energy transfer in the bioluminescent system of Aequorea. *Biochemistry* **13**: 2656-62.

Mornet D, Bertrand R, Pantel P, Audemard E and Kassab R (1981a) Structure of the actin-myosin interface. *Nature* **292**: 301-6.

Mornet D, Bertrand RU, Pantel P, Audemard E and Kassab R (1981b) Proteolytic approach to structure and function of actin recognition site in myosin heads. *Biochemistry* **20**: 2110-20.

Mornet D, Pantel P, Audemard E and Kassab R (1979) The limited tryptic cleavage of chymotryptic S-1: an approach to the characterization of the actin site in myosin heads. *Biochem Biophys Res Commun* **89**: 925-32.

Muldoon RR, Levy JP, Kain SR, Kitts PA and Link CJ, Jr. (1997) Tracking and quantitation of retroviral-mediated transfer using a completely humanized, red-shifted green fluorescent protein gene. *Biotechniques* **22**: 162-7.

Nagai T, Yamada S, Tominaga T, Ichikawa M and Miyawaki A (2004) Expanded dynamic range of fluorescent indicators for Ca(2+) by circularly permuted yellow fluorescent proteins. *Proc Natl Acad Sci U S A* **101**: 10554-9.

Nellen W, Silan C and Firtel RA (1984) DNA-mediated transformation in Dictyostelium discoideum: regulated expression of an actin gene fusion. *Mol Cell Biol* **4**: 2890-8.

Offer G and Elliott A (1978) Can a myosin molecule bind to two actin filaments? *Nature* **271**: 325-9.

Oiwa K, Eccleston JF, Anson M, Kikumoto M, Davis CT, Reid GP, Ferenczi MA, Corrie JE, Yamada A, Nakayama H and Trentham DR (2000) Comparative single-molecule and ensemble myosin enzymology: sulfoindocyanine ATP and ADP derivatives. *Biophys J* **78**: 3048-71.

Okamoto Y and Yount RG (1985) Identification of an active site peptide of skeletal myosin after photoaffinity labeling with N-(4-azido-2-nitrophenyl)-2-aminoethyl diphosphate. *Proc Natl Acad Sci U S A* **82**: 1575-9.

Ormo M, Cubitt AB, Kallio K, Gross LA, Tsien RY and Remington SJ (1996) Crystal structure of the Aequorea victoria green fluorescent protein. *Science* **273**: 1392-5.

Ostap EM and Pollard TD (1996) Biochemical kinetic characterization of the Acanthamoeba myosin-I ATPase. *J Cell Biol* **132**: 1053-60.

Pardee JD and Spudich JA (1982) Purification of muscle actin. *Methods Enzymol* **85 Pt B**: 164-81.

Patterson GH, Knobel SM, Sharif WD, Kain SR and Piston DW (1997) Use of the green fluorescent protein and its mutants in quantitative fluorescence microscopy. *Biophys J* **73**: 2782-90.

Periasamy M, Strehler EE, Garfinkel LI, Gubits RM, Ruiz-Opazo N and Nadal-Ginard B (1984) Fast skeletal muscle myosin light chains 1 and 3 are produced from a single gene by a combined process of differential RNA transcription and splicing. *J Biol Chem* **259**: 13595-604.

Pollard TD, Doberstein SK and Zot HG (1991) Myosin-I. *Annu Rev Physiol* **53**: 653-81.

Prasher DC, Eckenrode VK, Ward WW, Prendergast FG and Cormier MJ (1992) Primary structure of the Aequorea victoria green-fluorescent protein. *Gene* **111**: 229-33.

Presley JF, Cole NB, Schroer TA, Hirschberg K, Zaal KJ and Lippincott-Schwartz J (1997) ER-to-Golgi transport visualized in living cells. *Nature* **389**: 81-5.

Rayment I and Holden HM (1994) The three-dimensional structure of a molecular motor. *Trends Biochem Sci* **19**: 129-34.

Rayment I, Holden HM, Whittaker M, Yohn CB, Lorenz M, Holmes KC and Milligan RA (1993) Structure of the actin-myosin complex and its implications for muscle contraction. *Science* **261**: 58-65.

Ritchie MD, Geeves MA, Woodward SK and Manstein DJ (1993) Kinetic characterization of a cytoplasmic myosin motor domain expressed in Dictyostelium discoideum. *Proc Natl Acad Sci U S A* **90**: 8619-23.

Rizzuto R, Brini M, De Giorgi F, Rossi R, Heim R, Tsien RY and Pozzan T (1996) Double labelling of subcellular structures with organelle-targeted GFP mutants in vivo. *Curr Biol* **6**: 183-8.

Romoser VA, Hinkle PM and Persechini A (1997) Detection in living cells of Ca2+-dependent changes in the fluorescence emission of an indicator composed of two green fluorescent protein variants linked by a calmodulin-binding sequence. A new class of fluorescent indicators. *J Biol Chem* **272**: 13270-4.

Rosell FI and Boxer SG (2003) Polarized absorption spectra of green fluorescent protein single crystals: transition dipole moment directions. *Biochemistry* **42**: 177-83.

Sakamoto T, Amitani I, Yokota E and Ando T (2000) Direct observation of processive movement by individual myosin V molecules. *Biochem Biophys Res Commun* **272**: 586-90.

Sasaki N, Ohkura R and Sutoh K (2003) Dictyostelium myosin II mutations that uncouple the converter swing and ATP hydrolysis cycle. *Biochemistry* **42**: 90-5.

Schroder RR, Manstein DJ, Jahn W, Holden H, Rayment I, Holmes KC and Spudich JA (1993) Three-dimensional atomic model of F-actin decorated with Dictyostelium myosin S1. *Nature* **364**: 171-4.

Sellers JR, Han YJ and Kachar B (1991) The use of native thick filaments in in vitro motility assays. *J Cell Sci Suppl* **14**: 67-71.

Shammat IM and Welker DL (1999) Mechanism of action of the Rep protein from the Dictyostelium Ddp2 plasmid family. *Plasmid* **41**: 248-59.

Shih WM, Gryczynski Z, Lakowicz JR and Spudich JA (2000) A FRET-based sensor reveals large ATP hydrolysis-induced conformational changes and three distinct states of the molecular motor myosin. *Cell* **102**: 683-94.

Shimomura O, Johnson FH and Saiga Y (1962) Extraction, purification and properties of aequorin, a bioluminescent protein from the luminous hydromedusan, Aequorea. *J Cell Comp Physiol* **59**: 223-39.

Slade MB, Chang AC and Williams KL (1990) The sequence and organization of Ddp2, a high-copy-number nuclear plasmid of Dictyostelium discoideum. *Plasmid* **24**: 195-207.

Snyder GE, Sakamoto T, Hammer JA, 3rd, Sellers JR and Selvin PR (2004) Nanometer localization of single green fluorescent proteins: evidence that myosin V walks hand-over-hand via telemark configuration. *Biophys J* **87**: 1776-83.

Sowerby AJ, Seehra CK, Lee M and Bagshaw CR (1993) Turnover of fluorescent nucleoside triphosphates by isolated immobilized myosin filaments. Transient kinetics on the zeptomole scale. *J Mol Biol* **234**: 114-23.

Spudich JA (1994) How molecular motors work. *Nature* **372**: 515-8.

Squire (1981) *Structural basis of muscle contraction.*

Starr R and Offer G (1973) Polarity of the myosin molecule. *J Mol Biol* **81**: 17-31.

Suzuki Y, Yasunaga T, Ohkura R, Wakabayashi T and Sutoh K (1998) Swing of the lever arm of a myosin motor at the isomerization and phosphate-release steps. *Nature* **396**: 380-3.

Sweeney HL, De la Cruz, E. M., Wells, A. L., Safer, D., Rosenfeld, S. S., Ostap, E. M., (1999) Abstracts of the XXXVIII European Muscle Conference. *J Muscle Res Cell Motil* **20**: 812-813.

Szilagyi L, Balint M, Sreter FA and Gergely J (1979) Photoaffinity labelling with an ATP analog of the N-terminal peptide of myosin. *Biochem Biophys Res Commun* **87**: 936-45.

Thompson NL, Pearce KH and Hsieh HV (1993) Total internal reflection fluorescence microscopy: application to substrate-supported planar membranes. *Eur Biophys J* **22**: 367-78.

Trentham DR, Eccleston JF and Bagshaw CR (1976) Kinetic analysis of ATPase mechanisms. *Q Rev Biophys* **9**: 217-81.

Tsien RY (1998) The green fluorescent protein. *Annu Rev Biochem* **67**: 509-44.

van Thor JJ, Gensch T, Hellingwerf KJ and Johnson LN (2002) Phototransformation of green fluorescent protein with UV and visible light leads to decarboxylation of glutamate 222. *Nat Struct Biol* **9**: 37-41.

Vesalius A (1543) *De humani corporis fabrica.*

Vibert P and Cohen C (1988) Domains, motions and regulation in the myosin head. *J Muscle Res Cell Motil* **9**: 296-305.

Wachter RM and Remington SJ (1999) Sensitivity of the yellow variant of green fluorescent protein to halides and nitrate. *Curr Biol* **9**: R628-9.

Wakelin S, Bagshaw CR, (2002) A prism combination for near isotropic fluorescence excitation by total internal reflection. *Journal of Microscopy* **209:** 143-148

Ward WW (1997) *Green Fluorescent Protein; Properties, applications and protocols* (M. Chalfie SK, Ed.), John Wiley & Sons, New York.

Weeds AG and Lowey S (1971) Substructure of the myosin molecule. II. The light chains of myosin. *J Mol Biol* **61**: 701-25.

Weeds AG and Taylor RS (1975) Separation of subfragment-1 isoenzymes from rabbit skeletal muscle myosin. *Nature* **257**: 54-6.

Weiss S, Chizhov I and Geeves MA (2000) A flash photolysis fluorescence/light scattering apparatus for use with sub microgram quantities of muscle proteins. *J Muscle Res Cell Motil* **21**: 423-32.

Wells AL, Lin AW, Chen LQ, Safer D, Cain SM, Hasson T, Carragher BO, Milligan RA and Sweeney HL (1999) Myosin VI is an actin-based motor that moves backwards. *Nature* **401**: 505-8.

Werber MM, Szent-Gyorgyi AG and Fasman GD (1972) Fluorescence studies on heavy meromyosin-substrate interaction. *Biochemistry* **11**: 2872-83.

Wiemer EA, Wenzel T, Deerinck TJ, Ellisman MH and Subramani S (1997) Visualization of the peroxisomal compartment in living mammalian cells: dynamic behavior and association with microtubules. *J Cell Biol* **136**: 71-80.

Wollemann M, Feuer G and Straub FB (1950) [Suitability of actomyosin filaments for a model of muscles]. *Acta Physiol Hung* **1**: 34-43.

Xiao M, Reifenberger JG, Wells AL, Baldacchino C, Chen LQ, Ge P, Sweeney HL and Selvin PR (2003) An actin-dependent conformational change in myosin. *Nat Struct Biol* **10**: 402-8.

Xie X, Harrison DH, Schlichting I, Sweet RM, Kalabokis VN, Szent-Gyorgyi AG and Cohen C (1994) Structure of the regulatory domain of scallop myosin at 2.8 A resolution. *Nature* **368**: 306-12.

Yang F, Moss LG and Phillips GN, Jr. (1996) The molecular structure of green fluorescent protein. *Nat Biotechnol* **14**: 1246-51.

Yengo CM, Chrin LR, Rovner AS and Berger CL (2000) Tryptophan 512 is sensitive to conformational changes in the rigid relay loop of smooth muscle myosin during the MgATPase cycle. *J Biol Chem* **275**: 25481-7.

Yokoe H and Meyer T (1996) Spatial dynamics of GFP-tagged proteins investigated by local fluorescence enhancement. *Nat Biotechnol* **14**: 1252-6.

Zacharias DA, Violin JD, Newton AC and Tsien RY (2002) Partitioning of lipid-modified monomeric GFPs into membrane microdomains of live cells. *Science* **296**: 913-6.

Zeng W, Conibear PC, Dickens JL, Cowie RA, Wakelin S, Málnási-Csizmadia A, Bagshaw CR (2004) Dynamics of actomyosin interactions in relation to the crossbridge cycle. **in press**.